Frequency-Dependent Electronic Transport in Quantum Wires

Dissertation
zur Erlangung des Doktorgrades
des Fachbereichs Physik
der Universität Hamburg

vorgelegt von
Andrea Fechner
aus Hamburg

Hamburg
2000

Abstract

We investigate time and frequency-dependent transport and local field effects in single-channel quantum wires. Electron-electron interactions are taken into account exploiting the Luttinger model.

We discuss linear dc and ac transport in a "clean" quantum wire and derive a set of coupled integral equations which determine the local field in the wire self-consistently. Based on these equations we demonstrate the existence of a plasmon-polariton, induced by the coupling of collective charge excitations to the local transverse field, and discuss the dispersion relation of this polariton. We show that the influence of the induced transverse field on transport can be neglected.

In a "dirty" quantum wire, i.e. a wire containing a potential barrier, the dc current-voltage characteristic is non-linear due to the influence of the electron-electron interactions. We investigate in detail the non-linear ac current and here especially photon-assisted transport and higher harmonic generation. We show that the influence of the induced transverse field on the non-linear ac current can be neglected. Finally, the electromagnetic fields emitted by the non-linear ac current and the corresponding emitted power are derived and are studied as functions of position.

Zusammenfassung

Wir untersuchen zeit- und frequenzabhängigen Transport und die Rolle lokaler Felder in Quantendrähten mit einem besetzten Band. Die Elektron-Elektron Wechselwirkung wird mit Hilfe des Luttinger Modells behandelt.

Wir diskutieren linearen dc and ac Transport in einem "sauberen" Quantendraht und leiten ein System gekoppelter Integralgleichungen her, welche das lokale Feld im Draht selbstkonsistent bestimmt. Basierend auf diesen Gleichungen demonstrieren wir die Existenz eines Plasmonpolaritons, induziert durch die Kopplung zwischen kollektiven Ladungsanregungen und dem lokalen transversalen Feld, und diskutieren die Dispersionsrelation des Polaritons. Wir zeigen, dass der Einfluss des induzierten transversalen Feldes auf den Transport vernachlässigbar ist.

In einem "dreckigen" Quantendraht, d.h. einem Draht, der eine Potentialbarriere enthält, ist die Kennlinie nichtlinear aufgrund des Einflusses der Wechselwirkung zwischen den Elektronen. Wir untersuchen im Detail den nichtlinearen ac Strom und hier im besonderen photonenunterstützten Transport und die Erzeugung höherer Harmonischer. Wir zeigen, dass der Einfluss des induzierten transversalen Feldes auf den nichtlinearen ac Strom vernachlässigbar ist. Schließlich berechnen wir die elektromagnetischen Felder, die vom Draht ausgestrahlt werden, und die entsprechende abgestrahlte Leistung und untersuchen diese als Funktion des Ortes.

Contents

1 Introduction

In 1837, Michael Faraday put an insulator between the plates of a capacitor and found that the capacitance increased with respect to the empty capacitor. The insulator he called *dielectric* and the numerical factor by which the capacitance increased he called *dielectric constant*. At that time, the dielectric constant was just a phenomenological characteristic of each individual substance, however, it marked the beginning of the concept of *local fields* [1]: The charges inside the medium respond to the applied field and as a consequence induce a field themselves thus giving rise to a *local field* in the medium that is different from the external field. And such a local field can, for example, influence the properties of a capacitor.

Even though the chapter of local fields was opened over 160 years ago it is far from being closed any time soon. The reason is simple: The origin of local fields is the *longitudinal* Coulomb field associated with any charged particle plus the *transverse* field radiated by a charged particle that is accelerated. Hence, in order to take into account local fields rigorously, one has to solve a quantum many-body problem evaluating the dynamics of about 10^{23} electrons coupled by mutual Coulomb interactions *and* by the electromagnetic field the electrons radiate.

A heuristic treatment of local fields as initiated by Lorentz [2] makes sense – if at all – only for samples of macroscopic dimensions. One could also start out from a Fermi gas model [3], neglect the correlations between the charges, and then evaluate the local fields self-consistently. But one should keep in mind that such a mean-field like approach is an approximation.

Due to the complex nature of the problem, local fields are in many cases ignored in the literature. And even though this may *often* lead to results which accord with experiment, it does *not always* do so. We give a few examples of phenomena in which local fields play a crucial role.

First, the local *longitudinal* field is especially important in samples of reduced dimensions in which screening of the Coulomb potential is not as effective as in three-dimensional (3D) samples [4]. In quantum dots, for example, the local longitudinal field is responsible for the well-known Coulomb blockade. Second, the local *transverse* field is the origin for the fact that metals are opaque for visible light [3]. Third, any collective excitation of charges, leads to characteristic local field effects. Consider for example a phonon. The collective oscillation of the ionic lattice induces an electromagnetic field. Where frequency and wave vector of phonon and electromagnetic field are similar, the mechanical energy of the phonon and the electromagnetic energy of the photon are continuously transformed one into the other. Thus, one cannot distinguish between phonon and photon. This elementary excitation of the coupled systems – in principle nothing but a local field – is called phonon-polariton [5].

In this thesis, we investigate transport and local-field effects in "clean" and "dirty" quantum wires. For such quasi one-dimensional systems, a powerful tool exists that makes a rigorous treatment of the *longitudinal part of the local field* possible: The *Luttinger model* allows for the exact solution of the eigenvalue problem of a one-dimensional (1D) system of *interacting fermions* [6]. The elementary excitations

of the Luttinger liquid are of a collective nature and correspond to 1D plasma oscillations.

We derive the transport equation for a "clean" single-channel quantum wire of finite cross-section in linear response neglecting transitions to higher bands. We discuss dc and ac transport. We show that in a linear system like the clean Luttinger liquid the rigorous microscopic approach and the mean-field like approach used in order to incorporate the local *longitudinal* field lead to identical results. Further, we derive a set of integral equations that allows for a self-consistent determination of the local transverse field. We pursue an approximate approach to solve the local-field integral equations and identify the elementary excitation of the system of charges coupled to the electromagnetic field – the *plasmon-polariton*. We extract and discuss the dispersion relation of the plasmon-polariton. We estimate the magnitude of the induced transverse field and show that its influence on transport may be neglected.

In a dirty quantum wire, i.e. a Luttinger liquid containing a potential barrier, the influence of the local longitudinal field onto transport is particularly pronounced. The current-voltage characteristic of such a "dirty" wire is non-linear due to the simultaneous presence of the barrier *and* electron-electron interactions. Hence, interactions induce higher harmonics in time-dependent transport. We derive explicit expressions for the dc component and the harmonic components of the non-linear time-dependent current in the weak-tunneling regime. We investigate the current as a function of various parameters like driving voltage, frequency and interaction strength [7, 8, 9, 10, 11].

Discussing local field effects in the dirty quantum wire we show that the rigorous microscopic approach and the mean-field like approach used in order to incorporate the local longitudinal field lead to *different* results in non-linear transport, i.e. the mean-field like approach fails. We further approximate the induced transverse field in lowest order in the tunneling probability and find that its influence on the non-linear time-dependent current may be neglected.

Finally, we evaluate the electromagnetic field and the time-averaged power emitted by the dirty wire in time-dependent transport [7, 8]. In the far-field regime, we obtain analytic expressions and in the near-field regime, we perform numerical calculations. The spatial structure of the electromagnetic fields and of the Poynting vector in the near-field regime is discussed as a function of position [12].

This work is organized as follows. An overview of the field of time-dependent transport in mesoscopic devices is given in section 2. Section 3 introduces the model exploited during the course of this work: (i) the confinement of a quantum wire, (ii) the Luttinger liquid, and (iii) the technique to handle local fields self-consistently. Linear transport in a clean quantum wire is studied in section 4 and non-linear transport in a dirty quantum wire is investigated in section 5.

2 Overview on Mesoscopic Systems

The device that laid the basement for today's computer technology was announced rather modestly: "A three-element electronic device which utilizes a newly discovered principle involving a semiconductor as the basic element is described. It may be employed as an amplifier, oscillator, and for other purposes for which vacuum tubes are ordinarily used." Such the *transistor* was introduced by Bardeen and Brattain in 1948 [13, 14]. Since its invention the transistor has shrunk in size seemingly unstoppably allowing for a higher and higher density of these semiconductor devices on an integrated chip. Until today the shrinking process abides by *Moore's law* [15] which states that the density of semiconductor components on a chip would double in fixed time intervals – in praxis such a time interval consists of roughly 18 months. With continuing miniaturization one might in a couple of years be fabricating devices of mesoscopic dimensions whose performance is influenced by quantum effects.

The term *mesoscopic* denotes the regime between the macroscopic and the microscopic regime. A mesoscopic sample contains a macroscopically large number of electrons but the length over which these electrons move coherently is comparable to or smaller than the sample length [16, 17, 18]. Hence, quantum interference effects influence the transport properties of the sample, for example via *weak localization* [19] or the *Aharonov-Bohm* effect [20]. Further, in a submicron structure like a narrow wire the energy for an electron's motion perpendicular to this wire becomes quantized and the quantization of energy levels is revealed in the transport properties. Both, interference effects and quantization effects, might spoil the performance of an "ordinary" transistor at low temperatures if the transistor's dimensions are only small enough.

The intense research on submicron structures in recent years has produced a number of *new devices* whose performance *relies* on effects which originate from their small lateral dimensions of only a few hundred nanometres. A *quantum point contact*, for example, is a constriction in a two-dimensional electron gas (2DEG) narrow enough in order for only a few subbands to be occupied. Each subband in the point contact has a conductance of e^2/h and the total conductance of the point contact forms a staircase as a function of the number of occupied subbands with step height e^2/h [21].

In a *quantum wire*, the electron motion is not only parallel to the 2DEG but is confined along one further direction. Ideally, a quantum wire is just a "long quantum point contact" with discrete subbands and a conductance staircase [22]. In reality impurities inside the wire often mix up the subbands making it difficult to observe the staircase.

In a *quantum dot*, the electron motion is confined along all three directions. Transport through a quantum dot can be blocked when the dot is weakly coupled to leads and when in addition the capacitance of the dot is so small that the charging energy needed to add a single electron to the dot exceeds the thermal energy. If then the Fermi energy of the leads does not align with one of the discrete energy levels in the dot transport through the dot is not possible. This device is called *single electron transistor*, the phenomenon is known as *Coulomb blockade* [23, 24]. Strictly speaking,

the Coulomb blockade is a classical effect. Only when the separation of the energy levels which are due to the quantum mechanical confinement becomes comparable to the charging energy, Coulomb blockade shows also features of a quantum mechanical nature.

However, non of these new devices – quantum point contact, quantum wire or quantum dot – is by now "ready for application" in industry. The main problem is that they show their special *quantum properties* only at temperatures of a few Kelvin and not at room temperature. For example, the energetic distance between two subbands in a quantum wire or between two levels in a quantum dot has to be large in comparison to the thermal energy in order to be experimentally relevant. But it is expected that this problem disappears automatically the moment one succeeds to fabricate structures even smaller than the existing devices as with decreasing structure size the level separation increases.

The dc properties of the new quantum devices are quite well understood, but little is known so far about frequency- and time-dependent transport properties. Corresponding investigations have a high priority as they allow a deeper understanding of these devices and also because a thorough understanding of the ac properties of a device is vital for applications.

The outline of this overview is as follows: In section 2.1 it is explained how structures as quantum dots and quantum wires are fabricated. Experiments on mesoscopic systems probing interaction-dependent effects, frequency and time-dependent effects and local-field effects are presented in section 2.2. A selection of the corresponding theoretical works is introduced in section 2.3.

2.1 Fabrication of Mesoscopic Samples

Semiconductor quantum dots and quantum wires can be defined using a variety of different materials and fabrication techniques [22]. Mostly used are Si-based systems and AlGaAs/GaAs heterostructures. But also quantum devices fabricated from InGaAs/InP or InAs/AlGaSb heterostructures can be found.

The substrate consisting of a semiconductor heterostructure is grown by *molecular beam epitaxy* or *metal organic vapour phase epitaxy* [17, 25, 26, 27]. The first step in the structuring process is to spun a layer of resist onto the top layer of the heterostructure. Next, the desired pattern is written into this resist employing *optical lithography*, *holographic lithography*, or *electron beam lithography* [17, 28, 29]. The resist is then developed and either washed away where it was exposed (positive resist) or where it was not exposed (negative resist) [30]).

Different processing steps may follow. Most mesoscopic samples are either defined by gates or by etching. If a sample is to be defined by gates, the next step after having developed the resist is to evaporate a thin metal film onto the substrate, i.e. on the patterned and developed resist. Then, the rest of the resist is dissolved away. The metal film remains in those places where it directly touches the substrate. Where there is still the layer of resist between metal and substrate, the metal is dissolved away together with the resist. This process is called *lift-off* and is used to deposit metallic gates and contacts on the substrate [18, 30, 31, 32]. When applying

a negative voltage to such a metallic gate, the 2DEG beneath the gate is depleted. A so-called split-gate, for example, consists of two metallic gates with a narrow slit in between them. When a negative voltage is applied to these gates, a narrow wire forms below the slit.

If the device is to be defined by etching instead of gates, the resist pattern is used as a mask for selective etching. This etching process affects the substrate only in those areas where it is not protected by the resist. One employs either *wet chemical etching* or *dry etching* including *plasma etching*, *reactive ion etching*, and *reactive ion beam etching* [18, 30, 31, 32]. Where the top layer of the semiconductor heterostructure is partly or even fully etched away, the 2DEG below is depleted. By etching the substrate apart from a narrow channel one can define a quantum wire.

A few alternatives to these two most often used fabrication techniques – definition of the device by metal gates or by etching – can be found in the literature. For example, the pattern can be written directly into the semiconductor using *focused ion beam implantation* [30, 33]. Where the ions are implanted in the top layer, the 2DEG below is depleted. So-called V-groove GaAs wires are structured by growing GaAs and AlGaAs on a corrugated GaAs substrate into which V-grooves have been etched before [34, 35]. A technique used especially in order to define quantum wires is *cleaved edge overgrowth*. Here, a heterostructure with a 2DEG is cleaved at one edge. Then, a second heterostructure is grown at the cleaved edge, with the layers oriented perpendicular to the layers in the first heterostructure. A gate on the top layer of the substrate is biased negatively in order to deplete the 2DEG everywhere apart from directly at the edge where hence a T-shaped quantum wire forms [36, 37].

2.2 Experiments on Electronic Transport

2.2.1 Interaction-Dependent Effects

When asking in how far electron-electron interactions influence the transport properties of a sample, the experimentalist faces the difficulty that she or he cannot study the sample once with the interaction switched off and next with the interaction switched on; the interaction is always present. Thus, one has to rely on theory predicting certain effects which are based on the presence of the interaction. And indeed, the influence of interactions onto the transport properties of mesoscopic samples has many different facets.

Miscellaneous
First, electron-electron interactions cause corrections to the low-temperature conductivity. In the diffusive regime, the temperature dependence of these corrections was predicted to be proportional to $\ln(k_{\mathrm{B}}T\tau/\hbar)$ in two spatial dimensions and to $T^{-1/2}$ in one spatial dimension. In a magnetic field, the interaction-induced correction to the resistivity was predicted to be proportional to the square of the magnetic field strength [38, 39, 40]. Via these dependences on temperature and magnetic field, the interaction-induced corrections to the conductivity could be identified experimentally [41, 42, 43, 44, 45, 46].

Second, as the density of thermal excitations decreases with decreasing temperature, electron-electron interaction becomes the dominant dephasing mechanism at very low temperatures [16, 19, 39, 40, 47, 48]. Hence, any experiment studying the low-temperature phase coherence length is probing interaction effects. The number of corresponding experiments is huge. A few examples are [45, 49, 50, 51, 52, 53, 54, 55]. Most interesting are those publications in which a saturation of the phase coherence length with decreasing temperature was reported [45, 52, 53, 54, 55], because theoretically it was expected that the phase coherence length should diverge as the temperature approaches the absolute zero. Usually, the authors assigned the observed saturation to inelastic scattering at magnetic impurities or to heating. Only recently the discussion on the dephasing mechanism at low temperatures was renewed by an experiment in which the saturation of the phase coherence length could be attributed to neither of the two mechanisms [56].

A third transport phenomenon due to electron-electron interactions and present in quantum dots is the *Coulomb blockade* already discussed above. It was first observed in narrow quantum wires in which impurities subdivided the wires into small islands [57, 58, 59] before it was studied systematically in quantum dots [23, 24, 60].

Luttinger Liquid

The Luttinger liquid theory allows for the exact treatment of 1D systems of interacting electrons [6, 61, 62, 63]. It predicts that the current-voltage characteristic of a 1D wire containing a tunnel barrier obeys a power law, $J \propto V^{2/g-1}$, due to the simultaneous presence of the barrier *and* the electron-electron interaction. The parameter g characterizes the strength of the interaction. The power $2/g-1$ is different from 1 for interacting electrons. The dependence of the current on temperature is also governed by a power law according to the Luttinger model.

The first experimental verification of the power-law behaviour of the dc current in non-linear transport was reported in [64] where the 1D nature of the fractional quantum Hall edge states was exploited. Under certain conditions, these can be described by chiral Luttinger liquids, the interaction parameter g is replaced by the filling factor ν [65, 66, 67, 68, 69, 70, 71, 72]. A gate brought the two opposite edges of a GaAs 2DEG close together in a small region of the sample and backscattering between the two edge states became possible via a tunneling current. At any filling factor, the average conductance through this point contact decreased as the channel was slowly pinched of. A few transmission resonances were observed. The shape of the resonance peak and the off-resonance conductance was measured at filling factor $\nu = 1/3$ as a function of temperature in the millikelvin regime. Luttinger liquid theory predicted the half-width of the resonance peaks to scale as $T^{2/3}$ at $\nu = 1/3$ while the off-resonance conductance was expected to behave as T^4. The measured data were in agreement with the theoretical predictions.

In [73], also the 1D nature of the fractional quantum Hall edge states was exploited. The tunneling conductance and the current-voltage characteristics for electrons tunneling between a GaAs bulk normal metal and edge states were measured. For this kind of tunneling process, a power law for the current as a function of voltage with an exponent of 3 for $\nu = 1/3$ was predicted by the Luttinger model. The

measured current varied with the driving voltage as $V^{2.7\pm0.6}$ over one decade in the voltage at $T = 25$ mK and $\nu = 1/3$. The conductance varied with temperature as $T^{1.75\pm0.8}$ over one decade in temperature, an exponent of 2 had been expected. For $\nu = 1$, conductance was independent of temperature and the current-voltage characteristic was essentially linear. The measured data were in very good agreement with predictions based on Luttinger liquid theory.

The experiment [73] was then repeated for $\nu = 1/2$ [74]. A power law current-voltage characteristic was obtained with an average exponent of 1.91. The exponent governing the temperature-dependence of the conductance was 1.77 ± 0.07. The power-law behaviour was reminiscent of a chiral Luttinger liquid. Theoretically, the results were not well understood as Luttinger liquid behaviour had not been expected. The behaviour of a $\nu = 1/2$ edge state should have been markedly different from the behaviour of a $\nu = 1/3$ edge state.

Following [73] and [74], the current-voltage characteristics for tunneling into the edge states of a 2DEG for a continuum of filling factors from $\nu = 1/4$ to $\nu = 1$ was studied in [75]. At small and large voltages, the measured current-voltage characteristic was linear, while over a range of one decade in voltage in between, a continuum of power laws was observed. The exponent was approximately given by $1.16/\nu - 0.58$, it spanned the region in between 1 and 4. The edge appeared to behave as a single-mode Luttinger liquid for fillings with $1/\nu > 1.4$. For $1/\nu < 1.4$, the exponent saturated indicating an approach to Fermi liquid behaviour.

Also electrically conducting single-wall carbon nanotubes are expected to exhibit Luttinger liquid behaviour [76, 77]. In [78], the conductance of bundles of single wall carbon nanotubes was measured as a function of voltage and temperature. "End-contacted" samples with the metal electrode deposited on the tubes and "bulk-contacted" samples which were placed on top of the predefined metal leads were studied. The conductance as a function of gate voltage showed Coulomb blockade oscillations. The conductance as a function of temperature showed a power-law behaviour. It extended from 8 K to 300 K with exponents 0.33 and 0.38 for the bulk-contacted samples. Theory predicted an exponent of 0.24 for this system. The end-contacted samples showed a power-law behaviour from 10 K to 100 K with an exponent of ≈ 0.6, where an exponent of 0.65 had been expected. Also the current-voltage characteristic showed a power-law behaviour which extended over two decades in the voltage at 1.6 K. Luttinger liquid theory predicted a universal scaling curve for the differential conductance and it was indeed possible to collapse the measured data onto one single scaling curve in accordance with the prediction. The results were in very good agreement with theory.

Further, in [79] end-contacted single wall carbon nanotube ropes were studied which showed no Coulomb blockade at low temperature and a conductance $> e^2/h$ at room temperature. The samples showed almost no temperature-dependence for $T > 100$ K and large, reproducible fluctuations at lower T. The fluctuations were tentatively related to Luttinger liquid transport in a tube.

Transport through InSb in an asbestos matrix was studied in [80]. The current-voltage characteristic was non-linear. The conductance as a function of temperature followed a power law. The measured data was explained using Luttinger liquid

theory.

One further convincing proof of the relevance of the Luttinger model was found exploiting this model in order to describe the Coulomb blockade. In [81], evidence was reported for Luttinger liquid behaviour in a GaAs wire fabricated by cleaved edge overgrowth. The conductance of the wire as a function of carrier density showed deviations from the quantized conductance plateaus. These were attributed to the presence of impurities. For a density below the onset of the first plateau, the wire split into two parts as the potential barrier of an impurity crossed the Fermi energy. Decreasing the density further, another barrier due to another impurity crossed the Fermi energy and a single 1D island formed between these two impurities. Resonant tunneling through the island was observed. From the charging energy, the length of the island was estimated to be $100 - 200$ nm. The line shape of the resonance was measured for temperatures in the range $0.25\ \mathrm{K} < T < 2.5\ \mathrm{K}$. The line width decreased with decreasing temperature. According to conventional Coulomb blockade theory, the line shape should have been independent of temperature, while Luttinger liquid theory predicted the line width to be proportional to $T^{1/g-1}$, where the parameter $g\ (< 1)$ characterized the strength of the electron-electron interaction. Fitting the measured data of the line shapes at different Coulomb blockade peaks to Luttinger liquid theory yielded $g = 0.82$ at one peak and $g = 0.74$ at another. The change in carrier density in between the two peaks was responsible for the change in g. Similar power law behaviour was observed in three different wires. When in addition to the ground state also an excited state contributed to the resonant tunneling process, the behaviour of the line shape deviated from the simple power law it obeyed when tunneling occurred only via the ground state. Even this deviation was in perfect agreement with theoretical predictions based on the Luttinger model.

2.2.2 Frequency and Time-Dependent Effects

Noise

In 1984, discrete switching of the resistance of narrow Si wires with time was reported in [82]. The explanation was the following: The electrons in the wire suffered scattering from charged impurities. The ensuing electron trajectories constituted a large number of loops and the trajectories interfered coherently if half the circumference of such a loop was smaller than the phase coherence length. Whether interference was constructive or destructive depended on the phase shift between the trajectories which depended on the exact impurity configuration. Each loop thus either gave a positive or a negative contribution to conductance, depending on the details of the paths. Further, charged impurities could capture or emit electrons, hence become neutral which meant that they were turned off. Similarly, neutral impurities could capture or emit an electron and be thus turned on. And whenever an impurity was turned on or off the interference condition in the wire changed. Consequently also the conductance changed, namely by an amount of the order e^2/h. Thus, when the impurity configuration changed, a discrete jump in conductance or resistance was observed [83]. Further noise measurements on Si, GaAs and InAs wires can be found in [84, 85, 86, 87, 88, 89, 90, 91, 92].

Harmonic Generation

In 1985, a second harmonic signal was observed in a Si wire [93]. DC transport had been studied in the Si wires using an ac lock-in technique at 50 Hz. As the wire exhibited a non-linear current-voltage characteristic, a *second harmonic signal* of the 50 Hz driving voltage was observed. In 1988, a systematic study of second-harmonic generation in sub-micrometer GaAs wires was reported in [94]. The frequency was still very low, only 11 Hz.

Photoconductivity and Photovoltaic Effect

Starting in 1989, several authors investigated the *photoconductivity* of narrow semiconductor wires. Irradiating a semiconductor 2DEG or any sample fabricated from such a 2DEG leads to an increase in conductivity because the number of carriers available for transport increases due to the irradiation and hence the resistance drops. When the light source is removed, the photoconductivity decays slowly with time.

The photoconductivity in GaAs wires was reported to oscillate aperiodically as a function of time and as a function of magnetic field in [87, 95, 96]. The aperiodic oscillations were attributed to quantum interference effects as in case of the noise discussed above. Photoconductivity studies on GaAs wires patterned by etching revealed that the illumination changed the depletion depth by influencing the occupancy of traps generated during etching [97, 98]. The use of the time decay of the photoconductivity in order to measure conductance quantization of GaAs wires was reported in [99].

In addition to an increase of conductivity, irradiation of a sample can also generate a direct current when the sample lacks a centre of inversion. This phenomenon is called *photovoltaic effect*. In thermodynamic equilibrium, fluxes of particles with opposing momenta cancel each other and thus no net current flows. When the sample is irradiated with an electric field, the fraction of particles with velocity components parallel and anti-parallel to the direction of the electric field increases. Due to the intrinsic asymmetry of the system, the velocity distribution becomes anisotropic and a static particle current emerges.

Disordered samples always lack an inversion centre as the impurities are randomly distributed. But in a macroscopic disordered sample, the photovoltaic currents from different parts of the sample cancel each other, as the directions of the currents are random depending on the impurity configurations in the corresponding parts. This self-averaging takes place between sub-volumes of size $\approx l_\varphi^3$, where l_φ is the phase coherence length. In mesoscopic conductors, whose dimensions are of the order of l_φ, self-averaging is absent and the photovoltaic current is finite [100, 101]. Corresponding experiments on GaAs wires were performed in the GHz regime [95, 96, 102].

Surface Acoustic Waves

Only recently started the investigation of the influence of *surface acoustic waves* onto transport in narrow semiconductor wires. A surface acoustic wave propagating on a piezoelectric substrate generates a wave of electrostatic potential and thus interacts

with the charged carriers in the system. Due to this interaction, the damping and the velocity of the surface acoustic wave change. Further, because of momentum transfer from the surface acoustic wave to the electrons, a direct current is induced into a closed circuit. This current is called *acoustoelectric current*. Measurements of the acoustoelectric current induced by a surface acoustic wave in a GaAs channel are reported in [103].

Electron Turnstiles and Photon-Assisted Transport

In the presence of a low-frequency voltage signal, a quantum dot can be used as an *electron turnstile*. First, choose the energy level for the addition of one electron to the quantum dot aligned to the Fermi energies of the leads, hence transport through the dot is not blocked by the Coulomb blockade. Next, modulate the heights of the two barriers through which the electrons tunnel into and out of the dot by applying a time-dependent voltage with frequency f to the gates which define the barriers. The signals at the two gates should be phase-shifted by π with respect to each other, i.e. the height of one barrier should be decreased while at the same time the height of the other barrier should be increased by the time-dependent voltage and vice versa. Finally, a dc source-drain bias small with respect to the charging energy of the dot is applied.

Then, following the dc bias, an electron tunnels into the dot when the barrier it has to pass first is reduced by the time-dependent voltage at the gates. The electron does not immediately tunnel out of the dot on the other side as the height of the second barrier is enhanced with respect to the first and too large to be overcome. Due to the Coulomb blockade, a second electron cannot enter the dot through the first barrier. Then, half a cycle of the time-dependent voltage later, when the height of the second barrier is reduced, the electron leaves the dot. The next electron does not enter the dot immediately as now the first barrier is too large to be overcome. It enters half a cycle later when the first barrier is reduced again. Such a device is called turnstile as only one single electron can tunnel through the dot per cycle of the time-dependent voltage. The corresponding current is $I = ef$. For a dc drive larger than the charging energy but smaller than twice the charging energy the current is $I = 2ef$. In general, the current as a function of the dc drive exhibits the structure of a stair-case, $I = nef$, n integer [104]. Theoretical considerations on the accuracy of electron turnstiles can be found in [105, 106, 107].

The first metal turnstile was realized in 1990 [108]. A metal electron pump at zero dc bias was reported in 1991 [109]. In the same year, a semiconductor turnstile device was proposed and analyzed theoretically [110]. And indeed, the first GaAs turnstile was realized also in 1991 [111]. The frequency of the ac signal was roughly 10 MHz. It was a low-frequency signal in the sense that the corresponding energy was much smaller than the thermal energy and also smaller than the charging energy.

Further aspects of frequency-dependent transport through a quantum dot are revealed when a field with a frequency of the order of the charging energy is applied to the dot. When transport through the quantum dot is blocked due to charging effects, electrons might overcome this Coulomb blockade by absorbing energy quanta from the time-dependent field. Such *photon-assisted transport* was demonstrated

experimentally in semiconductor quantum dots in 1994 [112]. The Coulomb blockade peaks in the tunneling current vs. gate voltage developed "shoulders" in the presence of a microwave signal. In the derivative of the current with respect to gate voltage these shoulders appeared as additional peaks. The peaks shifted with frequency but not with microwave power, which was a strong evidence that they were due to electron tunneling via absorption of energy quanta from the external field. Further experiments on photon-assisted tunneling in quantum dots can be found in [104, 113, 114, 115].

2.2.3 Local-Field Effects

Local fields arise when an externally applied field causes a rearrangement of charges in a sample and these charges induce electromagnetic fields which superpose with the external field. One part of the induced field is due to the Coulomb field associated with any charged particle and is called *longitudinal* field. The other part of the induced field originates from accelerated charges which radiate electromagnetic waves and is called *transverse* field.

Phonon-Polariton

An electromagnetic field inside a sample couples to any excitation that includes dipole moments, thus it couples to transverse optical phonons. Due to the interaction between the electromagnetic field and the oscillation of the lattice, one cannot distinguish between photon and phonon. One obtains a "new" elementary excitation called *phonon-polariton* [5, 116, 117, 118, 119]. This polariton is nothing but the electromagnetic field in the presence of the medium, it is a *local field*.

In the absence of the coupling between photon and phonon – which can never be switched off in reality – both exhibit separate dispersion relations. The photon dispersion is linear and the dispersion relation of the transverse optical phonon can be assumed to be constant in the wave vector regime where the coupling of photon and phonon is most pronounced. The two dispersions cross at wave vector q_c.

In the presence of the coupling, when the polariton is the true elementary excitation of the system, the dispersions *do not cross* but a gap opens at q_c. The ensuing two branches constitute the dispersion relation of the polariton. The lower branch resembles the photon dispersion for $q \ll q_c$ while the upper branch resembles the phonon dispersion in this regime but with a frequency shifted slightly upwards due to the coupling. This shifted frequency coincides with the frequency of a longitudinal phonon at $q = 0$. Near q_c, the two branches deviate strongly from the original dispersion relations, they repel each other. Then, for $q \gg q_c$, the lower branch resembles the phonon dispersion while the upper branch resembles the photon dispersion. Typical values for q_c are around 5×10^4 m^{-1} which is extremely small in comparison to the zone boundary values of $\approx 10^{10}$ m^{-1} [5].

Phonon-polaritons can be probed experimentally via Raman scattering [120]. The first observation of phonon-polaritons was reported 1965 in [121], see also [5, 118]. Whenever an experiment probes the bulk properties of a material, the corresponding polaritons are called *bulk phonon-polaritons*. One distinguishes bulk polaritons from

surface phonon-polaritons which propagate along the surface of a sample. The latter were first detected in 1968 [122].

Localization of Electromagnetic Fields

In analogy to the localization of electrons in random media it was suspected that also electromagnetic waves should exhibit localization when propagating in media with random scatterers [123]. The incident field interacts strongly with the medium and the ensuing local field might become localized due to interference effects. And indeed, *weak localization of electromagnetic waves* was observed for different systems of randomly distributed scatterers [124, 125, 126]. This phenomenon is relatively well understood theoretically [127, 128, 129]. An experimental proof of *strong localization of electromagnetic waves* due to 2D random scattering was reported in [130]. A self-consistent theory of localization of classical waves was presented in [131]. Analogies between light and electrons like the density of states, screening and a criterion for localization were worked out in [132]. An investigation of the speed of propagation of classical waves in strongly scattering media may be found in [133]. An analytical approach to localization of electromagnetic waves in 2D systems based on Maxwell's equations was presented in [134].

Coulomb Blockade

A prominent example for local field effects in mesoscopic systems is the Coulomb blockade. One might either state that that transport is blocked by a large *local longitudinal field* or that transport is blocked by *charging effects*. Those are only two different names for the same phenomenon: the Coulomb field associated with any charged particle and the ensuing repulsion of equally charged particles.

Further, photon-assisted tunneling via sidebands in a quantum dot, i.e. via absorption and emission of energy quanta from the external time-dependent field, showed an asymmetry between absorption and emission peaks [135]. This asymmetry was attributed to a local-field effect. The internal potential in the dot was assumed to shift the occupation probabilities of the sidebands in [136].

2.3 Theories on Electronic Transport

Theoretical investigations of optical and transport properties of mesoscopic systems are numerous. A complete overview cannot be given here. We concentrate in the following on the most important concepts providing the background for the results derived in this thesis.

2.3.1 Interaction-Dependent Effects

Mean-Field Like Approaches

A complete description of the dynamics of $\approx 10^{23}$ particles coupled by mutual interaction is impossible – but fortunately also unnecessary. The knowledge of the low-energy excitation spectrum of a system is sufficient in order to predict its transport properties as experiments usually probe a system's response on energy scales small

in comparison to the Fermi energy. In 3D systems, the phenomenological *Fermi liquid theory* [3] is often employed to describe the influence of interaction onto the behaviour of a system. Fermi liquid theory models the low-lying excited states of a fermion liquid in terms of quasi-particles which consist of fermions "dressed" by the disturbance they cause in their immediate neighbourhood due to interaction with other fermions. The properties of such a Fermi liquid are qualitatively similar to the properties of a Fermi gas consisting of non-interacting electrons. Predictions of Fermi liquid theory concerning for example the temperature-dependence of the electronic specific heat agree well with experiments. Unfortunately, Fermi liquid theory cannot give account of microscopic phenomena or provide information on the ground state of the system of interacting electrons.

Microscopic theories, on the other hand, often yield reliable answers only in certain limits. For example, in an electron liquid in the limit of a high density, where the average energy due to the electron-electron interaction is small in comparison to the kinetic energy, the Coulomb interaction represents a small perturbation and it is sufficient to consider interaction effects in lowest order [3]. In the limit of a low electron density, the behaviour of the electron liquid is governed by the Coulomb interaction and the electrons form a *Wigner crystal*. The regime of intermediate electron densities, however, is difficult to handle. As kinetic and potential energies are comparable, neither one nor the other can be treated perturbatively.

An approach concerned with intermediate electron densities is the *Hartree-Fock approximation*. Instead of considering the interaction of one particle with all other particles individually, one constructs a *mean field*, originating from the Coulomb fields of all other particles, and considers the influence of this mean field onto the behaviour of a certain particle [137, 138]. In a uniform electron liquid, the Hartree-Fock approximation corresponds to lowest-order perturbation theory in the interaction potential. In a non-uniform system, the electron wave function and the mean-field have to be evaluated self-consistently and the Hartree-Fock approximation is more subtle than ordinary perturbation theory [3]. In spite of some success of the Hartree-Fock approximation, it fails when predicting the temperature-dependence of the electronic specific heat as this prediction does not accord with experiment [139]. One major problem of the Hartree-Fock approximation lies in the fact that it does not take into account the long-range correlations due to the Coulomb interactions [138].

A considerable improvement over the Hartree-Fock approximation was provided by the so-called *random phase approximation* (RPA) [3, 138, 139, 140]. This method has its name for historical reasons [3, 139], it was developed in the context of screening and collective behaviour of an electron liquid. The random phase approximation treats the long-range part of the Coulomb interactions by considering a *polarization* field and its influence onto the electron liquid. For methods leading to similar results as the random phase approximation like the *self-consistent field method* and the *equation-of-motion method* see [3, 138, 140].

The random phase approximation and corresponding methods allowed the evaluation of static and dynamic dielectric functions and hence the description of screening of a point charge in an electron liquid. Screening of a charged impurity comes about

because the surrounding electrons rearrange themselves with respect to the equilibrium distribution assumed in the absence of the impurity trying to restore the charge balance disturbed by the charged impurity. Far away from the charged impurity the field of the impurity is screened. But as the electrons have a certain kinetic energy and cannot stay fixed next to the impurity, screening can never be perfect close to the impurity. The corresponding length scale is given by the screening length, it governs the exponential decay of the screened Coulomb potential [4]. In order to calculate the screening length one needs the dielectric function. Depending on the approximation the evaluation of the dielectric function is based on one distinguishes between *Thomas-Fermi screening* [3, 140], *Hartree screening* [3], and *RPA screening* [3]. The latter is also known as *Lindhard screening* [4, 140].

An approach vaguely related to the Hartree-Fock approximation but definitely superior is the *density functional theory*. Ground state properties are expressed in terms of the electron density or the spin density instead of the many-electron wave function. The approach leads to self-consistent equations for the density similar to the ones encountered in the Hartree-Fock approximation. In density functional theory, however, correlation effects are included by the addition of the exchange-correlation potential. Density functional theory is in principle exact but in practice the exchange-correlation energy cannot be evaluated exactly. The simplest approximation to obtain this exchange-correlation energy is the *local-density approximation* which rests on a Monte Carlo calculation [141, 142].

When interacting electrons are considered on a lattice, this lattice model can be replaced by a single-site quantum impurity problem embedded in an effective medium which has to be determined self-consistently. This approach, called *dynamical mean-field method*, does not assume that all fluctuations are frozen, as in an ordinary mean-field approach like for example the Hartree-Fock approximation, but freezes only spatial fluctuations while taking into account local quantum fluctuations [143].

Electron-electron interactions may also be taken into account employing a local-field argument. As "interactions" and "induced longitudinal fields" are only different names for the same problem, namely the Coulomb potential associated with each charged particle, one might consider *either* one *or* the other. On the one hand, incorporating the Coulomb interaction into the many-body Hamiltonian leads to

$$H_{\rm int}^{\rm MB} = \frac{1}{2} \int {\rm d}\vec{r} \int {\rm d}\vec{r}\,' \, \rho(\vec{r}) V_{\rm ee}(\vec{r}-\vec{r}\,')\rho(\vec{r}\,'), \tag{1}$$

where $\rho(\vec{r}\,)$ denotes the density *operator* and the Coulomb interaction potential is

$$V_{\rm ee}(\vec{r}-\vec{r}\,') = \frac{1}{4\pi\epsilon_0} \frac{1}{|\vec{r}-\vec{r}\,'|}. \tag{2}$$

On the other hand, neglecting the interaction and considering the induced potential $V_{\rm ind}(\vec{r})$, obtained via the Poisson equation,

$$V_{\rm ind}(\vec{r}) = -\frac{1}{4\pi\epsilon_0} \int {\rm d}\vec{r}\,' \, \frac{\langle \rho(\vec{r}\,') \rangle}{|\vec{r}-\vec{r}\,'|}, \tag{3}$$

the corresponding Hamiltonian is

$$H_{\mathrm{ind}} = \int \mathrm{d}\vec{r} \int \mathrm{d}\vec{r}\,' \, \rho(\vec{r}) V_{\mathrm{ee}}(\vec{r}-\vec{r}\,') \langle \rho(\vec{r}\,') \rangle . \tag{4}$$

Now, the main difference between $H_{\mathrm{int}}^{\mathrm{MB}}$ in eq. (1) and H_{ind} in eq. (4) is the presence of the expectation value $\langle \rho(\vec{r}\,', t) \rangle$ in eq. (4). The consideration of H_{ind} instead of $H_{\mathrm{int}}^{\mathrm{MB}}$ corresponds to a mean-field like approach, sometimes also called RPA approach [2]. It is *not* equivalent to the consideration of $H_{\mathrm{int}}^{\mathrm{MB}}$ because the Poisson equation – or in general the set of Maxwell equations – is valid for functions and not for operators.

Renormalization Group Approach

Typically, the Hamiltonian and hence the action describing a system of interacting electrons contain a huge number of degrees of freedom at wave vectors up to a certain cut-off. In order to understand the system's properties only a small part of these degrees of freedom is needed. One has too much information which makes the task difficult to handle. One can obtain an *effective action* containing only the physically most interesting degrees of freedom by shifting the cut-off to some lower value with respect to the initial cut-off, integrating out all degrees of freedom between the old and the new cut-off and then perform a scale change of the wave vector that brings the cut-off back to its original value. Repeating these steps iteratively one obtains scaling equations for the system property of interest [61, 144]. This approach is called *renormalization group method*. A similar method based on the same idea of eliminating unwanted degrees of freedom is the *density matrix renormalization group method* [145].

Luttinger Liquid

The – for this thesis – most important theoretical approach designed to handle systems of interacting electrons is the *Luttinger liquid theory* [6, 61, 62, 63]. It allows for the exact treatment of 1D systems of interacting fermions based on three assumptions. First, the dispersion relation of the non-interacting fermions is linearized at the Fermi energy. One obtains two linear branches of the dispersion relation crossing at zero wave number. Second, these two branches of the linearized dispersion relation are extended beyond their point of intersection and the infinitely many "anti-particle" states at negative energies are assumed to be occupied. At excitation energies small in comparison to the Fermi energy neither of these two assumptions alters the physical properties of the system with respect to the "real" system. Third, backward scattering is excluded from the model as otherwise it would not be exactly solvable. The exclusion of backward scattering is justified under certain conditions based on renormalization group arguments [6]. Following these three assumptions the Hamiltonian describing the electron liquid can be diagonalized employing a bosonization technique.

The Luttinger model allows for the evaluation of a variety of properties of the 1D system of interacting particles. In the following, a few examples are given in a

flash-light manner without presenting any details. For a deeper understanding the reader is referred to the cited papers.

Correlation functions of interacting fermions in one dimension are presented in [146, 147]. The influence of boundaries on correlation functions is investigated in [148, 149, 150]. Raman scattering in a Luttinger liquid is described in [151, 152, 153]. The influence of contacts onto the dc transport properties of a Luttinger liquid is studied in [154, 155, 156, 157, 158, 159, 160, 161, 162]. Screening in a Luttinger liquid is considered in [163]. Results on shot noise in dc transport through a Luttinger liquid can be found in [164]. In [165, 166, 167, 168], the influence of the electron-electron interaction onto an applied electric potential is discussed. Time-dependent transport through a Luttinger liquid is investigated in [169, 170], see also section 2.3.2.

A Luttinger liquid containing a single tunneling barrier or also two barriers was and is subject of intense research activity. Transport through such a "dirty" Luttinger liquid is non-linear, the first systematical study can be found in [65, 66]. Under certain conditions transport through the tunneling barrier can be treated exactly [72, 171, 172]. Transport through a single barrier studied in terms of quantum Monte Carlo methods is presented in [173]. Transport through a dirty Luttinger liquid in the presence of leads is investigated in [174, 175]. Time-dependent non-linear transport through a dirty Luttinger liquid is investigated in [7, 8, 9, 10, 11, 12, 176, 177, 178, 179], see also section 2.3.2. A collapse of quantized conductance in a dirty Luttinger liquid is predicted in [180, 181]. The tunneling density of states at the location of the tunneling barrier is evaluated in [182]. The Green function for a general backward scattering potential in a Luttinger liquid is calculated in [183]. Friedel oscillations induced by the presence of the impurity are discussed in [184]. Charging effects and the Coulomb blockade in Luttinger liquids are investigated in [185, 186, 187, 188, 189, 190, 191]. A Wigner crystal in one dimensional systems and its behaviour in the presence of impurities are studied in [192, 193]. Anderson localization in connection with Luttinger liquid theory is discussed in [194, 195].

2.3.2 Frequency and Time-Dependent Effects

Scattering Matrix Approach for AC Transport

Time-dependent transport through small phase-coherent conductors can be studied employing the scattering matrix approach. Originally developed by Landauer and Büttiker [196, 197, 198] in order to investigate the dc properties of mesoscopic samples, it can be generalized to account also for time-dependent effects. The scattering matrix approach describes transport of electrons through a multi-probe conductor relating the current to the transmission amplitudes between the various contacts. Dephasing processes and dissipation are assumed to occur in the reservoirs. In dc transport, the current depends only on the total voltage drop between the contacts while in ac transport it depends in addition on the potential landscape inside the conductor. This internal potential can be taken into account in the following manner: First, the response to the external potentials is determined neglecting the interaction between the carriers. Second, the time-dependent inter-

nal potential caused by the charges injected into the conductor due to the external potentials is determined. Then, the response to this internal potential is evaluated. Finally, these two steps are combined in a self-consistent manner. The resulting dynamic conductances and capacitances of mesoscopic conductors can be found in [199, 200, 201, 202, 203, 204, 205, 206].

The scattering matrix approach does not take the electron-electron interaction directly into account, for example based on a microscopic Hamiltonian, but via the internal potential landscape of the conductor. The internal potential of the conductor is determined by employing Poisson's equation, neglecting the second inhomogeneous Maxwell equation. Thus, only the longitudinal part of the local field is considered, the transverse part is neglected.

Further, it is often stressed that any transport theory should be charge and current conserving [204], implying that a current between two contacts should only depend on the total voltage drop between these two contacts and not on the individual voltages applied to each contact. In order to achieve such a charge and current-conserving theory based on a microscopic model one has to consider the long-range nature of the Coulomb correlations in order correctly account for charge accumulation in a sample [204]. The scattering matrix approach is usually charge and current-conserving, but *not* because it considers long-range Coulomb correlations but because it uses current conservation as a condition enforced on the scattering matrix.

Following an idea similar in spirit to the scattering matrix approach, namely considering coherent propagation in the sample and dissipation in the reservoirs, second harmonic generation was studied in [207] by extending the microscopic linear Kubo formalism to second order. Also in [208], scattering theory was used for an investigation of harmonic generation.

AC Transport in Clean Quantum Wires

In [209], a self-consistent evaluation of the frequency-dependent conductance of a perfect ballistic wire of length L coupled to two reservoirs was presented. The internal potential of the wire was determined by a self-consistent integral equation based on the Poisson equation. For a single-channel wire and $\omega \ll v/L$, where v was the velocity of the charges, the 1D potential was close to one half of the external voltage drop everywhere in the wire. For $\omega \gg v/L$, the potential dropped linearly along the wire. The frequency-dependent conductance was a monotonic function of frequency,

$$\Gamma(\omega) = \frac{e^2}{2\pi} \left(1 - \frac{\mathrm{i}\omega L}{2v}\right)^{-1}. \tag{5}$$

In a wire with two channels, the internal potential and the conductance exhibited an oscillatory structure attributed to interchannel excitations.

In [210], the frequency-dependent conductance in a perfect ballistic wire of length L coupled capacitively to a gate and connected to two electron reservoirs was investigated. Zero-range interactions were considered, long-range correlations were taken care of within the random phase approximation. The internal potential of the wire

was evaluated self-consistently based on the Poisson equation which was adjusted in order to account for the short-range interaction potential. The capacitive part of the conductance was called gate conductance and the real part of this gate conductance exhibited peaks as a function of frequency. The height of these peaks was $4e^2/h$ independent of the interaction strength while the width of the peaks decreased with increasing interaction strength. The imaginary part of the gate conductance showed zeroes at those frequencies at which the real part exhibited maxima. Left and right of these zeroes it exhibited extrema. The exact positions of these extrema depended on the interaction strength, their height was $2e^2/h$ independent of interaction strength. It was proposed to study the low-frequency gate conductance experimentally in order to determine the interaction parameter g.

Linear time-dependent transport in an infinitely long Luttinger liquid without contacts was studied in [169, 170]. These publications are discussed in detail in section 4.3.

The response of a Luttinger liquid of length L connected to two reservoirs and subject to a low-amplitude ac voltage was investigated in [211]. The leads were modelled as Luttinger liquids with the electron-electron interaction switched off. The interaction in the central wire was assumed to be zero-ranged. The frequency-dependent conductance and impedance were evaluated. The impedance as a function of frequency was discussed. The real part of the impedance showed an oscillatory structure and vanishes at frequencies $2\pi nv/L$, n integer and v the renormalized Fermi velocity.

A further study of transport in a Luttinger liquid of finite length connected to two semi-infinite leads of non-interacting electrons was presented in [156]. The time-dependent non-local conductivity for a zero-range interaction was determined and its frequency-dependence discussed; an oscillatory behaviour was observed. Finally, also in [212] ac transport in an inhomogeneous Luttinger liquid was investigated. The interactions were switched off in the leads. The amplitude of the ac current depended on the distribution of the potential produced by a time-dependent field. An oscillatory behaviour of the current was found.

Photon-Assisted Transport and the Tien-Gordon Theory

Next, turn to ac transport involving tunneling. The presence of a time-dependent field may help the electrons to overcome the tunneling barrier as they can absorb energy quanta from the field. This process, called *photon-assisted tunneling*, is well-known from superconductor-insulator-superconductor junctions [213]. A corresponding theory for non-interacting quasi particles was developed by Tien and Gordon [214]. As this theory is often the starting point for the description of photon-assisted tunneling also in semiconductor devices, the main points of this theory are outline below.

Tien and Gordon assumed an external time-dependent voltage $V_{\rm ac}\cos(\omega_{\rm ext}t)$. They argued that if the time dependence of the quasi-particle wave function of the unperturbed Hamiltonian was

$$\Psi(\vec{r},t) = f(\vec{r})\cdot \mathrm{e}^{-\mathrm{i}Et/\hbar}, \tag{6}$$

then the wave function of the system perturbed by the external voltage should be

$$\Psi_{\rm ac}(\vec{r},t) = f(\vec{r}) \cdot {\rm e}^{-{\rm i}\int dt\,[E+eV_{\rm ac}\cos(\omega_{\rm ext}t)]/\hbar}. \tag{7}$$

Expanded into a power series this wave function of the perturbed system became

$$\Psi_{\rm ac}(\vec{r},t) = f(\vec{r}) \cdot {\rm e}^{-{\rm i}Et/\hbar} \cdot \left[\sum_{n=-\infty}^{\infty} J_n\left(\frac{eV_{\rm ac}}{\hbar\omega_{\rm ext}}\right)\,{\rm e}^{-{\rm i}n\omega_{\rm ext}t}\right], \tag{8}$$

where $J_n(z)$ are Bessel functions of the first kind. The wave functions in the presence of the ac field contain components with energies E, $E \pm \hbar\omega_{\rm ext}$, $E \pm 2\hbar\omega_{\rm ext}$, etc. These components at shifted energies imply that a quasi-particle with energy E in one superconductor cannot only tunnel to a state with the same energy in the other superconductor but also to states with energies $E \pm n\omega_{\rm ext}$, n integer. These additional energy states available for the tunneling quasi-particle are called *sidebands*.

Based on these considerations concerning the wave functions, Tien and Gordon derived the dc tunneling current for quasi-particles. When the tunneling current as a function of dc bias in the absence of an ac field is denoted by $J(V_{\rm dc})$, the tunneling current in the presence of the ac field is

$$J_{\rm TG}(V_{\rm dc},V_{\rm ac},\omega_{\rm ext}) = \sum_{n=-\infty}^{\infty} J_n^2\left(\frac{eV_{\rm ac}}{\hbar\omega_{\rm ext}}\right)\,J(V_{\rm dc}+n\hbar\omega_{\rm ext}/e). \tag{9}$$

The square of the Bessel function gives the occupation probability of the sidebands. The outward appearance of the result in eq. (9) is often encountered in the studies of photon-assisted tunneling.

Photon-Assisted Transport in Superlattices

Photon-assisted transport in a *superlattice* neglecting electron-electron interactions was studied in [215, 216, 217]. In [217], also higher harmonic generation was considered. A combination of a microscopic transport model with the standard model of Tien and Gordon was presented in [218] where electron-electron interactions were taken into account via the Thomas-Fermi approximation and via the random phase approximation and the corresponding results were compared with each other. In [219], photon-assisted tunneling in a superlattice was studied including interactions via a self-consistent mean-field approach. It was claimed that a Tien-Gordon like result is not valid when such a self-consistent approach is employed, see also [136].

Photon-Assisted Transport in Double-Barrier Structures

Transport through double-barrier resonant tunneling devices in the presence of ac fields was extensively discussed in the past and is still an active research field. Perturbative approaches assuming a small ac signal and neglecting interactions can be found in [220, 221, 222, 223, 224, 225, 226]. A high-frequency approach for non-interacting electrons was presented in [227, 228]. A generalization of the Landauer-Büttiker approach to frequency-dependent transport and its subsequent application

to ac transport through quantum dots considering non-interacting electrons was reported in [229, 230, 231, 232]. A general expression for the time-dependent current of electrons into an interacting mesoscopic sample was derived in [233, 234] and then applied to study time-dependent resonant tunneling of non-interacting electrons. Further theoretical approaches, all neglecting electron-electron interactions, were presented in [235, 236, 237, 238, 239, 240, 241, 242, 243, 244, 245, 246, 247, 248, 249].

Coherent and sequential tunneling of electrons through a quantum dot in the Coulomb blockade regime was investigated in [250, 251]. Quenching of resonant transmission of non-interacting electrons through a double-barrier was reported in [252, 253]. The non-linear current response of a resonant tunneling device and the corresponding higher harmonic generation was studied in [254] neglecting electron-electron interactions. Resonant reflection of electrons at a quantum dot due to the presence of an ac field was found in [255].

In [256], the spectral function in a single quantum well was evaluated and the result was used to analyze sequential photon-assisted tunneling. The occupation probabilities of the sidebands were found to scale with frequency as $1/\omega^2$ in contrast to the Tien-Gordon scale of $1/\omega$. Further, an asymmetry between the photon emitting and the photon absorbing channels was found. In a study of photon-assisted transport of non-interacting electrons through a single barrier, again a scaling of the sideband occupation probability with $1/\omega^2$ was found [257].

Publications on time-dependent resonant tunneling including electron-electron interactions are significantly less in number than those neglecting interactions. In [258], interactions were treated phenomenologically considering a charging energy of the quantum dot in order to account for the Coulomb blockade. An Anderson model with an infinitely strong interaction was studied in [259]. The interaction was included considering self-consistently the internal potential inside the tunneling device in [260, 261, 262, 263, 264].

In [136], the scattering-matrix approach was generalized to *non-linear* ac transport. Photon-assisted tunneling was investigated including the interaction via a self-consistent internal potential of the sample. As long as screening was neglected, the result was outwardly similar to the Tien-Gordon result. Taking into account screening, the sideband occupation probabilities changed, they were no longer given by Bessel functions. The interaction also gave rise to an asymmetry between absorption and emission peaks. Further, due to the non-linearity of the system, it exhibited higher harmonic generation. The leading order non-linear term in the current voltage characteristic was considered and an expression for the second harmonic current was given.

Photon-Assisted Transport in Dirty Quantum Wires

The conductance through a weak constriction in a Luttinger liquid was shown to vanish with frequency as $c_1\omega^2 + c_2\omega^{2/g-2}$ in [177] where g described the kind and the strength of the electron-electron interaction. The first term dominates for $g < 1/2$ while the second term dominates for $g > 1/2$. For a numerical study of the scaling behaviour of the dynamical conductance of a Luttinger liquid with frequency see [265].

The time-dependent current-voltage characteristic of a tunnel barrier in a Luttinger liquid without contacts was presented in [179]. The tunnel barrier had a δ-like shape, the interaction potential was zero-ranged. The applied time-dependent voltage was $V_{\rm P}\cos(\omega_{\rm P}t) + V_{\rm MW}\cos(\omega_{\rm MW}t)$, where the probe voltage $V_{\rm P}$ was assumed to be small and was considered in lowest order while the additional microwave potential $V_{\rm MW}$ was of arbitrary amplitude. In the limit of weak tunneling the absorptive ac conductance with respect to $V_{\rm P}$ in the presence of the microwave signal was

$$\Gamma_{\rm MW}(\omega_{\rm P}; V_{\rm MW}, \omega_{\rm MW}) = \sum_{n=-\infty}^{\infty} J_n^2\left(\frac{eV_{\rm MW}}{\hbar\omega_{\rm MW}}\right)\left(\frac{\omega_{\rm P}+n\omega_{\rm MW}}{\omega_{\rm P}}\right)\Gamma_{\rm P}(\omega_{\rm P}+n\omega_{\rm MW}). \quad (10)$$

Here, $\Gamma_{\rm P}$ is the absorptive conductance of the Luttinger liquid with a barrier in the absence of the microwave signal, $J_n(z)$ is a Bessel function of the first kind. This result for $\Gamma_{\rm MW}$ is outwardly similar to the one obtained by Tien and Gordon. The microscopic properties of the system are contained in $\Gamma_{\rm P}$ which is at zero temperature

$$\Gamma_{\rm P}(\omega) = \frac{1}{R_{\rm T}\Gamma(2/g)}\left(\frac{\omega}{\omega_{\rm c}}\right)^{2/g-2} {\rm e}^{-|\omega|/\omega_{\rm c}}, \quad (11)$$

where $R_{\rm T} = 2\omega_{\rm c}^2/\pi e^2\Delta^2$ is the tunneling resistance with the tunneling probability Δ^2 and the cut-off frequency $\omega_{\rm c}$. The $\Gamma(2/g)$ on the right hand side of eq. (11) is a Gamma-function. The parameter g characterizes the interaction. The process leading to the ω^2-scaling of the conductance as discussed in [177] was not considered in [179]. For g slightly less than 1, $\Gamma_{\rm MW}(0; V_{\rm MW}, \omega_{\rm MW})$ showed pronounced oscillations as a function of $eV_{\rm MW}/\hbar\omega_{\rm MW}$. The situation of a small barrier was also discussed in [179] as it was related to the large-barrier case via a duality transformation.

It was shown in [176] that also in non-linear transport through a Luttinger liquid with barrier the current depends only on the total voltage drop and not on the spatial shape of the driving field in the zero-frequency limit, while in ac transport the current depends on the spatial shape of the driving field. The ac currents at two different sites could be related and this relation was independent of the spatial shape of the field, see the discussion in section 5.1.

In [178], Lin and Fisher studied ac transport in the edge of a fractional quantum Hall device. A point-contact tunnel junction between two quantum Hall fluids corresponded to a tunnel barrier in a 1D quantum wire. The current-voltage characteristic in the presence of an ac drive was evaluated. It exhibited features which were attributed to mode-locking of current "plateaus". In the limit of weak backscattering, the plateaus were centred at currents given by integer multiples of $e\omega/2\pi$.

2.3.3 Local-Field Effects

Local Longitudinal Field

In parts, the problem of local fields has already been touched above – whenever a theoretical approach takes into account interactions by considering the internal scattering potential of a mesoscopic sample it uses the local longitudinal field. One may take *either* account of the Coulomb interaction between the electrons *or* of the

longitudinal local field. Considering both means considering the Coulomb potential twice which would be wrong. Hence, in a model like the Luttinger model one does not need to worry about the local longitudinal field as it is automatically included in the model.

Note, first, that the two approaches – Coulomb interaction vs. local longitudinal field – can only be identical when both consider the Coulomb potential to the same order. If the microscopic model includes the interaction exactly and the local longitudinal field is evaluated approximately, the two approaches necessarily differ. Second, one has to keep in mind that considering the local longitudinal field based on the *classical* Maxwell equations corresponds to a mean-field like approach which is not exact. Third, one has to be careful when using *a priori* a screened Coulomb interaction. Screening in quantum wires is usually due to nearby metallic gates. In order to proceed rigorously one should solve Maxwell equations for the whole system, quantum wire plus gates, and thus obtain a screened interaction from this calculation instead of assuming it from the beginning. In comparison, the mean-field like approach that determines the local field in a wire without gate assumes automatically an infinite-range Coulomb interaction as it is based on Maxwell equations.

Local Transverse Field

In contrast to the local longitudinal field, the local transverse field is not due to the simple presence of charges but to accelerated charges. If one had a solvable model taking full account of all time-dependent microscopic currents and the corresponding radiated electromagnetic waves, the local transverse field would be included automatically in the model and one would not have to worry about it. Unfortunately such a model does not yet exist. Hence, in contrast to the longitudinal component of the local field, the transverse component has to be inserted "by hand".

This means that first one derives an expression for the current in the system in terms of a general electric field. This field is either the complete local field, if the model on which the transport equation is based does not include Coulomb interactions, or it is the external longitudinal field plus the local transverse field. Second, one has to find an expression for the local fields in terms of the current. This expression can be obtained using Maxwell equations. Third, one has to combine these two expressions – current in terms of fields and fields in terms of current – self-consistently in order to obtain the current and the local fields.

Dielectric Function

The investigation of local field effects, also reflected in the dielectric function of a medium, is quite old [1, 2]. Williams and Bloch, for example, presented a detailed evaluation of the frequency and wave vector-dependent dielectric function of a quasi-1D electron gas in 1974 – but they neglected the transverse part of the local field [266]. For a quite exhaustive overview on local field effects on optical properties of semiconductor quantum wells and quantum dots and on local-field techniques in near-field optics see the article [2] by Keller and references therein.

3 The Model of the Quantum Wire

As discussed in section 2.1, a semiconductor quantum wire is usually defined from a semiconductor heterostructure either by applying a negative voltage to a split-gate or by etching the substrate apart from one long channel. Thus, a quantum wire is not a true 1D system but a confined 3D system. In section 3.1 below it is shown how such a confined wire can be described in terms of the eigenfunctions of the confinement potential. How one takes care of the electron-electron interactions in a single-channel quantum wire is explained in section 3.2 where the Luttinger model is introduced. The technique that allows for a self-consistent treatment of local fields in a quantum wire is introduced in section 3.3.

3.1 Confinement

It is assumed here that the wire extends along the x-direction, i.e. the 3D system is confined along the y and z-directions. The length of the wire is L. It is $\vec{r} = (x, \vec{R})$ and $\vec{q} = (q_x, \vec{Q})$ with $\vec{R} = (y, z)$ and $\vec{Q} = (q_y, q_z)$. As in this thesis transport in a clean wire and in a wire containing a potential barrier is considered, already in this section a quantum wire containing a potential barrier and coupled to an electromagnetic field is treated.

The many-body Hamiltonian of the quantum wire is

$$H^{\mathrm{MB}} = \int \mathrm{d}\vec{r}\, \Psi^{\dagger}(\vec{r}) \left[H^{\mathrm{SP}}_{\mathrm{kin}} + H^{\mathrm{SP}}_{\mathrm{em}} + H^{\mathrm{SP}}_{\mathrm{conf}} + H^{\mathrm{SP}}_{\mathrm{bar}} \right] \Psi(\vec{r}) + H^{\mathrm{MB}}_{\mathrm{int}}. \tag{12}$$

The single-particle Hamiltonians describing kinetic energy and coupling to the electromagnetic field are

$$H^{\mathrm{SP}}_{\mathrm{kin}} + H^{\mathrm{SP}}_{\mathrm{em}} = \frac{1}{2m} \left[\vec{p} - e\vec{A}(\vec{r}, t) \right]^2 + e\varphi_{\mathrm{ext}}(\vec{r}, t). \tag{13}$$

The electromagnetic vector potential $\vec{A}(\vec{r}, t)$ is the sum of the external and the induced vector potential while the electromagnetic scalar potential $\varphi_{\mathrm{ext}}(\vec{r}, t)$ is only the external one because the induced scalar potential is taken into account via the Coulomb interaction potential, see the discussion in sections 2.3 and 3.3. The single-particle Hamiltonian responsible for the confinement is for an arbitrary confinement potential denoted by $U_{\mathrm{conf}}(\vec{R})$, and hence $H^{\mathrm{SP}}_{\mathrm{conf}} = U_{\mathrm{conf}}(\vec{R})$. The potential of the scattering barrier is denoted by $U_{\mathrm{bar}}(\vec{r})$ and thus the corresponding Hamiltonian is $H^{\mathrm{SP}}_{\mathrm{bar}} = U_{\mathrm{bar}}(\vec{r})$. The electron-electron interaction potential $V_{\mathrm{ee}}(\vec{r} - \vec{r}\,')$ yields

$$H^{\mathrm{MB}}_{\mathrm{int}} = \int \mathrm{d}\vec{r} \int \mathrm{d}\vec{r}\,'\, \rho(\vec{r}) V_{\mathrm{ee}}(\vec{r} - \vec{r}\,') \rho(\vec{r}\,'). \tag{14}$$

Before an explicit expression for the many-body Hamiltonian in eq. (12) can be derived, the form of the 3D fermionic field operators $\Psi(\vec{r})$ has to be determined.

Projection of the Operators Ψ, ρ and $\vec{j}$

The eigenfunctions governing the motion of the electrons parallel to the wire are 1D plane waves while the eigenfunctions for the motion perpendicular to the wire are given by the eigenfunctions of the confinement potential which are denoted by $\Phi_n(\vec{R})$ with the quantum numbers $n = (n_y, n_z)$. The 3D fermionic field operator for spinless particles then is

$$\Psi(\vec{r}) = \frac{1}{\sqrt{L}} \sum_{q_x} \mathrm{e}^{\mathrm{i}q_x x} \sum_n \Phi_n(\vec{R})\, c_{nq_x}. \tag{15}$$

One can equivalently express $\Psi(\vec{r})$ in terms of the confinement eigenfunctions and a 1D fermionic field operator $\Psi_n(x)$,

$$\Psi(\vec{r}) = \sum_n \Phi_n(\vec{R})\Psi_n(x). \tag{16}$$

Here, the 1D fermionic field operator

$$\Psi_n(x) = \frac{1}{\sqrt{L}} \sum_{q_x} \mathrm{e}^{\mathrm{i}q_x x}\, c_{nq_x}, \tag{17}$$

acts on the subband corresponding to the quantum numbers (n_y, n_z) and c_{nq_x} is the annihilation operator for a fermion of wavenumber q_x in subband (n_y, n_z).

One could now use this expression for the fermionic field operator in order to reexpress the many-body Hamiltonian given above. However, it is useful to first express the particle density and the particle current density operators in terms of the eigenfunctions of the confinement potential as the many-body Hamiltonian can then be written in terms of those quantities. The 3D particle density is

$$\rho(\vec{r}) = \Psi^\dagger(\vec{r})\Psi\ (\vec{r}). \tag{18}$$

Inserting the expression given in eq. (16) yields

$$\rho(\vec{r}) = \sum_{n,l} \Phi_n^*(\vec{R})\Phi_l(\vec{R})\rho_{nl}(x), \tag{19}$$

with

$$\rho_{nl}(x) = \Psi_n^\dagger(x)\Psi_l(x). \tag{20}$$

Note that ρ_{nl} yields only a true 1D particle density for $n = l$.

One proceeds similarly in order to obtain the projected particle current density operator. In the absence of a vector potential it is

$$\vec{j}(\vec{r}) = \frac{i\hbar}{2m}\left\{[\vec{\nabla}\Psi^\dagger(\vec{r})]\Psi(\vec{r}) - \Psi^\dagger(\vec{r})[\vec{\nabla}\Psi(\vec{r})]\right\}. \tag{21}$$

Inserting also here the expression given in eq. (16) yields with $\alpha = x, y, z$,

$$j^\alpha(\vec{r}) = \sum_{n,l} B_{nl}^\alpha(\vec{R})\, j_{nl}^\alpha(x), \tag{22}$$

where the functions $B^{\alpha}_{nl}(\vec{R})$ contain the properties of the confinement potential,

$$B^{x}_{nl}(\vec{R}) = \Phi^{*}_{n}(\vec{R})\Phi_{l}(\vec{R}), \tag{23}$$

$$B^{\beta}_{nl}(\vec{R}) = d_{\beta}\left\{[\partial_{\beta}\Phi^{*}_{n}(\vec{R})]\Phi_{l}(\vec{R}) - \Phi^{*}_{n}(\vec{R})[\partial_{\beta}\Phi_{l}(\vec{R})]\right\}, \tag{24}$$

with $\beta = y, z$. The components of the 1D current operators are

$$j^{x}_{nl}(x) = \frac{\mathrm{i}\hbar}{2m}\left\{[\partial_{x}\Psi^{\dagger}_{n}(x)]\Psi_{l}(x) - \Psi^{\dagger}_{n}(x)[\partial_{x}\Psi_{l}(x)]\right\}, \tag{25}$$

$$j^{\beta}_{nl}(x) = \frac{\mathrm{i}\hbar}{2m\,d_{\beta}}\rho_{nl}(x). \tag{26}$$

The quantity d_{β} is the diameter of the wire along the direction β for $\beta = y, z$. It depends on the explicit choice of the confinement potential. Is is added here for dimensionality reasons only and drops out in the product $B^{\beta}_{nl}(\vec{R})\, j^{\beta}_{nl}(x)$.

In the presence of a vector potential, $\vec{A}(\vec{r}, t)$, the 3D current operator acquires an additional term proportional to the vector potential and to the particle density operator [140],

$$\vec{j}_{A}(\vec{r}, t) = -\frac{e^{2}}{m}\,\vec{A}(\vec{r}, t)\,\rho(\vec{r}, t). \tag{27}$$

Inserting the expression for the particle density operator given in eq. (19) and using the definition of $B^{x}_{nl}(\vec{R})$ given in eq. (23) yields

$$j^{\alpha}_{A}(\vec{r}, t) = -\frac{e^{2}}{m}\,A^{\alpha}(\vec{r}, t)\sum_{n,l} B^{x}_{nl}(\vec{R})\rho_{nl}(x, t). \tag{28}$$

Projection of the Continuity Equation

Usually, particle and current density operators are related via the 3D continuity equation,

$$\dot{\rho}(\vec{r}, t) + \vec{\nabla}\cdot\vec{j}(\vec{r}, t) = 0. \tag{29}$$

Inserting the expressions derived above for the particle density and the particle current density operators yields

$$\sum_{n,l}\Phi^{*}_{n}(\vec{R})\Phi_{l}(\vec{R})\left\{\dot{\rho}_{nl}(x, t) + \partial_{x}j^{x}_{nl}(x, t) - \mathrm{i}\Delta_{nl}\rho_{nl}(x, t)\right\} = 0. \tag{30}$$

Here, $\Delta_{nl} = (E_{n} - E_{l})/\hbar$, where E_{n} is the eigenenergy of the confinement Hamiltonian in the nth subband. Note that subbands with different indices are coupled, i.e. one does not obtain a continuity equation for each subband separately but a continuity equation mixing the subbands and thus taking into account inter-band transitions. However, one can get rid of the mixed terms with $n \neq l$ by integrating eq. (30) with respect to $\vec{R}$ exploiting the orthogonality of the confinement eigenfunctions,

$$\sum_{n}[\dot{\rho}_{nn}(x, t) + \partial_{x}j^{x}_{nn}(x, t)] = 0. \tag{31}$$

Also here the different subbands are coupled as eq. (31) has to be fulfilled as a whole and not just for each n separately. The expression in eq. (31) governs the conservation of the *total* current.

Projection of the Many-Body Hamiltonian

Now, turn back to the many-body Hamiltonian of eq. (12). Making use of the expressions derived for the fermionic field operator in eq. (16), the particle density operator in eq. (19), and the particle current density operator in eq. (22), one obtains for the Hamiltonian governing the kinetic energy

$$H_{\rm kin}^{\rm MB} = \sum_n \int {\rm d}x\, \Psi_n^\dagger(x) \left(\frac{-\hbar^2}{2m} \partial_x^2 \right) \Psi_n(x). \tag{32}$$

It is given by the kinetic energy of each subband summed over all subbands. The many-body Hamiltonian describing the coupling to the electromagnetic field is

$$\begin{aligned} H_{\rm em}^{\rm MB} &= -e \sum_\alpha \sum_{n,l} \int {\rm d}x\, j_{nl}^\alpha(x) \int {\rm d}\vec{R}\, B_{nl}^\alpha(\vec{R})\, A^\alpha(x,\vec{R},t) \\ &+ e \sum_{n,l} \int {\rm d}x\, \rho_{nl}(x) \int {\rm d}\vec{R}\, B_{nl}^x(\vec{R})\, \varphi_{\rm ext}(x,\vec{R},t) \\ &+ \frac{e^2}{2m} \sum_{n,l} \int {\rm d}x\, \rho_{nl}(x) \int {\rm d}\vec{R}\, B_{nl}^x(\vec{R})\, \vec{A}^{\,2}(x,\vec{R},t). \end{aligned} \tag{33}$$

For $n = l$, the right hand side of eq. (33) contains the typical expressions describing the coupling between charges and electromagnetic fields for each band separately. The first term contains the coupling between current density and vector potential for each subband, the second term gives the coupling between charge density and electric potential for each subband, and the third term gives the coupling between charge density and the square of the vector potential for each subband. Then the sum over all subbands is performed. For $n \neq l$, however, the expression in eq. (33) also takes inter-band transitions into account.

The many-body confinement Hamiltonian is given by the particle number in each subband, N_{n_β}, multiplied by the eigenenergy for that subband, E_{n_β}, summed over all subbands,

$$H_{\rm conf}^{\rm MB} = \sum_{n_y} N_{n_y} E_{n_y} + \sum_{n_z} N_{n_z} E_{n_z}. \tag{34}$$

The barrier potential leads for a general shape of the barrier to

$$H_{\rm bar}^{\rm MB} = \sum_{n,l} \int {\rm d}\vec{r}\, B_{nl}^x(\vec{R}) \Psi_n^\dagger(x) U_{\rm bar}(x,\vec{R}) \Psi_l(x). \tag{35}$$

The Hamiltonian taking care of the interaction potential becomes

$$H_{\rm int}^{\rm MB} = \sum_{n,l,s,p} \int {\rm d}x \int {\rm d}x'\, \rho_{nl}(x)\, V_{nlsp}(x-x')\, \rho_{sp}(x') \tag{36}$$

where $V_{nlsp}(x-x')$ is the projected interaction potential

$$V_{nlsp}(x-x') = \int {\rm d}\vec{R} \int {\rm d}\vec{R}'\, B_{nl}^x(\vec{R}) V_{\rm ee}(\vec{r}-\vec{r}\,') B_{sp}^x(\vec{R}'), \tag{37}$$

with the Fourier transform

$$V_{nlsp}(q_x) = \frac{1}{(2\pi)^2} \int \mathrm{d}\vec{Q}\, B_{nl}^{(x)}(-\vec{Q}) V_{\mathrm{ee}}(\vec{q}) B_{sp}^{(x)}(\vec{Q}). \tag{38}$$

Here, $V_{\mathrm{ee}}(\vec{q})$ denotes the Fourier transform of $V_{\mathrm{ee}}(\vec{r} - \vec{r}\,')$.

On first glance one might think that a *single-channel* wire can be described by simply assuming that only the lowest band with $n = l = (0,0)$ is occupied and setting all indices equal to zero in the above expressions for the many-body Hamiltonian. However, one has to keep in mind that following this procedure one neglects transitions to empty bands. It is hence only meaningful when only intra-band excitations are considered.

Harmonic Confinement

The expressions derived so far for the fermionic field operator, the particle and current density operators, the continuity equation and the many-body Hamiltonian are valid for any kind of confinement potential. What would be a realistic choice? The results of experiments probing the quantization of energy bands in quantum wires indicate that the confinement is roughly parabolic; for corresponding experiments on lateral superlattices of quantum wires see e.g. [267, 268, 269] and on single quantum wires [270, 271, 272]. Thus, a harmonic confinement potential is assumed,

$$U_{\mathrm{conf}}(\vec{R}) = \frac{m}{2} \sum_{\beta \neq x} \Omega_\beta^2 \beta^2, \tag{39}$$

where Ω_β is the curvature of the confinement potential along the direction β. The corresponding many-body Hamiltonian is obtained from eq. (34) by inserting $E_{n_\beta} = \hbar\Omega_\beta(n_\beta + 1/2)$ for $n = 0, 1, 2, \ldots$. The eigenfunctions $\Phi_n(\vec{R})$ are real for a harmonic confinement with $\Phi_n(\vec{R}) = \phi_{n_y}(y)\phi_{n_z}(z)$ where $\phi_{n_\beta}(\beta)$ is the eigenfunction of the 1D harmonic oscillator potential along the direction β. The 1D eigenfunction of the lowest subband, which is the only one needed throughout this thesis, is

$$\phi_0(\beta) = \left(\frac{4}{\pi d_\beta^2}\right)^{1/4} \mathrm{e}^{-2\beta^2/d_\beta^2}. \tag{40}$$

The diameter d_β of the wire is

$$d_\beta = 2\sqrt{\frac{\hbar}{m\Omega_\beta}}. \tag{41}$$

It corresponds to the full width of $\mathrm{e}^{-4\beta^2/d_\beta^2}$ at height $1/e$.

In a semiconductor quantum wire the confinement for a motion of the electrons perpendicular to the 2DEG is usually stronger than the confinement for motion in the plane of the 2DEG but perpendicular to the wire. A real quantum wire hence has an asymmetric cross section, or in other words, it is not rotationally symmetric. However, a symmetric confinement with $\Omega_y = \Omega_z$ is much easier to

handle mathematically than an asymmetric confinement with $\Omega_y \neq \Omega_z$. Hence, a symmetric confinement is assumed in the following.

As the functions $B^x_{00}(\vec{R})$ and the corresponding Fourier transform are used often throughout the course of this thesis, they are explicitly given here. Inserting the eigenfunction in eq. (40) into eq. (23) yields for $d_y = d_z \equiv d$,

$$B^x_{00}(\vec{R}) = \left(\frac{4}{\pi d^2}\right) \mathrm{e}^{-4R^2/d^2}. \tag{42}$$

The Fourier transform is

$$B^x_{00}(\vec{Q}) = \mathrm{e}^{-d^2|\vec{Q}|^2/16}. \tag{43}$$

From eq. (19) it can be seen that $B^x_{00}(\vec{R})$ gives the profile of the electron density for a single-channel quantum wire.

Finally, for the derivation of the transport equation of the clean quantum wire in section 4.1 certain sum rules are needed. They are given here for completeness. Using the orthogonality and the completeness of the confinement eigenfunctions one may derive with $\alpha \neq x$

$$\sum_b B^x_{ab}(\vec{Q}) B^x_{bc}(-\vec{Q}\,') = B^x_{ac}(\vec{Q} - \vec{Q}\,'), \tag{44}$$

$$\sum_b B^x_{ab}(\vec{Q}) B^\alpha_{bc}(-\vec{Q}\,') = B^\alpha_{ac}(\vec{Q} - \vec{Q}\,') + \mathrm{i} q_\alpha d_\alpha B^x_{ac}(\vec{Q} - \vec{Q}\,'), \tag{45}$$

where $B^x_{ab} = B^x_{ba}$ and $B^y_{ab} = -B^y_{ba}$.

3.2 Electron-Electron Interactions

In this section, it is shown how the electron-electron interaction in the quantum wire can be handled, i.e. it is mainly concerned with a certain part of the many-body Hamiltonian given in the previous section, namely

$$\begin{aligned} H^{\mathrm{MB}}_{\mathrm{kin}} + H^{\mathrm{MB}}_{\mathrm{int}} &= \sum_n \int \mathrm{d}x\, \Psi^\dagger_n(x) \left(\frac{-\hbar^2}{2m}\partial_x^2\right) \Psi_n(x) \\ &+ \sum_{n,l,s,p} \int \mathrm{d}x \int \mathrm{d}x'\, \rho_{nl}(x)\, V_{nlsp}(x - x')\, \rho_{sp}(x'). \end{aligned} \tag{46}$$

Is is assumed that only the lowest subband is occupied. Hence, in the kinetic part of the Hamiltonian all terms with $n \neq 0$ vanish where n consists of two numbers, $n = (n_y, n_z)$, and $n = 0$ is to be understood as $n = (0,0)$. In the part describing the interaction only those terms with $p \neq 0$ and $l \neq 0$ vanish, implying that the interaction allows for transitions to empty bands,

$$\begin{aligned} H^{\mathrm{MB}}_{\mathrm{kin,1b}} + H^{\mathrm{MB}}_{\mathrm{int,1b}} &= \int \mathrm{d}x\, \Psi^\dagger_0(x) \left(\frac{-\hbar^2}{2m}\partial_x^2\right) \Psi_0(x) \\ &+ \sum_{n,s} \int \mathrm{d}x \int \mathrm{d}x'\, \rho_{n0}(x)\, V_{n0s0}(x - x') \rho_{s0}(x'). \end{aligned} \tag{47}$$

The Luttinger model, employed in the following in order to take care of the electron-electron interaction, does not allow to consider transitions to empty bands. As the model describes the low-energy excitations of a system and inter-band transitions are improbable for excitation energies much smaller than the subband separation, inter-band transitions are neglected,

$$\begin{aligned} H^{\mathrm{MB}}_{\mathrm{kin,1b}} + H^{\mathrm{MB}}_{\mathrm{int,1b}} &\approx \int \mathrm{d}x\, \Psi_0^\dagger(x) \left(\frac{-\hbar^2}{2m} \partial_x^2 \right) \Psi_0(x) \\ &+ \int \mathrm{d}x \int \mathrm{d}x'\, \rho_{00}(x)\, V_{\mathrm{1b}}(x-x')\, \rho_{00}(x'), \end{aligned} \tag{48}$$

where the projected interaction potential of the lowest subband is $V_{\mathrm{1b}}(x) := V_{0000}(x)$.

In the following, the main ingredients of the Luttinger model are introduced. The model allows for an exact treatment of $H^{\mathrm{MB}}_{\mathrm{kin,1b}} + H^{\mathrm{MB}}_{\mathrm{int,1b}}$ when inter-band transitions are neglected. This means it provides a solution of the many-body problem! This introduction is kept short as several excellent reviews on this model can be found in the literature [6, 61, 62, 63]; see also [273, 274] for the rigorous mathematical background of the model.

The main ideas of the Luttinger model were published by Luttinger in 1963 [275]. However, this publication contains an error and the "correct" Luttinger model may be found in [276] presented by Mattis and Lieb in 1965. But even before, namely in 1950, a similar model had been proposed by Tomonaga [140, 277] and for this reason the model is sometimes also referred to as Tomonaga-Luttinger model. The research on 1D conductors of interacting electrons had been stimulated by experiments on quasi-1D organic conductors; for reviews on the Luttinger model in that field see [278, 279]. Fermi liquid theory could not be used to describe those organic conductors as it breaks down in 1D systems, see e.g. [6]. Loosely speaking, the definition of Fermi quasi particles is not possible in 1D systems.

Diagonalization of the Hamiltonian

The Luttinger model can be solved exactly based on a few assumptions. First, the dispersion relation of the non-interacting fermions is linearized at the Fermi energy. One obtains two linear branches which cross at zero wave number. This linearization is physically reasonable as long as only low-energy excitations are probed such that the deviation of the "real" dispersion relation from the linearized dispersion relation is small in the energy range probed. It is clear that the Luttinger model can hence not take account of inter-band transitions to empty bands as the dispersion relation of an empty band cannot be linearized at the Fermi energy when the Fermi energy lies below the bottom of this band [152, 280]. Second, the two branches of the linearized dispersion relation are extended beyond their point of intersection and the infinitely many "anti-particle" states lying energetically below this point of intersection are assumed to be occupied. This assumption has purely mathematical reasons. The "anti-particle" states do not play any physical role since only low-energy excitations are considered. Third, backward scattering is excluded from the model as otherwise it would not be exactly solvable. For spinless particles, the backward

scattering process is implicitly included as spinless particles are indistinguishable. As a consequence the forward scattering process cannot be distinguished from the backward scattering process, only the momentum transfer for the two processes is different. For particles with spin it is under certain conditions reasonable to neglect backward scattering. The corresponding argumentation based on renormalization group calculations can be found in [6].

Following these three assumptions, the Hamiltonian $H^{\mathrm{MB}}_{\mathrm{kin,1b}} + H^{\mathrm{MB}}_{\mathrm{int,1b}}$ as given in eq. (48) can be diagonalized [6, 274]. The diagonalization is based on a so-called bosonization approach: the 1D density operators obey exact bosonic commutation relations due to the presence of the "anti-particle" states assumed above. As a consequence, the Hamiltonian can be expressed by a bilinear form of bosonic operators which can then be diagonalized. The ground state is assigned zero energy and the elementary excitations are described by

$$H^{\mathrm{LL}}_{\mathrm{kin,1b}} + H^{\mathrm{LL}}_{\mathrm{int,1b}} = \sum_{q_x \neq 0} \hbar\omega_{\mathrm{LL}}(q_x) b^\dagger_{q_x} b_{q_x} + \frac{\hbar\pi}{2L}\left[\frac{v_{\mathrm{F}}}{g^2}N^2 + v_{\mathrm{F}}J^2\right]. \tag{49}$$

The bosonic operators $b^\dagger_{q_x}$ and b_{q_x} create and annihilate collective charge excitations with wave numbers q_x. The dispersion relation is

$$\omega_{\mathrm{LL}}(q_x) = |q_x| v_{\mathrm{F}} \sqrt{1 + \frac{V_{\mathrm{1b}}(q_x)}{\pi\hbar v_{\mathrm{F}}}}. \tag{50}$$

It contains the Fourier transform of the projected interaction potential $V_{\mathrm{1b}}(q_x)$. The bosonic operators $b^\dagger_{q_x}$ and b_{q_x} cannot handle excitations due to a changing particle number and the operators N and J describe excitations caused by an increase or decrease of the total particle number. They are present here for completeness but play no role throughout this thesis. The parameter g describes the kind and the strength of the interaction and is defined as

$$g = \sqrt{1 + \frac{V_{\mathrm{1b}}(q_x = 0)}{\pi\hbar v_{\mathrm{F}}}}^{-1}. \tag{51}$$

For non-interacting particles, $g = 1$. For repulsive interactions, $g < 1$ with $g = 0$ for an infinitely large $V_{\mathrm{1b}}(q_x = 0)$, and $g > 1$ for attractive interactions.

Interaction Potentials

Studying linear transport and local fields in a clean wire in section 4, an infinite-range Coulomb potential is considered,

$$V^{\mathrm{C}}_{\mathrm{ee}}(\vec{r} - \vec{r}\,') = \frac{1}{4\pi\epsilon_0}\frac{e^2}{|\vec{r} - \vec{r}\,'|}. \tag{52}$$

For a symmetric harmonic confinement, the Fourier transform of the projected potential is

$$V^{\mathrm{C}}_{\mathrm{1b}}(q_x) = \frac{e^2}{4\pi\epsilon_0}\, \mathrm{e}^{d^2 q_x^2/8}\, \mathrm{E}_1(d^2 q_x^2/8), \tag{53}$$

where $E_1(z)$ is an exponential integral [281]. This expression determines the behaviour of the dispersion relation of the collective excitations ω_{LL} with the wave number q_x: the dispersion relation is infinitely steep at $q_x = 0$ and converges to $v_{\mathrm{F}}|q_x|$ for large q_x, see figure 1.

During the investigation of non-linear transport in a quantum wire containing a scattering barrier in section 5, a screened Coulomb interaction and a zero-range interaction are considered for simplicity. For an exponentially screened Coulomb potential,

$$V_{\mathrm{ee}}^{\mathrm{scr}}(\vec{r}-\vec{r}\,') = \frac{1}{4\pi\epsilon_0}\,\frac{e^2}{|\vec{r}-\vec{r}\,'|}\,\mathrm{e}^{-\alpha|\vec{r}-\vec{r}\,'|}, \tag{54}$$

with an inverse screening length α, one obtains for a symmetric confinement in the Luttinger limit [169, 170, 282], i.e. for $\alpha d \gg 1$,

$$V_{\mathrm{1b}}^{\mathrm{scr,L}}(q_x) = \frac{e^2}{4\pi\epsilon_0}\,\frac{4}{d^2}\,\frac{1}{q_x^2+\alpha^2}. \tag{55}$$

In the Coulomb limit, i.e. for $\alpha d \ll 1$, one gets [169, 170]

$$V_{\mathrm{1b}}^{\mathrm{scr,C}}(q_x) = \frac{e^2}{4\pi\epsilon_0}\,2\,K_0\left(d\sqrt{q_x^2+\alpha^2}\right), \tag{56}$$

where $K_0(z)$ is a Bessel function [281]. For a screened Coulomb potential, the dispersion relation rises linearly at small q_x with a slope larger than $v_{\mathrm{F}}|q_x|$ and crosses over to $v_{\mathrm{F}}|q_x|$ at large q_x [63, 169].

For a zero-range interaction potential,

$$V_{\mathrm{ee}}^{\mathrm{ZR}}(\vec{r}-\vec{r}\,') = V_0\,\delta(\vec{r}-\vec{r}\,'), \tag{57}$$

the projected interaction potential is independent of q_x,

$$V_{\mathrm{1b}}^{\mathrm{ZR}} = \frac{2V_0}{\pi d^2}. \tag{58}$$

The dispersion relation of the collective excitations is then linear but with a slope larger than $v_{\mathrm{F}}|q_x|$, see figure 1.

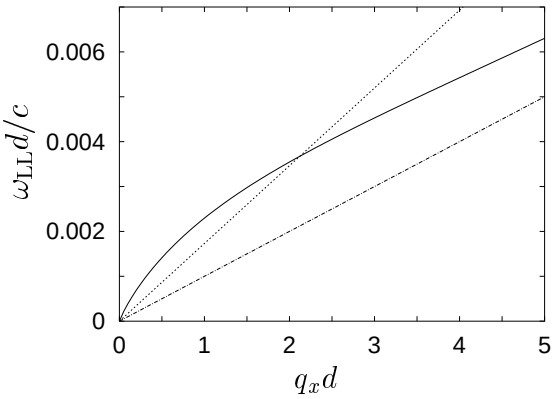

Figure 1: Dispersion relation of the collective excitations of the Luttinger liquid as a function of q_xd in the absence of interactions (dash-dotted), for a Coulomb interaction (solid), and a zero-range interaction with $g = 1/\sqrt{3} \approx 0.58$ (dashed).

Field Operators in Bosonic Form

The success of the Luttinger liquid theory is not only based on the fact that the Hamiltonian of the interacting system can be diagonalized exactly. One can further express the 1D fermionic field operator $\Psi_0(x)$ in terms of bosonic operators. In the Luttinger model, however, one does not use $\Psi_0(x)$ but a fermionic field operator that distinguishes between right and left-moving fermions,

$$\Psi_\pm(x) = \lim_{\lambda\to 0} \frac{1}{\sqrt{2\pi\lambda}} U_\pm \, \mathrm{e}^{\pm \mathrm{i}k_\mathrm{F}x \pm \mathrm{i}\sqrt{\pi}\vartheta(x) - \mathrm{i}\sqrt{\pi}\int^x \Pi(x')\mathrm{d}x'}. \tag{59}$$

Here, $\Psi_\pm(x)$ annihilates an electron at position x which moves to the right (upper sign) or to the left (lower sign). The bosonic fields $\vartheta(x)$ and $\Pi(x)$ are canonical conjugate fields [176],

$$\vartheta(x) = \frac{\mathrm{i}}{\sqrt{2L}} \sum_{q_x\neq 0} \frac{\mathrm{sgn}(q_x)}{\sqrt{|q_x|}} \mathrm{e}^{\varphi(q_x) - \mathrm{i}q_x x - \lambda|q_x|/2} \left[b^\dagger_{q_x} + b_{-q_x} \right] + \frac{\sqrt{\pi}}{L} xN, \tag{60}$$

$$\Pi(x) = -\frac{1}{\sqrt{2L}} \sum_{q_x\neq 0} \mathrm{sgn}(q_x) \sqrt{|q_x|} \mathrm{e}^{-\varphi(q_x) - \mathrm{i}q_x x - \lambda|q_x|/2} \left[b^\dagger_{q_x} - b_{-q_x} \right] - \frac{\sqrt{\pi}}{L} J, \tag{61}$$

with

$$[\vartheta(x), \Pi(x')] = \mathrm{i}\delta(x - x'). \tag{62}$$

The function $\varphi(q_x)$ is related to the dispersion relation ω_LL via

$$\mathrm{e}^{2\varphi(q_x)} = \frac{v_\mathrm{F}|q_x|}{\omega_\mathrm{LL}(q_x)}. \tag{63}$$

The operator $U_\pm$ annihilates a particle moving to the right or to the left. The presence of this operator is necessary as the bosonic operators $\vartheta(x)$ and $\Pi(x)$ cannot increase or decrease the particle number, see [274]. The fermionic field operator given in terms of $\vartheta(x)$ and $\Pi(x)$ allows for the evaluation of correlation functions. The explicit relation between $\Psi_0(x)$ and $\Psi_\pm(x)$ is quite complicated. Roughly $\Psi_0(x) \approx \Psi_+(x) + \Psi_-(x)$ holds, for details see [274].

In the special situation of a zero-range interaction potential, the diagonal Hamiltonian can be expressed in terms of the bosonic field operators $\vartheta(x)$ and $\Pi(x)$

$$H^\mathrm{LL}_\mathrm{kin,1b} + H^\mathrm{LL}_\mathrm{int,1b} = \frac{\hbar v_\mathrm{F}}{2} \int_{-L/2}^{L/2} \mathrm{d}x \left[\Pi^2(x) + \frac{1}{g^2} (\partial_x \vartheta(x))^2 \right]. \tag{64}$$

The interaction parameter g is given in eq. (51) and the dispersion relation of the collective excitations is here $\omega_\mathrm{LL}(q_x) = v_\mathrm{F}|q_x|/g$.

The 1D particle density operator and the 1D particle current density operator can be expressed in terms of the bosonic field $\vartheta(x)$. It is

$$\rho_{00}(x,t) = \frac{N_0}{L} + \frac{\partial_x \vartheta(x,t)}{\sqrt{\pi}}, \tag{65}$$

where N_0 is the particle number in the lowest subband with $n = (0,0)$. The projected continuity equation, eq. (31), yields for $n = 0$ the particle current density operator

$$j^x_{00}(x,t) = -\frac{\partial_t \vartheta(x,t)}{\sqrt{\pi}}. \tag{66}$$

Operators as $\rho_{n0}(x)$ or $j^x_{n0}(x)$ for $n \neq 0$, however, cannot be handled in the Luttinger model as transitions to empty bands cannot be handled.

3.3 Local Fields

Historically, local fields were often evaluated following a *heuristic approach*: A fictitious cavity was assumed around an atom in a sample, the cavity was chosen to be much larger than the interatomic distance but much smaller than the sample. Then, the medium outside the cavity was considered a continuum giving rise to a macroscopic field due to the presence of charges in this continuum. Further, the field induced by the other atoms inside the cavity was taken into account on a microscopic level. Finally, the field due to a polarization charge on the surface of the fictitious cavity was considered. All three fields taken together gave the local field at the position of the atom in the centre of the cavity. The reason for following such a heuristic approach lay more in the complex nature of the local field problem than in the quality of the approach, see e.g. the discussion in [2].

In order to proceed *rigorously* in the evaluation of local fields, one chooses a path completely different from the heuristic approach: One first derives an expression for the local field as a function of the current based on Maxwell equations, and second an expression for the current as a function of the local field. In a third and final step one combines the two expressions and the ensuing equation gives the local field in a self-consistent manner. During the course of this section, it is shown how to follow this path allowing for a rigorous evaluation of local fields. Further, the connection between local fields and the dielectric function is established. Finally, a simple example of local fields in a homogeneous 3D sample is discussed.

The Field in Terms of the Current

The starting point for the derivation of an expression giving the local field in terms of the current are Maxwell equations. In the frequency domain,

$$\begin{aligned}
\vec{\nabla} \cdot \vec{E}(\vec{r},\omega) &= \frac{1}{\epsilon_0}\rho_{\mathrm{tot}}(\vec{r},\omega), && (67)\\
\vec{\nabla} \cdot \vec{B}(\vec{r},\omega) &= 0, && (68)\\
\vec{\nabla} \times \vec{E}(\vec{r},\omega) &= \mathrm{i}\omega \vec{B}(\vec{r},\omega), && (69)\\
\vec{\nabla} \times \vec{B}(\vec{r},\omega) &= \mu_0 \vec{J}_{\mathrm{tot}}(\vec{r},\omega) - \mathrm{i}\epsilon_0\mu_0\omega\, \vec{E}(\vec{r},\omega), && (70)
\end{aligned}$$

where c is the velocity of light in vacuum, $\rho_{\mathrm{tot}}(\vec{r},\omega)$ and $\vec{J}_{\mathrm{tot}}(\vec{r},\omega)$ are microscopic charge and current densities, and $\vec{E}(\vec{r},\omega)$ and $\vec{B}(\vec{r},\omega)$ are the microscopic electric and magnetic field vectors. The charge and current densities include internal and

external charges. The term *external charges* refers to charges whose position is not inside the sample under study, in contrast to *internal charges*. The densities of internal charges and currents are denoted by ρ and $\vec{J}$, respectively. The fields include induced and external fields. The term *external field* refers to the field which is present in the absence of the sample under study, i.e. the field provided by the measurement apparatus used for the investigation of the sample. The *induced field* is the field due to the presence of the internal charges. The *local field* is the sum of external and induced field, it is always denoted by $\vec{E}$.

In the previous paragraph, $\vec{E}(\vec{r},\omega)$ and $\vec{B}(\vec{r},\omega)$ were called *microscopic* field vectors. What does *microscopic* mean in this context? The field containing the induced fields due to the fluctuations of all charged particles in the medium is a rapidly varying function of space and time and would be impossible to determine. In order to avoid this overkill of information one often replaces all local values by values averaged over a volume large compared to the interatomic distance but small compared to the sample size. However, neglecting from the outset the microscopic structure around each particle does not allow to relate the local field to this microscopic structure and is hence automatically a phenomenological approach. A procedure that averages out all fluctuations but retains the microscopic information is the averaging over an ensemble of samples. Therefore, $\vec{E}(\vec{r},\omega)$ and $\vec{B}(\vec{r},\omega)$ are to be understood as *microscopic* field vectors in the sense that they are ensemble-averaged but still contain all microscopically relevant informations. The same is true for the charge and current densities $\rho_{\rm tot}(\vec{r},\omega)$ and $\vec{J}_{\rm tot}(\vec{r},\omega)$; for details see [1].

It is straightforward to show that Maxwell equations together with a transport equation for the specific sample are sufficient in order to determine the local fields in this sample. Perform the "rotation" of eq. (69) and insert it into eq. (70),

$$\vec{\nabla}\times[\vec{\nabla}\times\vec{E}(\vec{r},\omega)] = \mathrm{i}\mu_0\omega\vec{J}_{\rm tot}(\vec{r},\omega) + \epsilon_0\mu_0\omega^2\,\vec{E}(\vec{r},\omega). \tag{71}$$

This equation relates the local electric field to the total current density, the magnetic field vector is not present. The absence of the magnetic field vector is quite comfortable, one can concentrate on the electric field and the current density and then at the end deduce the magnetic field from the electric field. Assume that an expression for the current as a function of the electric field is given, $\vec{J}_{\rm tot}(\vec{r},\omega) = F[\vec{E}(\vec{r},\omega)]$, where F is a function depending on the external source, the sample, and the microscopic model used. One then obtains

$$\vec{\nabla}\times[\vec{\nabla}\times\vec{E}(\vec{r},\omega)] = \mathrm{i}\mu_0\omega F[\vec{E}(\vec{r},\omega)] + \epsilon_0\mu_0\omega^2\,\vec{E}(\vec{r},\omega), \tag{72}$$

which is a closed expression that allows for the self-consistent evaluation of the local field.

Next, the vector fields in eq. (71) are divided into their longitudinal and transverse parts. The longitudinal part of the local electric field is defined via

$$\vec{\nabla}\times\vec{E}_{\rm L}(\vec{r},\omega) = 0, \tag{73}$$

while the transverse part is defined as

$$\vec{\nabla}\cdot\vec{E}_{\rm T}(\vec{r},\omega) = 0, \tag{74}$$

for all $\vec{r}$. Since $\vec{E} = \vec{E}_{\rm L} + \vec{E}_{\rm T}$, this splitting is unique. Fourier transformation yields

$$\vec{q} \times \vec{E}_{\rm L}(\vec{q},\omega) = 0, \tag{75}$$
$$\vec{q} \cdot \vec{E}_{\rm T}(\vec{q},\omega) = 0, \tag{76}$$

for all $\vec{q}$. When the total vector field $\vec{E}(\vec{q},\omega)$ is known, transverse and longitudinal parts can be obtained via

$$\vec{E}_{\rm L}(\vec{q},\omega) = \frac{\vec{q}\,[\vec{q}\cdot\vec{E}(\vec{q},\omega)]}{q^2} = \boldsymbol{L}(\vec{q})\cdot\vec{E}(\vec{q},\omega), \tag{77}$$
$$\vec{E}_{\rm T}(\vec{q},\omega) = \vec{E}(\vec{q},\omega) - \vec{E}_{\rm L}(\vec{q},\omega) = \boldsymbol{T}(\vec{q})\cdot\vec{E}(\vec{q},\omega), \tag{78}$$

where $\boldsymbol{L}(\vec{q})$ and $\boldsymbol{T}(\vec{q})$ are 3×3 matrices with the elements

$$L^{\alpha\beta}(\vec{q}) = \frac{q_\alpha q_\beta}{|\vec{q}|^2}, \tag{79}$$
$$T^{\alpha\beta}(\vec{q}) = \delta_{\alpha\beta} - \frac{q_\alpha q_\beta}{|\vec{q}|^2}, \tag{80}$$

for $\alpha,\beta = x,y,z$. The splitting of the field vectors into longitudinal and transverse parts is suggested by the structure of Maxwell equations. From eq. (67), for example, one can see that the *charge density* determines the *longitudinal* part of the electric field. The definitions given here for the longitudinal and transverse parts of the local electric field hold for any vector field, i.e. also for the current $\vec{J}_{\rm tot}(\vec{r},\omega)$.

Dividing local electric field and current density in eq. (71) into longitudinal and transverse parts yields [2]

$$-\epsilon_0\mu_0\omega^2\,\vec{E}_{\rm L}(\vec{r},\omega) = {\rm i}\mu_0\omega\vec{J}_{\rm L,tot}(\vec{r},\omega), \tag{81}$$
$$\vec{\nabla}\times[\vec{\nabla}\times\vec{E}_{\rm T}(\vec{r},\omega)] - \epsilon_0\mu_0\omega^2\,\vec{E}_{\rm T}(\vec{r},\omega) = {\rm i}\mu_0\omega\vec{J}_{\rm T,tot}(\vec{r},\omega). \tag{82}$$

The longitudinal part of the local electric field is already given in the desired form by eq. (81). The differential equation for the transverse part of the local electric field in eq. (82) is transformed into an integral equation via a Green's function approach. Making use of the microscopic Ewald-Oseen extinction theorem in order to relate the boundary terms of the integral equation to the external electric field one obtains, for details see [2],

$$\vec{E}_{\rm L}(\vec{q},\omega) = \vec{E}_{\rm L,ext}(\vec{q},\omega) + \frac{1}{{\rm i}\epsilon_0\omega}\vec{J}_{\rm L}(\vec{q},\omega), \tag{83}$$
$$\vec{E}_{\rm T}(\vec{q},\omega) = \vec{E}_{\rm T,ext}(\vec{q},\omega) + {\rm i}\mu_0\omega\, g_0(\vec{q},\omega)\vec{J}_{\rm T}(\vec{q},\omega), \tag{84}$$

where $\vec{E}_{\rm L,ext} + \vec{E}_{\rm T,ext}$ is the external electric field, $\vec{J}_{\rm L} + \vec{J}_{\rm T}$ is the internal current density, and $g_0(\vec{q},\omega)$ is the Fourier transform of the scalar Green's function

$$g_0(\vec{r},\omega) = \frac{{\rm e}^{{\rm i}\omega|\vec{r}\,|/c}}{4\pi|\vec{r}\,|}, \tag{85}$$

namely

$$g_0(\vec{q},\omega) = \lim_{\eta\to 0} \frac{1}{q^2 - \left(\frac{\omega}{c} + \mathrm{i}\eta\right)^2}. \tag{86}$$

The imaginary part $\mathrm{i}\eta$ was introduced during the Fourier transformation. It is often omitted in the following for brevity.

Note that, as the internal current density is zero outside of the sample, also the longitudinal and transverse parts of the current density have to be zero outside. This can be seen from the fact that for $|\vec{J}(\vec{r},\omega)| = 0$, the longitudinal and transverse parts of the current have to fulfil the condition $\vec{J}_{\mathrm{L}}(\vec{r},\omega) = -\vec{J}_{\mathrm{T}}(\vec{r},\omega)$. This means, following eqs. (73) and (74), that for any of the two parts of the current the divergence *and* the rotation have to be zero, implying $|\vec{J}_{\mathrm{L}}(\vec{r},\omega)| = 0$ and $|\vec{J}_{\mathrm{T}}(\vec{r},\omega)| = 0$.

The Current in Terms of the Field

Now, an expression for the internal current density as a function of the local field is needed. Consider for example linear response: The current density $\vec{J}(\vec{r},t)$ is related linearly but non-locally to the driving electric field via the conductivity tensor $\boldsymbol{\sigma}$ of the sample [140],

$$\vec{J}(\vec{r},t) = \int \mathrm{d}t' \int \mathrm{d}\vec{r}\,' \,\boldsymbol{\sigma}(\vec{r},\vec{r}\,',t,t') \cdot \vec{E}_?(\vec{r}\,',t'). \tag{87}$$

The question mark at the electric field indicates that it is not a priori clear if the field driving the current is the local or the external field. This point is discussed below. In a translationally invariant system exhibiting time-reversal symmetry, the conductivity tensor depends on $t - t'$ and $\vec{r} - \vec{r}\,'$. Fourier transforming to $\vec{q}$-space thus yields an algebraic relation between current and field,

$$\vec{J}(\vec{q},\omega) = \boldsymbol{\sigma}(\vec{q},\omega) \cdot \vec{E}(\vec{q},\omega). \tag{88}$$

A quantum wire is not translationally invariant along the y and z-direction, thus $\boldsymbol{\sigma}(\vec{r},\vec{r}\,',t,t') = \boldsymbol{\sigma}(x-x',\vec{R},\vec{R}\,',t-t')$. The relation between current and field remains an integral equation, the internal current density as a function of $\vec{q}$ and ω is

$$\vec{J}(\vec{q},\omega) = \int \mathrm{d}\vec{Q}\,' \,\boldsymbol{\sigma}(q_x,\vec{Q},\vec{Q}\,',\omega) \cdot \vec{E}_?(q_x,\vec{Q}\,',\omega). \tag{89}$$

Before this equation can be used in order to derive self-consistent local-field equations using eqs. (83) and (84) it has to be clarified which field has to be taken in order to evaluate the current in eq. (89).

The answer depends on the model used for the evaluation of the conductivity. On first glance one would suspect that – as the electrons naturally react to the local field – the field driving the current should be the local field, $\vec{E}_? = \vec{E}$. But this is only true when the microscopic model on which the conductivity $\boldsymbol{\sigma}$ is based neglects electron-electron interactions and the transverse fields emitted by time-dependent microscopic currents. The induced field responsible for the difference between the external and the local field is due to the presence of charges which always

"carry around" a longitudinal Coulomb field and to the presence of time-dependent currents which generate a transverse field. Assuming that the Coulomb potential and all atomic currents and emitted transverse fields were taken into account in the microscopic model and assuming that this model could be solved exactly, local fields would be inherent in the model [3]. Their effect would be hidden inside the conductivity and the choice $\vec{E}_? = \vec{E}$ would be equivalent to taking them into account twice, which would be wrong. Hence, if we had such a solvable "super" model, the current in eq. (89) would be driven by the external field, $\vec{E}_? = \vec{E}_{\rm ext}$.

On the other hand, if one takes into account neither the Coulomb field nor the microscopic currents, the field in eq. (89) indeed has to be the local field, $\vec{E}_? = \vec{E}$. One compensates for the shortcomings of the model by incorporating in a self-consistent way the induced fields. The approach is in general not identical to the incorporation of fields and currents into the microscopic model. First, is it a mean-field like approach, see section 2.3.1. Second, when linear response is considered, the exact microscopic model would be approximated linearly in the local fields and hence in the interaction potential.

In this thesis, as the quantum wire is described via the Luttinger model, the electron-electron interaction is taken into account microscopically while the transverse fields emitted by the time-dependent currents are neglected. Consequently, the field in eq. (89) is the external longitudinal field plus the local transverse field, $\vec{E}_? = \vec{E}_{\rm L,ext} + \vec{E}_{\rm T}$.

How to handle local fields in a system obeying a non-linear current-voltage characteristic is discussed in section 5.4.

Interaction vs. Local Longitudinal Field

Before performing the third step and closing the equations for the local field self-consistently, a few comments are in order if and when the two approaches based either on the electron-electron interaction or on the induced longitudinal field lead to equivalent results.

First, as already discussed in section 2.3.1, the consideration of the interaction potential and of the induced potential leads to different Hamiltonians. The Hamiltonians $H_{\rm int}^{\rm MB}$ and $H_{\rm ind}$, see section eqs. (1) and (4), differ as $H_{\rm int}^{\rm MB}$ contains the product of two density *operators* while $H_{\rm ind}$ contains the product of a density operator and the expectation value of a density operator. Whenever it is crucial that the Hamiltonian describing the interaction contains the product of two density *operators*, the mean-field like approach that considers the induced field instead of the microscopic Coulomb interaction fails, see section 5.4 for an example.

Second, consider linear transport and neglect for the moment the transverse field. Evaluating the conductivity based on a microscopic Hamiltonian for interacting particles leads to

$$\vec{J}(\vec{r},\omega) = \int {\rm d}\vec{r}\,' \, \boldsymbol{\sigma}_{\mathbf{ee}}(\vec{r},\vec{r}\,',\omega)\vec{E}_{\rm L,ext}(\vec{r}\,',\omega). \tag{90}$$

Neglecting the interactions and considering the induced longitudinal field in a self-

consistent manner yields

$$\vec{J}(\vec{r},\omega) = \int \mathrm{d}\vec{r}\,' \, \boldsymbol{\sigma}_{\mathbf{non-int}}(\vec{r},\vec{r}\,',\omega) \left[\vec{E}_{\mathrm{L,ext}}(\vec{r}\,',\omega) + \vec{E}_{\mathrm{L,ind}}(\vec{r}\,',\omega) \right]. \tag{91}$$

The conductivity of the non-interacting system, $\boldsymbol{\sigma}_{\mathbf{non-int}}$, in eq. (91) is strictly speaking not a response function as it relates the current to the external *and* the induced field. A response function by definition determines the response of a system to an *external* excitation [283]. True response functions satisfy the causality condition, and as a consequence their Fourier transforms are analytic in the upper half plane of the complex variable z, usually a complex frequency, and Kramers-Kronig relations are valid [283]. These statements are not valid for $\boldsymbol{\sigma}_{\mathbf{non-int}}$.

Next, the induced field can be represented as a function of the external field and this function can be absorbed into the conductivity, see e.g. [2] and section 4.4.1, turning eq. (91) into

$$\vec{J}(\vec{r},\omega) = \int \mathrm{d}\vec{r}\,' \, \boldsymbol{\sigma}_{\mathbf{MF}}(\vec{r},\vec{r}\,',\omega) \cdot \vec{E}_{\mathrm{L,ext}}(\vec{r}\,',\omega). \tag{92}$$

This expression is outwardly equivalent to the one in eq. (90). The conductivity seems to be the one of the interacting system. The index "MF" at the conductivity, however, is meant as a reminder that it is not evaluated based on a microscopic model of interacting electrons but by considering the induced potential which corresponds to a mean-field like approach. Now, is $\boldsymbol{\sigma}_{\mathbf{ee}}$ equivalent to $\boldsymbol{\sigma}_{\mathbf{MF}}$?

The conductivity evaluated via the Kubo formula [140] is based on a correlation function containing a commutator of two current operators, or alternatively two density operators, taken at different positions and times. An investigation of this commutator shows that, as long as its result is a number and not an operator, $H_{\mathrm{int}}^{\mathrm{MB}}$ and H_{ind} should lead to the same expressions for the conductivity tensors $\boldsymbol{\sigma}_{\mathbf{ee}}$ and $\boldsymbol{\sigma}_{\mathbf{MF}}$. This statement contains a "should" because there might still be a difference between $\boldsymbol{\sigma}_{\mathbf{ee}}$ and $\boldsymbol{\sigma}_{\mathbf{MF}}$ which is due to the linear-response approach. If the system is non-linear and hence the linear-response approach is an approximation in lowest order in the driving field, the conductivity $\boldsymbol{\sigma}_{\mathbf{MF}}$ contains the induced field – and hence the interaction – in linear order while the conductivity $\boldsymbol{\sigma}_{\mathbf{ee}}$ takes care of the interaction to any order. Thus, only if the system *is* linear, $\boldsymbol{\sigma}_{\mathbf{ee}}$ and $\boldsymbol{\sigma}_{\mathbf{MF}}$ are equivalent, see also section 4.4.1.

Third, consider the first non-linear correction to the above linear current, namely the second harmonic current

$$\vec{J}(\vec{r},2\omega) = \int \mathrm{d}\vec{r}\,' \int \mathrm{d}\vec{r}\,'' \, \boldsymbol{\Sigma}_{\mathbf{ee}}(\vec{r},\vec{r}\,',\vec{r}\,'';\omega,2\omega)\, \vec{E}_{\mathrm{L,ext}}(\vec{r}\,',\omega) \vec{E}_{\mathrm{L,ext}}(\vec{r}\,'',\omega), \tag{93}$$

which is related to the external field in second order and oscillates at frequency 2ω for a driving field that oscillates at ω. All possible effects of induced fields are contained in the non-linear conductivity $\boldsymbol{\Sigma}_{\mathbf{ee}}$ which is evaluated based on a microscopic Hamiltonian for interacting electrons.

Neglecting interactions, the second harmonic current is driven by the external plus the induced field,

$$\begin{aligned}\vec{J}^{(1)}(\vec{r},2\omega) &= \int \mathrm{d}\vec{r}' \int \mathrm{d}\vec{r}''\, \boldsymbol{\Sigma}_{\mathbf{non-int}}(\vec{r},\vec{r}',\vec{r}'';\omega,2\omega) \\ &\times \left[\vec{E}_{\mathrm{L,ext}}(\vec{r}',\omega)+\vec{E}_{\mathrm{L,ind}}(\vec{r}',\omega)\right]\left[\vec{E}_{\mathrm{L,ext}}(\vec{r}'',\omega)+\vec{E}_{\mathrm{L,ind}}(\vec{r}'',\omega)\right].\end{aligned} \tag{94}$$

Here, the induced field $\vec{E}_{\mathrm{L,ind}}(\vec{r},\omega)$ oscillates at frequency ω and has to be determined self-consistently from the linear current given in eq. (91) or (92). One has further to consider the induced field $\vec{E}^{(1)}_{\mathrm{L,ind}}(\vec{r},2\omega)$ oscillating at 2ω which has to be determined self-consistently from the second harmonic current $\vec{J}^{(1)}(\vec{r},2\omega)$. The induced field $\vec{E}^{(1)}_{\mathrm{L,ind}}(\vec{r},2\omega)$ drives a linear current $\vec{J}^{(2)}(\vec{r},2\omega)$ and further also the field induced by $\vec{J}^{(2)}(\vec{r},2\omega)$ has to be considered, leading to

$$\vec{J}^{(2)}(\vec{r},2\omega) = \int \mathrm{d}\vec{r}'\, \boldsymbol{\sigma}_{\mathbf{non-int}}(\vec{r},\vec{r}',2\omega)\left[\vec{E}^{(1)}_{\mathrm{L,ind}}(\vec{r}',2\omega)+\vec{E}^{(2)}_{\mathrm{L,ind}}(\vec{r}',2\omega)\right]. \tag{95}$$

In a way, $\vec{E}^{(1)}_{\mathrm{L,ind}}(\vec{r}',2\omega)$ may be interpreted as an external field for the linear current $\vec{J}^{(2)}(\vec{r},2\omega)$ and eq. (95) is like eq. (91) but at frequency 2ω.

Expressing the induced field $\vec{E}_{\mathrm{L,ind}}(\vec{r},\omega)$ as a function of the external field $\vec{E}_{\mathrm{L,ext}}(\vec{r},\omega)$ and the induced field $\vec{E}^{(2)}_{\mathrm{L,ind}}(\vec{r},2\omega)$ as a function of the induced field $\vec{E}^{(1)}_{\mathrm{L,ind}}(\vec{r},2\omega)$, absorbing these functions into the conductivities and adding $\vec{J}^{(1)}$ and $\vec{J}^{(2)}$ yields [2, 284]

$$\begin{aligned}\vec{J}(\vec{r},2\omega) &= \int \mathrm{d}\vec{r}' \int \mathrm{d}\vec{r}''\, \boldsymbol{\Sigma}_{\mathbf{MF}}(\vec{r},\vec{r}',\vec{r}'';\omega,2\omega)\, \vec{E}_{\mathrm{L,ext}}(\vec{r}',\omega)\vec{E}_{\mathrm{L,ext}}(\vec{r}'',\omega) \\ &+ \int \mathrm{d}\vec{r}'\, \boldsymbol{\sigma}_{\mathbf{MF}}(\vec{r},\vec{r}',2\omega)\, \vec{E}^{(1)}_{\mathrm{L,ind}}(\vec{r}',2\omega).\end{aligned} \tag{96}$$

This result is valid in the *parametric approach*, i.e. an approach in which the dynamics of the fundamental field evolves independently of the second-harmonic dynamics [2]. In the parametric approach it is assumed that the induced field at 2ω does not influence the current at ω via mixing. Comparing the expression in eq. (96) for the second harmonic current with the one in eq. (93) implies that the two approaches are conceptually different. While in eq. (93) "only" electron-electron interactions are considered, it seems that in eq. (96) both, interactions *and* induced fields are taken into account. But the non-linear conductivity $\boldsymbol{\Sigma}_{\mathbf{MF}}$ is not based on a microscopic theory of interacting electrons as is $\boldsymbol{\Sigma}_{\mathbf{ee}}$; $\boldsymbol{\Sigma}_{\mathbf{MF}}$ is obtained via a mean-field like approach and contains only the influence of the induced field at frequency ω while $\boldsymbol{\Sigma}_{\mathbf{ee}}$ contains the influence of the induced field at any frequency.

Self-Consistent Local-Field Equations

Now, the third and final step can be performed in order to determine the local fields in the quantum wire self-consistently. One closes eqs. (83) and (84) by dividing the current of eq. (89) into longitudinal and transverse parts, using the matrices $\boldsymbol{L}$ and

$\boldsymbol{T}$ given in eqs. (79) and (80), and inserting these parts into eqs. (83) and (84). The resulting integral equations are

$$\begin{aligned}\vec{E}_{\mathrm{L}}(\vec{q},\omega) &= \vec{E}_{\mathrm{L,ext}}(\vec{q},\omega) \qquad (97)\\ &+ \int \mathrm{d}\vec{Q}\,'\,\boldsymbol{K}_{\mathbf{L}}(q_x,\vec{Q},\vec{Q}\,',\omega)\cdot\left[\vec{E}_{\mathrm{L,ext}}(q_x,\vec{Q}\,',\omega)+\vec{E}_{\mathrm{T}}(q_x,\vec{Q}\,',\omega)\right],\\ \vec{E}_{\mathrm{T}}(\vec{q},\omega) &= \vec{E}_{\mathrm{T,ext}}(\vec{q},\omega) \qquad (98)\\ &+ \int \mathrm{d}\vec{Q}\,'\,\boldsymbol{K}_{\mathbf{T}}(q_x,\vec{Q},\vec{Q}\,',\omega)\cdot\left[\vec{E}_{\mathrm{L,ext}}(q_x,\vec{Q}\,',\omega)+\vec{E}_{\mathrm{T}}(q_x,\vec{Q}\,',\omega)\right],\end{aligned}$$

with the kernels

$$\begin{aligned}\boldsymbol{K}_{\mathbf{L}}(q_x,\vec{Q},\vec{Q}\,',\omega) &= \frac{1}{\mathrm{i}\epsilon_0\omega}\boldsymbol{L}(\vec{q})\cdot\boldsymbol{\sigma}(q_x,\vec{Q},\vec{Q}\,',\omega), \qquad (99)\\ \boldsymbol{K}_{\mathbf{T}}(q_x,\vec{Q},\vec{Q}\,',\omega) &= \mathrm{i}\mu_0\omega\, g_0(\vec{q},\omega)\,\boldsymbol{T}(\vec{q})\cdot\boldsymbol{\sigma}(q_x,\vec{Q},\vec{Q}\,',\omega). \qquad (100)\end{aligned}$$

These self-consistent local-field equations contain only the local and external fields – charge or current densities are no longer present – and the microscopic information on the medium which is hidden in the conductivity tensor. Solving these integral equations gives the local fields.

The integral equations determining the local fields appear somehow asymmetric. The local transverse field appears in the equation determining the local longitudinal field but the local longitudinal field does not appear in the equation determining the local transverse field. Hence, only the local transverse field needs to be determined *self-consistently*. The local longitudinal field is known the moment the local transverse field is known. The reason for this asymmetry is that the local longitudinal field is taken care of by the conductivity tensor evaluated for the interacting system. The local transverse field *does* depend on the local longitudinal field, namely via the conductivity of the interacting system which is hidden inside the kernels in eqs. (97) and (98). If the conductivity of the non-interacting system would be used for the evaluation of the current local longitudinal *and* local transverse fields would have to be determined self-consistently.

Local-Field Eigenmodes

The local-field integral equations are inhomogeneous Fredholm equations of the second kind [285, 286]. The two parts of the external field make up the inhomogeneities. Switching off the external field the integral equations turn into homogeneous Fredholm equations of the second kind for which non-trivial solutions can only be found under certain conditions [285, 286]. Here, this means that they are only solvable for certain combinations of wave vector $\vec{q}$ and frequency ω. Those non-trivial solutions are referred to as *eigenmodes*.

Fixing the wave vector $\vec{q}$, the frequency ω of the eigenmode is determined by the kernel of the integral equation. The kernel contains the conductivity which depends on the microscopic properties of the medium. Hence, the properties of the eigenmode depend on the microscopic properties of the system. The corresponding

relation between $\vec{q}$ and ω is the *dispersion relation* of the eigenmode. The latter corresponds to a local field inside the medium which can exist also in the absence of an external field. The eigenmode is the elementary excitation of the coupled system consisting of sample *and* electromagnetic field.

Already in section 2.3.3 an elementary excitation was discussed that consisted of an excitation of the medium coupled to electromagnetic fields – the phonon-polariton. Here, a quantum wire is studied and the typical elementary excitation of the electronic system as described by the Luttinger liquid is a collective charge excitation, namely a 1D plasmon. Following the discussion on the phonon coupled to an electromagnetic field we call the eigenmode of the integral equations in (97) and (98) *plasmon-polariton*.

Dielectric Function

Next, the relation between the local field and the dielectric function is established. As already mentioned, the dielectric function of a substance describes the modification of an electric field due to the presence of matter and hence determining the dielectric function for a given medium is closely related to the problem of finding the local field in this medium. par The dielectric function of a medium depends on frequency as the response of this medium to the field is not instantaneous but governed by the inertia of the charged particles. It further depends on the wavelength of the field as the response of the medium is spatially non-local, i.e. the polarization at a certain point in space is influenced by the field at that point and the field in its neighbourhood. Finally, in anisotropic media, the dielectric function depends on the direction of propagation of the field. It hence depends on ω and $\vec{q}$ [1].

In order to introduce the dielectric function one distinguishes between internal and external charge and current densities: ρ, $\vec{J}$ and ρ_{ext}, $\vec{J}_{\text{ext}}$. The two inhomogeneous Maxwell equations given in eqs. (67) and (70) become

$$\vec{\nabla} \cdot \vec{E}(\vec{r},\omega) = \frac{1}{\epsilon_0}\left[\rho(\vec{r},\omega) + \rho_{\text{ext}}(\vec{r},\omega)\right], \tag{101}$$

$$\vec{\nabla} \times \vec{B}(\vec{r},\omega) = \mu_0 \vec{J}(\vec{r},\omega) + \mu_0 \vec{J}_{\text{ext}}(\vec{r},\omega) - \mathrm{i}\epsilon_0\mu_0\omega\vec{E}(\vec{r},\omega). \tag{102}$$

Then, one introduces the displacement vector $\vec{D}(\vec{r},\omega)$ defined via

$$\mathrm{i}\omega\vec{D}(\vec{r},\omega) = \mathrm{i}\omega\vec{E}(\vec{r},\omega) - \frac{1}{\epsilon_0}\vec{J}(\vec{r},\omega). \tag{103}$$

Using the continuity equation that relates the internal charge to the internal current density, one obtains instead of eqs. (101) and (102)

$$\vec{\nabla} \cdot \vec{D}(\vec{r},\omega) = \frac{1}{\epsilon_0}\rho_{\text{ext}}(\vec{r},\omega), \tag{104}$$

$$\vec{\nabla} \times \vec{B}(\vec{r},\omega) = \mu_0 \vec{J}_{\text{ext}}(\vec{r},\omega) - \mathrm{i}\epsilon_0\mu_0\omega\vec{D}(\vec{r},\omega). \tag{105}$$

Contrary to $\vec{E}$, the displacement vector $\vec{D}$ does not have a direct physical meaning [283]. Only the longitudinal part of $\vec{D}$ has a physical meaning as it corresponds to the longitudinal part of the external field.

How are the electric field vector and the displacement vector related? The relation is given by the dielectric function. As, however, $\vec{E}$ and $\vec{D}$ are not necessarily parallel, one should in general rather consider a dielectric *tensor* defined via

$$\vec{D}(\vec{r},t) = \int \mathrm{d}\vec{r}\,' \int \mathrm{d}t' \boldsymbol{\epsilon}(\vec{r},\vec{r}\,',t,t') \cdot \vec{E}(\vec{r}\,',t'). \tag{106}$$

In a system exhibiting time-reversal symmetry, the dielectric tensor depends on $t-t'$. In a translationally invariant system it depends on $\vec{r}-\vec{r}\,'$ and in an isotropic system it reduces to a number, i.e. displacement vector and electric field are parallel.

If one is interested in a relation between *longitudinal* and *transverse* parts of $\vec{E}$ and $\vec{D}$, one has to define longitudinal and transverse dielectric tensors,

$$\vec{D}_{\mathrm{A}}(\vec{r},t) = \int \mathrm{d}\vec{r}\,' \int \mathrm{d}t' \boldsymbol{\epsilon}_{\mathbf{A}}(\vec{r},\vec{r}\,',t,t') \cdot \vec{E}_{\mathrm{A}}(\vec{r}\,',t'), \tag{107}$$

where the index A denotes either L or T. This expression cannot be derived from the expression for the total dielectric function in eq. (106). In order to turn eq. (106) into eq. (107) one would have to Fourier transform eq. (106) to $\vec{q}$-space and then insert $\boldsymbol{L}^{-1}(\vec{q}) \cdot \boldsymbol{L}(\vec{q})$ and $\boldsymbol{T}^{-1}(\vec{q}) \cdot \boldsymbol{T}(\vec{q})$ in between the dielectric tensor and the electric field vector – but the inverse of $\boldsymbol{L}$ and $\boldsymbol{T}$ cannot be defined as the corresponding determinants are zero. Hence, note that $\boldsymbol{\epsilon} \neq \boldsymbol{\epsilon_{\mathbf{L}}} + \boldsymbol{\epsilon_{\mathbf{T}}}$.

Dividing the expression in eq. (103) into one expression giving D_{L} and another expression giving D_{T}, expressing the currents $\vec{J}_{\mathrm{L}}$ and $\vec{J}_{\mathrm{T}}$ in terms of the fields using eqs. (83) and (84), and employing eq. (107) yields

$$\vec{E}_{\mathrm{L,ext}}(\vec{q},\omega) = \int \mathrm{d}\vec{q}\,' \boldsymbol{\epsilon}_{\mathbf{L}}(\vec{q},\vec{q}\,',\omega)\, \vec{E}_{\mathrm{L}}(\vec{q}\,',\omega), \tag{108}$$

$$\vec{E}_{\mathrm{T,ext}}(\vec{q},\omega) = \frac{\omega^2}{c^2q^2-\omega^2} \int \mathrm{d}\vec{q}\,' \left\{ \frac{c^2q^2}{\omega^2}\, \delta(\vec{q}-\vec{q}\,')\, \mathbf{1} - \boldsymbol{\epsilon}_{\mathbf{T}}(\vec{q},\vec{q}\,',\omega) \right\} \vec{E}_{\mathrm{T}}(\vec{q}\,',\omega). \tag{109}$$

These two equations relate the longitudinal and transverse dielectric tensors to the longitudinal and transverse local fields. Once the local fields are known, one can evaluate the dielectric tensors using these equations or vice versa.

Example: A 3D Homogeneous System

In the final part of this section, an example is discussed in order to demonstrate the difference between local and external field and in order to show how to obtain the dielectric function once the local field is known. Consider a 3D homogeneous system, see e.g. [3]. Only the diamagnetic part of the conductivity is taken into account for this simple example. Electron-electron interactions are considered via the local longitudinal field. The field driving the current is thus the local longitudinal plus the local transverse field. The conductivity depends on $\vec{r}-\vec{r}\,'$ and on $t-t'$, thus

$$\vec{J}(\vec{q},\omega) = \boldsymbol{\sigma_{\mathbf{3D}}}(\vec{q},\omega) \cdot \vec{E}(\vec{q},\omega). \tag{110}$$

The conductivity is diagonal and independent of $\vec{q}$ [3],

$$\boldsymbol{\sigma_{\mathbf{3D}}}(\omega) = \sigma_{\mathrm{3D}}(\omega) \cdot \mathbf{1} = \frac{\mathrm{i}n_{\mathrm{3D}}e^2}{m\omega} \cdot \mathbf{1}, \tag{111}$$

where n_{3D} is the particle density of the 3D homogeneous system.

Projecting the longitudinal and transverse parts of the current one finds that here the longitudinal part of the current is driven by the longitudinal part of the field alone and the transverse part of the current is driven by the transverse part of the field alone,

$$\vec{J}_{\rm A}(\vec{q},\omega) = \sigma_{\rm 3D}(\omega)\cdot\vec{E}_{\rm A}(\vec{q},\omega), \tag{112}$$

where A denotes either L or T. This is typical for an isotropic system. It will become clear in section 4 that the situation is different in a quantum wire.

Inserting the longitudinal part of the current into eq. (83) and the transverse part into eq. (84) one obtains

$$\vec{E}_{\rm L}(\vec{q},\omega) = \left[1-\frac{\sigma_{\rm 3D}(\omega)}{{\rm i}\epsilon_0\omega}\right]^{-1}\vec{E}_{\rm L,ext}(\vec{q},\omega), \tag{113}$$

$$\vec{E}_{\rm T}(\vec{q},\omega) = \left[1-{\rm i}\mu_0\omega g_0(\vec{q},\omega)\,\sigma_{\rm 3D}(\omega)\right]^{-1}\vec{E}_{\rm T,ext}(\vec{q},\omega). \tag{114}$$

Inserting the expressions given in eq. (86) for $g_0(\vec{q},\omega)$ and for the one for the conductivity $\sigma_{\rm 3D}(\omega)$ given in eq. (111) yields

$$\vec{E}_{\rm L}(\vec{q},\omega) = \frac{\omega^2}{\omega^2-\omega_{\rm P}^2}\vec{E}_{\rm L,ext}(\vec{q},\omega), \tag{115}$$

$$\vec{E}_{\rm T}(\vec{q},\omega) = \frac{c^2q^2-\omega^2}{c^2q^2-\omega^2+\omega_{\rm P}^2}\vec{E}_{\rm T,ext}(\vec{q},\omega), \tag{116}$$

where

$$\omega_{\rm P} = \sqrt{\frac{n_{\rm 3D}e^2}{m\epsilon_0}} \tag{117}$$

is the frequency of the 3D plasma oscillations [3].

The result for the local longitudinal field in eq. (115) implies that it is zero for zero frequency, $\omega = 0$. For $\omega \ll \omega_{\rm P}$, the local field is very small in comparison to the external field, $|\vec{E}_{\rm L}| \ll |\vec{E}_{\rm L,ext}|$. The external field is screened inside the medium by the charges. For $\omega \approx \omega_{\rm P}$, the local field may become huge, much larger than the external field. In this regime even a very small external excitation can excite collective plasma oscillations with frequency $\omega_{\rm P}$ and hence create a large local field. The plasma oscillation corresponds to the eigenmode of the system of charges coupled to the longitudinal field. The eigenmode dispersion is $\omega_{\rm 3D,L} = \omega_{\rm P}$, see figure 2. For $\omega \gg \omega_{\rm P}$, the external field oscillates so fast that the charges in the medium cannot follow to screen the field and hence $\vec{E}_{\rm L} \approx \vec{E}_{\rm L,ext}$.

The local transverse field is small when $|c^2q^2-\omega^2| \ll \omega_{\rm P}^2$. Local and external field are roughly equal when $|c^2q^2-\omega^2| \gg \omega_{\rm P}$. For $\omega = \omega_{\rm 3D,T} := \sqrt{c^2q^2+\omega_{\rm P}^2}$, the local transverse field diverges also for an arbitrarily small external field. It is the dispersion relation of the eigenmode of the charges coupled to the transverse field, see figure 2.

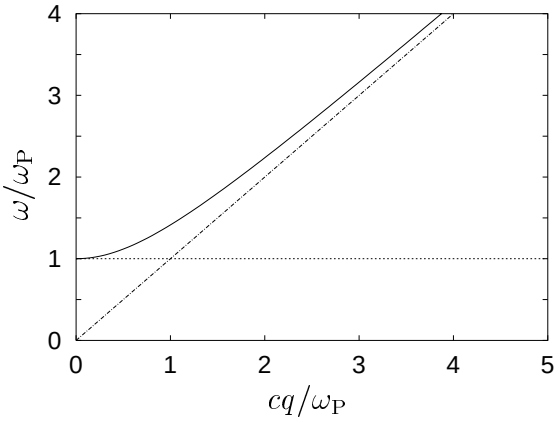

Figure 2: The dispersion relation of the longitudinal eigenmode $\omega_{3D,L} = \omega_P$ (dotted, in units of ω_P), the dispersion relation of the transverse eigenmode $\omega_{3D,T}$ (solid, in units of ω_P), and the frequency of the light $\omega = cq$ (dash-dotted, in units of ω_P) as a function of cq/ω_P.

The spatial shape of the local field can be obtained by Fourier transforming eqs. (115) and (116),

$$\vec{E}_L(\vec{r},t) = \frac{1}{(2\pi)^4}\int d\vec{q}\int d\omega\, e^{-i\vec{q}\vec{r}-i\omega t}\,\frac{\omega^2}{\omega^2-\omega_P^2}\,\vec{E}_{L,ext}(\vec{q},\omega), \tag{118}$$

$$\vec{E}_T(\vec{r},t) = \frac{1}{(2\pi)^4}\int d\vec{q}\int d\omega\, e^{-i\vec{q}\vec{r}-i\omega t}\,\frac{c^2q^2-\omega^2}{c^2q^2-\omega^2+\omega_P^2}\vec{E}_{T,ext}(\vec{q},\omega). \tag{119}$$

As the factor relating local and external longitudinal fields does not depend on $\vec{q}$, the spatial shape is identical for both fields. For a monochromatic external longitudinal field with frequency ω_{ext},

$$\vec{E}_L(\vec{r},t) = \frac{\omega_{ext}^2}{\omega_{ext}^2-\omega_{3D,P}^2}\,\vec{E}_{L,ext}(\vec{r},t). \tag{120}$$

The local longitudinal field diverges when the external frequency is equal to the plasma frequency.

In order to obtain the spatial shape of the local transverse field, one can evaluate the integral in eq. (119) in terms of residue. The modulus of the wave vector then assumes the value at the pole,

$$|\vec{q}_{pole}| = \frac{\sqrt{\omega_{ext}^2-\omega_P^2}}{c}, \tag{121}$$

for a monochromatic external field. The wave vector is imaginary when the external frequency is smaller than the plasma frequency ω_P. In that case the local field is exponentially damped. For $\omega_{ext} > \omega_P$, the wave vector is real and the local field can propagate inside the medium. However, specifying explicitly the spatial shape of the external transverse field one has to proceed carefully. The Fourier transform $\vec{E}_{T,ext}(\vec{q},\omega)$ has to be non-zero at $|\vec{q}_{pole}|$. It further should not contain a delta function which fixes any component of $\vec{q}$. Choosing a plane wave external field, for example, leads to a zero local transverse field as $\vec{q} = \vec{k}_{ext}$, $\omega = \omega_{ext}$, and $\omega_{ext} = c|\vec{k}_{ext}|$. The shape of a laser beam [287] might be an adequate choice but due to its complicated structure it cannot be Fourier transformed analytically.

Next, consider the dielectric tensors. For the 3D homogeneous system the expressions in eqs. (108) and (109) turn into

$$\vec{E}_{\mathrm{L,ext}}(\vec{q},\omega) = \boldsymbol{\epsilon}_{\mathbf{L}}(\vec{q},\omega)\,\vec{E}_{\mathrm{L}}(\vec{q},\omega), \tag{122}$$

$$\vec{E}_{\mathrm{T,ext}}(\vec{q},\omega) = \frac{\omega^2}{c^2q^2-\omega^2}\left\{\frac{c^2q^2}{\omega^2}\mathbf{1}-\boldsymbol{\epsilon}_{\mathbf{T}}(\vec{q},\omega)\right\}\vec{E}_{\mathrm{T}}(\vec{q},\omega). \tag{123}$$

Comparing these expressions with the ones in eqs. (115) and (116) shows that the longitudinal and transverse dielectric tensors reduce to functions. One obtains

$$\epsilon_{\mathrm{L/T}}(\vec{q},\omega) = \left(1-\frac{\omega_{\mathrm{P}}^2}{\omega^2}\right), \tag{124}$$

i.e. longitudinal and transverse dielectric functions are equivalent in this simple system. They are further independent of the wave vector $\vec{q}$.

One last comment on the physical meaning of longitudinal and transverse dielectric functions: The longitudinal dielectric function relates the internal charge density to the external charge density [283],

$$\rho(\vec{q},\omega) = \left[\frac{1}{\epsilon_{\mathrm{L}}(\vec{q},\omega)}-1\right]\rho_{\mathrm{ext}}(\vec{q},\omega) \tag{125}$$

$$= \frac{\omega_{\mathrm{P}}^2}{\omega^2-\omega_{\mathrm{P}}^2}\,\rho_{\mathrm{ext}}(\vec{q},\omega). \tag{126}$$

For frequencies much smaller than the plasma frequency the internal charge density is nearly equal to the negative of the external charge density, it hence screens the latter nearly perfectly.

The transverse dielectric function relates the transverse internal current density to the transverse external current density [283],

$$\vec{J}_{\mathrm{T}}(\vec{q},\omega) = \left[\frac{1}{\eta(\vec{q},\omega)}-1\right]\vec{J}_{\mathrm{T,ext}}(\vec{q},\omega), \tag{127}$$

where

$$\eta(\vec{q},\omega) = \frac{q^2c^2-\omega^2\epsilon_{\mathrm{T}}(\vec{q},\omega)}{q^2c^2-\omega^2}. \tag{128}$$

Inserting the above expression for ϵ_{T} yields

$$\vec{J}_{\mathrm{T}}(\vec{q},\omega) = -\frac{\omega_{\mathrm{P}}^2}{q^2c^2-\omega^2+\omega_{\mathrm{P}}^2}\,\vec{J}_{\mathrm{T,ext}}(\vec{q},\omega). \tag{129}$$

Hence, also the internal current screens the external current nearly perfectly as long as $\omega_{\mathrm{P}}^2 \gg |q^2c^2-\omega^2|$.

4 Clean Quantum Wire

In this section, time-dependent transport and local field effects in an infinitely long, clean quantum wire without contacts are studied. The infinite-range Coulomb interaction between the electrons is taken into account exploiting the Luttinger model. First, the transport equation of the clean wire is derived in section 4.1. Then, a short introduction into dc and ac transport in a clean quantum wire is given in sections 4.2 and 4.3. Section 4.4 contains the discussion of local field effects.

4.1 Transport Equation

In section 3.3, it was shown how to evaluate local fields inside a sample rigorously. The self-consistent local-field integral equations are given in eqs. (97) and (98). For their derivation, transport was assumed to be linear and to be determined by the conductivity $\boldsymbol{\sigma}(q_x, \vec{Q}, \vec{Q}\,', \omega)$ of the clean quantum wire of interacting electrons, see eq. (89). The derivation of an explicit expression for this conductivity based on the Kubo formula [140] and the Luttinger model is the subject of this section.

Linear Response

The current density in the wire is given by the expectation value of the current density operator,

$$\vec{J}(\vec{r}, t) = e\,\langle \vec{j}(\vec{r}, t) + \vec{j}_A(\vec{r}, t)\rangle. \tag{130}$$

A general expression for the particle current density operator in the absence of a vector potential, $\vec{j}(\vec{r}, t)$, is given in eq. (21) and the term to be added in the presence of a vector potential, $\vec{j}_A(\vec{r}, t)$, is given in eq. (27). The expectation value in eq. (130) is to be calculated using the eigenfunctions of the total Hamiltonian, given in section 3.1 and with the barrier switched off. The time evolution of the two current density operators, $\vec{j}(\vec{r}, t)$ and $\vec{j}_A(\vec{r}, t)$, is also governed by the total Hamiltonian. Neither the eigenfunctions of this total Hamiltonian containing the coupling of the wire to the electromagnetic field are known, nor can the time evolution of the current density operator be evaluated based on this total Hamiltonian.

One rewrites eq. (130) using for the expectation value the eigenfunctions of the Hamiltonian in the absence of the electromagnetic field and redefining the time evolution of the current operator also in terms of the Hamiltonian in the absence of the electromagnetic field. The electromagnetic field is not neglected, it appears inside the expectation value in form of a "time evolution operator" containing the Hamiltonian $H_{\rm em}^{\rm MB}$. This operator is then expanded in lowest order in the scalar electric potential $\varphi_{\rm ext}$ and the electromagnetic vector potential $\vec{A}$, leading to [140]

$$\begin{aligned} J^\alpha(\vec{r}, t) &= \langle j_A^\alpha(\vec{r}, t)\rangle_{\rm s} \\ &+ \frac{{\rm i}e^2}{\hbar} \sum_\beta \int_{-\infty}^{t} {\rm d}t' \int_{-\infty}^{\infty} {\rm d}\vec{r}\,' \langle [j^\alpha(\vec{r}, t), j^\beta(\vec{r}\,', t')]\rangle_{\rm s}\, A^\beta(\vec{r}\,', t') \end{aligned} \tag{131}$$

$$- \frac{\mathrm{i}e^2}{\hbar} \int\limits_{-\infty}^{t} \mathrm{d}t' \int\limits_{-\infty}^{\infty} \mathrm{d}\vec{r}\,' \langle [j^{\alpha}(\vec{r},t), \rho(\vec{r}\,',t')] \rangle_{\mathrm{s}}\, \varphi_{\mathrm{ext}}(\vec{r}\,',t'),$$

where $\alpha, \beta = x, y, z$. The index "s" at the expectation values indicates that only the eigenfunctions of the *system* in the absence of the electromagnetic field are considered.

Many Occupied Subbands

Next, one inserts the expressions for the projected particle and current density operators derived in section 3.1 into eq. (131) and obtains, see also eq. (89),

$$\vec{J}(\vec{q},\omega) = \int \mathrm{d}\vec{Q}\,' \boldsymbol{\sigma}(q_x, \vec{Q}, \vec{Q}\,', \omega) \cdot \left[\vec{E}_{\mathrm{L,ext}}(q_x, \vec{Q}\,', \omega) + \vec{E}_{\mathrm{T}}(q_x, \vec{Q}\,', \omega) \right]. \tag{132}$$

In the long wavelength limit, i.e. when the expectation value of the generalized density operator $\rho_{nl}(x)$ is independent of the position x, the elements of the conductivity tensor are

$$\begin{aligned} \sigma^{\alpha\beta}(q_x, \vec{Q}, \vec{Q}\,', \omega) &= \frac{1}{(2\pi)^2} \sum_{n,l} \sigma_{nl}^{\mathrm{dia}}(\omega)\, B_{nl}^{x}(\vec{Q} - \vec{Q}\,')\, \delta_{\alpha\beta} \\ &+ \frac{1}{(2\pi)^2} \sum_{n,l,s,p} \chi_{nlsp}^{\alpha\beta}(q_x, \omega)\, B_{nl}^{\alpha}(\vec{Q})\, B_{sp}^{\beta}(-\vec{Q}\,'). \end{aligned} \tag{133}$$

The generalized diamagnetic conductivity is

$$\sigma_{nl}^{\mathrm{dia}}(\omega) = \frac{\mathrm{i}e^2 \langle \rho_{nl}(q_x = 0) \rangle_{\mathrm{s}}}{m\omega L}, \tag{134}$$

where $\rho_{nl}(q_x)$ is the Fourier transform of $\rho_{nl}(x)$,

$$\rho_{nl}(q_x) = \sum_{k} c_{n,k+q_x}^{\dagger} c_{l,k}. \tag{135}$$

The correlation functions $\chi_{nlsp}^{\alpha\beta}$ contain the projected current operators,

$$\chi_{nlsp}^{\alpha\beta}(q_x,\omega) = \frac{e^2}{\hbar\omega L} \int\limits_{-\infty}^{\infty} \mathrm{d}\tau\, \Theta(\tau)\, \mathrm{e}^{\mathrm{i}\omega\tau} \langle [j_{nl}^{\alpha}(q_x,\tau), j_{sp}^{\beta}(-q_x,0)] \rangle_{\mathrm{s}}, \tag{136}$$

where $\Theta(\tau)$ is the Heavyside function. Remember that the expectation value is evaluated using the eigenfunctions of the Hamiltonian describing the wire of interacting electrons in the absence of the electromagnetic fields and also the time evolution of the projected 1D current operators is taken in the absence of the electromagnetic fields.

One Occupied Subband

When only the lowest subband is occupied, $l = 0$ in $\sigma^{\mathrm{dia}}_{nl}$ as can be seen from eq. (134) taking into account the definition of ρ_{nl}. Further, following the definitions of j^{α}_{nl} given in eqs. (25) and (26), it is $p = 0$ in $\chi^{\alpha\beta}_{nlsp}$. All other indices, namely n in $\sigma^{\mathrm{dia}}_{n0}$ and n, l, s in $\chi^{\alpha\beta}_{nls0}$, may be freely chosen. These other indices account for inter-band transitions to empty bands.

The remaining task is to evaluate the current-current correlation function in eq. (136) for a single-channel wire. For non-interacting electrons, this can be done for arbitrary indices, see appendix A.1 on page 109. For interacting electrons and arbitrary indices n, l, s, an evaluation of $\chi^{\alpha\beta}_{nls0}(q_x, \omega)$ is impossible. If all indices were zero, $\chi^{\alpha\beta}_{0000}$ could be obtained by exploiting the Luttinger model, see below. Now, one would expect that for a subband separation large in comparison to other energy scales in the system, transitions to empty bands are negligible and the term for $n = l = s = 0$ should be the dominant contribution to the conductivity. Under which conditions this is true is investigated in appendix A.1.

The conclusion drawn from these investigation is that for non-interacting electrons and a large subband separation, the element of the conductivity tensor relating the x-component of the current to the x-component of the field, σ^{xx}, is indeed dominated by intra-band transitions. However, for transport perpendicular to the wire, i.e. along y or z, the leading order contribution to the conductivity is provided by inter-band processes. Thus, the conductivity of the single channel wire may only be approximated by setting all indices to zero in eq. (133) when the x-component of the driving electric field is the dominant component of the field. Results for components of the current perpendicular to the wire should be interpreted with care. It is assumed that the arguments presented in appendix A.1 are qualitatively also valid for a system of interacting electrons.

In the following, the single-channel wire is approximated by setting all indices to zero in eq. (133). The conductivity tensor then is

$$\begin{aligned} \sigma^{\alpha\beta}_{1\mathrm{b}}(q_x, \vec{Q}, \vec{Q}\,', \omega) &= \frac{1}{(2\pi)^2}\, \sigma^{\mathrm{dia}}_{00}(\omega)\, B^{x}_{00}(\vec{Q} - \vec{Q}\,')\, \delta_{\alpha\beta} \\ &+ \frac{1}{(2\pi)^2}\, \chi^{xx}_{0000}(q_x, \omega)\, B^{x}_{00}(\vec{Q})\, B^{x}_{00}(-\vec{Q}\,')\delta_{\alpha x}\delta_{\beta x}, \end{aligned} \tag{137}$$

where

$$\sigma^{\mathrm{dia}}_{00}(\omega) = \frac{\mathrm{i}e^2 n_0}{m\omega}, \tag{138}$$

and $n_0 = N_0/L = m v_{\mathrm{F}}/\pi\hbar$ is the particle density in the lowest subband.

The correlation function $\chi^{xx}_{0000}(q_x, \omega)$ is evaluated based on the Luttinger model. First, rewrite $\chi^{xx}_{0000}(q_x, \omega)$ in terms of a density-density correlation function using the projected continuity equation in eq. (31): j^{α}_{00} is replaced by ρ_{00} and operators for higher bands, ρ_{nn} and j^{α}_{nn} with $n > 0$. All expectation values of terms containing ρ_{nn} and j^{α}_{nn} with $n > 0$ are zero when only the lowest subband is occupied. Then, the density operator ρ_{00} is expressed in terms of the bosonic field ϑ following eq. (65). An explicit expression for ϑ is given in eq. (60), it contains the bosonic operators $b^{\dagger}_{q_x}$

and b_{-q_x}. As the Hamiltonian of the system in the absence of the electromagnetic field is diagonal in these bosonic operators, the evaluation of the expectation value $\langle \ldots \rangle_{\mathrm{s}}$ needed in $\chi^{xx}_{0000}(q_x,\omega)$ is particularly simple and one obtains

$$\chi^{xx}_{0000}(q_x,\omega) = \sigma^{\mathrm{dia}}_{00}(\omega) \lim_{\eta\to 0} \frac{\omega^2_{\mathrm{LL}}(q_x)}{(\omega+\mathrm{i}\eta)^2 - \omega^2_{\mathrm{LL}}(q_x)}, \tag{139}$$

where the dispersion relation $\omega_{\mathrm{LL}}(q_x)$ is given in eq. (50). The explicit form of the Fourier transform of the projected interaction potential needed in $\omega_{\mathrm{LL}}(q_x)$ is for an infinite-range Coulomb interaction and a symmetric harmonic confinement given in eq. (53).

It can be shown that for a clean Luttinger liquid, linear response is exact [176, 154, 170, 288] due to the linearization of the dispersion relation [176]. Hence, the terms of higher order in the driving field neglected at the beginning of this section when an expression for the conductivity was derived yield no contribution in the Luttinger model anyway.

Note that in the expression for the conductivity of the single-channel quantum wire in eq. (137), the diamagnetic and the paramagnetic parts vary in a different manner with $\vec{Q}$ and $\vec{Q}\,'$. Thus, they also behave differently as a function of $\vec{R}$. The spatial behaviour of the two parts of the current with $\vec{R}$ is only identical in the limit of an infinitely strong confinement. Mathematically, this difference is due to the fact that when projecting the Kubo formula it is possible to explicitly perform two of the summations with respect to the band index in the diamagnetic part of the conductivity which cannot be done in the paramagnetic part of the conductivity. It is not assumed that this difference has a physical origin. It stems from the approximation in which inter-band transitions are neglected. As for an infinitely strong confinement only one band exists, and hence inter-band transitions cannot take place, the spatial behaviour of the two terms of the conductivity is equivalent in that case.

Further, with the conductivity of the single-channel wire as given in eq. (137) the current density in eq. (132) is related to the driving field via an integration. This is due to the anisotropy of the system and is in sharp contrast to transport in true 1D systems where current and driving field are related algebraically, see e.g. [170] and the discussion of the 1D limit below.

Finally, as the conductivity tensor is not proportional to the unity matrix, since it is diagonal but the diagonal elements are different from each other, it couples longitudinal and transverse components of the field. Even if the external field is purely longitudinal, the current acquires a transverse component and hence induces a local transverse field; and when the external field is purely transverse, a local longitudinal field is induced. This coupling between longitudinal and transverse field components is also due to the anisotropy of the system; such a coupling is absent in the example discussed in section 3.3.

The 1D Limit

As most of the investigations on transport in Luttinger liquids that can be found in the literature are concerned with true 1D systems, I this section is concluded

by showing how the 1D limit can be recovered from the transport equation derived here. Assume an infinitely strong confinement, $d = 0$. Then, the function $B^x_{00}(\vec{R})$ turns into a δ-function, $\lim_{d\to 0} B^x_{00}(\vec{R}) = \delta(\vec{R})$. As a consequence, $B^x_{00}(\vec{Q})$ becomes independent of $\vec{Q}$, $\lim_{d\to 0} B^x_{00}(\vec{Q}) = 1$. Neglecting transport perpendicular to the wire, the conductivity of the 1D system then consists of the term for $\alpha = \beta = x$ of the the single-band conductivity given in eq. (137) when the functions B^x_{00} are omitted. However, a factor of $1/(2\pi)^2$ remains that is not present when true 1D systems are studied [170]. This factor can be understood by looking at the transport equation in (132). The electric field in (132) is a 3D field. Define a 1D field projected onto the single subband,

$$E^x_{1\mathrm{b}}(x,\omega) = \int \mathrm{d}\vec{R}\, B^x_{00}(\vec{R}) E^x(x,\vec{R},\omega). \tag{140}$$

Fourier transforming the expressions on both sides yields

$$E^x_{1\mathrm{b}}(q_x,\omega) = \frac{1}{(2\pi)^2} \int \mathrm{d}\vec{Q}\, B^x_{00}(-\vec{Q}) E^x(q_x,\vec{Q},\omega). \tag{141}$$

For an infinitely strong confinement this turns into

$$E^x_{1\mathrm{b},d=0}(q_x,\omega) = \frac{1}{(2\pi)^2} \int \mathrm{d}\vec{Q}\, E^x(q_x,\vec{Q},\omega). \tag{142}$$

One can now rewrite eq. (132) for an infinitely strong confinement by putting the conductivity of the zero-diameter wire in front of the integral as it no longer depends on $\vec{Q}$. The remaining integral over the field yields $(2\pi)^2 E^x_{1\mathrm{b},d=0}(q_x,\omega)$. The factor $(2\pi)^2$ cancels the one present in the conductivity and the transport equation becomes

$$J^x_{d=0}(q_x,\vec{Q},\omega) = \sigma^{xx}_{1\mathrm{b},d=0}(q_x,\omega)\,[E^x_{\mathrm{L,ext},1\mathrm{b},d=0}(q_x,\omega) + E^x_{\mathrm{T},1\mathrm{b},d=0}(q_x,\omega)], \tag{143}$$

where

$$\begin{aligned} \sigma^{xx}_{1\mathrm{b},d=0}(q_x,\omega) &= \sigma^{\mathrm{dia}}_{00}(\omega) + \chi^{xx}_{0000}(q_x,\omega), & (144)\\ &= \sigma^{\mathrm{dia}}_{00}(\omega)\,\frac{\omega^2}{\omega^2 - \omega^2_{\mathrm{LL}}(q_x)}. & (145) \end{aligned}$$

The expression for the conductivity in eq. (145) is the one usually found in the literature [176].

As the right hand side of eq. (143) does not depend on $\vec{Q}$, the current is proportional to $\delta(\vec{R})$ in $\vec{r}$-space. Components of the current or the electric field other than the x-component are not considered. One can see that the true 1D system is much easier to handle than the projected 3D system as the current is related to the driving field via an algebraic expression and not via an integration in $\vec{q}$-space. On the other hand, rigorous local field studies cannot be performed on such a 1D system as Maxwell equations are only valid for 3D system.

4.2 DC Transport

The conductance of an infinitely long, clean Luttinger liquid without contacts can be derived from the conductivity given in eq. (145) by evaluating first the frequency-dependent absorbed power, then relating the time-averaged absorbed power to the frequency-dependent absorptive conductance, and finally performing the limit $\omega \to 0$, see [63, 169, 170] and the discussion in section 2.3.2. It turns out that the conductance is renormalized by the presence of the interactions, $\Gamma(\omega = 0) = ge^2/h$ [65, 289].

For quite some time it was believed that this renormalization of the conductance should be experimentally observable but experimentalists never succeeded to do so, see e.g. [37, 290]. As a consequence, theorists began to search for a reason why the conductance should remain e^2/h also in the presence of interactions. Two different possible explanations emerged.

It was suggested that the presence of leads might be responsible for the discrepancy between the theoretical prediction and the experimental finding. The prediction that the conductance should be ge^2/h is based on an infinitely long Luttinger liquid without contacts while any "real" quantum wire is of finite length and connected to 3D leads. Several groups then considered a so-called inhomogeneous Luttinger liquid. It consists of an infinitely long Luttinger liquid with a central part where the interaction parameter is different from one, $g \neq 1$, i.e. the electrons interact with each other. To the left and the right of this central wire the interaction is assumed to be switched off, $g = 1$. Those parts of the wire with the interaction switched off are meant to model the leads. Of course, in "real" leads the electrons also interact. But leads are usually 3D and in 3D systems screening is very effective [4] such that from a phenomenological point of view the electrons behave effectively as if they were not interacting [3]. Instead to describe explicitly this screening, the idea from which the inhomogeneous Luttinger liquid originated was to model the screening in the leads by assuming them to consist of non-interacting electrons. On the one hand, this is definitely a reasonable assumption, but on the other hand, the leads are still 1D instead of 3D and in 1D system screening is not strong – the idea of the inhomogeneous Luttinger liquid is not consistent.

However, despite slight difficulties concerning the interpretation of the inhomogeneous Luttinger liquid, the result seemed to justify the model. In [154, 155, 156, 158], a conductance of e^2/h for the Luttinger liquid "with leads" was derived. See also [157] where a Luttinger liquid with contacts is treated based on the Landauer-Büttiker approach. Notice that, strictly speaking, the result of [154, 155, 156, 158] is that the conductance of the central wire is determined by the properties of the leads and e^2/h is recovered because $g = 1$ is assumed in the leads. The idea that the transport properties of a system are determined by the contacts between this system and the outside world is not new, see the discussion on the "contact resistance" in [196, 198, 291]. Further, already in [65] it was discussed that any "real" quantum wire would be of finite length and connected to 3D leads and that one would have to make sure that one really probes the properties of the wire and not the properties of the leads in an experiment, see also [170].

The second approach chosen by some groups in order to explain why the conductance is not renormalized by the interactions is based on an attempt to include local field effects. It is argued that the electron-electron interaction not only affects the current, and hence leads to a renormalization of the conductance, but affects also the applied potential. As the conductance is the ratio of current and applied potential, the effects of the interaction on the current *and* the potential cancel and a conductance of e^2/h remains [166, 167, 168]. Even though also this approach leads to the desired result, namely a conductance of e^2/h, it is difficult to understand how the potential drop can be renormalized when it is usually provided by a battery which is introduced to keep this potential drop fixed.

Anyhow, for the clean quantum wire studied in this section, the conductance is ge^2/h because the wire is infinitely long and not connected to leads. This result is not in contradiction with experiments where wires of finite lengths are investigated.

4.3 AC Transport

Linear time-dependent transport in an infinitely long Luttinger liquid without contacts was studied by Cuniberti, Sassetti and Kramer in [169, 170]. An exponentially screened Coulomb potential is assumed, projected onto a parabolically confined quantum wire. The dispersion relation of the collective elementary excitations of the Luttinger liquid, $\omega_{\mathrm{LL}}(k)$, was discussed. The derivative of the inverse of the dispersion relation, $k_{\mathrm{LL}}(\omega)$, exhibited a peak as a function of ω which was reflected in the ac conductance, see below.

The absorptive part of the ac conductance of the system was found to be

$$\Gamma_{\mathrm{a}}(\omega) = \frac{e^2 v_{\mathrm{F}}}{h} \cdot \frac{\mathrm{d}k_{\mathrm{LL}}(\omega)}{\mathrm{d}\omega} \cdot L[k_{\mathrm{LL}}(\omega)], \tag{146}$$

where $k_{\mathrm{LL}}(\omega)$ is the inverse of the dispersion relation of the collective excitations of the Luttinger liquid and $L(k)$ is the Fourier transform of the spatial autocorrelation function of the probe field. It was pointed out that a zero-range interaction influences the ac conductance only quantitatively with respect to the non-interacting case while a finite-range interaction influences Γ_{a} also qualitatively via the behaviour of $\mathrm{d}k_{\mathrm{LL}}(\omega)/\mathrm{d}\omega$. It was argued that, as the ac conductance displays directly the features of the dispersion relation of the elementary excitations, the internal properties of the quantum wire could be determined from its ac conductance when the spatial shape of the probe field is known. The reactive part of the conductance was obtained from the absorptive one via a Kramers-Kronig transformation. The results for the complex conductance were analyzed with respect to "resistive", "capacitive", and "inductive" behaviour. The Luttinger liquid was compared with an equivalent classical circuit.

Further, screening in the quantum wire was examined by evaluating the 1D longitudinal dielectric function ϵ_{L} defined in [170] by the ratio of external to local electric potential,

$$\epsilon_{\mathrm{L}}(k,\omega) = \frac{\omega_{\mathrm{LL}}^2(k) - \omega^2}{v_{\mathrm{F}}^2 k^2 - \omega^2}. \tag{147}$$

It was then demonstrated that the current in the wire can either be related to the conductivity of the interacting system in connection with the external electric field or to the conductivity of the non-interacting system in connection with the local electric field. The transverse field was not considered. It was argued that this equivalence is due to the fact that linear response is exact in a Luttinger liquid, see also section 4.4. It was also shown that it makes no difference if the external or the local longitudinal field is used when the absorbed power is evaluated as the final expression for the absorbed power, and hence also the result for the absorptive conductance, is independent of this choice. This finding is in accordance with a statement of Keldysh [1] that the action of the local field on the particles in the medium is an internal interaction and cannot change the medium's energy, i.e. it cannot contribute to dissipation.

4.4 Local Field Effects

With the local field formalism introduced in section 3.3 and the conductivity tensor derived in section 4.1, it is now possible to investigate the local fields in a clean quantum wire. The self-consistent integral equations determining the local fields are, see also eqs. (97) and (98),

$$\begin{aligned} \vec{E}_{\mathrm{L}}(\vec{q},\omega) &= \vec{E}_{\mathrm{L,ext}}(\vec{q},\omega) \\ &+ \int \mathrm{d}\vec{Q}\,'\, \boldsymbol{K}_{\mathbf{L}}(q_x,\vec{Q},\vec{Q}\,',\omega)\cdot\left[\vec{E}_{\mathrm{L,ext}}(q_x,\vec{Q}\,',\omega)+\vec{E}_{\mathrm{T}}(q_x,\vec{Q}\,',\omega)\right], \end{aligned} \tag{148}$$

$$\begin{aligned} \vec{E}_{\mathrm{T}}(\vec{q},\omega) &= \vec{E}_{\mathrm{T,ext}}(\vec{q},\omega) \\ &+ \int \mathrm{d}\vec{Q}\,'\, \boldsymbol{K}_{\mathbf{T}}(q_x,\vec{Q},\vec{Q}\,',\omega)\cdot\left[\vec{E}_{\mathrm{L,ext}}(q_x,\vec{Q}\,',\omega)+\vec{E}_{\mathrm{T}}(q_x,\vec{Q}\,',\omega)\right]. \end{aligned} \tag{149}$$

Inserting the conductivity given in eq. (137) into the expressions for the Kernels in eqs. (99) and (100) yields

$$K_{\mathrm{L}}^{\alpha\beta}(q_x,\vec{Q},\vec{Q}\,',\omega) = \frac{1}{\mathrm{i}\epsilon_0\omega}\, L^{\alpha\beta}(\vec{q})\,\sigma_{\mathrm{1b}}^{\beta\beta}(q_x,\vec{Q},\vec{Q}\,',\omega), \tag{150}$$

$$K_{\mathrm{T}}^{\alpha\beta}(q_x,\vec{Q},\vec{Q}\,',\omega) = \mathrm{i}\mu_0\omega\, g_0(\vec{q},\omega)\, T^{\alpha\beta}(\vec{q})\,\sigma_{\mathrm{1b}}^{\beta\beta}(q_x,\vec{Q},\vec{Q}\,',\omega), \tag{151}$$

where the matrices $\boldsymbol{L}$ and $\boldsymbol{T}$ are given in eqs. (79) and (80) and the function $g_0(\vec{q},\omega)$ can be found in eq. (86).

An approximative approach for the solution of the local-field integral equations is presented in section 4.4.2. But before, in section 4.4.1, it is demonstrated that the rigorous microscopic approach and the mean-field like approach used to take into account electron-electron interactions lead to identical results in a clean quantum wire.

4.4.1 Interaction vs. Local Longitudinal Field

In this section, the *projected* local longitudinal field is derived for a specific choice of the external field; the local transverse field is neglected. Instead of using eq. (148),

first the current is evaluated and then the induced longitudinal field. The approach is equivalent to the usage of eq. (148) and it is applied here in order to obtain not only an expression for the local field but also one for the current. The induced longitudinal field is then projected onto the quantum wire. Based on this derivation of the projected induced longitudinal field it is demonstrated that the current can *either* be expressed via the projected *external* field in connection with the conductivity of the interacting system *or* via the projected *local* field in connection with the conductivity of the non-interacting system.

Assume an external longitudinal field parallel to the wire and independent of $\vec{R}$, $\vec{E}_{\mathrm{L,ext}}(\vec{r},\omega) = (E_0(x,\omega),0,0)$. The Fourier transform is

$$E^x_{\mathrm{L,ext}}(\vec{q},\omega) = (2\pi)^2\,\delta(\vec{Q})\,E_0(q_x,\omega). \tag{152}$$

Inserting this field into the expression for the current in eq. (132) yields

$$J^x(\vec{q},\omega) = (2\pi)^2\,\sigma^{xx}_{\mathrm{1b}}(q_x,\vec{Q},\vec{Q}\,'=\vec{0},\omega)\,E_0(q_x,\omega). \tag{153}$$

The local longitudinal field is related to the longitudinal part of the current via eq. (83) and the longitudinal part of the current is obtained from the total current using eq. (77). Then, the induced field, i.e. the local minus the external field, is

$$E^x_{\mathrm{L,ind}}(\vec{q},\omega) = \frac{q_x^2\,V^{\mathrm{C}}_{\mathrm{ee}}(q)}{\mathrm{i}\omega e^2}\,J^x(\vec{q},\omega), \tag{154}$$

with the Fourier transformed Coulomb potential $V^{\mathrm{C}}_{\mathrm{ee}}(q) = e^2/\epsilon_0 q^2$.

Now, project the fields in eqs. (152) and (154) onto the lowest subband following eq. (141): multiply both sides by $B^x_{00}(-\vec{Q})/(2\pi)^2$ and integrate with respect to $\vec{Q}$. Further, insert the expression for the conductivity given in eq. (137). Employing the expression for the projected interaction potential in eq. (38) and using $E^x_{\mathrm{L,ext,1b}}(q_x,\omega) = E_0(q_x,\omega)$ yields

$$E^x_{\mathrm{L,ind,1b}}(q_x,\omega) = \frac{q_x^2\,V^{\mathrm{C}}_{\mathrm{1b}}(q_x)}{\mathrm{i}\omega e^2}\;\sigma^{xx}_{\mathrm{1b},d=0}(q_x,\omega)\,E^x_{\mathrm{L,ext,1b}}(q_x,\omega). \tag{155}$$

Here, $\sigma^{xx}_{\mathrm{1b},d=0}(q_x,\omega)$ given in eq. (144) is used in order to abbreviate the expression $\sigma^{\mathrm{dia}}_{00}(\omega) + \chi^{xx}_{0000}(q_x,\omega)$; it does not imply that a wire of zero diameter is assumed. Inserting for $\sigma^{xx}_{\mathrm{1b},d=0}(q_x,\omega)$, see eq. (145), and using the explicit expression for the dispersion relation ω_{LL} given in eq. (50), it is straightforward to show, see also [170],

$$E^x_{\mathrm{L,ind,1b}}(q_x,\omega) = \left[\frac{\sigma^{xx}_{\mathrm{1b},d=0}(q_x,\omega)}{\sigma^{xx}_{\mathrm{1b,non-int},d=0}(q_x,\omega)} - 1\right] E^x_{\mathrm{L,ext,1b}}(q_x,\omega), \tag{156}$$

where $\sigma^{xx}_{\mathrm{1b,non-int},d=0}$ is the conductivity of the non-interacting system which follows from $\sigma^{xx}_{\mathrm{1b},d=0}$ by replacing ω^2_{LL} in eq. (145) with $v_{\mathrm{F}}^2 q_x^2$, see eq. (50). The projected local field is hence related to the projected external field via

$$\sigma^{xx}_{\mathrm{1b,non-int},d=0}(q_x,\omega)E^x_{\mathrm{L,1b}}(q_x,\omega) = \sigma^{xx}_{\mathrm{1b},d=0}(q_x,\omega)E^x_{\mathrm{L,ext,1b}}(q_x,\omega). \tag{157}$$

This result demonstrates that the conductivity of the interacting system times the projected external longitudinal field is equivalent to the conductivity of the non-interacting systems times the projected local longitudinal field. This equivalence is due to the fact that linear response is exact in a Luttinger liquid, see also [170], and further to the fact that, for the evaluation of the correlation function that gives the conductivity, the difference between $H_{\rm int}^{\rm MB}$ in eq. (1) and $H_{\rm ind}$ in eq. (4) has no consequences.

It is further important to consider a Coulomb interaction potential and not an *ad hoc* finite-range potential. The appearance of $V_{\rm ee}^{\rm C}(q)$ in eqs. (154) and (155) is due to the nature of Maxwell equations – a Coulomb interaction is contained inherently in Maxwell equations. The conductivity $\sigma_{{\rm 1b},d=0}^{xx}$ contains the interaction potential *assumed* in the wire. If this is not also a Coulomb potential, eq. (157) is strictly speaking not valid. In order to consider a finite-range interaction potential one would have to incorporate explicitly gates or change Maxwell equations in a consistent manner in order to account for a different interaction potential.

Finally, the current in terms of the projected external field is, following eq. (153),

$$J^x(\vec{q},\omega) = B_{00}^x(\vec{Q})\,\sigma_{{\rm 1b},d=0}^{xx}(q_x,\omega)\,E_{{\rm L,ext,1b}}^x(q_x,\omega). \tag{158}$$

Using eq. (157), one can replace the external field by the local field and obtains the current in terms of the projected local field,

$$J^x(\vec{q},\omega) = B_{00}^x(\vec{Q})\,\sigma_{{\rm 1b,non-int},d=0}^{xx}(q_x,\omega)\,E_{{\rm L,1b}}^x(q_x,\omega). \tag{159}$$

The two equivalent expressions for the current in eqs. (158) and (159) show that one may *either* consider the Coulomb interactions directly *or* the local longitudinal field instead. However, this argument has one slight flaw: The expressions for the current in eqs. (158) and (159) contain the projected fields.

Could two expressions for the current similar to the ones in eqs. (158) and (159) be obtained for the *full* local and external fields and a *general* shape of the external field? The obstacle that would have to be overcome in order to do so is the integral in the transport equation. In the derivation of eqs. (158) and (159), this obstacle is circumvented by choosing a particular shape of the external field which is proportional to $\delta(\vec{Q})$ in $\vec{q}$-space and thus removes the integral. Then, because the induced field depends in a more complicated manner on $\vec{Q}$ than the external field does, the fields are projected in order to get rid of the $\vec{Q}$-dependence. Whenever the information on the $\vec{Q}$-dependence of the fields is retained, one ends up with integrations instead of algebraic equations. Hence, for the full field and a general external field it is impossible to arrive at analytic expressions similar to the ones in eqs. (158) and (159).

However, it is reasonable to project the fields when the local transverse field is neglected. The integral in the transport equation that is responsible for the encountered problems is related to the anisotropy of the system. This anisotropy also causes a coupling of local longitudinal and local transverse fields as can be seen from eqs. (148) and (149); this coupling is absent in an isotropic system, see the example in section 3.3. If the longitudinal and transverse components of the local

electric field were not coupled, the transverse field would not need to be neglected as it would simply not enter the equation determining the local longitudinal field. Hence, the anisotropy is neglected together with the local transverse field. It is reasonable to neglect it then also in the evaluation of the local longitudinal field by projecting the electric fields.

4.4.2 Plasmon-Polariton

In this section, the local-field integral equations given in (148) and (149) are tackled following an approximative approach. In contrast to the previous section, the local *transverse* field is fully taken into account. The coupling between the collective charge excitations in the quantum wire and the electromagnetic field gives rise to a local field eigenmode which is studied in detail below.

Discretization of the Local-Field Equations

The approximative approach employed here is based on a discretization of the integral equations: The integrals with respect to q_y' in eqs. (148) and (149) are replaced by sums over N abscissas and the integrals with respect to q_z' are replaced by sums over M abscissas. This approach leads to two systems of $3NM$ coupled linear equations instead of two integral equations [292]; the factor of 3 is due to the fact that the integral equations define vectors which have three components. In the limit of an infinite number of abscissas, $N, M \to \infty$, this approach is exact. Solving the system of linear equations for finite N, M analytically or numerically, one obtains the local field at the discrete values of the abscissas. Investigating the condition under which the system of linear equations is solvable also in the absence of an external field, the local field eigenmodes can be found.

For an explicit demonstration of the discretization of the integral equations see appendix A.2 on page 112. Here, only those details of the discretization process are given which are necessary in order to understand the following discussion: The abscissas used for the discretization are denoted by $\nu_{N,n}$ for the integration with respect to q_y' and by $\nu_{M,m}$ for the integration with respect to q_z', where $1 \leq n \leq N$ and $1 \leq m \leq M$. The abscissas are chosen in accordance to the rule of the Gaussian quadrature in order to assure a good accuracy, see appendix A.2.1. For odd N, one of the abscissas is always zero, namely the one with $n = (N+1)/2$. The other abscissas are distributed symmetrically to both sides of $\nu_{N,(N+1)/2}$, for example $\nu_{5,5} = -\nu_{5,1}$ and $\nu_{5,4} = -\nu_{5,2}$. For even N, all abscissas are different from zero but also distributed symmetrically around zero, for example $\nu_{4,4} = -\nu_{4,1}$ and $\nu_{4,3} = -\nu_{4,2}$. The components of the local field, of the external field and the kernels in eqs. (148) and (149) are then taken at the discrete values of $\vec{Q}$ and $\vec{Q}\,'$. The variables q_x and ω remain continuous. Following appendix A.2.1, the discretized local-field equations can be written in terms of matrix equations,

$$\vec{\mathcal{E}}_{\mathrm{L}}(q_x,\omega) = \boldsymbol{M}_{\mathbf{LL}}(q_x,\omega)\cdot\vec{\mathcal{E}}_{\mathrm{L,ext}}(q_x,\omega) + \boldsymbol{M}_{\mathbf{LT}}(q_x,\omega)\cdot\vec{\mathcal{E}}_{\mathrm{T,ext}}(q_x,\omega), \quad (160)$$

$$\vec{\mathcal{E}}_{\mathrm{T}}(q_x,\omega) = \boldsymbol{M}_{\mathbf{TL}}(q_x,\omega)\cdot\vec{\mathcal{E}}_{\mathrm{L,ext}}(q_x,\omega) + \boldsymbol{M}_{\mathbf{TT}}(q_x,\omega)\cdot\vec{\mathcal{E}}_{\mathrm{T,ext}}(q_x,\omega). \quad (161)$$

The elements of the vectors $\vec{\mathcal{E}}_{\mathrm{L}}$ and $\vec{\mathcal{E}}_{\mathrm{T}}$ are the local fields $\vec{E}_{\mathrm{L}}$ and $\vec{E}_{\mathrm{T}}$ evaluated at the discrete values $q_y = 4\nu_{N,n}/d$ and $q_z = 4\nu_{M,m}/d$, see appendix A.2.1, where d is the diameter of the wire. The elements of the $(3NM \times 3NM)$ matrices $\boldsymbol{M}_{\mathbf{AB}}(q_x, \omega)$, where A and B denote L and T, are explicitly given in appendix A.2.1. The matrix $\boldsymbol{M}_{\mathbf{AB}}$ for A≠B is non-zero, hence longitudinal and transverse fields are coupled in the quantum wire in contrast to the example discussed in section 3.3.

When the external field is either longitudinal or transverse, the discretized local field equations become

$$\boldsymbol{M}_{\mathbf{AB}}{}^{-1}(q_x, \omega) \cdot \vec{\mathcal{E}}_{\mathrm{A}}(q_x, \omega) = \vec{\mathcal{E}}_{\mathrm{B,ext}}(q_x, \omega). \tag{162}$$

How the i-th component of the discretized local field vector $\vec{\mathcal{E}}_{\mathrm{A}}$ can be obtained from eq. (162) is shown in appendix A.2.2. For completeness, the discretized dielectric function following from eq. (162) is given in appendix A.2.3.

Local-Field Eigenmodes

From eq. (162) and the theory on coupled linear equations, see e.g. [285], it is clear that a local field may exist even in the absence of an external field when the matrix $\boldsymbol{M}_{\mathbf{AB}}{}^{-1}$ is singular, i.e. its determinant is zero because then a system of *homogeneous* linear equations is solvable. Hence, in order to find a local-field eigenmode one has to search for the values of q_x and ω for which

$$\det[\boldsymbol{M}_{\mathbf{AB}}{}^{-1}(q_x, \omega)] = 0. \tag{163}$$

The matrices $\boldsymbol{M}_{\mathbf{AB}}$ for any A and B are all based on $\boldsymbol{M}_{\mathbf{TT}}$, see appendix A.2.1. It is shown in appendix A.2.4 that the zeroes of the determinants of the other matrices are given by the zeroes of the determinant of $\boldsymbol{M}_{\mathbf{TT}}$. Hence, only $\boldsymbol{M}_{\mathbf{TT}}$ is discussed here.

One knows that an arbitrary square matrix $\boldsymbol{A}$ of dimension $N \times N$ with elements a^{ij} *is not singular* when

$$|a^{ii}| > \sum_{j \neq i} |a^{ij}|, \tag{164}$$

for any i with $1 \leq i \leq N$ [293, 294]. Now, the diagonal elements of the matrix $\boldsymbol{M}_{\mathbf{TT}}{}^{-1}$ and also the sum over the off-diagonal elements of $\boldsymbol{M}_{\mathbf{TT}}{}^{-1}$ are estimated in appendix A.2.4, see eqs. (292) and (294). Due to the presence of poles in the corresponding expressions, the diagonal elements and the sums over the off-diagonal elements diverge when ω and q_x are chosen such that they either lie exactly on the light or on the Luttinger dispersion; q_y and q_z may not be chosen freely but are fixed by the discretization procedure. Away from these poles, the diagonal elements of $\boldsymbol{M}_{\mathbf{TT}}{}^{-1}$ are roughly of the order of 1 while the sums over the off-diagonal elements are roughly of the oder of

$$Z = \frac{4e^2}{\pi^2 \hbar \epsilon_0 c} \frac{v_{\mathrm{F}}}{c} \approx 3 \times 10^{-2} \cdot \frac{v_{\mathrm{F}}}{c}. \tag{165}$$

For a realistic value of the Fermi velocity around 10^5 m/s, $Z \approx 10^{-5}$. Hence, only when ω and q_x are chosen close to the light or to the Luttinger dispersion, the sums

over the off-diagonal elements of $\boldsymbol{M_{TT}}^{-1}$ become large enough in order to be equal to or larger than the diagonal elements – then, the matrix $\boldsymbol{M_{TT}}^{-1}$ can be singular and thus local-field eigenmodes can exist. For values of ω and q_x away from the light and the Luttinger dispersion, local-field eigenmodes cannot exist.

The combinations of ω and q_x for which $\boldsymbol{M_{TT}}^{-1}$ *is* singular determine the dispersion relation of the eigenmode of the local field. Now, the discussion in the preceding paragraph implies that, if eigenmodes exist at all, their dispersion relation is closely related to the light and the Luttinger dispersions. This is in analogy to the dispersion relation of the phonon-polariton – the local-field eigenmode in a system consisting of a ionic lattice and an electromagnetic field –which was discussed in section 2.2.3. Thus, near the crossing of light and Luttinger dispersions, where the coupling between charge excitations and electromagnetic field is strongest, the opening of a gap is expected.

In analogy to the phonon-polariton, the local field eigenmode studied here is called *plasmon-polariton* as it is based on the coupling of a collective plasma oscillation of the charges in the quantum wire and an electromagnetic field. The names "local-field eigenmode" and "plasmon-polariton" are used synonymously in the following. Note that the coupling of a plasma oscillation to a transverse field is only possible due to the anisotropy of the system. In 3D isotropic systems, the plasma oscillation can only couple to a longitudinal field [3].

Now, the above discussion on when the matrix $\boldsymbol{M_{TT}}^{-1}$ can be singular and when it cannot be singular gives an idea on what should be expected for the local-field eigenmodes in the quantum wire. However, it does not proof that $\boldsymbol{M_{TT}}^{-1}$ *does* become singular at all. To ascertain that local-field eigenmodes exist in the quantum wire, to study their dispersion relation and to investigate the gap in this dispersion is the remaining task of this section.

Plasmon and Photon Dispersions

The branches of the dispersion relation of plasmon-polariton are expected to lie close to the dispersion relations of the light and of the collective excitations of the Luttinger liquid. The greatest deviation of the polariton dispersion from the light and the Luttinger dispersions is expected to appear near the crossing of these two dispersions.

The dispersion relation of the photon for a $\vec{q}$-vector parallel to the wire is denoted by $\omega_{\mathrm{Ph}\parallel}$ and is $\omega_{\mathrm{Ph}\parallel} = cq_x$ because $|\vec{Q}| = 0$. When the $\vec{q}$-vector is not parallel to the wire, the dispersion relation of the photon is denoted by $\omega_{\mathrm{Ph}\perp}$ and is, as $|\vec{Q}| \neq 0$, $\omega_{\mathrm{Ph}\perp} = c(q_x^2 + Q^2)^{1/2}$. Now, the dispersion $\omega_{\mathrm{Ph}\parallel}$ intersects the Luttinger dispersion ω_{LL} twice as a function of q_x, see figure 3. One point of intersection is at $q_x = q_{1\parallel} = 0$. A second point of intersection exists because for a Coulomb potential the Luttinger dispersion is infinitely steep at $q_x = 0$ and crosses over to a linear behaviour $v_{\mathrm{F}}q_x$ for large q_x, see section 3.2, while the light dispersion for $|\vec{Q}| = 0$ rises as cq_x with c finite and $c > v_{\mathrm{F}}$. Following eqs. (50) and (53), one can estimate the position of the second crossing between the photon dispersion for $\vec{q}$ parallel to the wire and the Luttinger dispersion to be at $q_{2\parallel} \approx \sqrt{8}\,\mathrm{e}^{-8/Z}$, where Z is given in eq. (165).

The light dispersion for a $\vec{q}$-vector not parallel to the wire intersects the Luttinger

dispersion only if the component of $\vec{q}$ perpendicular to the wire is not too large, see figure 3. For a small enough $|\vec{Q}|$, also the light dispersion $\omega_{\mathrm{Ph}\perp}$ intersects the Luttinger dispersion twice. The positions of the intersection are denoted by $q_{1\perp}$ and $q_{2\perp}$. These two positions cannot be estimated analytically, but one knows $q_{1\parallel} < q_{1\perp} < q_{2\perp} < q_{2\parallel}$, see figure 3. The photon and Luttinger dispersions are displayed as functions of q_x and $|\vec{Q}|$ in figure 4.

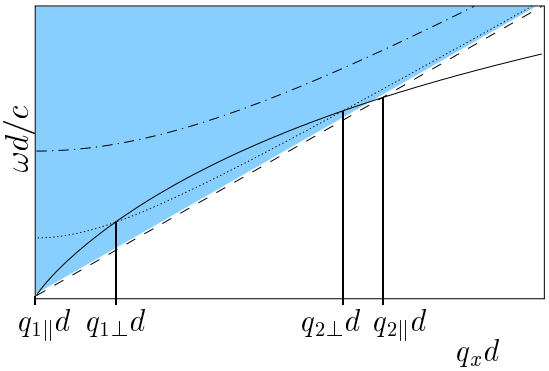

Figure 3: The Luttinger dispersion ω_{LL} (solid), the photon dispersion $\omega_{\mathrm{Ph}\parallel}$ (dashed), a photon dispersion $\omega_{\mathrm{Ph}\perp}$ that intersects ω_{LL} (dotted), and a photon dispersion $\omega_{\mathrm{Ph}\perp}$ that does not intersect ω_{LL} (dash-dotted). The shaded area illustrates the continuum of photon dispersions with any possible Q. The picture is to be understood qualitatively.

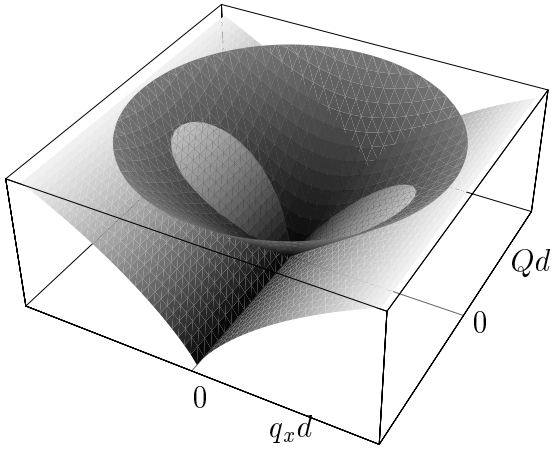

Figure 4: The Luttinger dispersion (light grey) and the photon dispersion (dark grey) as functions of $q_x d$ and Qd. The picture is to be understood qualitatively.

Polariton Dispersion Approached Analytically

One could now in principle determine the eigenmode dispersions numerically by searching for the zeroes of the determinant of $\boldsymbol{M}_{\mathbf{TT}}{}^{-1}$ using a numerical algorithm, see below. However, the region of the crossing between light and Luttinger dispersions, which is the most interesting regime here as it promises the largest deviation of the eigenmode dispersion from light and Luttinger dispersions, cannot be reached numerically for realistic values of the Fermi velocity. But, in order to obtain a qualitative picture, it can be approached analytically in the limit of very few abscissas. Choose $N = 3$ and $M = 1$, evaluate $\boldsymbol{M}_{\mathbf{TT}}{}^{-1}$, take the determinant and look for the zeroes. One obtains three branches of the polariton dispersion, see appendix A.2.4,

$$\left(\frac{\omega_{\mathrm{T,LL}}(q_x)d}{c}\right)^2 \approx \left(\frac{\omega_{\mathrm{LL}}(q_x)d}{c}\right)^2 \left[1 - \frac{\mathrm{e}^{-3/2}\,Z}{72}\right], \tag{166}$$

$$\left(\frac{\omega_{\mathrm{T,Ph}\parallel}(q_x)d}{c}\right)^2 \approx (q_x d)^2 + \frac{2\,Z}{3}, \tag{167}$$

$$\left(\frac{\omega_{\mathrm{T,Ph}\perp}(q_x)d}{c}\right)^2 \approx (q_x d)^2 + (4\nu_{3,1})^2 + \frac{\mathrm{e}^{3/2}\,Z}{6}, \tag{168}$$

where Z is given in eq. (165). The value of $|\vec{Q}|d$ is here for $N = 3$ and $M = 1$ given by $4\nu_{3,1} = 2\sqrt{6}$. These three expressions in (166) - (168) are not valid for any value of q_x. However, for the following discussion the conditions imposed on eqs. (166) - (168) are not important, details can be found in appendix A.2.4.

The dispersions (166) - (168) are displayed qualitatively in figure 5. The plasmon-like mode $\omega_{\mathrm{T,LL}}$ lies below the Luttinger dispersion ω_{LL}. The difference between $\omega_{\mathrm{T,LL}}$ and ω_{LL} is given by the multiplicative factor $[1 - \mathrm{e}^{-3/2}\,Z/72]$, it depends mainly on v_{F}/c, see eq. (165), and increases with increasing v_{F}/c. The photon-like modes $\omega_{\mathrm{T,Ph}\parallel}$ and $\omega_{\mathrm{T,Ph}\perp}$ lie above the photon dispersions $\omega_{\mathrm{Ph}\parallel}$ and $\omega_{\mathrm{Ph}\perp}$. The difference between $\omega_{\mathrm{T,Ph}\parallel}$ and $\omega_{\mathrm{Ph}\parallel}$ is given by the additive term $2Z/3$ and the difference between $\omega_{\mathrm{T,Ph}\perp}$ and $\omega_{\mathrm{Ph}\perp}$ is given by the additive term $\mathrm{e}^{3/2}Z/6$ – these differences depend on Z and hence on v_{F}/c. Near the crossing of the dispersions ω_{LL} and $\omega_{\mathrm{Ph}\parallel}$, the branches $\omega_{\mathrm{T,LL}}$ and $\omega_{\mathrm{T,Ph}\parallel}$ cross without showing any repulsion. This is due to the fact that for $\omega_{\mathrm{Ph}\parallel}$ the $\vec{q}$-vector is parallel to the wire and hence the corresponding transverse field is perpendicular to the wire. It has no component parallel to the wire that could couple to the plasmons. At $q_x = 0$, however, the branches of the polariton dispersion $\omega_{\mathrm{T,LL}}$ and $\omega_{\mathrm{T,Ph}\parallel}$ do show an anti-crossing because for $|\vec{q}| = 0$ the transverse field is not well defined and can have any direction. The repulsion between the branches $\omega_{\mathrm{T,Ph}\parallel}$ and $\omega_{\mathrm{T,LL}}$ at $q_x = 0$ is

$$\left(\frac{\omega_{\mathrm{T,Ph}\parallel}(0)d}{c}\right)^2 - \left(\frac{\omega_{\mathrm{T,LL}}(0)d}{c}\right)^2 = \frac{2\,Z}{3}. \tag{169}$$

The size of the gap at $q_x = 0$ increases with increasing v_{F}/c. This ratio determines the strength of the coupling between charges and electromagnetic fields.

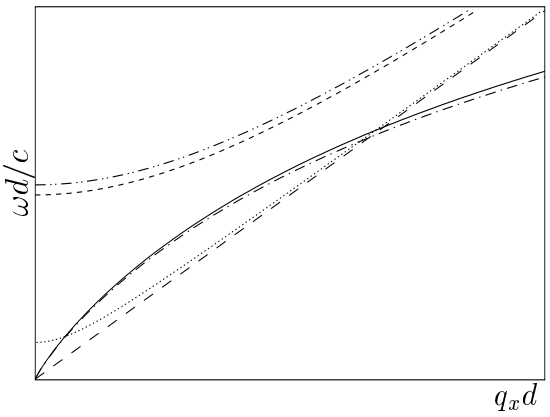

Figure 5: The Luttinger dispersions ω_{LL} (solid), the photon dispersions $\omega_{\mathrm{Ph}\parallel}$ (long dashes) and $\omega_{\mathrm{Ph}\perp}$ (short dashes), and the corresponding branches of the eigenmode dispersion $\omega_{\mathrm{T,LL}}$ (dash-dot), $\omega_{\mathrm{T,Ph}\parallel}$ (dots), and $\omega_{\mathrm{T,Ph}\perp}$ (dash-dot-dot) displayed qualitatively. The deviations of the eigenmode branches from the dispersions of the uncoupled systems are greatly exaggerated.

In the eigenmode dispersion derived above for $N = 3$ and $M = 1$, no gap was found at finite $q_x d$ as ω_{LL} and $\omega_{\mathrm{Ph}\parallel}$ do not couple at finite $q_x d$ due to symmetry reasons and ω_{LL} and $\omega_{\mathrm{Ph}\perp}$ do not cross, see figure 5. The reason for the absence

of a crossing between ω_{LL} and $\omega_{\mathrm{Ph}\perp}$ is that the value of $|\vec{Q}|d$, which is fixed by the discretization procedure, is too large. In the limit of infinitely many abscissas, there are of course discrete values of Q small enough in order to allow for an intersection of ω_{LL} and $\omega_{\mathrm{Ph}\perp}$ – but that limit cannot be approached analytically. In order to be able to study the gap at a crossing of ω_{LL} and $\omega_{\mathrm{Ph}\perp}$ for finite $q_x d$ nevertheless, choose $N = M = 1$. But then, the abscissas $\nu_{N=1,1} = \nu_{M=1,1} = 0$, and hence $|\vec{Q}| = 0$, thus $\vec{q}$ is parallel to the wire. Now, shift $\nu_{N=1,1}$ slightly to the left and to the right, splitting it into two abscissas: $\nu_{N=1,1} \to \pm\varepsilon$, where $0 < \varepsilon \ll 1$. The choice $\varepsilon \neq 0$ ensures $|\vec{Q}| \neq 0$ and hence the presence of $\omega_{\mathrm{Ph}\perp}$ with $\omega_{\mathrm{Ph}\perp} d/c = (q_x^2 d^2 + 16\varepsilon^2)^{1/2}$. The explicit expressions for the branches of the ensuing eigenmode dispersion can be found in appendix A.2.4. They are denoted by $\omega_{\mathrm{T},+}$ and $\omega_{\mathrm{T},-}$. It is impossible to call either of them photon-like or plasmon-like as such an assignment would inevitably depend of $q_x d$. At $q_x d = 0$, it is, for the conditions see appendix A.2.4,

$$\left(\frac{\omega_{\mathrm{T}\pm}(q_x = 0)d}{c}\right)^2 \approx \begin{cases} (4\varepsilon)^2 + Z, \\ 0. \end{cases} \tag{170}$$

Here, in the regime where $q_x d$ is much smaller than the position of the first crossing between ω_{LL} and $\omega_{\mathrm{Ph}\perp}$, $q_x d \ll q_{1\perp} d$, $\omega_{\mathrm{T}-}$ is a plasmon-like mode and $\omega_{\mathrm{T}+}$ is a photon-like mode. As $\varepsilon^2 \ll Z$, the relative deviation of the dispersion of the photon-like mode from the dispersion $\omega_{\mathrm{Ph}\perp}$ is huge at $q_x d = 0$. The result in eq. (170) is not equivalent to the one in eq. (167) as in (170) the deviation is given by Z, while it is given by $2Z/3$ in (167). This difference is due to the crude approximations performed taking so few abscissas. However, in both equations the deviation is determined by Z and hence by v_{F}/c!

At the two intersections of the dispersions ω_{LL} and $\omega_{\mathrm{Ph}\perp}$, namely at $q_x d = q_{i\perp} d$ for $i = 1, 2$, define

$$\kappa_i d := (q_{i\perp} d)^2 + (4\varepsilon)^2 = \left(\frac{\omega_{\mathrm{LL}}(q_{i\perp})d}{c}\right)^2. \tag{171}$$

Here, a gap opens and one obtains in lowest order in ε^2

$$\left(\frac{\omega_{\mathrm{T}\pm}(q_x = q_{i\perp})d}{c}\right)^2 \approx \begin{cases} (\kappa_i d)^2 + Z\,\frac{(4\varepsilon)^2}{(\kappa_i d)^2}, \\ (\kappa_i d)^2. \end{cases} \tag{172}$$

In the regime $q_{1\perp} d < q_x d < q_{2\perp} d$, $\omega_{\mathrm{T}-}$ is a photon-like mode while $\omega_{\mathrm{T}+}$ is a plasmon-like mode in contrast to the regime $q_x d \ll q_{1\perp} d$. For $q_x d \gg q_{2\perp}$, $\omega_{\mathrm{T}-}$ is again a plasmon-like mode and $\omega_{\mathrm{T}+}$ is again a photon-like mode, see appendix A.2.4. As $\varepsilon/(\kappa_i d) < 1$, the deviation of $\omega_{\mathrm{T}+}$ from the photon dispersion $\omega_{\mathrm{Ph}\perp}$ is smaller at $q_x d = q_{i\perp} d$ than at $q_x d = 0$ and it is further smaller at $q_{2\perp} d$ than at $q_{1\perp} d$. The deviation of $\omega_{\mathrm{T}-}$ from the Luttinger dispersion is of higher order in ε^2 than the expression given in eq. (172) and thus much smaller than the deviation of the photon mode from $\omega_{\mathrm{Ph}\perp}$. The size of the gap between the two branches of the eigenmode dispersion at $q_{i\perp} d$ is in lowest order in ε^2

$$\left(\frac{\omega_{\mathrm{T}+}(q_x = q_{i\perp})d}{c}\right)^2 - \left(\frac{\omega_{\mathrm{T}-}(q_x = q_{i\perp})d}{c}\right)^2 = Z\,\frac{(4\varepsilon)^2}{(\kappa_i d)^2}. \tag{173}$$

It is smaller at $q_{2\perp}d$ than at $q_{1\perp}d$ and increases with increasing v_{F}/c. The results are displayed qualitatively in figure 6.

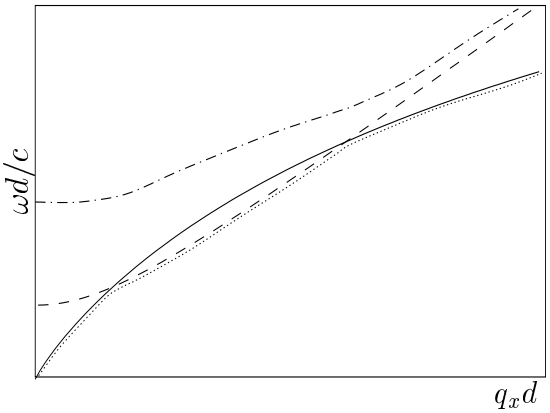

Figure 6: The Luttinger dispersion ω_{LL} (solid), the photon dispersion $\omega_{\mathrm{Ph},\perp}$ (dashes), and the corresponding branches of the eigenmode dispersion, $\omega_{\mathrm{T}+}$ (dash-dot) and $\omega_{\mathrm{T}-}$ (dots), displayed qualitatively. The deviations of the eigenmode dispersions from the dispersions of the uncoupled systems are greatly exaggerated.

Note that a gap in between the branches of the polariton dispersion opens only if the corresponding dispersion relations of the light and the Luttinger liquid cross. The crossing at $q_x d = 0$ is independent of the shape of the interaction potential but a crossing at finite $q_x d$ depends crucially on the form of V_{ee}. Apart from the fact that choosing *a priori* a finite-range interaction potential is not consistent with Maxwell equations, the light and the Luttinger dispersion *do not cross* at finite $q_x d$ if the interaction potential is not an infinitely-ranged Coulomb potential. In fact, the light and the Luttinger dispersion cross only because the slope of the Luttinger dispersion for $q_x d \to 0$ is infinitely steep which is due to the infinite range of the Coulomb potential. For a finite-range potential, the Luttinger dispersion rises linearly for small $q_x d$, see section 3.2, with a slope smaller than the slope of the light dispersion and hence the two dispersions never cross. A gap in between the branches of the dispersion relation of the plasmon-polariton at finite $q_x d$ in analogy to the phonon-polariton is hence only present when a Coulomb potential is considered.

In contrast to the plasmon in a 3D homogeneous system discussed in section 3.3, here one does not find a gap in the dispersion that exists for any value of the wave vector. This is due to the fact that the dispersion relation of the 1D plasma oscillation starts at zero frequency for a zero wave vector.

Polariton Dispersion Approached Numerically

From the above analytical approaches for $N = 3$, $M = 1$ and $N = M = 1$, it is clear what to expect qualitatively for dispersion relation of the plasmon polariton near the crossing of light and Luttinger dispersion. Nothing is yet known about the regime $q_x d \gg q_{2\|} d$. In the following, this regime is probed numerically: The determinant of $\boldsymbol{M_{\mathbf{TT}}}^{-1}$ is evaluated for arbitrary q_x and ω, then q_x and ω are varied in order to find a zero of $\det[\boldsymbol{M_{\mathbf{TT}}}^{-1}]$. The search for the zeroes of the determinant of $\boldsymbol{M_{\mathbf{TT}}}^{-1}$ is concentrated on the regime close to the light and the Luttinger dispersions as away from these dispersions $\boldsymbol{M_{\mathbf{TT}}}^{-1}$ cannot be singular, see above. As the determinant has to be evaluated quite often during the search for zeroes, this search becomes very slow for $N, M > 9$.

It is found that the determinant of $\boldsymbol{M_{\mathbf{TT}}}^{-1}$ has zeroes for q_x and ω close to the Luttinger dispersion relation, see figure 7. As the determinant exhibits sign changes in connection with these roots, this mode is quite easy to find and can be evaluated to a relative accuracy as small as 10^{-10}. The mode is called plasmon-like as for $q_x d \gg q_{2\|} d$ it shows only plasmon like behaviour. It lies below the Luttinger dispersion, $\omega_{\mathrm{T,LL}}(q_x) < \omega_{\mathrm{LL}}(q_x)$. The exact quantitative result for this plasmon-like mode depends on the number of abscissas chosen. The relative deviation of the Luttinger dispersion from the corresponding branch of the eigenmode is defined as

$$\Delta_{\mathrm{LL}}(q_x) = \frac{\omega_{\mathrm{LL}}(q_x) - \omega_{\mathrm{T,LL}}(q_x)}{\omega_{\mathrm{LL}}(q_x)}, \tag{174}$$

see figure 8. The definition was chosen in order to ensure $\Delta_{\mathrm{LL}} > 0$. The relative deviation Δ_{LL} is of the order 10^{-6}. It increases with increasing N, M, but figure 8 indicates a convergence of Δ_{LL} with increasing N, M. Further, the relative deviation Δ_{LL} decreases with increasing $q_x d$. This is due to the fact that with increasing $q_x d$ the dispersion relations of the light and of the Luttinger liquid move further apart and hence the coupling between charges and electromagnetic field becomes weaker.

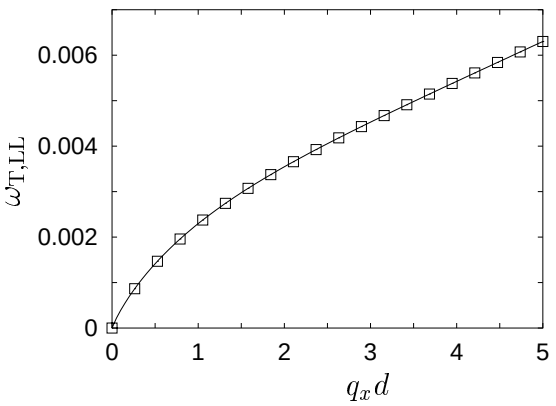

Figure 7: The Luttinger dispersion ω_{LL} (solid) and the numerically found eigenmode $\omega_{\mathrm{T,LL}}$ for $N = M = 9$ ($\square$) and $v_{\mathrm{F}}/c = 10^{-3}$. The smallest value for $q_x d$ is 10^{-4}.

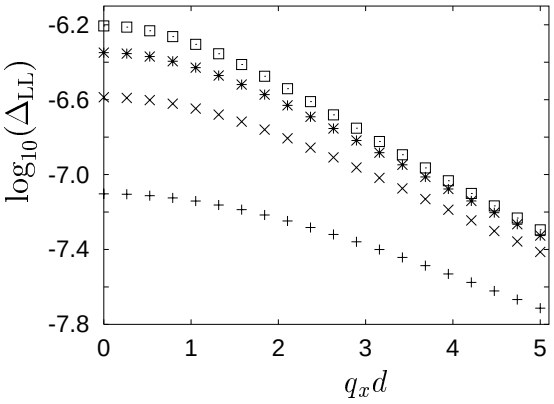

Figure 8: The logarithm (base 10) of the relative deviation of the plasmon-like mode from the Luttinger dispersion for $v_{\mathrm{F}}/c = 10^{-3}$ and $N = M = 3$ (+), $N = M = 5$ ($\times$), $N = M = 7$ ($*$), and $N = M = 9$ ($\square$).

The light dispersion is here denoted by $\omega_{\mathrm{Ph},nm}(q_x)$, it also depends on N and M, and follows from $\omega_{\mathrm{Ph}\perp}$ by replacing $q_y = 4\nu_{N,n}/d$ and $q_z = 4\nu_{M,m}/d$. When $\nu_{N,n}$ and $\nu_{M,m}$ are both equal to zero, the light dispersion $\omega_{\mathrm{Ph},nm}$ corresponds to $\omega_{\mathrm{Ph}\|}$, otherwise $\omega_{\mathrm{Ph},nm}$ corresponds to $\omega_{\mathrm{Ph}\perp}$. Hence, one obtains a dispersion that correspond to $\omega_{\mathrm{Ph}\|}$ when $n = m = 2$ for $N = M = 3$, when $n = m = 3$ for $N = M = 5$, when $n = m = 4$ for $N = M = 7$, when $n = m = 5$ for $N = M = 9$, and so on. For all other combinations of n, m and N, M, the dispersion $\omega_{\mathrm{Ph},nm}$ corresponds to $\omega_{\mathrm{Ph}\perp}$ where the explicit value of $|\vec{Q}|d$ depends on these combinations,

$|\vec{Q}|d = d[(4\nu_{N,n})^2 + (4\nu_{M,m})^2]^{1/2}$. Further, the choice of the abscissas depends on a rule given in appendix A.2.1.

Now, for q_x and ω close to these light dispersions $\omega_{\mathrm{Ph},nm}$, zeroes of the determinant of $\boldsymbol{M}_{\mathbf{TT}}{}^{-1}$ are found which are not always accompanied by a change of sign: A zero is sometimes related to an extremum which is zero at its smallest (for a minimum) or its largest (for a maximum) value. These zeroes are difficult to find. Further, one sometimes obtains even two or more zeroes lying very close together. These double or triple zeroes are attributed to the finite number of abscissas and are assumed to merge into one single zero for $N, M \to \infty$, see also the discussion in appendix A.2.4. In the dispersion relations displayed in the following, one of the zeroes was selected in order to represent the eigenmode dispersion relation and consequently the exact quantitative behaviour of this dispersion depends on the choice of the zero. The overall qualitative behaviour, however, is independent of this choice. The relative accuracy lies roughly in between 10^{-10} and 10^{-6}. The branch of the eigenmode whose dispersion lies in the vicinity of a light dispersion is called photon-like.

Despite the encountered difficulties, the mode $\omega_{\mathrm{T,Ph},nm}(q_x)$ is always present and lies slightly above the corresponding light dispersion, $\omega_{\mathrm{T,Ph},nm}(q_x) > \omega_{\mathrm{Ph},nm}(q_x)$. The relative deviation of the photon-like branch from the photon dispersion is

$$\Delta_{\mathrm{Ph},nm}(q_x) = \frac{\omega_{\mathrm{T,Ph},nm}(q_x) - \omega_{\mathrm{Ph},nm}(q_x)}{\omega_{\mathrm{Ph},nm}(q_x)}. \tag{175}$$

The definition was chosen in order to ensure $\Delta_{\mathrm{Ph},nm} > 0$. Four photon dispersions for different discrete values of Q at $N = M = 7$ and the corresponding branches of the eigenmode dispersion are displayed in figure 9. The photon dispersion with $n = m = 4$ for $N = M = 7$ in figure 9 corresponds to $\omega_{\mathrm{Ph}\parallel}$. The relative deviations between photon dispersions and photon-like modes are shown in figure 10, but only for the photon modes which correspond to $\omega_{\mathrm{Ph}\perp}$. The deviation decreases with increasing q_x and with increasing Q, i.e. with increasing distance of the light dispersion from the Luttinger dispersion indicating that the coupling between charge excitations and electromagnetic fields decreases. Figures 11 and 12 display the relative deviation for the photon mode that corresponds to $\omega_{\mathrm{Ph}\parallel}$ for $N, M = 3,\ 5,\ 7,\ 9$. The data in the two figures is the same, the only difference is that $q_x d$ is displayed logarithmically in figure 12 but not in figure 11 and that the range of $q_x d$ is smaller in figure 12 than in figure 11. The deviation is much larger than the one displayed in figure 10 and even diverges for $q_x d \to 0$. This is due to the fact that $\Delta_{\mathrm{Ph},nm}$ in eq. (175) contains a $\omega_{\mathrm{Ph},nm}$ in the denominator which goes to zero with $q_x d \to 0$ for the data in figures 11 and 12. Further, the deviation decreases with increasing N, M but shows a tendency to convergence.

In figures 11 and 12, the relative deviation of the photon-like eigenmode from the photon dispersion diverges for $q_x d \to 0$ because $\omega_{\mathrm{Ph},nm} \to 0$. As an alternative, consider the absolute deviation, i.e. $\Delta_{\mathrm{Ph},nm} \cdot \omega_{\mathrm{Ph},nm}$, which should remain finite for $q_x d \to 0$. In figure 13, this absolute deviation of the photon-like mode $\omega_{\mathrm{T,Ph},nm}$ that corresponds to $\omega_{\mathrm{T,Ph}\parallel}$ from the photon dispersion that corresponds to $\omega_{\mathrm{Ph}\parallel}$ is displayed. This absolute deviation indeed converges to a finite value for $q_x d \to 0$. That the absolute deviation does not vanish with $q_x d \to 0$ indicates that $\omega_{\mathrm{T,Ph}nm}$

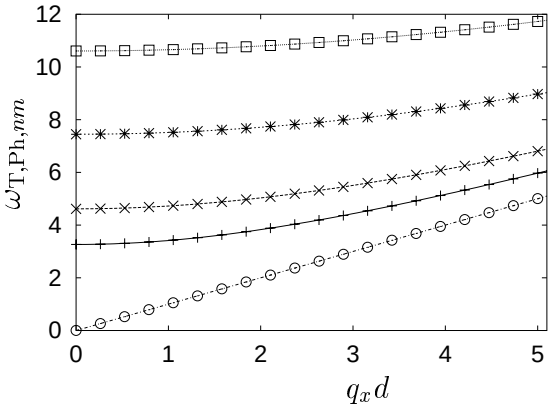

Figure 9: The photon dispersions $\omega_{\mathrm{Ph},nm}$ (lines) and the numerically obtained branches of the eigenmode $\omega_{\mathrm{T,Ph},nm}$ (symbols) for $N = M = 7$ and $n = m = 4$ (dash-dotted, $\circ$), $n = 4$, $m = 5$ (solid, $+$), $n = 4$, $m = 7$ (long dashes, $\times$), $n = 5$, $m = 5$ (short dashes, $*$) $n = 5$, $m = 6$ (dotted, $\Box$) for $v_{\mathrm{F}}/c = 10^{-3}$.

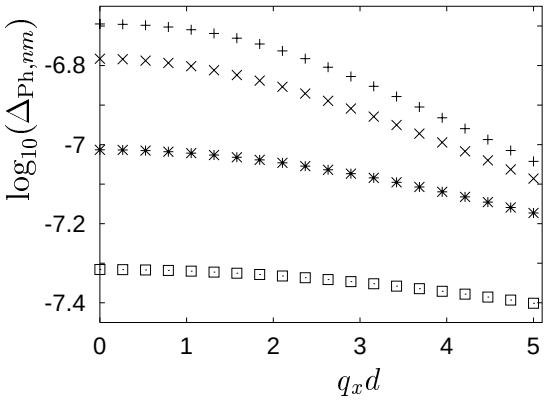

Figure 10: The logarithm (base 10) of the relative deviation of the photon-like mode from the photon dispersion for $v_{\mathrm{F}}/c = 10^{-3}$, $N = M = 7$, and $n = 4$, $m = 5$ ($+$), $n = 4$, $m = 7$ ($\times$), $n = 5$, $m = 5$ ($*$) $n = 5$, $m = 6$ ($\Box$).

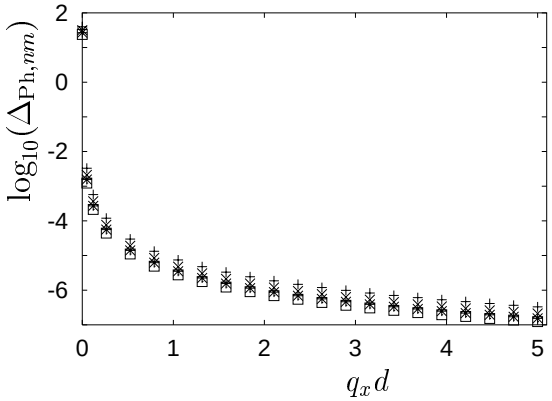

Figure 11: The logarithm (base 10) of the relative deviation of the photon-like mode that corresponds to $\omega_{\mathrm{T,Ph}\|}$ from the photon dispersion that corresponds to $\omega_{\mathrm{Ph}\|}$ for $v_{\mathrm{F}}/c = 10^{-3}$ and $N = M = 3$ with $n = m = 2$ ($+$), $N = M = 5$ with $n = m = 3$ ($\times$), $N = M = 7$ with $n = m = 4$ ($*$), $N = M = 9$ with $n = m = 5$ ($\Box$).

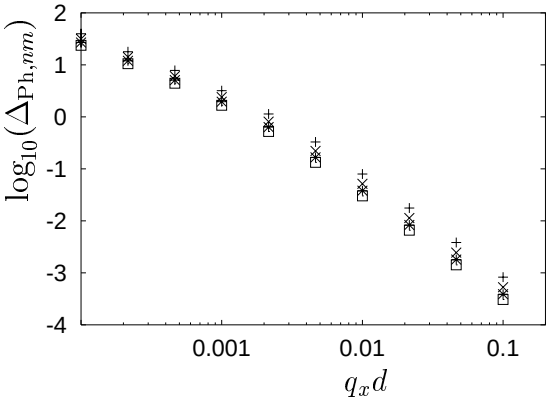

Figure 12: Same data as in figure 11 but on a logarithmic scale in $q_x d$ and in the regime $10^{-4} < q_x d < 10^{-1}$.

does not go to zero with $q_x d \to 0$. This finding is qualitatively in accordance with the behaviour of the photon-like eigenmodes derived analytically for $N = 3$, $M = 1$ and $N = M = 1$, see for example eq. (167).

The absolute deviation of the plasmon-like mode, from the corresponding dispersion, $\Delta_{\mathrm{LL}} \cdot \omega_{\mathrm{LL}}$, goes to zero with $q_x d \to 0$, see figure 14. Here, the deviation increases with increasing N, M. That the absolute deviation of plasmon-like mode and Luttinger dispersion vanishes for $q_x d \to 0$ is in accordance with the behaviour of the plasmon-like mode derived analytically for $N = 3$, $M = 1$ and $N = M = 1$, see eq. (166).

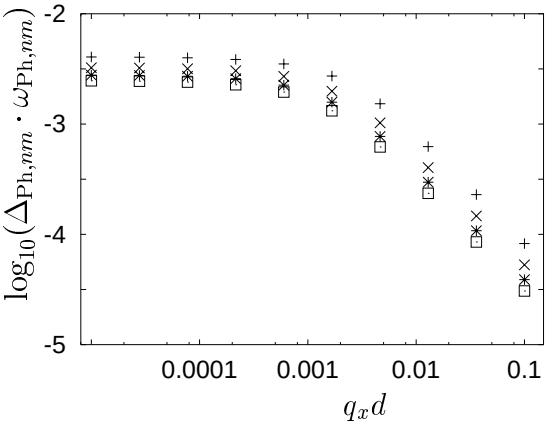

Figure 13: The logarithm (base 10) of the absolute deviation of the photon-like mode that corresponds to $\omega_{\mathrm{T,Ph}\|}$, $n = \mathrm{int}(N/2)+1$ and $m = \mathrm{int}(M/2)+1$, from the corresponding dispersion for $v_{\mathrm{F}}/c = 10^{-3}$ and $N = M = 3$ (+), $N = M = 5$ ($\times$), $N = M = 7$ ($*$), and $N = M = 9$ ($\Box$).

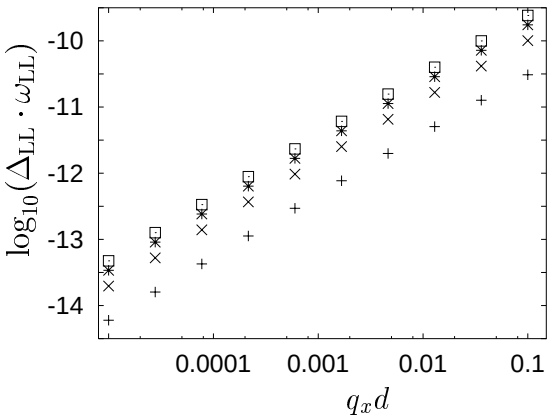

Figure 14: The logarithm (base 10) of the absolute deviation of the plasmon-like mode from the corresponding dispersion for $v_{\mathrm{F}}/c = 10^{-3}$, and $N = M = 3$ (+), $N = M = 5$ ($\times$), $N = M = 7$ ($*$), and $N = M = 9$ ($\Box$).

Further, in the above analytic results for the dispersion relation of the plasmon-polariton for $N = 3$, $M = 1$ and $N = M = 1$, the deviation of the branches of the polariton dispersion from the light and the Luttinger dispersion increases with increasing v_{F}/c, indicating that the coupling between charge excitations and electromagnetic field depends on v_{F}/c. The numerical results displayed so far were all obtained for fixed $v_{\mathrm{F}}/c = 10^{-3}$. The relative deviations of several branches of the eigenmode dispersion for different v_{F}/c are displayed in figures 15 - 18. The deviations increase with increasing v_{F}/c in accordance to the analytic findings.

In analogy to the phonon-polariton discussed in section 2.2.3 and to the plasmon in a 3D homogeneous system discussed in section 3.3, the branches of the polariton dispersion for away from the gap are practically identical to the photon and the plasmon dispersions of the uncoupled systems.

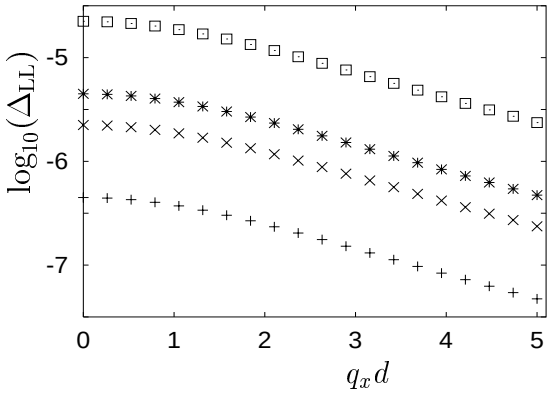

Figure 15: The logarithm (base 10) of the relative deviation of the plasmon-like mode from the Luttinger dispersion for $N = M = 7$ and $v_{\mathrm{F}}/c = 10^{-3}$ (+), 5×10^{-3} (×), 10^{-2} (∗), and $\times 10^{-2}$ (□).

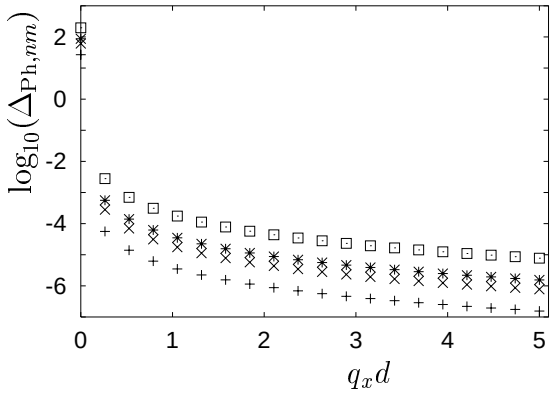

Figure 16: The logarithm (base 10) of the relative deviation of the photon-like mode that corresponds to $\omega_{\mathrm{T,Ph}\parallel}$ from the corresponding photon dispersion for $N = M = 7$, $n = m = 4$, and $v_{\mathrm{F}}/c = 10^{-3}$ (+), 5×10^{-3} (×), 10^{-2} (∗), and 5×10^{-2} (□).

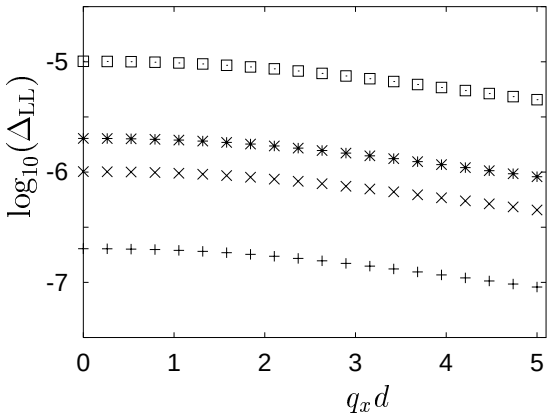

Figure 17: The logarithm (base 10) of the relative deviation of a photon-like mode that corresponds to $\omega_{\mathrm{T,Ph}\perp}$ from the corresponding photon dispersion for $N = M = 7$, $n = 4$, $m = 5$, and $v_{\mathrm{F}}/c = 10^{-3}$ (+), 5×10^{-3} (×), 10^{-2} (∗), and 5×10^{-2} (□).

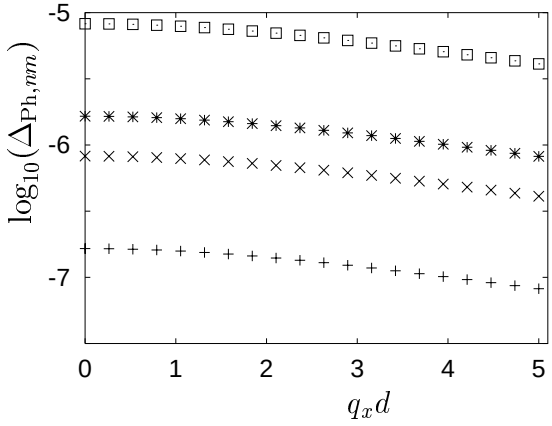

Figure 18: The logarithm (base 10) of the relative deviation of a photon-like mode that corresponds to $\omega_{\mathrm{T,Ph}\perp}$ from the corresponding photon dispersion for $N = M = 7$, $n = m = 5$, and $v_{\mathrm{F}}/c = 10^{-3}$ (+), 5×10^{-3} (×), 10^{-2} (∗), and 5×10^{-2} (□).

4.4.3 Induced Transverse Field

In the following, we estimate the magnitude of the induced transverse field based on the discretization procedure employed in section 4.4.2.

The explicit form of the local transverse field as a function of q_x and ω for discrete values of q_y and q_z can be obtained using the matrix-form of the local-field equations in eq. (162). Based on the usual technique for the solution of coupled linear equations [285], the local transverse field is expressed in terms of the determinant of the matrix $\boldsymbol{M_{TT}}^{-1}$ and the determinant of another matrix $\boldsymbol{M_{TT}^{ext,i}}$ which is obtained from $\boldsymbol{M_{TT}}^{-1}$ by replacing the ith column in $\boldsymbol{M_{TT}}^{-1}$ with the discretized vector of the external field, see appendix A.2.2.

We evaluate the determinants of the matrices $\boldsymbol{M_{TT}}^{-1}$ and $\boldsymbol{M_{TT}^{ext,i}}$ analytically. As the dimension of the matrices is $(3NM \times 3NM)$, such an evaluation can only be performed for very small N, M, i.e. a very small number of abscissas. Following the discussion in section 4.4.2, we choose $N = 2$ with $q_y = \pm 4\varepsilon/d$ and $M = 1$ with $q_z = 0$. The details of the evaluation can be found in appendix A.2.5. The result obtained for the induced transverse field, i.e. the local transverse field minus the external transverse field, is

$$E^x_{\mathrm{T,ind}}(q_x, q_y = \pm 4\varepsilon/d, q_z = 0, \omega) \approx E_{\mathrm{T,ext,av}}(q_x, \omega) \tag{176}$$

$$\times \left\{ \frac{\zeta'_+(q_x,\varepsilon)}{[(\omega d/c)^2 - (\omega_{\mathrm{T}+}(q_x)d/c)^2]} - \frac{\zeta_-(q_x,\varepsilon)}{[(\omega d/c)^2 - (\omega_{\mathrm{T}-}(q_x)d/c)^2]} \right.$$

$$\left. - \frac{\zeta'_+(q_x,\varepsilon)\,\zeta_-(q_x,\varepsilon)}{[(\omega d/c)^2 - (\omega_{\mathrm{T}+}(q_x)d/c)^2]\,[(\omega d/c)^2 - (\omega_{\mathrm{T}-}(q_x)d/c)^2]} \right\},$$

where $E_{\mathrm{T,ext,av}}(q_x, \omega)$ is the external transverse field integrated with respect to $\vec{R}$. The eigenmode dispersions $\omega_{\mathrm{T}\pm}(q_x)$ were discussed in section 4.4.2 and are explicitly given in appendix A.2.4, the quantity d is the diameter of the wire. The functions $\zeta'_+(q_x,\varepsilon)$ and $\zeta_-(q_x,\varepsilon)$ are of the order of Z, see eq. (165), or smaller, i.e. they are dominated by the ratio v_{F}/c. Their magnitude is determined by the deviation of the local-field eigenmode dispersion from the dispersion of the uncoupled systems.

The expression for the induced transverse field given in eq. (176) diverges when q_x and ω are chosen such that $\omega = \omega_{\mathrm{T}\pm}(q_x)$. This implies that the Fourier transform $q_x \to x$ is dominated by these poles, i.e. the behaviour of the induced transverse field along x is governed by the eigenmode dispersion $\omega_{\mathrm{T}\pm}(q_x)$. The magnitude of the induced transverse field as a function of x is given by the residue of the expression in eq. (176) at the poles. These residue are mainly the functions $\zeta'_+(q_x,\varepsilon)$ and $\zeta_-(q_x,\varepsilon)$. Hence, the induced transverse field as a function of x is suppressed with respect to the external transverse field by a factor v_{F}/c! Following the discussion in appendix A.2.5, the induced transverse field is also strongly suppressed with respect to an external longitudinal field. Its influence on transport may therefore be neglected.

Even though this result was obtained for a very small number of abscissas, we believe it to be generally valid. With increasing N and M, the results for $\det[\boldsymbol{M_{TT}}^{-1}]$

and $\det[\boldsymbol{M}^{\mathbf{ext},i}_{\mathbf{TT}}]$ become extremely complicated but the overall structure of these results remains unchanged. As a consequence, also the structure of the expression of the induced transverse field remains unchanged: in $\vec{q}$-space it contains poles exactly at the local-field eigenmode dispersions and the corresponding residue are governed by v_{F}/c.

4.5 Summary

The transport equation of a confined 3D quantum wire was derived in section 4.1 using linear response theory. A single-channel wire was modelled by assuming only the lowest subband to be occupied and neglecting transitions to empty bands. The validity of this assumption was discussed and it was found that inter-band transitions may be neglected when one is interested in the component of the current parallel to the wire, or in other words, when the component of the driving electric field parallel to the wire is the dominant one. For the single-channel quantum wire, an explicit expression for the conductivity including Coulomb interactions was derived using the Luttinger model. Even for the single-channel wire, the current is given by an integral instead of an algebraic relation – in contrast to true 1D systems – due to the anisotropic nature of the quasi 1D quantum wire.

The dc and ac transport properties of the clean single-channel quantum wire were shortly discussed in sections 4.2 and 4.3.

The transport equation of the single-channel wire was used in order to close self-consistently the local-field equations, see section 4.3. Two coupled integral equations were obtained. Considering an external longitudinal field and neglecting the induced transverse field, an explicit expression for the projected local longitudinal field was derived in section 4.4.1. It was shown that using the conductivity of the interacting system in combination with the projected external field is equivalent to using the conductivity of the non-interacting system in combination with the projected local field. This result is based on the fact that linear response is exact in a Luttinger liquid.

Then, the local-field equations were tackled via a discretization of the integral equations. The local-field equations yield a non-trivial solution also in the absence of an external field for certain combinations of the frequency and the wave vector. These combinations determine the dispersion relation of the local-field eigenmodes. In analogy to the phonon-polariton this eigenmode was called plasmon-polariton.

Considered as a function of $q_x d$ instead of $|\vec{q}|d$, the polariton dispersion consists of infinitely many branches, namely one for each $|\vec{Q}|$ plus one emerging from the plasmon dispersion. The branches of the polariton dispersion lie close to either the photon or the Luttinger dispersion, which represent the elementary excitations of the uncoupled systems. The light dispersion $\omega_{\mathrm{Ph}\|}$ and the plasmon dispersion ω_{LL} cross at $dq_{1\|} = 0$ and at $dq_{2\|}$ while the corresponding eigenmode dispersions $\omega_{\mathrm{T,Ph}\|}$ and $\omega_{\mathrm{T,LL}}$ repel each other at $dq_{1\|}$ and cross near $dq_{2\|}$. The absence of repulsion at $dq_{2\|}$ is due to symmetry reasons. Further, the light dispersion $\omega_{\mathrm{Ph}\perp}$ and the plasmon dispersion ω_{LL} cross at $dq_{1\perp}$ and at $dq_{2\perp}$ if Q is sufficiently small. The corresponding branches of the eigenmode dispersion exhibit repulsion at both, $dq_{1\|}$ and $dq_{2\|}$. The

coupling strength and hence the deviation of the eigenmode dispersion from the photon or the plasmon dispersion is governed by the ratio v_F/c. These results for the dispersion relation of the plasmon-polariton are in analogy with the phonon-polariton.

The gap in the polariton dispersion opens for extremely small values of the wave vector. However, when inter-band transitions are taken into account, at least one branch of the dispersion relation of the charge system starts at finite frequency for a zero wave vector. Hence, the point of intersection between light and charge dispersion moves to much larger values of the wave vector and so does the gap in the dispersion. For a subband spacing of 5 meV, the gap in the polariton dispersion would roughly open around $q \approx 3 \times 10^4$ m^{-1}. This value for the wave vector is of the same order of magnitude as the wave vector for which the dispersion of the phonon-polariton shows a gap [5].

Finally, we estimated the magnitude of the induced transverse field in section 4.4.3. We showed that it is suppressed by a factor v_F/c with respect to the external field. Its influence on transport may hence be neglected.

5 Dirty Quantum Wire

In this section, transport and local fields in a "dirty" quantum wire, i.e. a quantum wire containing a potential barrier, are studied. First, the transport equation of the dirty wire is derived in section 5.1. Due to the presence of the barrier *and* electron-electron interactions, the dirty wire exhibits a non-linear dc current-voltage characteristic as discussed in section 5.2. It is thus an ideal system in order to investigate higher harmonic generation in time-dependent transport: Driven by a monochromatic field with frequency $\omega_{\rm ext}$, the current oscillates in time with frequencies $n\omega_{\rm ext}$, n integer. The corresponding non-linear time-dependent current is studied in detail in section 5.3. The influence of local fields on this current is discussed in section 5.4. Finally, the electromagnetic fields emitted by the time-dependent current and the corresponding emitted power are investigated in section 5.5.

5.1 Transport Equation

Hamiltonian

Before the transport equation for the dirty single-channel quantum wire is evaluated, it is clarified how the Hamiltonian that describes this wire looks like. We use the projected Hamiltonian derived in section 3.1 and set all summation indices to zero. The electron-electron interaction is treated within the Luttinger model, see section 3.2. The Hamiltonian describing the barrier is given in eq. (35). The extension of the barrier perpendicular to the wire is assumed to be much larger than the diameter of the wire, thus its shape along $\vec{R}$ is approximately constant. The barrier is positioned at $x = 0$ and is assumed to have the shape of a delta-function along x, $U_{\rm bar}(\vec{r}) = U_{\rm bar}\delta(x)$. Then, in the Luttinger formalism, one obtains for the single-channel wire [65, 63, 66]

$$H^{\rm MB}_{\rm bar,1b} = U_{\rm bar}\cos[2\sqrt{\pi}\vartheta(x=0)]. \tag{177}$$

The bosonic field operator $\vartheta(x)$ is given in eq. (60).

In the part of the Hamiltonian describing the coupling of the wire to the electromagnetic field, see eq. (33), the term quadratic in the vector potential is omitted in order to be consistent with the linearization of the dispersion relation in the Luttinger model. Local fields are neglected for the moment to be discussed later in section 5.4. Then

$$H^{\rm MB}_{\rm em,1b} = e\int {\rm d}x\,\rho_{00}(x)\varphi_{\rm ext,1b}(x,t) - e\sum_\alpha \int {\rm d}x j^\alpha_{00}(x)A^\alpha_{\rm ext,1b}(x,t), \tag{178}$$

where $\varphi_{\rm ext,1b}(x,t)$ and $A^\alpha_{\rm ext,1b}(x,t)$ are the projected 3D external potentials,

$$\varphi_{\rm ext,1b}(x,t) = \int {\rm d}\vec{R}\,B^x_{00}(\vec{R})\,\varphi_{\rm ext}(x,\vec{R},t), \tag{179}$$

$$A^\alpha_{\rm ext,1b}(x,t) = \int {\rm d}\vec{R}\,B^x_{00}(\vec{R})\,A^\alpha_{\rm ext}(x,\vec{R},t). \tag{180}$$

The projected external electric field parallel to the wire is related to the projected potentials via

$$E^x_{\mathrm{ext,1b}}(x,t) = -\partial_x \varphi_{\mathrm{ext,1b}}(x,t) - \partial_t A^x_{\mathrm{ext,1b}}(x,t). \tag{181}$$

The components of the external field perpendicular to the wire are chosen to be zero. For the particle density operator and the particle current density operator in eq. (178), $\rho_{00}(x)$ and $j^x_{00}(x)$, the Luttinger representations given in eqs. (65) and (66) are used.

Transport Equation in the Weak Tunneling Regime

Now, based on the above Hamiltonian, the current as a function of the driving electric field is evaluated. The space- and time-dependent current density is given by the expectation value of the 3D current density operator. Here and in the following, only the component of the current parallel to the wire is considered. In the single-channel system, following eq. (22), the current density operator $j^x(\vec{r},t)$ is given by the function $B^x_{00}(\vec{R})$, which contains the eigenfunctions of confinement potential, times the 1D current density operator $j^x_{00}(x,t)$. Using the Luttinger representation for $j^x_{00}(x,t)$, see eq. (66), yields for the x-component of the current density in the wire

$$J^x(\vec{r},t) = -\frac{e}{\sqrt{\pi}}\, B^x_{00}(\vec{R})\, \langle \partial_t \vartheta(x,t) \rangle. \tag{182}$$

Hence, one has to determine the time evolution of the bosonic field operator $\vartheta(x)$, given in eq. (60), in order to evaluate the current. This time evolution is governed by the Hamiltonian of the total system, including the barrier, $H^{\mathrm{MB}}_{\mathrm{bar,1b}}$, and the electromagnetic fields, $H^{\mathrm{MB}}_{\mathrm{em,1b}}$. An exact evaluation of the time evolution of $\vartheta(x)$ is in general impossible.

For a large barrier, the time evolution of the bosonic field operator $\vartheta(x,t)$ and hence the current can be evaluated in lowest order in the tunneling probability Δ^2 of the barrier by mapping the Luttinger liquid with impurity onto a dissipative quantum system, for details see appendix B.1 and [63, 179, 282, 295]. One obtains for the current at the position of the barrier [9]

$$J^x(x=0,\vec{R},t) = e\Delta^2\, B^x_{00}(\vec{R}) \int_0^\infty \mathrm{d}\tau\, \mathrm{e}^{-S(\tau)} \sin[R(\tau)] \sin\left[\frac{e}{\hbar}\int_{t-\tau}^{t} \mathrm{d}t'\, V_{\mathrm{eff}}(t')\right]. \tag{183}$$

Here, Δ^2 is the probability for one electron to tunnel through the barrier. The function $B^x_{00}(\vec{R})$ governs the behaviour of the current along $\vec{R}$, see eq. (42). The functions $S(t)$ and $R(t)$ are given in appendix B.1. Their explicit form depends on the shape of the interaction potential. For a zero-range interaction, algebraic expressions can be given for $S(t)$ and $R(t)$, see appendix B.1, while for a finite-range interaction they have to be evaluated numerically [9, 282]. The effective driving voltage $V_{\mathrm{eff}}(t)$ is [9]

$$V_{\mathrm{eff}}(t) = \int_{-\infty}^{\infty} \mathrm{d}x \int_{-\infty}^{t} \mathrm{d}t'\, E^x_{\mathrm{ext,1b}}(x,t')\, r(x,t-t'). \tag{184}$$

The field $E^x_{\mathrm{ext,1b}}(x,t)$ is the projected driving field as defined in eq. (140) and the function

$$r(x,\omega) = \frac{\sigma^{xx}_{\mathrm{1b},d=0}(x,\omega)}{\sigma^{xx}_{\mathrm{1b},d=0}(0,\omega)} \tag{185}$$

contains the conductivity of the clean quantum wire of zero diameter, see eq. (145). The explicit form of $\sigma^{xx}_{\mathrm{1b},d=0}$ and hence of $r(x,\omega)$ depends on the shape of the interaction potential. Thus, the effective potential $V_{\mathrm{eff}}(t)$ depends on the shape of the interaction potential via the function $r(x,t-t')$ and on the spatial shape of the driving electric field via $E^x_{\mathrm{ext,1b}}(x,t')$.

The expression for the current in eq. (183) represents the current at the position of the barrier, i.e. at $x=0$. The current at any position x is related to the current at the barrier via, see appendix B.1 and [176],

$$J^x(x,\vec{R},\omega) \;=\; J^x_{\mathrm{clean}}(x,\vec{R},\omega) - r(x,\omega)\, J^x_{\mathrm{clean}}(0,\vec{R},\omega) + r(x,\omega)\, J^x(0,\vec{R},\omega). \tag{186}$$

Here, the current denoted by J^x_{clean} is the linear current in the clean quantum wire studied in section 4.1. Note that the expression in eq. (186) was originally derived for a true 1D wire of zero diameter [176], hence J^x_{clean} should be the linear current in a wire of zero diameter, see eq. (143). In order to account for a wire of finite diameter one might replace the delta-function $\delta(\vec{R})$ which then governs the $\vec{R}$-dependence of J^x_{clean} by the function $B^x_{00}(\vec{R})$. However, the ensuing expression for the linear current is not equivalent to the expression for the linear current in a quantum wire of finite diameter derived in section 4.1. In order to be consistent with the results of section 4.1 one should thus use eq. (186) only for a truely 1D wire.

For a delta-form electric field localized at the barrier and an infinitely thin wire, the two linear currents in eq. (186) cancel exactly. This is true for any shape of the interaction potential. Assuming in addition a zero-range interaction potential – then the dispersion relation of the elementary excitations of the Luttinger liquid is $\omega_{\mathrm{LL}} = |q_x| v_{\mathrm{F}}/g$, where the interaction parameter g renormalizes the Fermi velocity in the presence of interactions – one obtains for the spatial shape of the non-linear current density

$$J^x(x,\vec{R},\omega) = \mathrm{e}^{\mathrm{i}|x|\omega g/v_{\mathrm{F}}} J^x(x=0,\vec{R},\omega). \tag{187}$$

The current is distributed symmetrically around the barrier as it depends on the modulus of x. It further oscillates as a function of x with a spatial period of $2\pi v_{\mathrm{F}}/\omega g$.

When the tunneling probability is zero, the current at the barrier vanishes and thus the whole current is zero, see eq. (187). This is a strange result as in time-dependent transport one would expect finite currents in the two disconnected parts of the wire. The result is due to the fact that the electric field is localized at the barrier. The electrons left and right of the barrier do not feel the field. For an extended electric field, the two linear currents in eq. (186) do not cancel and as they are independent of the tunneling probability they survive for $\Delta^2 = 0$. Then, the current in the two disconnected parts of the wire is finite also for an infinitely high barrier. This linear current is much larger than the tunneling current because it does not depend on Δ^2, but it does not contribute to the higher harmonics discussed in section 5.3 as it oscillates only with the frequency of the driving field.

5.2 DC Transport

For a time-independent driving field, the effective driving potential in eq. (184) reduces to an integral over the electric field because in dc transport the conductivity of the clean Luttinger wire, contained in the function $r(x,\omega)$ in eq. (185), is independent of position x [176]. Hence, the dc current is determined by the external voltage drop alone and does not depend on the spatial shape of the driving electric field [176]. Further, for a zero-range interaction potential, the integration with respect to τ in the expression for the current in eq. (183) can be performed analytically. In the zero-temperature limit one obtains the well-known non-linear relation between current and driving voltage, see appendix B.2 and [65, 66],

$$J^x_{\rm dc}(\vec{R}, V_{\rm dc}) \propto V_{\rm dc}^{2/g-1}, \tag{188}$$

for $V_{\rm dc} > 0$. The parameter g describes the kind and the strength of the interaction and is given in eq. (51). For non-interacting electrons, $g = 1$, and the current is linear. For a repulsive interaction, $g < 1$, and the non-linear current is suppressed with respect to the linear current, obtained for $g = 1$, at small voltages. The stronger the interaction, the more pronounced is the suppression. With increasing driving voltage, the non-linear current can become larger than the linear one, but then one leaves the range of validity of the model, see appendix B.2.

As the current in a clean quantum wire is linear, see section 4, and the current through a dirty quantum wire consisting of *non-interacting* electrons is also linear, see eq. (188) for $g = 1$, the non-linearity of the system is obviously due to the presence of both, the barrier and the electron-electron interaction. Of course, for any barrier of intermediate height, the current would also be non-linear for non-interacting electrons as the tunneling probability then depends in a non-linear manner on the energy of the electrons and hence on the driving voltage. Here, however, the driving voltage is small in comparison to the barrier height, and the tunneling probability is independent of the voltage. The non-linearity of a dirty quantum wire containing a high tunneling barrier thus depends crucially on the presence of the electron-electron interactions.

The relation for the dc current given above in eq. (188) is valid for a zero-range interaction potential. For a finite range interaction potential it cannot be given by an analytic expression but has to be evaluated numerically as then the functions $S(t)$ and $R(t)$ appearing in eq. (183) cannot be given analytically. For a screened 3D Coulomb interaction potential projected onto the lowest subband of the quantum wire, the dc current is evaluated in [10, 191]. In the so-called Luttinger limit, i.e. for a screening length much smaller than the diameter of the wire, the dc current for finite-range interactions behaves similarly to the dc current for zero-range interactions at small driving voltages. With increasing driving voltage, however, the dc current for finite-range interactions converges to the linear current, see [10, 191].

Keeping the temperature finite and choosing a vanishing driving voltage, $k_{\rm B}T > eV_{\rm dc}$, one can show that the current varies with temperature as $\propto T^{2/g-2}$ based on eq. (357) in appendix B.2, see also [65, 66]. Thus, also the dependence of the current on temperature is non-linear and governed by the interaction strength.

The power-law dependences of the current on voltage and temperature are often referred to as "non-Fermi liquid behaviour". This is due to the fact that in Fermi liquid theory electron-electron interactions only influence prefactors and do not change the dependence of a quantity on voltage or temperature [3]. Power-law dependences like that of the dc current vs. driving voltage or vs. temperature are typical for the Luttinger model.

For experimental verifications of the non-Fermi liquid behaviour in dc transport predicted by the Luttinger model see the discussion in section 2.2.1.

5.3 AC Transport

A time-dependent driving field applied to a system exhibiting a non-linear current-voltage characteristic – like the dirty quantum wire investigated here – leads to higher harmonic generation and frequency mixing. If the system has a centre of inversion, only odd harmonics can be generated, i.e. a driving frequency ω_{ext} leads to currents at frequencies ω_{ext}, $3\omega_{\text{ext}}$, $5\omega_{\text{ext}}$ and so on. If the inversion symmetry of the system is broken also even harmonics can be generated. In particular, an ac driving field can then also lead to a dc current. In the following, the inversion symmetry of the dirty quantum wire is broken by a dc bias. The resulting dc component of the ac current is studied in section 5.3.1. Higher harmonic generation is investigated in section 5.3.2. Frequency mixing is not studied in this thesis.

5.3.1 DC Component of the AC Current

In this section, a 3D screened Coulomb potential with an inverse screening length α is chosen as interaction potential, see section 3.2. It is projected onto a quantum wire of diameter d, see section 3.1, and the regime $\alpha^{-1} \ll d$ is considered. The projected driving electric field, see eq. (140), is assumed to contain a time-independent and a time-dependent part,

$$E^x_{\text{ext,1b}}(x,t) = E^x_{\text{dc}}(x) + E^x_{\text{ac}}(x)\cos(\omega_{\text{ext}}t). \tag{189}$$

The time-independent part $E^x_{\text{dc}}(x)$ is taken into account in order to break the inversion symmetry of the wire. The voltages V_{dc} and V_{ac} are defined as the integrals over the corresponding components of the fields

$$V_{\text{dc/ac}} \equiv -\int_{-\infty}^{\infty} \mathrm{d}x\, E_{\text{dc/ac}}(x). \tag{190}$$

The spatial shape of $E^x_{\text{dc}}(x)$ does not need to be specified as the current is independent of this shape, only the total voltage drop V_{dc} is of importance. For the ac part of the field it is assumed

$$E^x_{\text{ac}}(x) = E^x_{\text{ac}}\,\mathrm{e}^{-|x|/\Lambda}, \tag{191}$$

where Λ denotes the range of the electric field. When $\Lambda \to 0$, the spatial shape of $E^x_{\text{ac}}(x)$ turns into a delta-function for $E^x_{\text{ac}} \to \infty$.

Transport via Sidebands

With the explicit forms of the interaction potential and of the driving electric field specified, the effective driving potential $V_{\text{eff}}(t)$, see eq. (184), needed in the expression for the current in eq. (183) can be evaluated, see appendix B.3.1. Then as, apart from the dc component, the driving field is monochromatic, the phase factor in eq. (183) can be expressed in terms of a sum over Bessel functions. The dc component of the ac current in the quantum wire does not depend on the position x and is hence directly given by the expression for the current at the barrier. One obtains, see appendix B.3.1 and [10],

$$J^x_{\text{ac,dc}}(x=0,\vec{R}) = \sum_{n=-\infty}^{\infty} J_n^2(|z|)\, J^x_{\text{dc}}(\vec{R}, V_{\text{dc}} + n\hbar\omega_{\text{ext}}/e), \tag{192}$$

where the index "ac,dc" denotes the dc component of the ac current and J^x_{dc} is the true dc current discussed in section 5.2. For the shape of the interaction potential chosen here, no simple algebraic expression can be given for J^x_{dc}, it has to be determined numerically. The explicit form of the argument of the Bessel function, $|z|$, depends on the spatial shape of the driving electric field and on the form of the interaction potential. The scaling of $|z|$ with frequency is discussed below. As this scaling cannot be seen directly from the analytic expression for $|z|$ but is determined numerically, the expression for $|z|$ is not given here but only in eq. (365) in appendix B.3.1.

The expression for the dc component of the ac current in eq. (192) is outwardly similar to the result obtained by Tien and Gordon [214], see the discussion in section 2.3.2. Obviously, also for interacting particles transport occurs via sidebands and the dc component of the ac current is given by the sum over the true dc current evaluated at the voltages $V_{\text{dc}}+n\hbar\omega_{\text{ext}}/e$ and weighted by the occupation probabilities of the sidebands, $J_n^2(|z|)$. The properties of the system, like for example the influence of the electron-electron interaction or the temperature dependence, are hidden in the dc current J^x_{dc}. A difference between the expression in eq. (192) and the Tien-Gordon result is the scaling of the occupation probability of the sidebands with frequency. In the Tien-Gordon current, see eq. (9), the argument of the Bessel function is $eV_{\text{ac}}/\hbar\omega_{\text{ext}}$ and it consequently scales with frequency as $1/\omega_{\text{ext}}$. Here, the argument of the Bessel function is $|z|$ whose explicit shape depends on the forms of the interaction potential and of the driving field. As is discussed below, $|z|$ exhibits a whole range of different scalings with frequency depending on the range of the driving electric field.

Consider the differential conductance $\mathrm{d}J^x_{\text{ac,dc}}/\mathrm{d}V_{\text{dc}}$ as a function of $eV_{\text{dc}}/\hbar\omega_{\text{ext}}$. Based on the details given in appendix B.3.1, it can be evaluated numerically and the results are presented in figures 19 and 20 [10]. The difference between figure 19 and figure 20 is the strength of the finite range interaction: in figure 19 the interaction parameter, see eq. (51), is $g = 0.9$ while in figure 20 it is $g = 0.5$, hence the interaction potential is stronger in figure 20 than in figure 19.

For $g = 0.9$, sharp minima are observed in the differential conductance which occur near integer values of $eV_{\text{dc}}/\hbar\omega_{\text{ext}}$. Further, the region in which the current

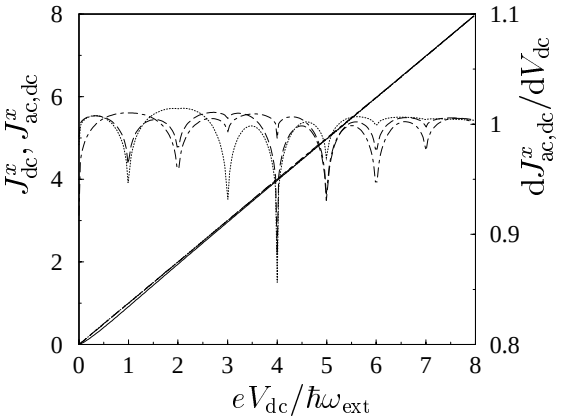

Figure 19: Currents $J^x_{\rm dc}$, $J^x_{\rm ac,dc}$, and differential conductance ${\rm d}J^x_{\rm ac,dc}/{\rm d}V_{\rm dc}$ at zero temperature as a function of $eV_{\rm dc}/\hbar\omega_{\rm ext}$ for an interaction parameter $g = 0.9$, a frequency $\omega_{\rm ext} = v_{\rm F}\alpha$, a zero-range of the electric field $\Lambda = 0$, and an ac drive of $eV_{\rm ac}/\hbar v_{\rm F}\alpha = 5$ (dotted), 6 (dashed), 7 (dash-dotted). The currents (left axis) are given in units of $\hbar v_{\rm F}\alpha/eR_{\rm T}$ and the differential conductance (right axis) is given in units of $1/R_{\rm T}$ where the tunneling resistance $R_{\rm T}$ is given in eq. (358) in appendix B.2.

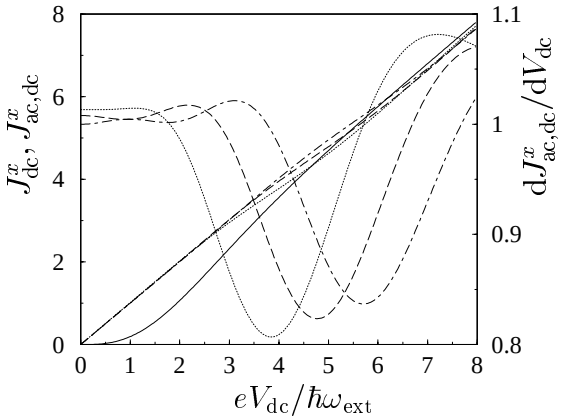

Figure 20: Currents $J^x_{\rm dc}$, $J^x_{\rm ac,dc}$, and differential conductance ${\rm d}J^x_{\rm ac,dc}/{\rm d}V_{\rm dc}$ at zero temperature as a function of $eV_{\rm dc}/\hbar\omega_{\rm ext}$ for an interaction parameter $g = 0.5$, a frequency $\omega_{\rm ext} = v_{\rm F}\alpha$, a zero-range of the electric field $\Lambda = 0$, and an ac drive of $eV_{\rm ac}/\hbar v_{\rm F}\alpha = 5$ (dotted), 6 (dashed), 7 (dash-dotted). The currents (left axis) are given in units of $\hbar v_{\rm F}\alpha/eR_{\rm T}$ and the differential conductance (right axis) is given in units of $1/R_{\rm T}$ where the tunneling resistance $R_{\rm T}$ is given in eq. (358) in appendix B.2.

$J^x_{\mathrm{ac,dc}}$ is strongly suppressed below the linear current, i.e. where it has a very shallow slope as a function of V_{dc}, $\mathrm{d}J^x_{\mathrm{ac,dc}}/\mathrm{d}V_{\mathrm{dc}} \ll 1$, is limited to $eV_{\mathrm{dc}}/\hbar\omega_{\mathrm{ext}} < 1$. One can estimate that for $eV_{\mathrm{dc}} \approx \hbar\omega_{\mathrm{ext}}$ and a not too strong interaction potential [10]

$$\frac{\mathrm{d}J^x_{\mathrm{ac,dc}}}{\mathrm{d}V_{\mathrm{dc}}} \propto \left(\frac{2}{g} - 1\right) |eV_{\mathrm{dc}} - \hbar\omega_{\mathrm{ext}}|^{2/g-2}. \tag{193}$$

Further, for $eV_{\mathrm{dc}} \approx m\hbar\omega_{\mathrm{ext}}$, m integer, it is [10]

$$\frac{\mathrm{d}J^x_{\mathrm{ac,dc}}}{\mathrm{d}V_{\mathrm{dc}}} \approx 1 - J_m^2(|z|) + \mathrm{const} \cdot J_m^2(|z|)\, |eV_{\mathrm{dc}} - m\hbar\omega_{\mathrm{ext}}|^{2/g-2}. \tag{194}$$

Hence, for $g > 2/3$, the cusp-like structure of the differential conductance in figure 19 appears due to the presence of the modulus $|eV_{\mathrm{dc}} - m\hbar\omega_{\mathrm{ext}}|$ with an exponent that is smaller than 1. The depths of the minima are approximately given by $1 - J_m^2(|z|)$ and hence depend on the ac driving voltage and on frequency. For the frequency locking effect observed in figure 19, the finite range of the interaction potential is crucial as for a zero-range interaction the effect is not present. For an increasing interaction strength, $g < 2/3$, the exponent at the modulus in eq. (194) would be bigger than one and the shape of the minima would no longer be pointed. In addition, with increasing interaction strength, the region of eV_{dc} in which $J^x_{\mathrm{ac,dc}}$ is suppressed below the linear current becomes larger than $\hbar\omega_{\mathrm{ext}}$. As a consequence, for $g = 0.5$ no minima near integer values of $\hbar\omega_{\mathrm{ext}}$ exist, see figure 20.

Scaling of the Sidebands with Frequency

Next, consider the scaling of the argument of the Bessel function $|z|$ with the ac drive and with the frequency. From the expression for $|z|$ given in appendix B.3.1 one can see that it scales linearly with the ac drive, $|z| \propto V_{\mathrm{ac}}$. The scaling with frequency is characterized by the scaling exponent ν defined by

$$\nu = -v_{\mathrm{F}}\alpha \frac{\mathrm{d}\log|z|}{\mathrm{d}\log\omega_{\mathrm{ext}}}. \tag{195}$$

The scaling exponent is displayed in figure 21 as a function of $\omega_{\mathrm{ext}}/v_{\mathrm{F}}\alpha$ for different values of $\alpha\Lambda$, where α is the inverse screening length of the interaction potential and Λ is the range of the electric field.

At small $\omega_{\mathrm{ext}}/v_{\mathrm{F}}\alpha$, one observes $\nu = 1$, or equivalently $|z| \propto \omega_{\mathrm{ext}}^{-1}$, for any of the values of $\alpha\Lambda$ displayed in figure 21. However, the smaller the value of $\alpha\Lambda$, the larger the value of $\omega_{\mathrm{ext}}/v_{\mathrm{F}}\alpha$ at which still $\nu = 1$. Thus, the scaling $|z| \propto \omega_{\mathrm{ext}}^{-1}$, which is the one also found by Tien and Gordon [214], is valid for $\Lambda \to 0$. At large $\omega_{\mathrm{ext}}/v_{\mathrm{F}}\alpha$, one observes $\nu = 2$, or equivalently $|z| \propto \omega_{\mathrm{ext}}^{-2}$, for any of the values of $\alpha\Lambda$ displayed in figure 21. This scaling is valid for $\Lambda \to \infty$; for an analytic estimate of the scaling of $|z|$ in these two limits see appendix B.3.1.

A scaling of $|z| \propto \omega_{\mathrm{ext}}^{-2}$ was also discussed in [256], see the discussion in section 2.3. But as in the work of Tien and Gordon [214], also in [256] non-interacting particles were considered.

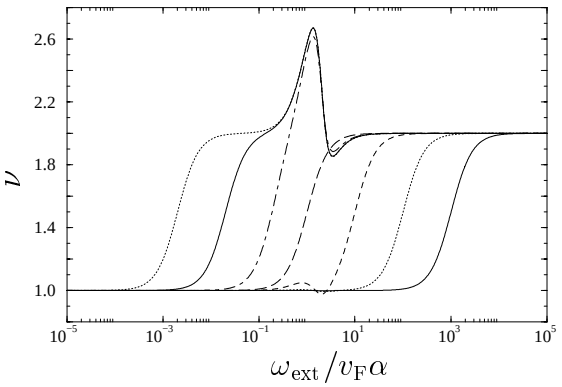

Figure 21: Scaling exponent ν, see eq. (195), of the argument $|z|$ of the Bessel functions in the expression for the current, eq. (192), as a function of $\omega_{\rm ext}/v_{\rm F}\alpha$ for ranges of the ac driving field (curves from right to left) $\alpha\Lambda = 10^{-3}$, 10^{-2}, 10^{-1}, 1, 10, 10^2, 10^3, for an interaction parameter $g = 0.5$.

It can be seen here that, first of all, the two scalings $|z| \propto \omega_{\rm ext}^{-1}$ and $|z| \propto \omega_{\rm ext}^{-2}$ which are known from the literature [214, 256] are also present in systems of interacting particles. The different scalings are due to different ranges of the driving ac electric field. Second, it is obvious from figure 21 that $|z| \propto \omega_{\rm ext}^{-1}$ and $|z| \propto \omega_{\rm ext}^{-2}$ are not the only two possible scalings of the occupation probabilities of the sidebands with frequency. The exponent ν assumes a variety of values in between 1 and ≈ 2.7.

Concluding, we state that the outward form of the Tien-Gordon expression for the dc tunneling current in the presence of an ac drive holds also for photon-assisted transport in a dirty quantum wire of interacting electrons. Due to the presence of electron-electron interactions, the dc component of the non-linear ac current shows frequency locking. Further, the scaling of the occupation probability of the sidebands with frequency varies as a function of the range of the ac electric field.

5.3.2 Harmonic Components of the AC Current

In this section, the higher harmonics of the non-linear ac current are investigated. It is for simplicity assumed that the ac component of the driving electric field has a delta-like shape and is localized at the barrier. Further, it is assumed to vary monochromatically with time. A dc component of the driving electric field is taken into account in order to break the inversion symmetry of the quantum wire. The interaction potential in the wire is chosen to be of zero range. These simplified conditions are chosen as otherwise one could not proceed analytically in the following. The effective driving voltage, see eq. (184), is then equivalent to the external driving voltage, $V_{\rm eff}(t) = V_{\rm dc} + V_{\rm ac}\cos(\omega_{\rm ext}t)$.

The Current Amplitudes

The voltage phase factor in eq. (183) can for a monochromatic driving be expressed in terms of Bessel functions, see appendix B.3.2. The resulting expression for the current at the barrier displays the generation of higher harmonics [9],

$$J^x(x=0,\vec{R},t) = B_{00}^x(\vec{R}) \sum_{n=-\infty}^{\infty} A_n(\omega_{\rm ext})\, {\rm e}^{-{\rm i}n\omega_{\rm ext}t}. \tag{196}$$

The dc component of the ac current investigated in the previous section corresponds to the term with $n = 0$ in eq. (196) and is not discussed here. The complex current

amplitude

$$A_n(\omega_{\rm ext}) = A_n^{(+)}(\omega_{\rm ext}) + {\rm i}A_n^{(-)}(\omega_{\rm ext}) \tag{197}$$

of the n-th harmonic can be expressed in terms of series over Bessel functions and a complex function $C(\zeta)$,

$$\begin{aligned} A_n^{(\pm)}(\omega_{\rm ext}) &= \frac{1}{2}\sum_{k=-\infty}^{\infty} C^{(\pm)}(V_{\rm dc} + k\hbar\omega_{\rm ext}/e)\cdot J_k\left(\frac{eV_{\rm ac}}{\hbar\omega_{\rm ext}}\right) \\ &\times \left[J_{k+n}\left(\frac{eV_{\rm ac}}{\hbar\omega_{\rm ext}}\right) \pm J_{k-n}\left(\frac{eV_{\rm ac}}{\hbar\omega_{\rm ext}}\right)\right], \end{aligned} \tag{198}$$

where the signs $(\pm)$ at the function C denote the real, $(+)$, and imaginary, $(-)$, parts of

$$C(\zeta) = {\rm i}e\Delta^2 \int_0^\infty {\rm d}\tau\, {\rm e}^{-S(\tau)} \sin[R(\tau)]\, {\rm e}^{-{\rm i}e\zeta\tau/\hbar}. \tag{199}$$

The real part of this expression is equivalent to the $\vec{R}$-independent part of the dc current following from eq. (183) by choosing a time-independent driving voltage, see section 5.2 and appendix B.2.

The expression for the higher harmonics of the current given in eq. (196) with the current amplitudes as given in eq. (198) differs from the Tien-Gordon like expression for the dc component of the ac current in two respects. First, only the real part of the current amplitude $A_n^{(+)}$ is given in terms of the true dc current. The imaginary part of the current amplitude $A_n^{(-)}$ is given in terms of the imaginary part of the function $C(\zeta)$ which, though also a dc property of the system, is *not equivalent* to the dc current. Second, the contributions to the sum in eq. (198) are not weighted by squares of Bessel functions. Here, the weights are given by combinations of Bessel functions of different orders and this difference in order is exactly the number of the harmonic of the current. Hence, the harmonic generation is related to tunneling processes via different sidebands separated in energy by $n\hbar\omega_{\rm ext}$.

The meaning of the real and imaginary parts of the current amplitude A_n becomes clear when writing the expression for the current in eq. (196) in terms of a sine and a cosine instead of an exponential. With $A_{-n}^{(+)} = A_n^{(+)}$, $A_0^{(-)} = 0$, and $A_{-n}^{(-)} = -A_n^{(-)}$, one finds that the real part of the complex current amplitude yields the in-phase part of the time-dependent current, i.e. the part of the current oscillating in phase with the driving voltage, while the imaginary part of A_n yields the out-phase part of the current,

$$\begin{aligned} J^x(x=0,\vec{R},t) &= B_{00}^x(\vec{R})\, A_0^{(+)}(\omega_{\rm ext}) + 2B_{00}^x(\vec{R})\sum_{n=1}^{\infty} A_n^{(+)}(\omega_{\rm ext})\cos(n\omega_{\rm ext}t) \\ &- 2B_{00}^x(\vec{R})\sum_{n=1}^{\infty} A_n^{(-)}(\omega_{\rm ext})\sin(n\omega_{\rm ext}t). \end{aligned} \tag{200}$$

The phase shift in the current, i.e. the presence of an out-phase part oscillating as $\sin(n\omega_{\rm ext}t)$ instead of $\cos(n\omega_{\rm ext}t)$, is due to the non-linearity of the current-voltage characteristic.

Evaluating in- and out-phase part of the current explicitly, one finds that both scale differently with the cut-off frequency ω_c. The presence of such a cut-off frequency is necessary whenever a zero-range interaction is considered in order to avoid divergencies. This cut-off frequency has to be at least of the order of the subband separation. Now, the in-phase part of the current scales in leading order as $\omega_c^{-2/g}$ for all g. The out-phase part scales in leading order as $\omega_c^{-2/g}$ for values of g above certain critical values $g_c(n)$ which depends on the number of the harmonic, $g_c(n) = 2/(n+2+s)$ with $s = [1+(-1)^n]/2$. For $g < g_c(n)$, the out-phase current scales in leading order as $\omega_c^{-(n+2+s)}$ [10]. As in this regime, the out-phase part dominates the current, in the following only the regime $g > g_c(n)$ is considered. The function $C(\zeta)$ is given for this regime in eq. (375) in appendix B.3.2. Performing the zero-temperature limit and inserting the result for $C(\zeta)$ into the above expressions for the complex current amplitudes yields in leading order in ω_c

$$\begin{aligned} A_n^{(+)}(\omega_{\rm ext}) &= \frac{\hbar\omega_c}{eR_T}\left(\frac{\omega}{\omega_c}\right)^{2/g-1}\frac{1}{2\Gamma(2/g)}\sum_{k=-\infty}^{\infty}J_k\left(\frac{eV_{\rm ac}}{\hbar\omega_{\rm ext}}\right) \\ &\times \left[J_{k+n}\left(\frac{eV_{\rm ac}}{\hbar\omega_{\rm ext}}\right)+J_{k-n}\left(\frac{eV_{\rm ac}}{\hbar\omega_{\rm ext}}\right)\right]\left|k+\frac{eV_{\rm dc}}{\hbar\omega_{\rm ext}}\right|^{2/g-1} \\ &\times \operatorname{sgn}\left(k+\frac{eV_{\rm dc}}{\hbar\omega_{\rm ext}}\right), \end{aligned} \tag{201}$$

$$\begin{aligned} A_n^{(-)}(\omega_{\rm ext}) &= \frac{\hbar\omega_c}{eR_T}\left(\frac{\omega}{\omega_c}\right)^{2/g-1}\frac{1}{2\Gamma(2/g)}\tan(\pi/g)\sum_{k=-\infty}^{\infty}J_k\left(\frac{eV_{\rm ac}}{\hbar\omega_{\rm ext}}\right) \\ &\times \left[J_{k+n}\left(\frac{eV_{\rm ac}}{\hbar\omega_{\rm ext}}\right)-J_{k-n}\left(\frac{eV_{\rm ac}}{\hbar\omega_{\rm ext}}\right)\right]\left|k+\frac{eV_{\rm dc}}{\hbar\omega_{\rm ext}}\right|^{2/g-1}. \end{aligned} \tag{202}$$

The tunneling resistance R_T is given in eq. (358) in appendix B.2. Due to the different scalings of $A_n^{(+)}$ and $A_n^{(-)}$ with the cut-off frequency, these results are only valid for interactions strengths $g > 2/3$ for $n = 1$, $g > 2/5$ for $n = 2$ and $n = 3$, $g > 2/7$ for $n = 4$ and $n = 5$, and so on.

Non-Fermi Liquid Behaviour of the Current Amplitudes

At low frequencies, $\hbar\omega_{\rm ext} < \max(eV_{\rm dc}, k_BT/g)$, one can estimate the behaviour of the complex current amplitude with the driving voltage [9], see appendix B.3.2. For $V_{\rm dc} \ll V_{\rm ac}$,

$$A_n^{(+)}(V_{\rm dc}, V_{\rm ac}, g) \propto \left(\frac{V_{\rm dc}}{V_{\rm ac}}\right)^s \left(\frac{eV_{\rm ac}}{\hbar\omega_c}\right)^{2/g-1}, \tag{203}$$

and for $V_{\rm dc} \gg V_{\rm ac}$,

$$A_n^{(+)}(V_{\rm dc}, V_{\rm ac}, g) \propto \left(\frac{eV_{\rm ac}}{\hbar\omega_c}\right)^n \left(\frac{eV_{\rm dc}}{\hbar\omega_c}\right)^{2/g-n-1}, \tag{204}$$

where the out-phase part $A_n^{(-)}$ is small in comparison to the in-phase part $A_n^{(+)}$. Obviously, also the non-linear *time-dependent* current exhibits non-Fermi liquid be-

haviour as a function of the driving voltage. Here, however, also the order of the higher harmonic enters into the exponent of the power law, see eq. (204).

At finite temperature the above results remain valid as long as $k_{\mathrm{B}}T/g < eV_{\mathrm{dc}}$ or $eV_{\mathrm{ac}} > k_{\mathrm{B}}T/g > eV_{\mathrm{dc}}$. When $eV_{\mathrm{ac}} < k_{\mathrm{B}}T/g$,

$$A_n^{(+)}(V_{\mathrm{dc}}, V_{\mathrm{dc}}, T, g) \propto \left(\frac{eV_{\mathrm{ac}}}{\hbar\omega_{\mathrm{c}}}\right)^n \left(\frac{eV_{\mathrm{dc}}}{k_{\mathrm{B}}T}\right)^s \left(\frac{k_{\mathrm{B}}T}{\hbar\omega_{\mathrm{c}}}\right)^{2/g-n-1}. \tag{205}$$

The non-Fermi liquid behaviour is then reflected by the temperature dependence of the current [9] as was already the case in dc transport, see section 5.2.

Numerical Investigation of the Current Amplitudes

The expressions for the current amplitudes given in eqs. (201) and (202) can be evaluated numerically. The sums with respect to the summation index k converge quite fast as the Bessel functions decay exponentially when the order becomes larger than the argument. The dependence of the current amplitudes on the order of the harmonic, on frequency, on the strength of dc and ac drive, and on the interaction strength are discussed below.

The modulus of the complex current amplitude $|A_n|$ as a function of the order of the harmonic for different strengths of the dc drive is displayed in figure 22. The amplitudes decrease roughly exponentially with n for the parameters chosen. Further, with decreasing strength of the dc drive, the amplitudes of the even harmonics decrease for fixed n. This is due to the fact that in the absence of the dc drive, the system exhibits inversion symmetry and thus no even harmonics can be generated. In figure 23, the modulus of the complex current amplitude $|A_n|$ is displayed as a function of the order of the harmonics for different strength of the ac drive. The amplitudes decrease faster with n as the ac drive is reduced.

In figure 24, the modulus of the complex current amplitude $|A_n|$ is displayed as a function of the order of the harmonic for different values of the external frequency. With decreasing frequency, a plateau develops, i.e. the current amplitude decreases slowly over a finite range of values of n. The limit $\omega_{\mathrm{ext}} \to 0$, however, cannot be performed numerically as the sum and the limit must not be interchanged in eqs. (201) and (202). Changing the interaction parameter g hardly affects the behaviour of the current amplitude with the harmonic order n.

The in-phase part, the out-phase part and the modulus of the current amplitude for the second and the third harmonic as a function of the external frequency for two different values of the ac drive are displayed in figures 25 and 26. At low frequencies, the in-phase part is much larger than the out-phase part while at large frequencies it is much smaller than the out-phase part. At intermediate frequencies, the in-phase part decreases monotonically for the larger ac drive and the second harmonic in figure 25. For the smaller ac drive in figure 26, it shows a very small maximum. The out-phase part of the second harmonic shows a maximum at intermediate frequencies for both values of the ac drive. The two parts of the current amplitude combine to yield a monotonically decreasing modulus of the second harmonic amplitude for the lower ac drive while the modulus of the second harmonic amplitude shows a

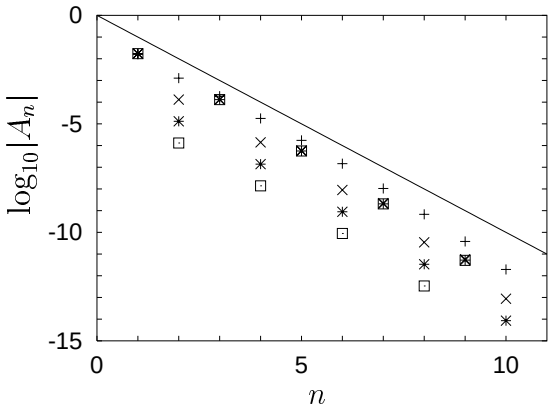

Figure 22: The logarithm (base 10) of the modulus of the complex current amplitude $|A_n|$ in units of $\hbar\omega_c/eR_T$ as a function of the order n of the higher harmonic for $g = 0.7$, $\omega_{ext}/\omega_c = 10^{-1}$, $eV_{ac}/\hbar\omega_c = 10^{-1}$, $eV_{dc}/\hbar\omega_c = 10^{-1}$ (+), 10^{-2} (×), 10^{-3} (∗), and 10^{-4} (□). The tunneling resistance R_T is given in eq. (358) in appendix B.2. The solid line is a guide to the eye with the slope $-n$.

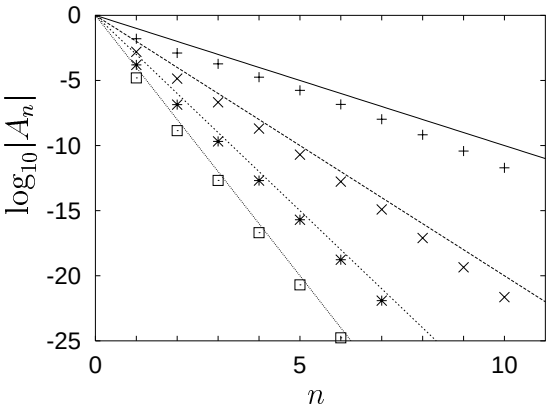

Figure 23: The logarithm (base 10) of the modulus of the complex current amplitude $|A_n|$ in units of $\hbar\omega_c/eR_T$ as a function of the order n of the higher harmonic for $g = 0.7$, $\omega_{ext}/\omega_c = 10^{-1}$, $eV_{dc}/\hbar\omega_c = 10^{-1}$, $eV_{ac}/\hbar\omega_c = 10^{-1}$ (+), 10^{-2} (×), 10^{-3} (∗), and 10^{-4} (□). The tunneling resistance R_T is given in eq. (358) in appendix B.2. The solid lines are guides to the eye with the slopes $-n$, $-2n$, $-3n$, and $-4n$.

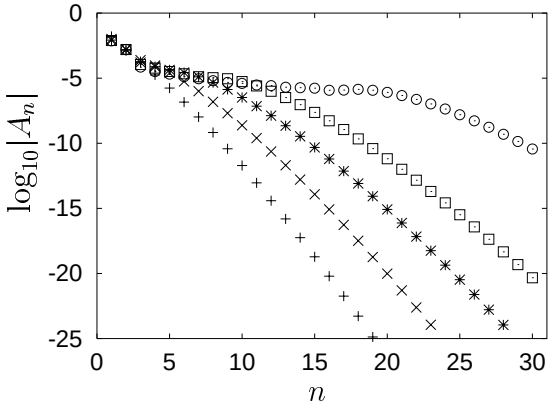

Figure 24: The logarithm (base 10) of the modulus of the complex current amplitude $|A_n|$ in units of $\hbar\omega_c/eR_T$ as a function of the order n of the higher harmonic for $g = 0.7$, $eV_{dc}/\hbar\omega_c = 10^{-1}$, $eV_{ac}/\hbar\omega_c = 10^{-1}$, $\omega_{ext}/\omega_c = 10^{-1}$ (+), 5×10^{-2} (×), 3×10^{-2} (∗), 2×10^{-2} (□), and 10^{-2} (○). The tunneling resistance R_T is given in eq. (358) in appendix B.2.

maximum for the larger ac drive. For the third harmonic, the modulus of the current amplitude shows a maximum for both values of the ac drive, see figures 25 and 26

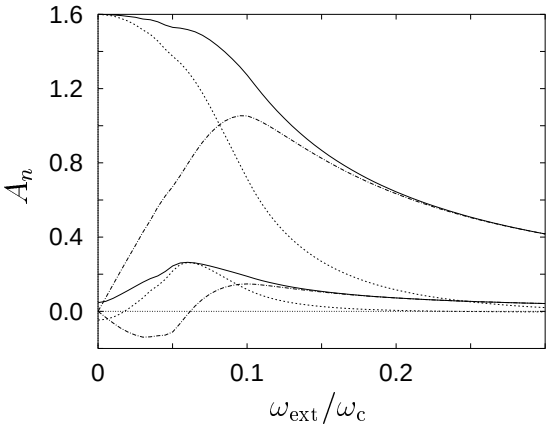

Figure 25: In-phase part (dotted), out-phase part (dash-dotted), and modulus (solid) of the complex current amplitude A_n in units $(\hbar\omega_{\rm c}/eR_{\rm T}) \times 10^{-3}$ for the 2nd (upper three curves) and the 3rd (lower three curves) harmonic as a function of the external frequency for $g = 0.7$, $eV_{\rm ac}/\hbar\omega_{\rm c} = 10^{-1}$, $eV_{\rm dc}/\hbar\omega_{\rm c} = 10^{-1}$. The tunneling resistance $R_{\rm T}$ is given in eq. (358) in appendix B.2.

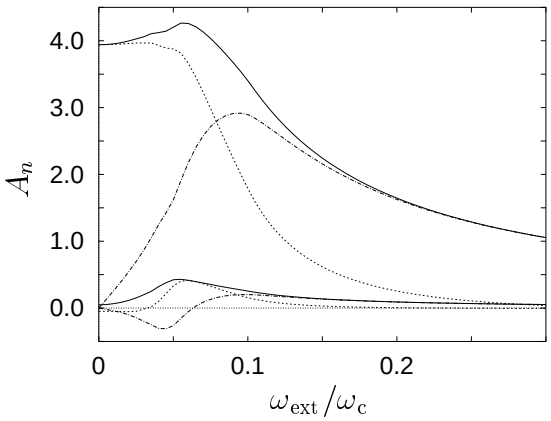

Figure 26: In-phase part (dotted), out-phase part (dash-dotted), and modulus (solid) of the complex current amplitude A_n in units $(\hbar\omega_{\rm c}/eR_{\rm T})\times 10^{-4}$ for the 2nd (upper three curves) and the 3rd (lower three curves) harmonic as a function of the external frequency for $g = 0.7$, $eV_{\rm ac}/\hbar\omega_{\rm c} = 5 \times 10^{-2}$, $eV_{\rm dc}/\hbar\omega_{\rm c} = 10^{-1}$. The tunneling resistance $R_{\rm T}$ is given in eq. (358) in appendix B.2.

When varying the interaction strength, one finds that for weak interactions oscillations of A_n vs. frequency develop at small frequencies. The modulus of the current amplitude of the second harmonic as a function of the external frequency for different interaction strengths is displayed in figure 27. Oscillations are clearly visible for $g = 0.9$ and $g = 0.8$ which then decay and disappear completely around $g = 0.65$. These oscillations are present in both, the in-phase and the out-phase parts of the current, see figure 28. They are further also present in the third harmonic, see figure 28.

Figure 29 displays the modulus of the current amplitude of the second harmonic as a function of the dc drive for several values of the interaction strength. The amplitude is zero for zero dc drive due to inversion symmetry. As a function of g the current amplitude shows a non-monotonic behaviour, see also figures 36 and 37. For $g = 0.98$ and $g = 0.9$, $|A_2|$ shows a kink exactly at $eV_{\rm dc}/\hbar\omega_{\rm c} = 0.1$ which can be understood from eqs. (201) and (202). The modulus occurring in the real and the imaginary part of the current amplitude is not differentiable for $g = 1$ at $k + eV_{\rm dc}/\hbar\omega_{\rm ext} = 0$ where k is the summation index. It shows a pointed extremum at these positions. For $g < 1$, the modulus is differentiable, but it still looks as if it were not for g only slightly smaller than 1. In the real part of A_n in eq. (201), the signum

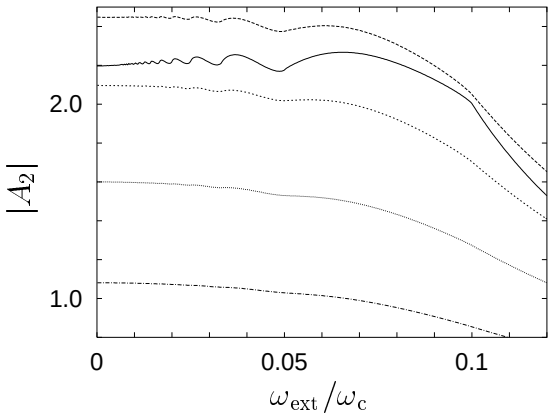

Figure 27: Modulus of the complex current amplitude of the 2nd harmonic $|A_2|$ in units $(\hbar\omega_{\rm c}/eR_{\rm T}) \times 10^{-3}$ as a function of the external frequency for $eV_{\rm ac}/\hbar\omega_{\rm c} = 10^{-1}$, $eV_{\rm dc}/\hbar\omega_{\rm c} = 10^{-1}$, $g = 0.9$ (solid, second curve from the top), $g = 0.8$ (long dashes, top curve), $g = 0.75$ (short dashes, third curve from the top), $g = 0.7$ (dotted, second curve from the bottom), and $g = 0.65$ (dash-dotted, bottom curve). The tunneling resistance $R_{\rm T}$ is given in eq. (358) in appendix B.2.

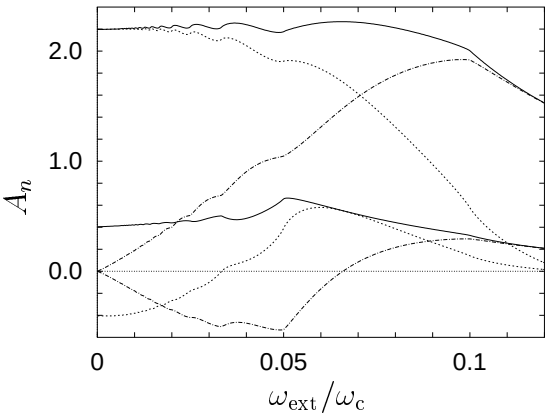

Figure 28: In-phase part (dotted), out-phase part (dash-dotted), and modulus (solid) of the complex current amplitude A_n for $n = 2$ (upper three curves) and $n = 3$ (lower three curves) in units $(\hbar\omega_{\rm c}/eR_{\rm T}) \times 10^{-3}$ as a function of the external frequency for $g = 0.9$, $eV_{\rm ac}/\hbar\omega_{\rm c} = 10^{-1}$, $eV_{\rm dc}/\hbar\omega_{\rm c} = 10^{-1}$. The tunneling resistance $R_{\rm T}$ is given in eq. (358) in appendix B.2.

turns the pointed extremum into a saddle point, thus $A_n^{(+)}$ shows no kink, see figure 30. The imaginary part of A_n in eq. (202) contains no signum. One expects kinks in $A_n^{(-)}$ whenever $eV_{\rm dc}/\hbar\omega_{\rm ext}$ is an integer number, i.e. at $eV_{\rm dc}/\hbar\omega_{\rm c} = 0.1$, 0.2, 0.3, 0.4, and 0.5, because one term in the sum exhibits a kink at these values. But only as long as this term is of the same order of magnitude as the sum over all remaining terms, $A_n^{(-)}$ shows the kink. When this one term is small in comparison to the sum over the remaining terms, the kink becomes indistinguishable, see figure 30. With increasing interaction strength, i.e. decreasing g, the kinks disappear. The higher the number of the harmonic, the more kinks are visible for g close to 1, see figures 31 and 32.

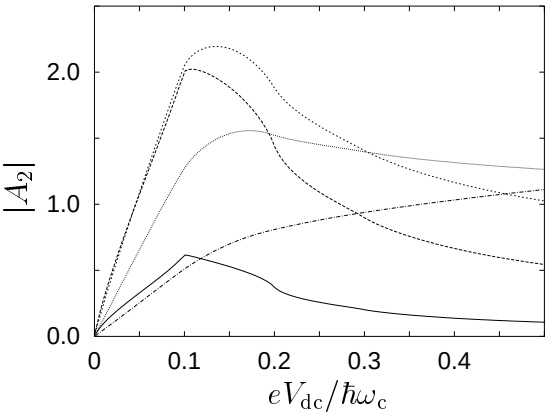

Figure 29: Modulus of the complex current amplitude $|A_2|$ in units $(\hbar\omega_{\rm c}/eR_{\rm T})\times 10^{-3}$ as a function of the dc drive for $\omega_{\rm ext}/\omega_{\rm c} = 10^{-1}$, $eV_{\rm ac}/\hbar\omega_{\rm c} = 10^{-1}$, $g = 0.98$ (solid), $g = 0.9$ (long dashes), $g = 0.8$ (short dashes), $g = 0.7$ (dotted), and $g = 0.6$ (dash-dotted). The tunneling resistance $R_{\rm T}$ is given in eq. (358) in appendix B.2.

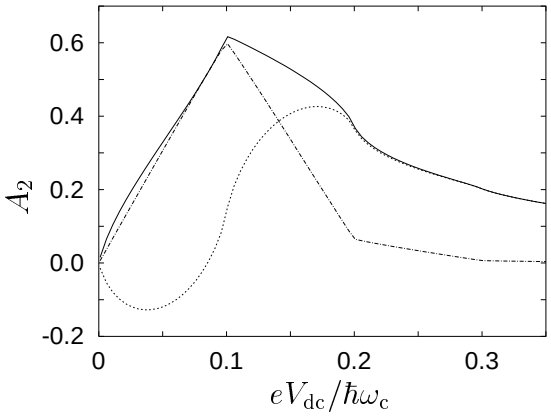

Figure 30: In-phase part (dotted), out-phase part (dash-dotted), and modulus (solid) of the complex current amplitude A_2 in units $(\hbar\omega_{\rm c}/eR_{\rm T}) \times 10^{-3}$ as a function of the dc drive for $g = 0.98$, $\omega_{\rm ext}/\omega_{\rm c} = 10^{-1}$, $eV_{\rm ac}/\hbar\omega_{\rm c} = 10^{-1}$. The tunneling resistance $R_{\rm T}$ is given in eq. (358) in appendix B.2.

When the frequency is reduced, the maxima of $|A_n|$ as a function of the dc drive move to smaller dc voltages, see figures 33 and 34 for the second and the third harmonic at $g = 0.7$. The magnitude of $|A_2|$ at the maximum hardly varies with changing frequency in contrast to the magnitude of $|A_3|$.

The modulus of the current amplitude of the second harmonic as a function of the ac drive for different interaction strengths is displayed in figure 35. The amplitude rises in a non-linear manner at small ac driving voltages for any interaction strength. At large driving voltages the increase becomes linear.

Figure 36 displays the complex current amplitude of the second harmonic as a function of the interaction parameter g. For small g, the amplitudes of the harmonics are strongly suppressed. For g close to 1, on the other hand, the current-voltage characteristic is nearly linear and harmonic generation is inefficient. At $g = 1$, all harmonics with $n > 1$ are zero. At intermediate values of g, $|A_n|$ shows a

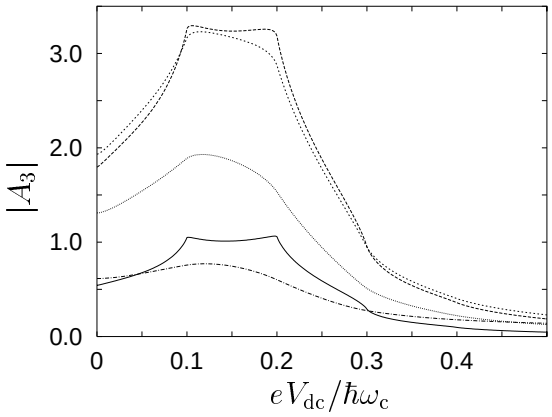

Figure 31: Modulus of the complex current amplitude $|A_3|$ in units $(\hbar\omega_{\rm c}/eR_{\rm T})\times 10^{-4}$ as a function of the dc drive for $\omega_{\rm ext}/\omega_{\rm c} = 10^{-1}$, $eV_{\rm ac}/\hbar\omega_{\rm c} = 10^{-1}$, $g = 0.98$ (solid), $g = 0.9$ (long dashes), $g = 0.8$ (short dashes), $g = 0.7$ (dotted), and $g = 0.6$ (dash-dotted). The tunneling resistance $R_{\rm T}$ is given in eq. (358) in appendix B.2.

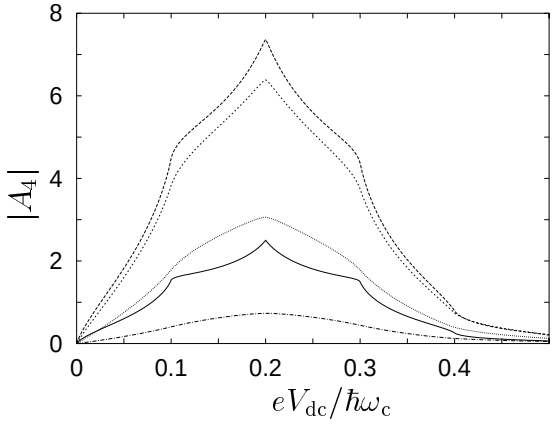

Figure 32: Modulus of the complex current amplitude $|A_4|$ in units $(\hbar\omega_{\rm c}/eR_{\rm T})\times 10^{-5}$ as a function of the dc drive for $\omega_{\rm ext}/\omega_{\rm c} = 10^{-1}$, $eV_{\rm ac}/\hbar\omega_{\rm c} = 10^{-1}$, $g = 0.98$ (solid), $g = 0.9$ (long dashes), $g = 0.8$ (short dashes), $g = 0.7$ (dotted), and $g = 0.6$ (dash-dotted). The tunneling resistance $R_{\rm T}$ is given in eq. (358) in appendix B.2.

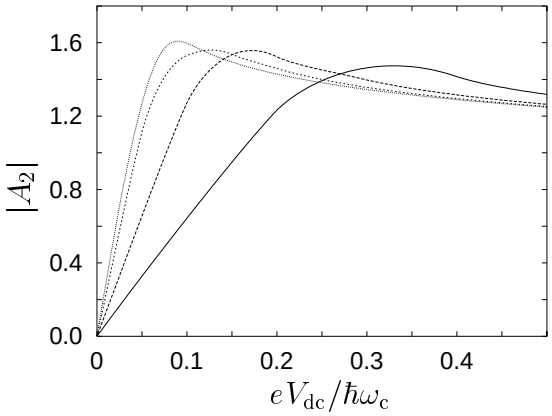

Figure 33: Modulus of the complex current amplitude $|A_2|$ in units $(\hbar\omega_{\rm c}/eR_{\rm T})\times 10^{-3}$ as a function of the dc drive for $g = 0.7$, $eV_{\rm ac}/\hbar\omega_{\rm c} = 10^{-1}$, $\omega_{\rm ext}/\omega_{\rm c} = 2\times 10^{-1}$ (solid), 10^{-1} (long dashes), 5×10^{-2} (short dashes), 10^{-2} (dotted). The tunneling resistance $R_{\rm T}$ is given in eq. (358) in appendix B.2.

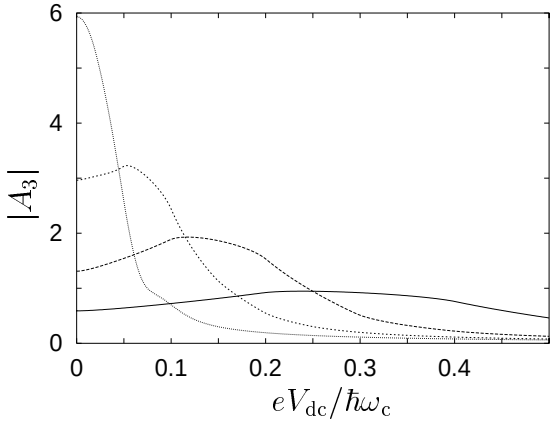

Figure 34: Modulus of the complex current amplitude $|A_3|$ in units $(\hbar\omega_{\rm c}/eR_{\rm T})\times 10^{-4}$ as a function of the dc drive for $g = 0.7$, $eV_{\rm ac}/\hbar\omega_{\rm c} = 10^{-1}$, $\omega_{\rm ext}/\omega_{\rm c} = 2\times 10^{-1}$ (solid), 10^{-1} (long dashes), 5×10^{-2} (short dashes), 10^{-2} (dotted). The tunneling resistance $R_{\rm T}$ is given in eq. (358) in appendix B.2.

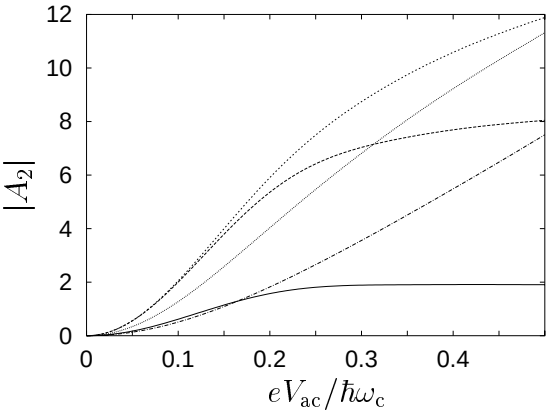

Figure 35: The modulus of the complex current amplitude $|A_2|$ in units of $(\hbar\omega_{\rm c}/eR_{\rm T}) \times 10^{-3}$ as a function of the ac driving voltage for $\omega_{\rm ext}/\omega_{\rm c} = 10^{-1}$, $eV_{\rm dc}/\hbar\omega_{\rm c} = 10^{-1}$, $g = 0.98$ (solid), $g = 0.9$ (long dashes), $g = 0.8$ (short dashes), $g = 0.7$ (dotted), $g = 0.6$ (dash-dotted). The tunneling resistance $R_{\rm T}$ is given in eq. (358) in appendix B.2.

maximum. The maxima of the in-phase and the out-phase parts are at slightly different positions. Figure 37 displays the modulus of the current amplitude for different harmonics as a function of the interaction parameter g. With increasing harmonic number, the maxima move to larger values of g.

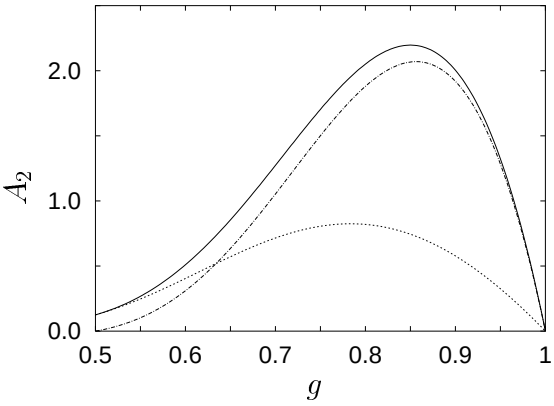

Figure 36: In-phase part (dotted), out-phase part (dash-dotted) and modulus (solid) of the complex current amplitude A_2 in units $(\hbar\omega_{\rm c}/eR_{\rm T}) \times 10^{-3}$ as a function of the interaction strength for $\omega_{\rm ext}/\omega_{\rm c} = 10^{-1}$, $eV_{\rm ac}/\hbar\omega_{\rm c} = 10^{-1}$, $eV_{\rm dc}/\hbar\omega_{\rm c} = 10^{-1}$. The tunneling resistance $R_{\rm T}$ is given in eq. (358) in appendix B.2.

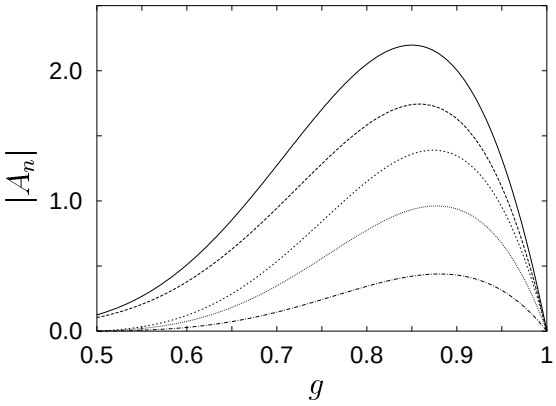

Figure 37: Modulus of the complex current amplitude $|A_n|$ in units $(\hbar\omega_{\rm c}/eR_{\rm T}) \times 10^{-3}$ as a function of the interaction strength for $\omega_{\rm ext}/\omega_{\rm c} = 10^{-1}$, $eV_{\rm ac}/\hbar\omega_{\rm c} = 10^{-1}$, $eV_{\rm dc}/\hbar\omega_{\rm c} = 10^{-1}$, $n = 2$ (solid), $n = 3$ (long dashes, multiplied by 5), $n = 4$ (short dashes, multiplied by 30), $n = 5$ (dotted, multiplied by 200), $n = 6$ (dash-dotted, multiplied by 1000). The tunneling resistance $R_{\rm T}$ is given in eq. (358) in appendix B.2.

From the detailed discussion of the behaviour of the current amplitude with harmonic number, dc and ac drive, frequency and interaction strength it is obvious that A_n shows a large variety of different features. The parameter space is so large and the behaviour of A_n with all parameters so rich, that it is very difficult to make even qualitative predictions for the behaviour of A_n for a certain set of parameters

without first evaluating A_n numerically for this parameter set. In other words, one can hardly deduce the unknown behaviour of A_n at one parameter set from the known behaviour of A_n at another parameter set.

Finally, the magnitude of the current amplitude is estimated. Choosing $\hbar\omega_c$ to be of the order of the subband spacing, say ≈ 1 meV, the ratio of the frequencies ω_{ext} and ω_c becomes $\omega_{ext}/\omega_c \approx \omega_{ext} \times 10^{-12}$ s. Choosing $\omega_{ext} = 100$ GH, it is $\omega_{ext}/\omega_c \approx 0.1$. The ratio $eV_{ac}/\hbar\omega_c = 0.1$ then corresponds to $V_{ac} \approx 0.1$ mV, and similarly $V_{dc} \approx 0.1$ mV. From figure 25 one can see that under these conditions the modulus of the amplitude of the second harmonic is of the order of $10^{-3} \cdot (\hbar\omega_c/eR_T)$. The tunneling resistance is chosen to be $R_T = 10 \cdot (h/e^2) \approx 10^5\ \Omega$. Then, $\hbar\omega_c/eR_T \approx 10^{-8}$ A and hence the current amplitude of the second harmonic is of the order of 10^{-11} A.

5.4 Local Field Effects

Local Fields in Non-Linear Transport

In the following, it is discussed how local fields can be incorporated into the theory on non-linear ac transport and their influence on the non-linear current is estimated.

First of all it has to be clarified which field is driving the current. Of course, the argument presented in section 3.3 is true also in non-linear transport: On the one hand, if the transport equation is based on a microscopic theory that neglects Coulomb interactions and also microscopic currents and the corresponding induced transverse field, the current should be driven by the complete local field, i.e. local longitudinal plus local transverse field. On the other hand, if the underlying microscopic theory takes into account Coulomb interactions, the influence of the local longitudinal field is included in the transport equation and the current should be driven by the external longitudinal field plus the local transverse field.

There can be found local-field studies in the literature which seem to imply that in non-linear transport one has to take into account both, electron-electron-interactions *and* local longitudinal fields [2]. But these studies are not based on a microscopic theory of interacting electrons but on a mean-field like approach, see the discussions in sections 2.3.1 and 3.3, and due to the nature of such a mean-field like approach, one indeed has to consider interactions and local longitudinal fields.

Infinitely Many Local-Field Equations

Before discussing local field effects in a dirty single-channel quantum wire, consider a very general example of non-linear transport – it illustrates nicely that a rigorous self-consistent treatment of local fields in non-linear transport is virtually impossible.

Take a monochromatic driving electric field of arbitrary spatial shape,

$$\vec{E}_{ext}(\vec{r},t) = \vec{E}_{ext}(\vec{r})\, e^{-i\omega_{ext}t}. \tag{206}$$

Assume that the response of the system under study is a non-linear current containing higher harmonics,

$$\vec{J}(\vec{r},t) = \sum_{n=-\infty}^{\infty} \vec{J}_n(\vec{r})\, e^{-in\omega_{ext}t}, \tag{207}$$

where the current amplitudes $\vec{J}_n(\vec{r})$ depend on position, on the driving electric field, on the driving frequency, on the interaction strength, on temperature and so on, but not on time.

Following eqs. (83) and (84) in section 3.3, the local field is related to the longitudinal and transverse parts of the current via

$$\vec{E}_{\rm L}(\vec{q},\omega) = \vec{E}_{\rm L,ext}(\vec{q},\omega) + \frac{1}{{\rm i}\epsilon_0\omega}\vec{J}_{\rm L}(\vec{q},\omega), \tag{208}$$

$$\vec{E}_{\rm T}(\vec{q},\omega) = \vec{E}_{\rm T,ext}(\vec{q},\omega) + {\rm i}\mu_0\omega\, g_0(\vec{q},\omega)\vec{J}_{\rm T}(\vec{q},\omega). \tag{209}$$

Fourier transforming the current in eq. (207) to $\vec{q}$-space, the transverse and longitudinal parts of the current can be obtained using eqs. (77) and (78). Performing also the Fourier transform to frequency one obtains

$$\vec{E}_{\rm L}(\vec{q},\omega) = 2\pi\,\vec{E}_{\rm L,ext}(\vec{q})\,\delta(\omega-\omega_{\rm ext}) + \frac{1}{{\rm i}\epsilon_0\omega}\,2\pi\sum_{n=-\infty}^{\infty}\vec{J}_{{\rm L},n}(\vec{q})\,\delta(\omega-n\omega_{\rm ext}), \tag{210}$$

$$\begin{aligned}\vec{E}_{\rm T}(\vec{q},\omega) &= 2\pi\,\vec{E}_{\rm T,ext}(\vec{q})\,\delta(\omega-\omega_{\rm ext}) \\ &+ {\rm i}\mu_0\omega\, g_0(\vec{q},\omega)2\pi\sum_{n=-\infty}^{\infty}\vec{J}_{{\rm T},n}(\vec{q})\,\delta(\omega-n\omega_{\rm ext}).\end{aligned} \tag{211}$$

Hence, a finite local field is obtained for any $\omega = n\omega_{\rm ext}$, n integer, if $\vec{J}_{{\rm L/T},n}$ is finite for that value of n. The local longitudinal and transverse fields are not monochromatic but contain all harmonics. Further, due the non-linearity of the system, a local transverse field at frequency $n\omega_{\rm ext}$ induces currents at all possible harmonics, $m(n\omega_{\rm ext})$, m integer. These currents again induce fields at frequencies of $m(n\omega_{\rm ext})$. As a consequence, a local field at frequency $k\omega_{\rm ext}$ is influenced by any local field with frequency $n\omega_{\rm ext}$ if k/n is an integer number. Finally, due to mixing, local fields with different frequencies $n\omega_{\rm ext}$ and $k\omega_{\rm ext}$ combine to drive currents at frequencies $(\pm n \pm k)\omega_{\rm ext}$ and the corresponding higher harmonics. Thus, if e.g. $n-k=1$, they also influence the fundamental mode.

Based on these considerations, it is obvious that the equations for the local fields in eqs. (210) and (211) do not decouple, to yield one separate equation for any frequency $n\omega_{\rm ext}$, because the local fields at different frequencies influence each other. This cross-influence leads to a set of infinitely many coupled equations for the local fields which is in general impossible to solve.

One approach that simplifies the task is the so-called parametric approximation. This approximation neglects the coupling that allows a local field at frequency $n\omega_{\rm ext}$ to influence another field at a smaller frequency $m\omega_{\rm ext}$, $m<n$, i.e. it neglects mixing [2]. The parametric approach is justified when mixing is an inefficient process such that the cross-influence between the fields is small. But still the local field equations are coupled as via harmonic generation a field at frequency $k\omega_{\rm ext}$ is influenced by any field at $n\omega_{\rm ext}$ with k/n integer. This coupling might be neglected when also harmonic generation is inefficient and the current amplitudes decrease rapidly with increasing harmonic number. Then, the impact of the fundamental mode, which contains also the external field, on a field at frequency $n\omega_{\rm ext}$ is much larger than the impact of a local field at $k\omega_{\rm ext}$, n/k integer, on a field at frequency $n\omega_{\rm ext}$.

5.4.1 Interaction vs. Local Longitudinal Field

The following paragraphs are dedicated to a comparison between the microscopic consideration of electron-electron interactions and the mean-field like approach discussed in sections 2.3.1, 3.3, and 4.4.1.

Choose a longitudinal external driving field parallel to the wire and constant as a function of $\vec{R}$, and neglect the induced transverse field. For an infinitely high tunneling barrier, $\Delta^2 = 0$, the ac current in the wire is purely linear, see eq. (186),

$$J^x(x,\vec{R},\omega) = J^x_{\rm clean}(x,\vec{R},\omega) - r(x,\omega)\, J^x_{\rm clean}(x=0,\vec{R},\omega). \tag{212}$$

Here, $J^x_{\rm clean}$ is the linear current in an infinitely thin wire without a barrier, see eq. (132). The function $r(x,\omega)$ is given in eq. (185). The induced longitudinal field for an external longitudinal field parallel to the wire and in the absence of a transverse field is given in eq. (154) in section 4.4.1,

$$E^x_{\rm L,ind}(\vec{q},\omega) = \frac{q_x^2\, V^{\rm C}_{\rm ee}(\vec{q})}{{\rm i}\omega e^2}\, J^x(\vec{q},\omega). \tag{213}$$

Inserting the expression for the current given in eq. (212) into eq. (213), multiplying both sides by $B^x_{00}(-\vec{Q})/(2\pi)^2$, integrating with respect to $\vec{Q}$ and defining the projected field as in eq. (140), one obtains for the projected induced longitudinal field in terms of the projected external field [12]

$$\begin{aligned} E^x_{\rm L,ind,1b}(q_x,\omega) \;=\; & \left[\frac{\sigma^{xx}_{{\rm 1b},d=0}(q_x,\omega)}{\sigma^{xx}_{{\rm 1b,non-int},d=0}(q_x,\omega)} - 1\right] \Bigg\{ E^x_{\rm L,ext,1b}(q_x,\omega) \\ & - \frac{\int {\rm d}q_x\, \sigma^{xx}_{{\rm 1b},d=0}(q_x,\omega)\, E^x_{\rm L,ext,1b}(q_x,\omega)}{2\pi\, \sigma^{xx}_{{\rm 1b},d=0}(x=0,\omega)} \Bigg\}, \end{aligned} \tag{214}$$

where $\sigma^{xx}_{{\rm 1b},d=0}$ is the conductivity of the clean single-channel quantum wire of zero diameter, see eq. (145), and $\sigma^{xx}_{{\rm 1b,non-int},d=0}$ is the conductivity of the non-interacting system which is obtained from eq. (145) by replacing $\omega^2_{\rm LL}(q_x)$ with $v_{\rm F}^2 q_x^2$. The first term in the curly brackets in eq. (214) is equivalent to the one derived for the clean quantum wire in section 4.4.1, the second term represents the influence of the barrier.

The same result for the projected induced longitudinal field is obtained when driving the current with the projected local field using the conductivity of the non-interacting system [12]. Hence, the two approaches, considering *either* electron-electron interactions *or* the induced longitudinal field, are here equivalent. This result is in complete analogy to the one found in section 4.4.1 and might have been expected. For a barrier of finite height, however, the situation changes completely.

For a barrier of finite height, $\Delta^2 \neq 0$, the current in the wire is non-linear if and only if the current is evaluated based on a microscopic model that considers interacting electrons. As a consequence, one observes higher harmonic generation in ac transport as discussed in detail in section 5.3.2 and in particular one obtains induced fields at all harmonic frequencies. The mean-field like approach that neglects interactions and considers self-consistently the induced longitudinal field yields a current

at the fundamental frequency provided by the external field as for non-interacting electrons, the dirty quantum wire exhibits a linear-current voltage characteristic and hence does not show harmonic generation. As Maxwell equations are linear, the induced field also contains only the fundamental mode.

Hence, the two approaches, considering *either* the interaction *or* the longitudinal induced field lead in the case of a dirty quantum wire with a barrier of finite height to qualitatively completely different results. Entering into the details of the evaluation of the non-linear current, see appendix B.1, it turns out that it is crucial for the appearance of a non-linear current-voltage characteristic that the interaction is represented by a term in the Hamiltonian that contains the product of two density *operators*, see eq. (14). From the discussion of the mean-field like approach in section 2.3.1, it is known that the Hamiltonian taking into account the self-consistent induced field, see eq. (4), contains the product of one density operator and an expectation value of another density operator. This seemingly slight difference leads here to two qualitatively completely different results: a linear vs. a non-linear current-voltage characteristic. Choosing a mean-field like approximation, one therefore misses important features of the system.

5.4.2 Induced Transverse Field

In the following, the magnitude of the local transverse field in the dirty single-channel quantum wire is estimated. Consider a current amplitude at frequency $n\omega_{\rm ext}$ that is driven by the external field alone. For $n > 1$, this current is a pure tunneling current proportional to the tunneling probability Δ^2. When the driving electric field is not localized at the barrier, a displacement current that is independent of Δ^2 is also present, see the discussion in section 5.1, but it contributes only to the fundamental mode, $n = 1$. The induced field at $n\omega_{\rm ext}$ is thus also proportional to Δ^2 for $n > 1$. The correction to the tunneling current at another frequency $k\omega_{\rm ext}$ due to this induced field at frequency $n\omega_{\rm ext}$ is of correspondingly higher order in Δ^2. As the total current was evaluated in section 5.1 only in order Δ^2 it would be inconsistent to take into account corrections of higher order. Hence, harmonics induced by local fields of frequency $n\omega_{\rm ext}$, $n > 1$, and mixing have to neglected. The induced transverse field at $n\omega_{\rm ext}$, however, also drives the displacement current at the same frequency and this current is linear in the driving field. The corresponding correction to the total current is exactly of order Δ^2 and has to be taken into account.

In appendix B.4 it is shown how to evaluate this induced transverse field in lowest order in Δ^2. An infinitely thin wire is assumed. The induced field $E^x_{\rm T,ind}(\vec{r},\omega)$ consists of two terms, one diverges at $|\vec{R}| = 0$ while the other remains finite "within" the wire. Now, as for an infinitely thin wire the non-linear ac current $J^x(\vec{r},\omega)$ is proportional to $\delta(\vec{R})$, one indeed expects the induced field to reflect this delta-function. As we are interested in a correction to the current caused by the induced transverse field, the term that does not diverge at $|\vec{R}| = 0$ is neglected with respect to the other term. Then, the current $J^x(\vec{r},\omega)$ and the induced field $E^x_{\rm T,ind}(\vec{r},\omega)$ are averaged with respect to $\vec{R}$. The resulting expression for the induced field is for

$x \neq 0$

$$E^x_{\mathrm{T,ind,av}}(x \neq 0, \omega) \approx -\frac{\mathrm{i}}{\epsilon_0 \omega} \left(\frac{v_\mathrm{F}/g}{c}\right)^2 J^x_{\mathrm{av}}(x, \omega), \tag{215}$$

where $J^x_{\mathrm{av}}(x, \omega)$ is the averaged time-dependent non-linear current,

$$J^x_{\mathrm{av}}(x, \omega) = 2\pi\, \mathrm{e}^{\mathrm{i}\omega g|x|/v_\mathrm{F}} \sum_{n=-\infty}^{\infty} A_n(\omega_{\mathrm{ext}})\, \delta(\omega - n\omega_{\mathrm{ext}}). \tag{216}$$

The amplitudes of the current, $A_n(\omega_{\mathrm{ext}})$, are given in section 5.3.2.

The induced transverse field in eq. (215) drives a linear current following eq. (186) as it is not localized at the barrier. This linear current is proportional to Δ^2 as the induced transverse field is proportional to Δ^2 and represents a correction to the time-dependent non-linear current. The expression in eq. (215) shows that the field $E^x_{\mathrm{T,ind,av}}(x \neq 0, \omega)$ is suppressed by a factor of $(v_\mathrm{F}/gc)^2$ with respect to the average current $J^x_{\mathrm{av}}(x, \omega)$, the correction to this current caused by $E^x_{\mathrm{T,ind,av}}(x \neq 0, \omega)$ is thus negligible.

Hence, the results derived for the non-linear ac current in section 5.3 remain valid when the local transverse field is taken into account apart from corrections of the order of $(v_\mathrm{F}/gc)^2$.

5.5 Emitted Electromagnetic Fields

Finally, in order to provide a means for a possible detection of the non-linear ac current that does not rely on contacts, we evaluate the electromagnetic field emitted by the wire based on the ac current evaluated in section 5.3.2 and Maxwell equations. In the following, the emitted magnetic field, the emitted electric field and the Poynting vector, i.e. the emitted power, are evaluated based on the non-linear current density that is given as a function of position in section 5.1 and as a function of time in section 5.3.2. The wire is assumed to be infinitely thin.

Magnetic Field

The vector potential created by a space- and time-dependent current is [296]

$$\vec{A}(\vec{r}, t) = \frac{\mu_0}{4\pi} \int \mathrm{d}\vec{r}\,' \, \frac{\vec{J}(\vec{r}\,', t - |\vec{r} - \vec{r}\,'|/c)}{|\vec{r} - \vec{r}\,'|}. \tag{217}$$

The current density $\vec{J}(\vec{r}, t)$ has here only an x-component. For an infinitely thin wire, $\lim_{d\to 0} B^x_{00}(\vec{R}) = \delta(\vec{R})$, it is, see eqs. (187) and (196),

$$J^x(x, \vec{R}, t) = \sum_{n=-\infty}^{\infty} A_n(\omega_{\mathrm{ext}})\, \mathrm{e}^{-\mathrm{i}n\omega_{\mathrm{ext}}t} \cdot \mathrm{e}^{\mathrm{i}n\omega_{\mathrm{ext}}g|x|/v_\mathrm{F}}\, \delta(R). \tag{218}$$

The current amplitude A_n at finite temperature is given in eqs. (373) and (375) in appendix B.3.2 and at zero temperature in eqs. (201) and (202) in section 5.3.2.

Inserting the expression for the current given in eq. (218) into the expression for the vector potential in eq. (217) yields

$$A^x(\vec{r},t) = \frac{\mu_0}{4\pi} \sum_{n=-\infty}^{\infty} A_n(\omega_{\rm ext})\, {\rm e}^{-{\rm i}n\omega_{\rm ext}t} L_n(\vec{r}), \tag{219}$$

with the function

$$L_n(\vec{r}) = \int_{-\infty}^{\infty} {\rm d}x' \, \frac{{\rm e}^{{\rm i}(n\omega/c)\,[(x-x')^2+R^2]^{1/2}}}{[(x-x')^2+R^2]^{1/2}} \, {\rm e}^{{\rm i}gn\omega_{\rm ext}|x'|/v_{\rm F}}. \tag{220}$$

This integral can in general not be evaluated analytically, see below.

The magnetic field is related to the vector potential via $\vec{B}(\vec{r},t) = \vec{\nabla} \times \vec{A}(\vec{r},t)$. In the following, ϕ denotes the angle between the vector $\vec{R}$ and the y-axes. Then, $y = R\cos(\phi)$ and $z = R\sin(\phi)$, and one obtains for the magnetic field vector

$$\vec{B}(\vec{r},t) = \sum_{n=-\infty}^{\infty} \vec{b}_n(\vec{r})\, {\rm e}^{-{\rm i}n\omega_{\rm ext}t}, \tag{221}$$

with the complex amplitude

$$\vec{b}_n(\vec{r}) = \frac{\mu_0}{4\pi} A_n(\omega_{\rm ext}) \frac{\partial L_n(\vec{r})}{\partial R} \cdot (0, \sin(\phi), -\cos(\phi)). \tag{222}$$

At a certain frequency $n\omega_{\rm ext}$ $(n > 0)$, the magnetic field vector is

$$\vec{B}_n(\vec{r},t) = 2{\rm Re}[\vec{b}_n(\vec{r})\, {\rm e}^{-{\rm i}n\omega_{\rm ext}t}]. \tag{223}$$

Here it was used that as $A_{-n} = A_n^*$ and also $L_{-n} = L_n^*$, thus $\vec{b}_{-n} = \vec{b}_n^*$.

It can be seen from eq. (221) that the magnetic field has contributions which oscillate in phase and out of phase with respect to the external driving field which is due to the fact that the current has an in-phase and an out-phase part. The x-component of the magnetic field is zero, the symmetry of the magnetic field along y and z is displayed schematically in figure 38.

Only in the far-field limit, defined by the condition that the dimension of the oscillating dipole is much smaller than the wavelength of the emitted radiation and that this wavelength is again much smaller than the distance from the dipole, the function $L_n(\vec{r})$ and hence the complex amplitude of the magnetic field vector can be evaluated analytically,

$$\vec{b}_{n,{\rm ff}}(\vec{r}) = -\mu_0\, A_n(\omega_{\rm ext}) \frac{R}{2\pi} \frac{v_{\rm F}}{gc} \frac{{\rm e}^{{\rm i}2\pi|\vec{r}|/\lambda_{\rm rad}}}{r^2} (0, \sin\phi, -\cos\phi). \tag{224}$$

Here, $\lambda_{\rm rad}$ is the wavelength of the emitted radiation, $\lambda_{\rm rad} = 2\pi c/n\omega_{\rm ext}$. The amplitude of the magnetic field decays with the distance from the dipole, $|\vec{r}|$. It is reduced with respect to the current amplitude by the factor $v_{\rm F}/gc$.

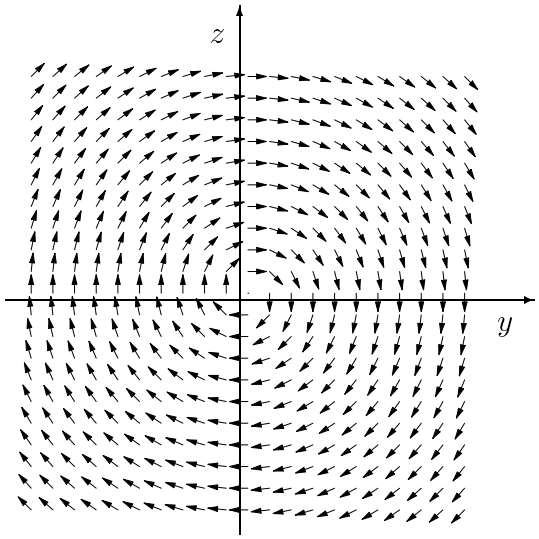

Figure 38: The orientation of the magnetic field vector in the y-z plane. The x-component of the magnetic field is zero. The arrows all have the same length, they contain no information on the magnitude of the field. The position of the quantum wire is at the crossing of the y- and the z-axes.

Close to the wire, the amplitude of the magnetic field vector may be evaluated numerically. Due to the oscillatory nature of the integrand of the function $L_n(\vec{r})$ in eq. (220) it is difficult to achieve a high accuracy of the result of the integration in reasonable time. The larger the ratio $R/\lambda_{\rm el}$, where $\lambda_{\rm el} = 2\pi v_{\rm F}/gn\omega_{\rm ext}$ is the "wavelength" of the electrons inside the wire, the more difficult it becomes to obtain results for $\vec{b}_n(\vec{r})$ with sufficient accuracy. Thus, all numerical results presented in the following are evaluated for $R/\lambda_{\rm el} \leq 1$.

Figure 39 shows the magnitude of the z-component of $\vec{b}_n/A_n$ as a function of x for different R. The angle ϕ is zero, thus the y-component of $\vec{b}_n$ is zero. As the system exhibits rotational symmetry with respect to the x-axes this choice does not imply a loss of generality. Both, x and R are given in units of $\lambda_{\rm el}$. The real and the imaginary parts of b_n^y/A_n oscillate roughly with the wavelength $\lambda_{\rm el}$ for small R. With increasing R, this behaviour remains true only for the real part of b_n^z/A_n. The imaginary part develops a maximum around $x/\lambda_{\rm el} = 0$ with increasing R.

The moduli of the real and imaginary parts of the z-component of $\vec{b}_n/A_n$, $\mathrm{Re}[b_n^z/A_n]$ and $\mathrm{Im}[b_n^z/A_n]$, as functions of $R/\lambda_{\rm el}$ for various $x/\lambda_{\rm el}$ are displayed in figure 40. The behaviour of $|\mathrm{Re}[b_n^z/A_n]|$ at $x/\lambda_{\rm el} = 0.5$ and 1 is nearly identical to the one at $x/\lambda_{\rm el} = 0$ and is not displayed. At $x/\lambda_{\rm el} = 0.25$ and 0.75, $\mathrm{Re}[b_n^z/A_n]$ is zero. The decrease of $|\mathrm{Im}[b_n^z/A_n]|$ at $x/\lambda_{\rm el} = 0$ is much slower than the decrease of $|\mathrm{Re}[b_n^z/A_n]|$ at that position. At $x/\lambda_{\rm el} = 0.25$, $|\mathrm{Im}[b_n^z/A_n]|$ decreases similarly to $|\mathrm{Re}[b_n^z/A_n]|$ at $x/\lambda_{\rm el} = 0$ until $R/\lambda_{\rm el} \approx 0.1$ and decreases more slowly for $R/\lambda_{\rm el} > 0.1$. At $x/\lambda_{\rm el} = 0.5$, $|\mathrm{Im}[b_n^z/A_n]|$ even increases with increasing R. Comparison with figure 39 shows that for $R/\lambda_{\rm el} = 10^{-2}$ and $R/\lambda_{\rm el} = 10^{-1}$, $|\mathrm{Im}[b_n^z/A_n]|$ is zero at $x/\lambda_{\rm el} = 0.5$ which is no longer true for $R/\lambda_{\rm el} = 5 \times 10^{-1}$, which is the reason for the increase of $|\mathrm{Im}[b_n^z/A_n]|$ with increasing $R/\lambda_{\rm el}$. (The oscillating structure of $|\mathrm{Im}[b_n^z/A_n]|$ at $x/\lambda_{\rm el} = 0.5$ in figure 40 at small $R/\lambda_{\rm el}$ is due to problems with the numerical accuracy.) At $x/\lambda_{\rm el} = 0.75$, $\mathrm{Im}[b_n^z/A_n]$ exhibits a change of sign with increasing R and thus $|\mathrm{Im}[b_n^z/A_n]|$ shows a dip as $\mathrm{Im}[b_n^z/A_n]$ moves through zero at $R/\lambda_{\rm el} \approx 0.6$.

From the numerically obtained data on the complex amplitude of the magnetic

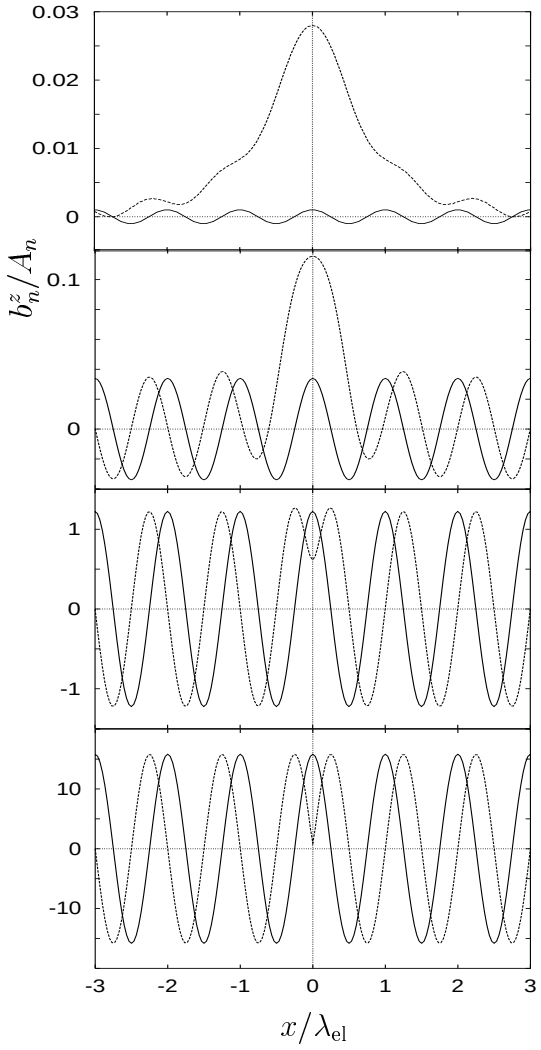

Figure 39: The real (solid) and the imaginary (dashed) parts of the z-component of the complex amplitude of the magnetic field vector divided by the complex current amplitude $\vec{b}_n(\vec{r})/A_n$ (in units of $\mu_0/\lambda_{\rm el}$) as a function of the position $x/\lambda_{\rm el}$ for $R/\lambda_{\rm el} = 10^{-2}$ (bottom), 10^{-1} (second from the bottom), 5×10^{-1} (second from the top), and 1 (top). The angle ϕ between R and the y-axes is 0. The ratio of Fermi velocity to velocity of light is $v_{\rm F}/gc = 10^{-3}$.

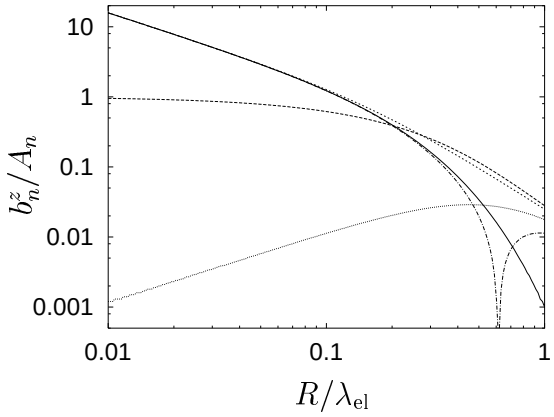

Figure 40: The moduli of the real and imaginary parts of the z-component of $\vec{b}_n/A_n$ (in units of $\mu_0/\lambda_{\rm el}$) for $\phi = 0$ as functions of R. The solid line displays the modulus of the real part of b_n^z/A_n at $x/\lambda_{\rm el} = 0$. The modulus of the imaginary part of b_n^z/A_n is displayed at $x/\lambda_{\rm el} = 0$ (long dashes), 0.25 (short dashes), 0.5 (dotted), and 0.75 (dash-dotted). It is $\phi = 0$ and $v_{\rm F}/gc = 10^{-3}$.

field vector, one can estimate the magnitude of the magnetic field. For an external frequency of 100 GH and $v_{\rm F}/gc = 10^{-3}$, it is $\lambda_{\rm el} \approx 10^{-5}$ m for the second harmonic. With a magnitude of the current amplitude of $\approx 10^{-11}$ A, see section 5.3.2, the magnetic field has a magnitude of $\approx 10^{-11}$ T at $x/\lambda_{\rm el} = 0$ and $R/\lambda_{\rm el} = 0.01$.

Electric Field

Next, turn to the emitted transverse electric field. It is related to the magnetic field by $\partial \vec{E}_{\rm T}(\vec{r},t)/\partial t = c^2 \vec{\nabla} \times \vec{B}(\vec{r},t)$ and thus

$$\vec{E}_{\rm T}(\vec{r},t) = \sum_{n=-\infty}^{\infty} \vec{e}_n(\vec{r})\, {\rm e}^{-{\rm i}n\omega_{\rm ext}t} \tag{225}$$

where the complex amplitude of the transverse electric field is

$$\begin{aligned} \vec{e}_n(\vec{r}) &= \frac{{\rm i}\, A_n(\omega_{\rm ext})}{4\pi\epsilon_0\, n\omega_{\rm ext}} \\ &\times \left(-\left[2 + R\frac{\partial}{\partial R}\right] \frac{\partial L_n(\vec{r})}{R\partial R}, \frac{\partial^2 L_n(\vec{r})}{\partial x \partial R}\, \cos(\phi), \frac{\partial^2 L_n(\vec{r})}{\partial x \partial R}\, \sin(\phi) \right). \end{aligned} \tag{226}$$

In contrast to the magnetic field vector, non of the components of the electric field vector is zero for a general angle ϕ. At a certain frequency, $n\omega_{\rm ext}$ $(n > 0)$, the electric field vector is

$$\vec{E}_{{\rm T},n}(\vec{r},t) = 2{\rm Re}[\vec{e}_n(\vec{r})\, {\rm e}^{-{\rm i}n\omega_{\rm ext}t}], \tag{227}$$

as $\vec{e}_{-n} = \vec{e}_n^{\,*}$. In analogy to the current and the magnetic field, also the electric field has contributions which oscillate in phase and out of phase with respect to the external driving field. In the far-field limit, the amplitude of the electric field vector can be evaluated analytically,

$$\vec{e}_{n,{\rm ff}}(\vec{r}) = -\mu_0 c\, A_n(\omega_{\rm ext})\, \frac{R}{2\pi}\, \frac{v_{\rm F}}{gc}\, \frac{{\rm e}^{{\rm i}2\pi|\vec{r}|/\lambda_{\rm rad}}}{r^3}\, (R, -x\cos\phi, -x\sin\phi). \tag{228}$$

It decays with the distance from the wire and just like the complex amplitude of the magnetic field vector contains a factor $v_{\rm F}/gc$.

The behaviour of the transverse electric field close to the wire is obtained numerically. The directions of the real and the imaginary parts of $\vec{e}_n/A_n$ for $\phi = 0$ are displayed in figures 41 - 44. The real part of $\vec{e}_n/A_n$ is shown in figures 41 and 42 and the imaginary part of $\vec{e}_n/A_n$ is shown in figures 43 and figure 44. In all figures, $R/\lambda_{\rm el}$ ranges from 0.05 to 1. The arrows indicating the directions of ${\rm Re}[\vec{e}_n/A_n]$ and ${\rm Im}[\vec{e}_n/A_n]$ are scaled to have all have the same length, hence the figures do not contain any information on the magnitude of ${\rm Re}[\vec{e}_n/A_n]$ and ${\rm Im}[\vec{e}_n/A_n]$. Seemingly discontinuous changes of direction, for example at $x/\lambda_{\rm el} = 0$ and $R/\lambda_{\rm el}$ between 0.6 and 0.65 in figures 41 and 42, are due to changes of sign in the x- or the y-component of the amplitude of the electric field, see figures 45 and 46. Both, ${\rm Re}[\vec{e}_n/A_n]$ and ${\rm Im}[\vec{e}_n/A_n]$ show whirls appearing around certain values of $x/\lambda_{\rm el}$ and rather close to the wire. The appearance of these whirls is also due to changes of sign in e_n^x/A_n or e_n^y/A_n.

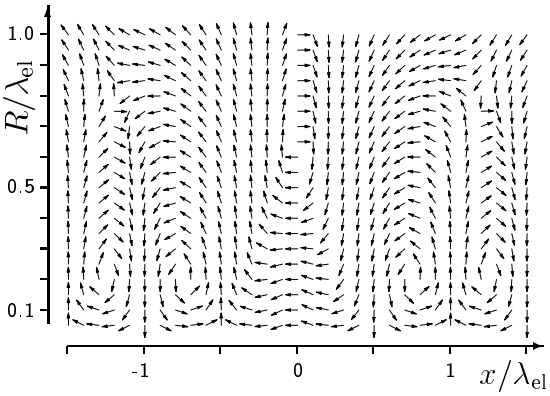

Figure 41: The real part of $\vec{e}_n/A_n$ as a function of $x/\lambda_{\rm el}$ and $R/\lambda_{\rm el}$ (in units of $c\mu_0/\lambda_{\rm el}$) for $-1.5 < x/\lambda_{\rm el} < 1.5$.

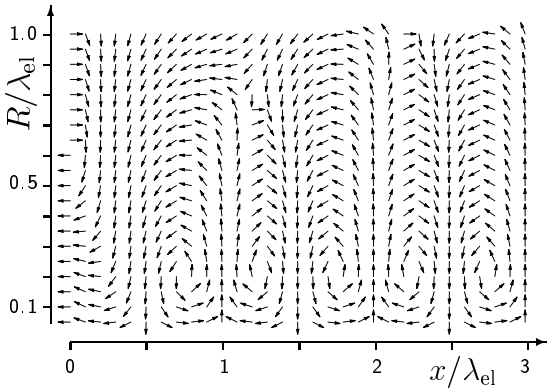

Figure 42: The real part of $\vec{e}_n/A_n$ as a function of $x/\lambda_{\rm el}$ and $R/\lambda_{\rm el}$ (in units of $c\mu_0/\lambda_{\rm el}$) for $0 < x/\lambda_{\rm el} < 3$.

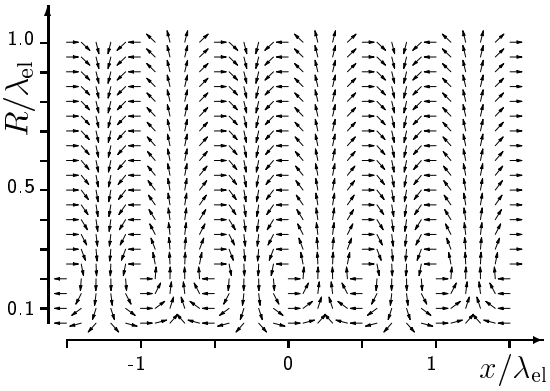

Figure 43: The imaginary part of $\vec{e}_n/A_n$ as a function of $x/\lambda_{\rm el}$ and $R/\lambda_{\rm el}$ (in units of $c\mu_0/\lambda_{\rm el}$) for $-1.5 < x/\lambda_{\rm el} < 1.5$.

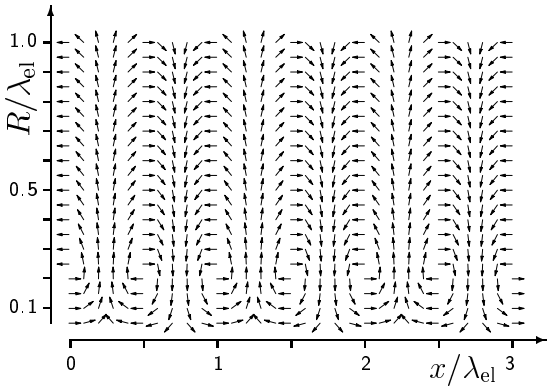

Figure 44: The imaginary part of $\vec{e}_n/A_n$ as a function of $x/\lambda_{\rm el}$ and $R/\lambda_{\rm el}$ (in units of $c\mu_0/\lambda_{\rm el}$) for $0 < x/\lambda_{\rm el} < 3$.

Information on the magnitude of $\mathrm{Re}[\vec{e}_n/A_n]$ and $\mathrm{Im}[\vec{e}_n/A_n]$ as a function of x is given in figures 45 and 46. Figure 45 shows the real and the imaginary parts of e_n^x/A_n and figure 46 shows the real and the imaginary part of e_n^y/A_n. At small R, real and imaginary parts of both components oscillate with a wavelength $\approx \lambda_{\mathrm{el}}$. With increasing R, the imaginary parts of both components maintain their oscillatory behaviour but change in amplitude. In addition, $\mathrm{Im}[e_n^x/A_n]$ shows a phase shift by π in between $R/\lambda_{\mathrm{el}} = 0.1$ and 0.5. The behaviour of the real parts changes quite drastically with increasing R. They show regular oscillations only for the two smallest values of R/λ_{el} displayed in figures 45 and 46.

The change of magnitude of the moduli of the real and imaginary parts of e_n^x/A_n and e_n^y/A_n with R for different x is displayed in figures 47 and 48. The modulus of the real part of e_n^x/A_n as a function of R/λ_{el} is shown at $x/\lambda_{\mathrm{el}} = 0$, 0.75 and 1 in figure 47. For $x/\lambda_{\mathrm{el}} = 0$ and 0.75, it shows dips close to $R/\lambda_{\mathrm{el}} = 0.6$ and 0.2, respectively, as e_n^x/A_n changes sign and thus passes through zero. The modulus of the imaginary part of e_n^x/A_n as a function of R/λ_{el} for $x/\lambda_{\mathrm{el}} = 0$ shows a dip close to $R/\lambda_{\mathrm{el}} = 0.2$ due to a phase shift by π in this regime. At $x/\lambda_{\mathrm{el}} = 0.5$, the behaviour is nearly identical to the one at $x/\lambda_{\mathrm{el}} = 0$ and at $x/\lambda_{\mathrm{el}} = 0.25$ and 0.75, $|\mathrm{Im}[e_n^x/A_n]|$ is zero. The modulus of the real part of e_n^y/A_n as a function of R/λ_{el} is shown at $x/\lambda_{\mathrm{el}} = 0.25$, 0.5, 0.75, and 1 in figure 48. For $x/\lambda_{\mathrm{el}} = 1$, it shows a dip around $R/\lambda_{\mathrm{el}} = 0.9$ due to a sign change of $\mathrm{Re}[e_n^y/A_n]$. The modulus of the imaginary part of e_n^y/A_n is displayed for $x/\lambda_{\mathrm{el}} = 0.25$. The behaviour at $x/\lambda_{\mathrm{el}} = 0.75$ is nearly identical to the one at $x/\lambda_{\mathrm{el}} = 0.25$ and at $x/\lambda_{\mathrm{el}} = 0.$, 0.5, and 1, $|\mathrm{Im}[e_n^y/A_n]|$ is zero.

Based on the numerically obtained data for the complex amplitude of the electric field vector, the magnitude of the electric field emitted by the wire can be estimated. For an external frequency of 100 GH and $v_{\mathrm{F}}/gc = 10^{-3}$, it is $\lambda_{\mathrm{el}} \approx 10^{-5}$ m for the second harmonic. With a magnitude of the current amplitude of $\approx 10^{-11}$ A, see section 5.3.2, the electric field has a magnitude of ≈ 10 V/m at $x/\lambda_{\mathrm{el}} = 0$ and $R/\lambda_{\mathrm{el}} = 0.01$.

Poynting Vector

Using the expressions for the magnetic and electric field vectors at a certain frequency $n\omega_{\mathrm{ext}}$ derived above, the Poynting vector at frequency $n\omega_{\mathrm{ext}}$ can be evaluated [296] ,

$$\vec{S}_n(\vec{r},t) = \frac{1}{\mu_0}\left(\vec{E}_{\mathrm{T},n}(\vec{r},t) \times \vec{B}_n(\vec{r},t)\right). \tag{229}$$

Inserting the expressions in eqs. (223) and (227) for the electromagnetic fields and averaging with respect to time yields for $n > 0$ [7, 8, 9]

$$\langle \vec{S}_n(\vec{r},t)\rangle_t = \frac{2}{\mu_0}\mathrm{Re}[\vec{e}_n(\vec{r}) \times \vec{b}_n^*(\vec{r})]. \tag{230}$$

In the far-field approximation, one may obtain an analytic result for the Poynting vector [8, 9],

$$\langle \vec{S}_n(\vec{r},t)\rangle_t = \mu_0 c\, \frac{|A_n(\omega_{\mathrm{ext}})|^2}{2\pi^2}\left(\frac{v_{\mathrm{F}}}{gc}\right)^2 \frac{R^2}{r^5}\,(x, R\cos\phi, R\sin\phi). \tag{231}$$

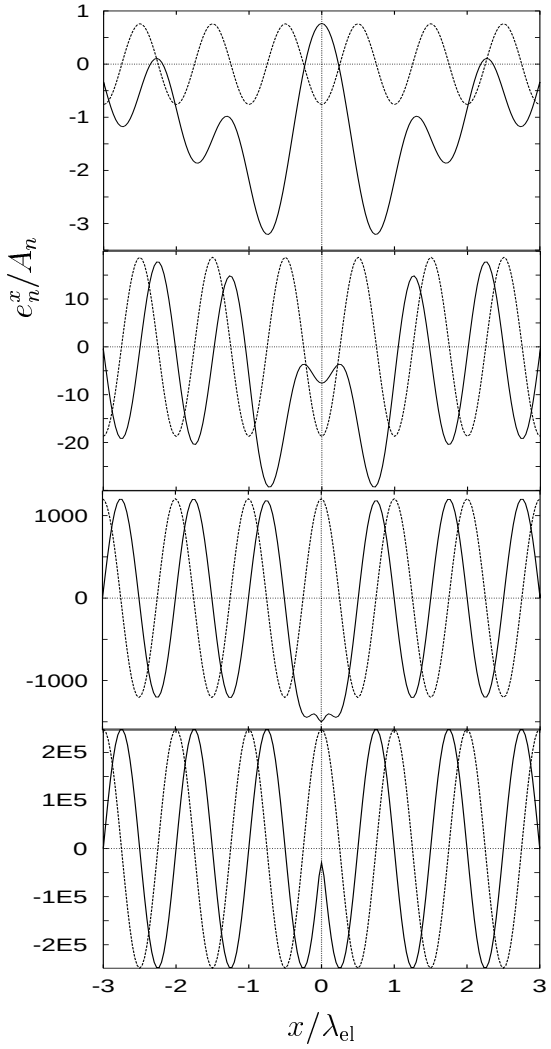

Figure 45: The real (solid) and the imaginary (dashed) parts of the x-component of $\vec{e_n}(\vec{r})/A_n$ (in units of $c\mu_0/\lambda_{\rm el}$) as a function of $x/\lambda_{\rm el}$ for $R/\lambda_{\rm el} = 10^{-2}$ (bottom), 10^{-1} (second from the bottom), 5×10^{-1} (second from the top), and 1 (top). The angle ϕ between R and the y-axes is 0. The ratio of Fermi velocity to velocity of light is $v_{\rm F}/gc = 10^{-3}$.

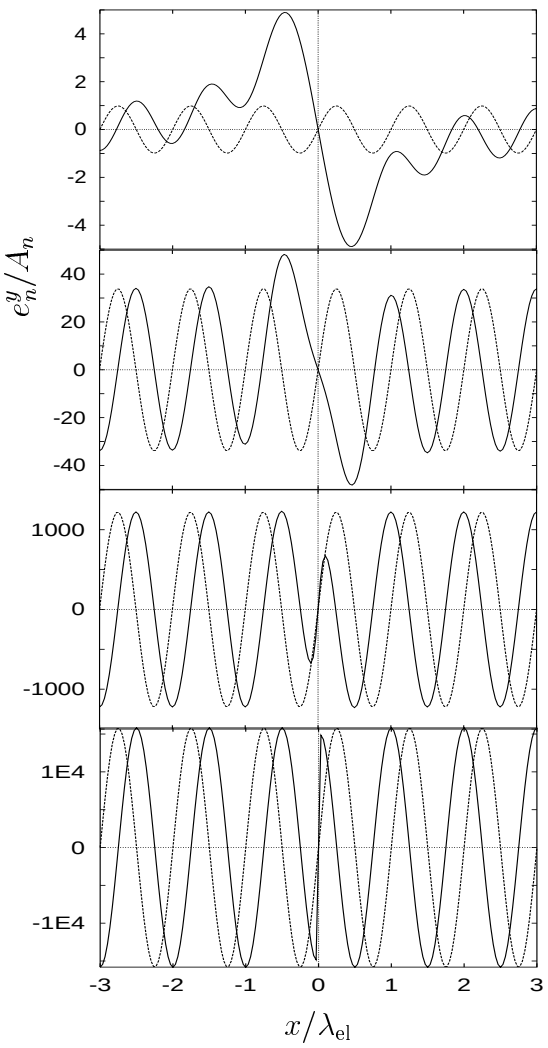

Figure 46: The real (solid) and the imaginary (dashed) parts of the y-component of $\vec{e_n}(\vec{r})/A_n$ (in units of $c\mu_0/\lambda_{\rm el}$) as a function of the position $x\lambda_{\rm el}$ for $R/\lambda_{\rm el} = 10^{-2}$ (bottom), 10^{-1} (second from the bottom), 5×10^{-1} (second from the top), and 1 (top). The angle ϕ between R and the y-axes is 0. The ratio of Fermi velocity to velocity of light is $v_{\rm F}/gc = 10^{-3}$.

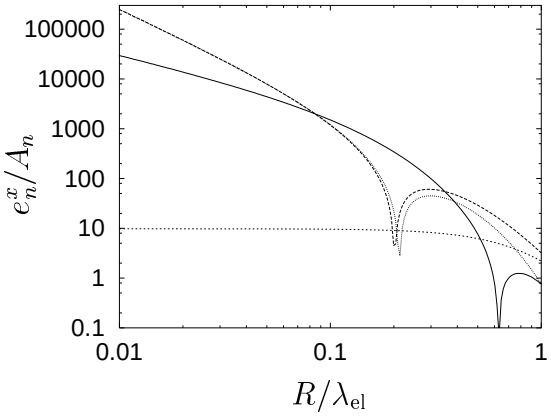

Figure 47: The moduli of the real and imaginary parts of the x-component of $\vec{e}_n/A_n$ as a function of R (in units of $c\mu_0/\lambda_{\rm el}$). The modulus of the real part of e_n^x/A_n is displayed at $x/\lambda_{\rm el} = 0$ (solid), 0.75 (long dashes), and 1 (short dashes). The modulus of the imaginary part of e_n^x/A_n is displayed at $x/\lambda_{\rm el} = 0$ (dotted).

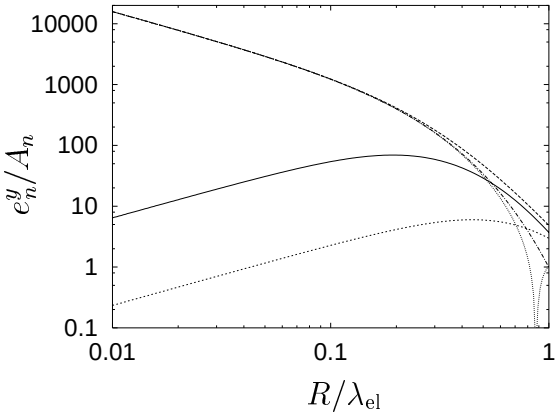

Figure 48: The moduli of the real and imaginary parts of the y-component of $\vec{e}_n/A_n$ as a function of R (in units of $c\mu_0/\lambda_{\rm el}$). The modulus of the real part of e_n^y/A_n is displayed at $x/\lambda_{\rm el} = 0.25$ (solid), 0.5 (long dashes), 0.75 (short dashes), and 1 (dotted). The modulus of the imaginary part of e_n^y/A_n is displayed at $x/\lambda_{\rm el} = 0.25$ (dash-dotted).

The factor $(v_{\rm F}/gc)^2$ indicates that in the far-field regime the emitted power is strongly suppressed for any realistic value of the Fermi velocity. For a current amplitude of the order of $\approx 10^{-11}$ A for the second harmonic, see section 5.3.2, and $v_{\rm F}/gc = 10^{-3}$, the emitted power in the far-field limit has at $x = 0$ a magnitude of $\approx 0.4 \times R^{-2} \times 10^{-26}$ W.

The time-averaged Poynting vector close to the wire can be evaluated numerically [7, 8]. The directions of $\langle \vec{S}_n \rangle_t$ for $\phi = 0$ and $-1.5 < x/\lambda_{\rm el} < 1.5$ are displayed in figure 49 and for $0 < x/\lambda_{\rm el} < 3$ in figure 50. The arrows in figures 49 and 50 all have the same lengths, they do not contain any information on the magnitude of $\langle \vec{S}_n \rangle_t$. Directly at the barrier, $x/\lambda_{\rm el} = 0$, the Poynting vector is perpendicular to the wire for $0.05 < R/\lambda_{\rm el} < 1.0$. Close to the wire, $R/\lambda_{\rm el} \leq 0.1$, but at some distance from the barrier, $x/\lambda_{\rm el} \geq 0.5$, the Poynting vector is parallel to the wire. Around $|x/\lambda_{\rm el}| \approx 0.75$, and $R/\lambda_{\rm el} \approx 0.6$, or $|x/\lambda_{\rm el}| \approx 1.75$ and $R/\lambda_{\rm el} \approx 0.85$, or $|x/\lambda_{\rm el}| \approx 2.75$ and $R/\lambda_{\rm el} \approx 1$, $\langle \vec{S}_n \rangle_t$ shows whirls.

The magnitude of the x-component, the y-component and the modulus of $\langle \vec{S}_n \rangle_t$ as functions of x for different values of R is displayed in figure 51. The x-component of $\langle \vec{S}_n \rangle_t$ is always zero at $x/\lambda_{\rm el} = 0$ while the y-component always has a maximum at that position, compare with figures 49 and 50. For values of x away from the barrier, the x-component of $\langle \vec{S}_n \rangle_t$ is large in comparison to the y-component for $R/\lambda_{\rm el} < 1$.

The behaviour of the x-component and the y-component of $\langle \vec{S}_n \rangle_t$ as functions of R is displayed in figure 52. The solid and the dashed lines represent the decrease of the x-component at $x/\lambda_{\rm el} = 0.25$ and 3, respectively. The dash-dotted line represents

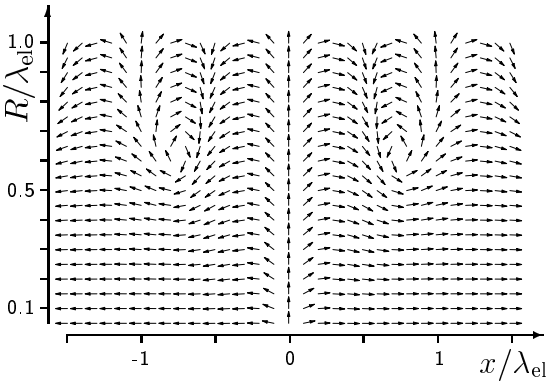

Figure 49: The time-averaged Poynting vector $\langle \vec{S}_n \rangle_t$ as a function of $x/\lambda_{\rm el}$ and $R/\lambda_{\rm el}$ for $-1.5 < x/\lambda_{\rm el} < 1.5$.

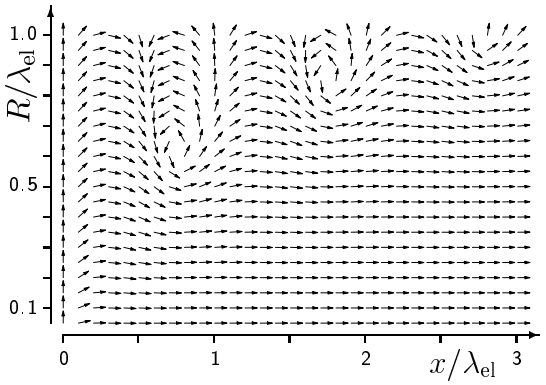

Figure 50: The time-averaged Poynting vector $\langle \vec{S}_n \rangle_t$ as a function of $x/\lambda_{\rm el}$ and $R/\lambda_{\rm el}$ for $0 < x/\lambda_{\rm el} < 3$.

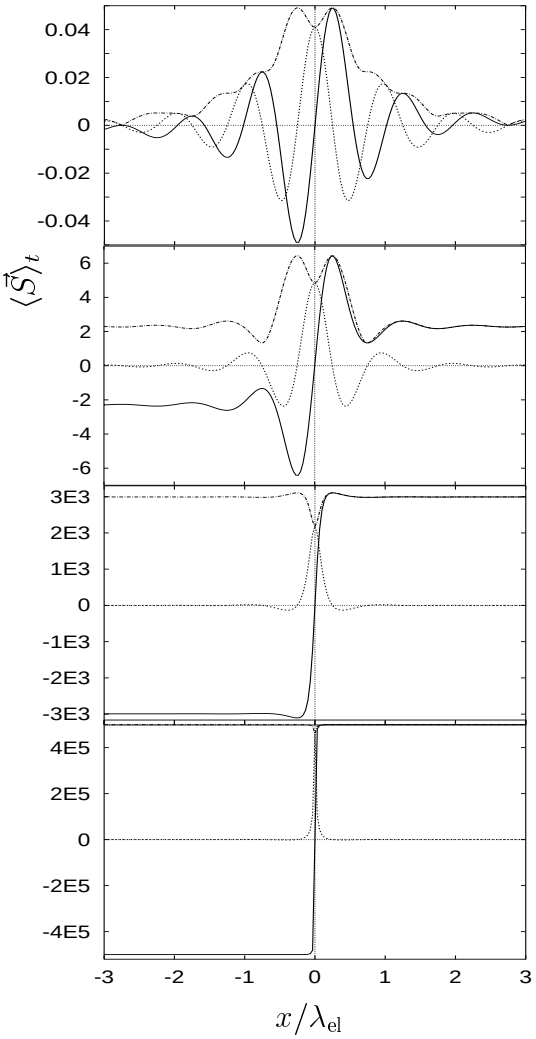

Figure 51: The x-component (solid), the y-component (dashed), and the modulus (dash-dotted) of the time-averaged Poynting vector (in units of $c\mu_0 \, |A_n(\omega_{\rm ext})|^2/\lambda_{\rm el}^2$) as a function of $x/\lambda_{\rm el}$ for $R/\lambda_{\rm el} = 10^{-2}$ (bottom), 10^{-1} (second from the bottom), 5×10^{-1} (second from the top), and 1 (top). The angle ϕ between R and the y-axes is 0. The ration of Fermi velocity to velocity of light is $v_{\rm F}/gc = 10^{-3}$.

the decrease of the y-component at $x/\lambda_{\rm el} = 0$. The behaviour in all three cases is quite similar.

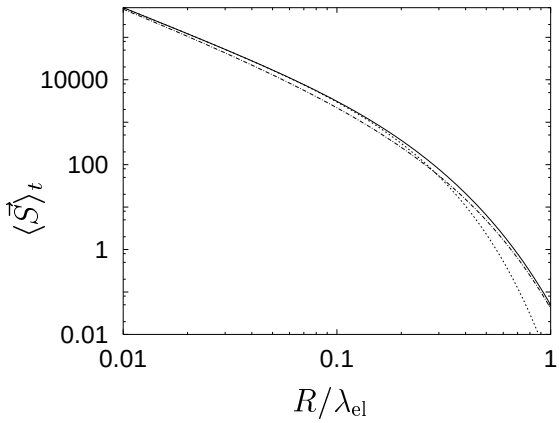

Figure 52: The modulus of the x-component of $\langle \vec{S} \rangle_t$ (in units of $c\mu_0 \, |A_n(\omega_{\rm ext})|^2/\lambda_{\rm el}^2$) as a function of $R/\lambda_{\rm el}$ at $x/\lambda_{\rm el} = 0.25$ (solid) and $x/\lambda_{\rm el} = 3$ (dashed) and the modulus of the y-component of $\langle \vec{S} \rangle_t$ (in units of $c\mu_0 \, |A_n(\omega_{\rm ext})|^2/\lambda_{\rm el}^2$) as a function of $R/\lambda_{\rm el}$ at $x/\lambda_{\rm el} = 0$ (dash-dotted). It is $\phi = 0$ and $v_{\rm F}/gc = 10^{-3}$.

The magnitude of the emitted power close to the wire can be estimated based on the numerical data. For an external frequency of 100 GH and $v_{\rm F}/gc = 10^{-3}$, the wavelength $\lambda_{\rm el} \approx 10^{-5}$ m for the second harmonic. With a magnitude of the current amplitude of $\approx 10^{-11}$ A, the modulus of the y-component of the Poynting vector has a magnitude of $\approx 10^{-7}$ W/m^2 at $x/\lambda_{\rm el} = 0$ and $R/\lambda_{\rm el} = 0.01$ which is much larger than in the far-field regime. The x-component of the Poynting vector is zero at $x/\lambda_{\rm el} = 0$.

5.6 Summary

A single-channel quantum wire containing a potential scattering barrier was studied. The current in such a "dirty" quantum wire as a function of space and time was derived in section 5.1 in the limit of a high scattering barrier and based on the Luttinger model. In section 5.2, dc transport in the dirty wire was discussed. It was shown that the dc current-voltage characteristic is non-linear due to the presence of the scattering barrier *and* electron-electron interactions. The dc current shows non-Fermi liquid behaviour as a function of driving voltage and temperature.

Due to the non-linear current-voltage characteristic, the wire shows higher harmonic generation in ac transport, see section 5.3. In addition to an ac driving voltage, a dc drive was applied in order to break the inversion symmetry of the wire. The resulting dc component of the current, $J^x_{\rm ac,dc}$, was for a screened Coulomb interaction and a finite range of the driving electric field investigated in section 5.3.1. The outward form of the expression for the dc component of the ac current in the dirty quantum wire resembles closely the well-known expression of Tien and Gordon for photon-assisted transport: The dc component of the ac current is given by the true dc current of the system evaluated at the driving voltages $V_{\rm dc} + n\hbar\omega_{\rm ext}/e$, weighted by the occupation probabilities of the sidebands, given by Bessel functions, and summed over all sidebands. What is of course different between the result derived in section 5.3 and the Tien-Gordon formula is the explicit form of the true dc current in the wire: here, it contains the influence of the electron-electron interaction. A further difference is the scaling of the occupation probability of the sidebands with

frequency. In the theory of Tien and Gordon, the argument of the Bessel functions which govern the occupation probability scale with frequency as $\omega_{\rm ext}^{-1}$. We found for the quantum wire scaling exponents between -1 and ≈ -2.7, depending on the range of the driving electric field.

Further, a signature of frequency-locking was found in the differential conductance, $\mathrm{d}J^x_{\rm ac,dc}/\mathrm{d}V_{\rm dc}$. The differential conductance vs. dc drive showed pronounced dips close to integer values of $eV_{\rm dc}/\hbar\omega_{\rm ext}$ for not too large values of the interaction parameter. The frequency-locking depended crucially on the finite range of the electron-electron interaction.

The higher harmonics in the current for a zero-range interaction potential, a zero-range electric field, and a wire of zero diameter were investigated in section 5.3.2. The amplitude of an individual harmonic at frequency $n\omega_{\rm ext}$ was given by a sum over the dc current weighted by Bessel functions. This result was similar to the Tien-Gordon result but with the difference that the tunneling processes via the sidebands, and hence the weight factors of the dc currents, depend on the number of the harmonic. The complex amplitudes of the harmonics of the ac current were investigated numerically as a function of various parameters. As a function of the order of the harmonic, the current amplitudes decrease rapidly. They showed maxima as functions of frequency, dc voltage and interaction strength.

In the discussion of the ac current in the dirty quantum wire the local transverse field was neglected. What one would have to do in order to incorporate the induced transverse field self-consistently into the calculations was discussed in section 5.4. It was argued that an exact treatment of local fields in non-linear transport is virtually impossible. An estimate of the induced transverse field in the dirty quantum wire was presented in section 5.4.2. It is suppressed by a factor $(v_{\rm F}/gc)^2$ with respect to the current and its influence may hence be neglected.

Neglecting the transverse field, the difference between the two approaches that consist of considering *either* electron-electron interactions *or* the local longitudinal field was discussed in section 5.4.1. For an infinitely high barrier, both approaches lead to the same results. For a barrier of finite height, the first approach leads to a non-linear system while the second approach leads to a linear system, i.e. the mean-field like approach fails.

The electromagnetic fields *emitted* by the wire were evaluated in section 5.5. In the far-field limit, explicit expressions could be obtained for the electromagnetic field vectors. Close to the wire, the fields were studied numerically. They showed oscillatory structure as a function of the position x along the wire and decayed fast with increasing distance from the wire, R. The Poynting vector, i.e. the emitted power, given by the vector product of electric and magnetic field was obtained. An analytic expression for the time-averaged Poynting vector was given in the far-field limit. Close to the wire, the emitted power was evaluated numerically. At the barrier, the Poynting vector was perpendicular to the wire while at large x it was parallel to the wire. The Poynting vector decayed with increasing R.

6 Conclusion

Whenever the electronic or the optical properties of a medium in response to an electromagnetic field are to be described theoretically, one faces the task to take account of *local fields* [2]. Especially in time-dependent transport, where the current does not only depend on the total voltage drop but on the explicit spatial shape of the driving field, the consideration of local fields is important. However, in order to take local fields into account rigorously one has to solve the many-body problem of 10^{23} particles correlated via mutual Coulomb interactions *and* via the fields they emit when they are accelerated. This task is in general not solvable. A possible way to tackle local fields without considering the many-body problem is to evaluate the current distribution in the sample and the local field it induces in a self-consistent manner.

For quantum wires with only one subband occupied, a powerful tool exists that allows one to study at least the local longitudinal field rigorously – this tool is the *Luttinger model*. Based on a few assumptions, the many-body Hamiltonian of a 1D system, i.e. a single-channel quantum wire, can be diagonalized exactly [6]. As a consequence, the transport properties of this quantum wire can be evaluated taking microscopic account of electron-electron interactions and hence of the local longitudinal field. The local transverse field can then be evaluated self-consistently based on Maxwell equations [2].

The quantum wire studied in this thesis was modelled as a 3D system confined by a harmonic potential in section 3.1. A "dirty" wire was obtained by introducing a tunneling barrier into the wire. Both wires, the clean one and the dirty one, were assumed to be infinitely long and were not connected to leads. Electron-electron interactions in the wire were taken into account on a microscopic level by exploiting the Luttinger model, see section 3.2. How to evaluate the transverse part of the local field in the wire self-consistently was shown in section 3.3.

Transport Equation
For the clean single-channel quantum wire, a transport equation was derived based on a linear response approach in section 4.1. It was shown that inter-band transitions can be neglected with respect to intra-band transitions when the components of the driving electric field perpendicular to the wire are negligible with respect to the component parallel to the wire. The linear conductivity of the clean single-channel wire was then evaluated based on the Luttinger model.

The transport equation for the dirty quantum wire was evaluated by mapping the Luttinger liquid with impurity onto a dissipative quantum system, section 5.1. The tunneling barrier was assumed to be high and the current in the wire was obtained in lowest order in the tunneling probability. Inter-band transitions were neglected.

DC Transport
Employing the transport equations for the clean wire, we discussed its dc properties in section 4.2. We reproduced for an infinitely strong confinement and a zero-range interaction potential the result that the dc conductance of e^2/h associated with a

single-channel wire should be renormalized by the electron-electron interaction and should be ge^2/h [65], where the parameter g describes the kind and the strength of the interaction. We discussed that this result is true for an infinitely long wire without contacts and that the conductance is e^2/h when contacts are taken into account [154, 155, 156, 158].

For the dirty quantum wire, we derived in section 5.2 the well-known result that, for a zero-range interaction potential, the dc current is proportional to the dc driving voltage to the power of $2/g-1$ [65]: For interacting electrons, $0 < g < 1$, the current-voltage characteristic of the dirty quantum wire is non-linear and this non-linearity is due to the simultaneous presence of the scattering barrier *and* the electron-electron interaction. We also discussed the dc current for a finite-range interaction potential [10, 191].

AC Transport

Coming to time-dependent transport, we discussed the ac conductance of a clean zero-diameter wire in section 4.3 based on [169, 170]. It is expected to reflect the shape of the dispersion relation of the collective excitations of the Luttinger liquid and hence to show features of the electron-electron interaction.

The time-dependent current in the dirty quantum wire was investigated in section 5.3. We studied the dc component of the ac current for a wire of zero diameter, a finite-range interaction potential, and a finite range of the external field in section 5.3.1. The structure of this expression resembled the well-known result of Tien and Gordon [214] for photon-assisted transport: The dc component of the ac current is given by the true dc tunneling current of the system, $J_{\rm dc}$, evaluated at the externally applied dc voltage *plus* a sideband "voltage" $k\hbar\omega_{\rm ext}/e$, weighted by the occupation probability for each sideband of number k and summed over all sidebands. What is different between the expressions obtained by us in section 5.3.1 and the one of Tien and Gordon [214] is the form of the true dc tunneling current, $J_{\rm dc}$. Here, this tunneling current explicitly reflects the influence of the electron-electron interactions. A further difference between the two expressions is the scaling of the occupation probability of the sidebands with frequency. In both expressions, the occupation probability of an individual sideband of number k is given by the square of a Bessel function, $J_k^2(z)$. In [214], the argument of the Bessel function is proportional to $\omega_{\rm ext}^{-1}$. We showed in section 5.3.1 that z exhibits a variety of different scalings depending of the range of the externally applied field and we reproduced the scaling $z \propto \omega_{\rm ext}^{-1}$ for a short ranged field localized at the barrier.

Investigating the differential conductance as a function of the dc voltage, we observed cusps near $eV_{\rm dc} \approx \hbar\omega_{\rm ext}$ for a not too strong electron-electron interaction. This frequency locking effect was only present for an interaction potential of finite range.

In section 5.3.2, we investigated the higher harmonics of the current in the dirty quantum wire. In order to obtain closed analytic expressions for the amplitudes of the harmonics of the current, we assumed a zero-range interaction potential and a delta-form external electric field localized at the barrier. The current amplitudes showed non-Fermi liquid behaviour similar to the dc current in section 5.2. Following

a numerical approach, we discussed the behaviour of the current amplitudes as functions of various parameters in detail. We observed a rich behaviour that could not be condensed into a few universal statements. The most important aspects were that the current amplitudes decreased fast when the order of the harmonic increased. As function, of frequency, dc voltage, and interaction strength, maxima in the current amplitudes were observed. Displayed vs. the ac voltage, the current amplitudes showed a non-linear increase at small ac voltages.

Local Field Effects

Local field effects in the clean single-channel quantum wire were studied in section 4.4. We showed in section 4.4.1 that the linear current given by the conductivity of the interacting system times the *projected external field* is equivalent to the current given by the conductivity of the non-interacting system times the *projected local longitudinal field*. Hence, the mean-field like approach leads to the same result for the current in the wire as does the microscopic consideration of the electron-electron interactions via the Luttinger model. This finding relies crucially on the fact that linear response is exact in the Luttinger model.

For the dirty quantum wire, we showed in section 5.4.1 that for an infinitely high barrier – transport in linear in that case – the mean-field like approach also yields the same result for the current in the wire as does the microscopic approach based on the Luttinger model. For a barrier of finite height, the microscopic approach based on the Luttinger model, on the one hand, leads to a non-linear transport equation and consequently to higher harmonics in the current *and* in the local fields. The mean-field like approach, on the other hand, always leads to a linear system with currents and induced fields oscillating at the frequency of the external driving field only. It fails to capture essential features of the system.

The influence of the local *transverse* field on the properties of the clean wire was investigated in section 4.4.2. We derived a set of coupled integral equations giving the local transverse field in a self-consistent manner. As these integral equations could not be solved analytically, we followed an approximative approach which consisted of discretizing the integral equations. Based on subsequent analytical and numerical investigations of the eigenmodes of the local field we identified a *plasmon polariton* induced by the coupling of the collective charge excitations in the quantum wire and the electromagnetic field. We discussed the dispersion relation of this plasmon polariton and showed that the branches of the dispersion relation exhibit an anti-crossing. The size of the gap at the anti-crossing scales as v_{F}/c. It occurs at the position where the dispersion relations of the two uncoupled systems – charge excitations in the wire and electromagnetic fields – cross.

Further, we estimated the magnitude of the induced transverse field in the clean quantum wire in section 4.4.3. We showed that it is suppressed by a factor v_{F}/c with respect to the external field. Its influence on transport may hence be neglected.

In the dirty quantum wire, a rigorous self-consistent treatment of local fields is virtually impossible due to higher harmonic generation and mixing in the non-linear system, as we discussed in section 5.4. However, we estimated the magnitude of the corrections to the ac current due to an induced transverse field in section 5.4.2. We

showed that this correction was suppressed by a factor $(v_F/gc)^2$ with respect to the current obtained in the absence of the induced transverse field. Hence, the influence of the induced transverse field on transport in the dirty wire can be neglected.

Emitted Electromagnetic Fields

Finally, we evaluated the electromagnetic fields emitted by the dirty wire in section 5.5. The calculations were based on the ac current obtained in section 5.3.2 and Maxwell equations. The magnetic and electric field vectors could in the far-field limit be obtained analytically while in the near-field limit, they were evaluated numerically. In the near-field limit, the components of the complex amplitudes of the fields showed oscillations as functions of the position along the wire. As a function of the distance perpendicular to the wire, the components of the complex amplitudes of the electromagnetic fields decayed. Based on the expressions for the magnetic and electric field vectors, we then evaluated the Poynting vector, i.e. the emitted power. In the far-field limit, we obtained an analytic expression for the time-averaged Poynting vector while in the near-field limit, we evaluated the time-averaged Poynting vector numerically. Also the Poynting vector decayed with the distance from the wire.

A Clean Quantum Wire

The transport equation for the clean quantum wire is derived in appendix A.1. In appendix A.2, it is demonstrated how the the local-field integral equations for a clean quantum wire can be tackled by discretizing them.

A.1 Transport Equation

Linear Response

The linear current through a single-channel wire is, following the Kubo approach [140], compare section 4.1,

$$\vec{J}(\vec{q},\omega) = \int \mathrm{d}\vec{Q}\,'\,\boldsymbol{\sigma}(q_x,\vec{Q},\vec{Q}\,',\omega)\cdot\vec{E}(q_x,\vec{Q}\,',\omega), \tag{232}$$

where the conductivity tensor is in the long wavelength limit for an arbitrary number of occupied subbands

$$\begin{aligned}\sigma^{\alpha\beta}(q_x,\vec{Q},\vec{Q}\,',\omega) &= \frac{1}{(2\pi)^2}\sum_{n,l}\sigma^{\mathrm{dia}}_{nl}(\omega)\,B^x_{nl}(\vec{Q}-\vec{Q}\,')\,\delta_{\alpha\beta} \\ &+ \frac{1}{(2\pi)^2}\sum_{n,l,s,p}\chi^{\alpha\beta}_{nlsp}(q_x,\omega)\,B^{\alpha}_{nl}(\vec{Q})\,B^{\beta}_{sp}(-\vec{Q}\,'),\end{aligned} \tag{233}$$

and the generalized diamagnetic conductivity is

$$\sigma^{\mathrm{dia}}_{nl}(\omega) = \frac{\mathrm{i}e^2\langle\rho_{nl}(q_x=0)\rangle_{\mathrm{s}}}{m\omega L}. \tag{234}$$

The current-current correlation functions $\chi^{\alpha\beta}_{nlsp}$ are

$$\chi^{\alpha\beta}_{nlsp}(q_x,\omega) = \frac{e^2}{\hbar\omega L}\int\limits_{-\infty}^{\infty}\mathrm{d}\tau\,\Theta(\tau)\,\mathrm{e}^{\mathrm{i}\omega\tau}\,\langle[j^{\alpha}_{nl}(q_x,\tau),j^{\beta}_{sp}(-q_x,0)]\rangle_{\mathrm{s}}. \tag{235}$$

The remaining task is to evaluate these current-current correlation functions.

It is to be studied under which conditions it is reasonable to assume $n=l=s=p=0$ in eq. (233) in order to model a single-channel wire. Therefore, the current-current correlation functions are evaluated for non-interacting electrons, where it is possible to consider inter-band transitions, and then the contribution of these inter-band transitions to the conductivity is compared with the contribution of the intra-band transitions.

Many Occupied Subbands

Consider the current-current correlation functions for non-interacting electrons and arbitrary indices. One inserts for j^{α}_{nl} the expressions given in eqs. (25) and (26). It

is then straightforward to perform the commutators and to obtain the expectation values. For $\alpha, \beta \neq x$ it is

$$\chi^{xx}_{nlsp}(q_x,\omega) = \frac{\mathrm{i}e^2}{\hbar\omega L}\left(\frac{\hbar}{2m}\right)^2 \sum_k \frac{(2k+q_x)^2(n_{n,k+q_x}-n_{l,k})\,\delta_{pn}\delta_{sl}}{\omega+\Delta_{k+q_x,k}+\Delta_{nl}}, \quad (236)$$

$$\chi^{x\beta}_{nlsp}(q_x,\omega) = -\frac{e^2}{\hbar\omega L d}\left(\frac{\hbar}{2m}\right)^2 \sum_k \frac{(2k+q_x)(n_{n,k+q_x}-n_{l,k})\,\delta_{pn}\delta_{sl}}{\omega+\Delta_{k+q_x,k}+\Delta_{nl}}, \quad (237)$$

$$\chi^{\alpha x}_{nlsp}(q_x,\omega) = -\frac{e^2}{\hbar\omega L d}\left(\frac{\hbar}{2m}\right)^2 \sum_k \frac{(2k+q_x)(n_{n,k+q_x}-n_{l,k})\,\delta_{pn}\delta_{sl}}{\omega+\Delta_{k+q_x,k}+\Delta_{nl}}, \quad (238)$$

$$\chi^{\alpha\beta}_{nlsp}(q_x,\omega) = -\frac{\mathrm{i}e^2}{\hbar\omega L d^2}\left(\frac{\hbar}{2m}\right)^2 \sum_k \frac{(n_{n,k+q_x}-n_{l,k})\,\delta_{pn}\delta_{sl}}{\omega+\Delta_{k+q_x,k}+\Delta_{nl}}, \quad (239)$$

where

$$\Delta_{nl} = \frac{E_n - E_l}{\hbar}, \quad (240)$$

$$\Delta_{k+q_x,k} = \frac{E_{k+q_x} - E_k}{\hbar}, \quad (241)$$

$$E_k = \frac{\hbar^2 k^2}{2m}. \quad (242)$$

The expectation value of the particle number operator for a certain wave number k in subband n is

$$n_{n,k} = \langle c^\dagger_{n,k} c_{n,k}\rangle_{\mathrm{s}}. \quad (243)$$

The right hand sides of eqs. (237) - (239) do not depend on α or β in an explicit way. This is due to the rotational symmetry of system: $\chi^{x\beta}_{nlsp}$ is equal for $\beta = y$ and $\beta = z$, $\chi^{\alpha x}_{nlsp}$ is equal for $\alpha = y$ and $\alpha = z$, and also $\chi^{\alpha\beta}_{nlsp}$ is equal for any combination of $\alpha = y, z$ and $\beta = y, z$.

One Occupied Subband

Any of the expressions in eqs. (236) - (239) contains a combination of particle numbers $n_{n,k+q_x} - n_{l,k}$. When only the lowest subband is occupied, $n_{n,k+q_x} = 0$ for $n \neq 0$ and $n_{l,k} = 0$ for $l \neq 0$. But for $n_{n,k+q_x}$, l may have any value and for $n_{l,k}$, n may have any value. Hence, one cannot put generally either n or l to zero in eqs. (236) - (239) but one has to consider also inter-band transitions.

In order to judge the importance of inter-band transitions, proceed by inserting the expressions for the correlation functions into the expression for the conductivity in eq. (233). Concentrate on the paramagnetic part of the conductivity,

$$\sigma^{\mathrm{para},\alpha\beta}(q_x,\vec{Q},\vec{Q}\,',\omega) = \frac{1}{(2\pi)^2}\sum_{n,l,s,p} \chi^{\alpha\beta}_{nlsp}(q_x,\omega)\, B^\alpha_{nl}(\vec{Q})\, B^\beta_{sp}(-\vec{Q}\,'). \quad (244)$$

Using the above expressions for $\chi^{\alpha\beta}_{nlsp}(q_x,\omega)$, can the sums with respect to n, l, s, p be performed? When the functions $B^\alpha_{nl}(\vec{Q})$ and $B^\beta_{sp}(-\vec{Q}\,')$ are expressed in terms of

their Fourier transforms, $B^{\alpha}_{nl}(\vec{R})$ and $B^{\beta}_{sp}(\vec{R}\,')$, it turns out that the sum in eq. (244) is similar to the expression of the Fourier transform of a time-dependent Green's function $G(\vec{R},\vec{R}\,',t)$ [297, 298]. The explicit result for the latter may be found in [297, 298]. But it is impossible to perform analytically the Fourier transform of $G(\vec{R},\vec{R}\,',t)$ in order to obtain $G(\vec{R},\vec{R}\,',z)$ with $z=\omega+\Delta_{k+q_x,k}+\Omega/2$ as is needed here.

Instead to attempt an exact summation of the paramagnetic conductivity in eq. (244), consider the limit of a large subband separation, $\omega+\Delta_{k+q_x,k}\ll\Omega$, and estimate how large the contribution of inter-band transitions is with respect to the contribution due to intra-band transitions. As the largest value for the wave number giving a non-zero contribution to the sums in eqs. (236) - (239) at zero temperature is $k_{\rm F}$, $\Delta_{k+q_x,k}$ is bounded above for finite q_x. Take χ^{xx}_{nlsp} and insert it into eq. (244). Assume the lowest subband occupied, interchange the summations over the band indices with the summation over k, and use $B^{x}_{nl}(\vec{Q})=B^{x}_{ln}(\vec{Q})$, then

$$\begin{aligned}\sigma^{{\rm para},xx}(q_x,\vec{Q},\vec{Q}\,',\omega) &= \frac{1}{(2\pi)^2}\frac{{\rm i}e^2}{\hbar\omega L}\left(\frac{\hbar}{2m}\right)^2\sum_k(2k+q_x)^2 \\ &\times \sum_{n=0}^{\infty}\left\{\frac{n_{0,k+q_x}}{\omega+\Delta_{k+q_x,k}-\Delta_{n0}}-\frac{n_{0,k}}{\omega+\Delta_{k+q_x,k}+\Delta_{n0}}\right\} \\ &\times B^{x}_{n0}(\vec{Q})\,B^{x}_{n0}(-\vec{Q}\,').\end{aligned} \tag{245}$$

Split off the term with $n=0$ and use the definition of Δ_{nl},

$$\begin{aligned}\sigma^{{\rm para},xx}(q_x,\vec{Q},\vec{Q}\,',\omega) &= \frac{1}{(2\pi)^2}\frac{{\rm i}e^2}{\hbar\omega L}\left(\frac{\hbar}{2m}\right)^2\sum_k(2k+q_x)^2 \\ &\times \left\{\left(\frac{n_{0,k+q_x}}{\omega+\Delta_{k+q_x,k}}-\frac{n_{0,k}}{\omega+\Delta_{k+q_x,k}}\right)B^{x}_{00}(\vec{Q})\,B^{x}_{00}(-\vec{Q}\,')\right. \\ &+ \sum_{n=1}^{\infty}\left(\frac{n_{0,k+q_x}}{\omega+\Delta_{k+q_x,k}-n\Omega}-\frac{n_{0,k}}{\omega+\Delta_{k+q_x,k}+n\Omega}\right) \\ &\times \left. B^{x}_{n0}(\vec{Q})\,B^{x}_{n0}(-\vec{Q}\,')\right\},\end{aligned} \tag{246}$$

where Ω is the curvature of the harmonic confinement potential.

Now, compare the terms describing intra-band transitions, $n=0$, with those describing inter-band transitions, $n>0$, in eq. (246). For $\omega+\Delta_{k+q_x,k}\ll\Omega$, already the first order term with $n_y=1$ or $n_z=1$ is much smaller than the lowest order term with $n_y=n_z=0$ if $q_x\neq 0$. One may hence choose ω and q_x ($\neq 0$) small enough, namely well below the values at which they can induce inter-band transitions of excitation energy $\hbar\Omega$, in order to assure that the term for $n=0$ is bigger than the remaining sum. For a large subband spacing it is thus reasonable to set all summation indices to zero when evaluating the element of the conductivity tensor for $\alpha=\beta=x$.

Considering the off-diagonal elements of the conductivity one can in principle proceed as above. However, for $\alpha=x$ or $\beta=x$ with $\alpha\neq\beta$, the term with

$n = l = 0$ in the paramagnetic conductivity vanishes as $B^{\alpha}_{00}(\vec{Q}) = 0$ for $\alpha \neq x$. The leading term is obtained for $n = 0$ and $l = 1$ or $n = 1$ and $l = 0$, the diamagnetic conductivity is not present. Can this term be neglected with respect to the diagonal terms of the conductivity? The leading order terms of $\chi^{x\beta}_{nlsp}$ or $\chi^{\alpha x}_{nlsp}$ for $\alpha, \beta \neq x$ contain an Ω in the denominator, in contrast to the leading order term of χ^{xx}_{nlsp}. On the other hand, the former two have a prefactor proportional to $1/d$ and hence proportional to $\sqrt{\Omega}$. However, they still vary with $1/\sqrt{\Omega}$ for large Ω, while the leading order term of χ^{xx}_{nlsp} does not depend on Ω. But assume a driving field that has only a y-component. Then, χ^{xx}_{nlsp} would not contribute at all to the current in contrast to χ^{xy}_{nlsp}. As a consequence, the off-diagonal terms cannot be neglected which implies that inter-band transitions cannot be neglected. Therefore, a condition for the neglect of inter-band transitions is that the driving field must have a component parallel to the wire which should further be comparable to or larger than the y and z-components of the driving field.

When α and β are both different from x, the term with $n = l = 0$ in the paramagnetic conductivity also vanishes. The lowest order term in the conductivity then consists of the diamagnetic term plus the paramagnetic term at $n = 0$ and $l = 1$ or $n = 1$ and $l = 0$ for $\alpha = \beta$ or of the paramagnetic term at $n = 0$ and $l = 1$ or $n = 1$ and $l = 0$ alone for $\alpha \neq \beta$. One encounters the difficulty that the prefactor of $\chi^{\alpha\beta}_{nlsp}$ is proportional to $1/d^2$ and hence to Ω. Hence, despite the Ω in the denominator, the paramagnetic term does not decrease with increasing Ω. For $\alpha = \beta$, one might say that the paramagnetic part renormalizes the diamagnetic conductivity. Also the off-diagonal terms give contributions to the current which do not vanish for large Ω. These terms may only be neglected when the x-component is the dominant part of the driving electric field.

In summary, it was shown that for a large subband separation, σ^{xx} is dominated by intra-band transitions, i.e. inter-band transitions can be neglected. However, for transport perpendicular to the wire, the leading order contribution to the conductivity is provided by inter-band processes. Hence, the conductivity of the single channel wire may only be approximated by taking the general expression for the conductivity in eq. (233) and setting all indices to zero when the x-component of the driving electric field is the dominant component of the field. Results for components of the current perpendicular to the wire should be interpreted with care.

It is assumed that the arguments presented here are qualitatively also valid for a system of interacting electrons.

A.2 Local Field Effects

Below, the discretized local-field equations are derived and it is shown that they can be written in terms of matrix equations. An explicit expression for the discretized local field is given and also for the discretized dielectric function. Based on the discrete local-field matrix equations, it is discussed under which conditions local-field eigenmodes exist.

A.2.1 Discretization of the Local-Field Integral Equations

Local-Field Integral Equations

The local field integral equations for linear transport in a clean quantum wire are, see sections 3.3 and 4.4 for the derivation,

$$\begin{aligned}\vec{E}_{\rm L}(\vec{q},\omega) &= \vec{E}_{\rm L,ext}(\vec{q},\omega) \qquad (247)\\ &+ \int {\rm d}\vec{Q}\,'\, \boldsymbol{K}_{\mathbf{L}}(q_x,\vec{Q},\vec{Q}\,',\omega)\cdot\left[\vec{E}_{\rm L,ext}(q_x,\vec{Q}\,',\omega)+\vec{E}_{\rm T}(q_x,\vec{Q}\,',\omega)\right],\\ \vec{E}_{\rm T}(\vec{q},\omega) &= \vec{E}_{\rm T,ext}(\vec{q},\omega) \qquad (248)\\ &+ \int {\rm d}\vec{Q}\,'\, \boldsymbol{K}_{\mathbf{T}}(q_x,\vec{Q},\vec{Q}\,',\omega)\cdot\left[\vec{E}_{\rm L,ext}(q_x,\vec{Q}\,',\omega)+\vec{E}_{\rm T}(q_x,\vec{Q}\,',\omega)\right],\end{aligned}$$

with the Kernels

$$\begin{aligned}K_{\rm L}^{\alpha\beta}(q_x,\vec{Q},\vec{Q}\,',\omega) &= \frac{1}{{\rm i}\epsilon_0\omega}\, L^{\alpha\beta}(\vec{q})\,\sigma_{\rm 1b}^{\beta\beta}(q_x,\vec{Q},\vec{Q}\,',\omega), \qquad (249)\\ K_{\rm T}^{\alpha\beta}(q_x,\vec{Q},\vec{Q}\,',\omega) &= {\rm i}\mu_0\omega\, g_0(\vec{q},\omega)\, T^{\alpha\beta}(\vec{q})\,\sigma_{\rm 1b}^{\beta\beta}(q_x,\vec{Q},\vec{Q}\,',\omega). \qquad (250)\end{aligned}$$

The matrices $\boldsymbol{L}$ and $\boldsymbol{T}$ are, see eqs. (79) and (80),

$$\begin{aligned}L^{\alpha\beta}(\vec{q}) &= \frac{q_\alpha q_\beta}{|\vec{q}|^2}, \qquad (251)\\ T^{\alpha\beta}(\vec{q}) &= \delta_{\alpha\beta}-\frac{q_\alpha q_\beta}{|\vec{q}|^2}, \qquad (252)\end{aligned}$$

the function $g_0(\vec{q},\omega)$ is given in eq. (86),

$$g_0(\vec{q},\omega)=\lim_{\eta\to 0}\frac{1}{q^2-\left(\frac{\omega}{c}+{\rm i}\eta\right)^2}, \qquad (253)$$

and the elements of the conductivity tensor of the single-channel wire are, following eq. (137),

$$\begin{aligned}\sigma_{\rm 1b}^{\alpha\beta}(q_x,\vec{Q},\vec{Q}\,',\omega) &= \frac{1}{(2\pi)^2}\,\sigma_{00}^{\rm dia}(\omega)\,B_{00}^{x}(\vec{Q}-\vec{Q}\,')\,\delta_{\alpha\beta} \qquad (254)\\ &+ \frac{1}{(2\pi)^2}\,\chi_{0000}^{xx}(q_x,\omega)\,B_{00}^{x}(\vec{Q})\,B_{00}^{x}(-\vec{Q}\,')\delta_{\alpha x}\delta_{\beta x},\end{aligned}$$

with, see eq. (138),

$$\sigma_{00}^{\rm dia}(\omega)=\frac{{\rm i}e^2 n_0}{m\omega}, \qquad (255)$$

where $n_0=N_0/L=mv_{\rm F}/\pi\hbar$ is the particle density in the lowest subband and the correlation function χ_{0000}^{xx} is, see eq. (139),

$$\chi_{0000}^{xx}(q_x,\omega)=\sigma_{00}^{\rm dia}(\omega)\,\lim_{\eta\to 0}\frac{\omega_{\rm LL}^2(q_x)}{(\omega+{\rm i}\eta)^2-\omega_{\rm LL}^2(q_x)}, \qquad (256)$$

where the dispersion relation $\omega_{\rm LL}(q_x)$ is given in eq. (50). The explicit form of the Fourier transform of the projected interaction potential needed in $\omega_{\rm LL}(q_x)$ is for an infinite-range Coulomb interaction and a symmetric harmonic confinement given in eq. (53).

Discretization Procedure

Now, the local-field integral equations in (247) and (248) are discretized, i.e. the integrals are replaced by sums. A single integral can be discretized expressing it in terms of a sum using N abscissas,

$$\int_a^b \mathrm{d}x\, w(x) f(x) \approx \sum_{k=1}^{N} w_{N,k} f(\nu_{N,k}). \tag{257}$$

For $N \to \infty$, the expressions on the left and the right hand sides of eq. (257) are exactly identical. Choose the weight function $w(x) = \mathrm{e}^{-x^2}$ and the limits of integration $a = -\infty$, $b = \infty$. Then, according to the Gaussian quadrature, the abscissas $\nu_{N,k}$ are given by the N zeroes of the Hermite polynomials $H_N(x)$ and the weights are [299]

$$w_{N,k} = \frac{2^{N+1}\, N!\, \sqrt{\pi}}{[H_{N+1}(\nu_{N,k})]^2}. \tag{258}$$

It is $\nu_{N,k} < \nu_{N,k+1}$, further $\nu_{N,k} < 0$ for $1 \le k \le \mathrm{int}[N/2]$, where $\mathrm{int}[u/v]$ gives the integer part of u/v cutting all decimals, and $\nu_{N,k} \ge 0$ for $\mathrm{int}[N/2] < k \le N$ with $\nu_{N,k} = -\nu_{N,N+1-k}$, see figure 53. For odd N, $\nu_{N,\mathrm{int}[N/2]+1} = 0$. With increasing N, the abscissas move closer together. The weights are always positive with $w_{N,k} < \sqrt{\pi}$ for any N and k. They have a maximum at $k = \mathrm{int}[N/2]+1$ for odd N or at $k = N/2$ and $k = N/2+1$ for even N. They decrease with decreasing k for $k < (N+1)/2$ and with increasing k for $k > (N+1)/2$, see figure 54.

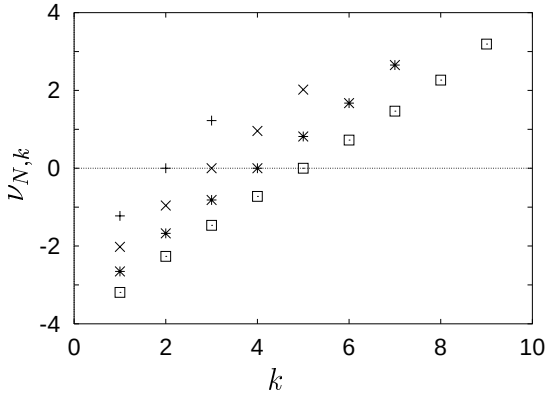

Figure 53: The abscissas $\nu_{N,k}$ as a function of k for $N = 3$ (+), $N = 5$ (×), $N = 7$ (∗), and $N = 9$ (□).

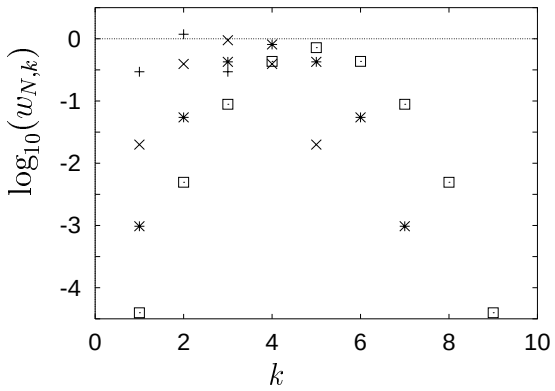

Figure 54: The logarithm (base 10) of the weight $w_{N,k}$ as a function of k for $N = 3$ (+), $N = 5$ (×), $N = 7$ (∗), and $N = 9$ (□).

In order to discretize the local field integral equations, proceed in the following manner. Choose N abscissas for the integration with respect to q_y' and M abscissas for the integration with respect to q_z'. Substitute $\vec{Q}\,'$ on the right hand sides of eqs. (247) and (248) by $\vec{Q}\,' = 4\vec{Q}\,''/d$. Due to the choice of the weight function, the kernels $\boldsymbol{K_{L/T}}(q_x, \vec{Q}, 4\vec{Q}\,''/d, \omega)$ have to be multiplied by $\mathrm{e}^{Q''^2}$. This product times

the electric fields is to be taken at $q_y'' = \nu_{N,l}$ and $q_z'' = \nu_{M,k}$ for $l = 1, \ldots, N$ and $k = 1, \ldots, M$. The whole product is then multiplied by the weights $w_{N,l}$ and $w_{M,k}$ and summed with respect to l and k. In order to have electric fields evaluated at the same discrete values on the left and on the right hand side of the integral equations, choose $q_y = (4/d)\nu_{N,n}$ and $q_z = (4/d)\nu_{M,m}$ in the electric fields on the left hand side of eqs. (247) and (248) and also in the kernels on the right hand side. Finally, define

$$
\begin{aligned}
f_{nm}(q_x) &= f(q_x, 4\nu_{N,n}/d, 4\nu_{M,m}/d), && (259)\\
g_{nmlk}(q_x) &= g(q_x, 4\nu_{N,n}/d, 4\nu_{M,m}/d, 4\nu_{N,l}/d, 4\nu_{M,k}/d), && (260)
\end{aligned}
$$

where f is any function depending on $\vec{q}$ and g is any function depending on $\vec{q}$ and $\vec{Q}\,'$. Note that the functions f_{nm} and g_{nmlk} depend also on the choice of N and M.

Discretized Local-Field Equations

Following the steps outlined above, one obtains instead of eqs. (247) and (248),

$$
\begin{aligned}
E^{\alpha}_{\mathrm{L},nm}(q_x,\omega) &= E^{\alpha}_{\mathrm{L,ext},nm}(q_x,\omega) && (261)\\
&+ \sum_{\beta}\sum_{\substack{l=1,\\ k=1}}^{N,M}\left(\frac{4}{d}\right)^2 w_{N,l}\, w_{M,k}\, \mathrm{e}^{\nu_{N,l}^2+\nu_{M,k}^2}\, K^{\alpha\beta}_{\mathrm{L},nmlk}(q_x,\omega)\\
&\times \left[E^{\beta}_{\mathrm{L,ext},lk}(q_x,\omega) + E^{\beta}_{\mathrm{T},lk}(q_x,\omega)\right],\\
E^{\alpha}_{\mathrm{T},nm}(q_x,\omega) &= E^{\alpha}_{\mathrm{T,ext},nm}(q_x,\omega) && (262)\\
&+ \sum_{\beta}\sum_{\substack{l=1,\\ k=1}}^{N,M}\left(\frac{4}{d}\right)^2 w_{N,l}\, w_{M,k}\, \mathrm{e}^{\nu_{N,l}^2+\nu_{M,k}^2}\, K^{\alpha\beta}_{\mathrm{T},nmlk}(q_x,\omega)\\
&\times \left[E^{\beta}_{\mathrm{L,ext},lk}(q_x,\omega) + E^{\beta}_{\mathrm{T},lk}(q_x,\omega)\right],
\end{aligned}
$$

with $\alpha, \beta = x, y, z$. This set of $3NM$ coupled linear equations can be written in terms of matrix equations,

$$
\begin{aligned}
\vec{\mathcal{E}}_{\mathrm{L}}(q_x,\omega) &= \boldsymbol{M_{LL}}(q_x,\omega)\cdot\vec{\mathcal{E}}_{\mathrm{L,ext}}(q_x,\omega) + \boldsymbol{M_{LT}}(q_x,\omega)\cdot\vec{\mathcal{E}}_{\mathrm{T,ext}}(q_x,\omega), && (263)\\
\vec{\mathcal{E}}_{\mathrm{T}}(q_x,\omega) &= \boldsymbol{M_{TL}}(q_x,\omega)\cdot\vec{\mathcal{E}}_{\mathrm{L,ext}}(q_x,\omega) + \boldsymbol{M_{TT}}(q_x,\omega)\cdot\vec{\mathcal{E}}_{\mathrm{T,ext}}(q_x,\omega). && (264)
\end{aligned}
$$

The $(3NM)$-dimensional discretized field vectors are

$$\vec{\mathcal{E}}_{\mathrm{L/T}} = \begin{pmatrix} E^x_{\mathrm{L/T},11} \\ \vdots \\ E^x_{\mathrm{L/T},1M} \\ E^x_{\mathrm{L/T},21} \\ \vdots \\ E^x_{\mathrm{L/T},2M} \\ \vdots \\ E^x_{\mathrm{L/T},NM} \\ E^y_{\mathrm{L/T},11} \\ \vdots \\ E^y_{\mathrm{L/T},NM} \\ E^z_{\mathrm{L/T},11} \\ \vdots \\ E^z_{\mathrm{L/T},NM} \end{pmatrix} \quad \text{and} \quad \vec{\mathcal{E}}_{\mathrm{L/T,ext}} = \begin{pmatrix} E^x_{\mathrm{L/T,ext},11} \\ \vdots \\ E^x_{\mathrm{L/T,ext},1M} \\ E^x_{\mathrm{L/T,ext},21} \\ \vdots \\ E^x_{\mathrm{L/T,ext},2M} \\ \vdots \\ E^x_{\mathrm{L/T,ext},NM} \\ E^y_{\mathrm{L/T,ext},11} \\ \vdots \\ E^y_{\mathrm{L/T,ext},NM} \\ E^z_{\mathrm{L/T,ext},11} \\ \vdots \\ E^z_{\mathrm{L/T,ext},NM} \end{pmatrix}. \tag{265}$$

Comparison of eq. (264) with eq. (262) yields for the elements of the inverse of the $(3NM \times 3NM)$ matrix $\boldsymbol{M_{TT}}$,

$$\begin{aligned} \left(\boldsymbol{M_{TT}}^{-1}(q_x,\omega)\right)^{ij} &= \delta_{ij} - \left(\frac{4}{d}\right)^2 w_{N,\vartheta(j)} w_{M,\varphi(j)}\, \mathrm{e}^{\nu^2_{N,\vartheta(j)}+\nu^2_{M,\varphi(j)}} \\ &\times \quad K^{\gamma(i)\gamma(j)}_{\mathrm{T},\vartheta(i)\varphi(i)\vartheta(j)\varphi(j)}(q_x,\omega). \end{aligned} \tag{266}$$

The integer i denotes a line and the integer j a column of the matrix. The functions $\vartheta(s)$, $\varphi(s)$ and $\gamma(s)$ are given below. Further, comparing again eq. (264) with eq. (262) using eq. (266) yields for the elements of the $(3NM \times 3NM)$ matrix $\boldsymbol{M_{TL}}$,

$$\boldsymbol{M_{TL}}(q_x,\omega) = \boldsymbol{M_{TT}}(q_x,\omega) \cdot \left[\mathbf{1} - \boldsymbol{M_{TT}}^{-1}(q_x,\omega)\right]. \tag{267}$$

The $(3NM \times 3NM)$ matrices giving the local longitudinal field are related to those giving the local transverse field, as can be seen by comparing eq. (263) with eq. (261) inserting eq. (262) for the local transverse field,

$$\boldsymbol{M_{LL}}(q_x,\omega) = \mathbf{1} + \boldsymbol{M}(q_x,\omega) \cdot [\mathbf{1} + \boldsymbol{M_{TL}}(q_x,\omega)], \tag{268}$$

$$\boldsymbol{M_{LT}}(q_x,\omega) = \boldsymbol{M}(q_x,\omega) \cdot \boldsymbol{M_{TT}}(q_x,\omega), \tag{269}$$

where the elements of the $(3NM \times 3NM)$ matrix $\boldsymbol{M}$ are

$$\begin{aligned} \left(\boldsymbol{M}(q_x,\omega)\right)^{ij} &= \left(\frac{4}{d}\right)^2 w_{N,\vartheta(j)} w_{M,\varphi(j)}\, \mathrm{e}^{\nu^2_{N,\vartheta(j)}+\nu^2_{M,\varphi(j)}} \\ &\times \quad K^{\gamma(i)\gamma(j)}_{\mathrm{L},\vartheta(i)\varphi(i)\vartheta(j)\varphi(j)}(q_x,\omega). \end{aligned} \tag{270}$$

The interrelation between the matrices $\boldsymbol{M_{TA}}$ and $\boldsymbol{M_{LA}}$ with A standing for L or T is due to the fact that only the integral equation for the local transverse field is

really a self-consistent equation. The local longitudinal field is known the moment one knows the local transverse field. Further, the discretized kernels are

$$\mathrm{e}^{\nu^2_{N,\vartheta(j)}+\nu^2_{M,\varphi(j)}}\, K^{\gamma(i)\gamma(j)}_{\mathrm{L},\vartheta(i)\varphi(i)\vartheta(j)\varphi(j)}(q_x,\omega) = \tag{271}$$

$$\frac{\sigma^{\mathrm{dia}}_{00}(\omega)\mathrm{e}^{-\nu^2_{N,\vartheta(i)}-\nu^2_{M,\varphi(i)}}\, L^{\gamma(i)\gamma(j)}_{\vartheta(i)\varphi(i)}(q_x)}{\mathrm{i}\epsilon_0\omega(2\pi)^2}$$

$$\times \quad \left\{ \mathrm{e}^{2\nu_{N,\vartheta(i)}\nu_{N,\vartheta(j)}+2\nu_{M,\varphi(i)}\nu_{M,\varphi(j)}} + \frac{\omega^2_{\mathrm{LL}}(q_x)\delta_{\gamma(j)1}}{\omega^2-\omega^2_{\mathrm{LL}}(q_x)} \right\},$$

$$\mathrm{e}^{\nu^2_{N,\vartheta(j)}+\nu^2_{M,\varphi(j)}}\, K^{\gamma(i)\gamma(j)}_{\mathrm{T},\vartheta(i)\varphi(i)\vartheta(j)\varphi(j)}(q_x,\omega) = \tag{272}$$

$$\frac{\mathrm{i}\mu_0\omega\,\sigma^{\mathrm{dia}}_{00}(\omega)\,\mathrm{e}^{-\nu^2_{N,\vartheta(i)}-\nu^2_{M,\varphi(i)}}\, T^{\gamma(i)\gamma(j)}_{\vartheta(i)\varphi(i)}(q_x)}{(2\pi)^2\left[q_x^2+\left(\frac{4\nu_{N,\vartheta(i)}}{d}\right)^2+\left(\frac{4\nu_{M,\varphi(i)}}{d}\right)^2-\left(\frac{\omega}{c}\right)^2\right]}$$

$$\times \quad \left\{ \mathrm{e}^{2\nu_{N,\vartheta(i)}\nu_{N,\vartheta(j)}+2\nu_{M,\varphi(i)}\nu_{M,\varphi(j)}} + \frac{\omega^2_{\mathrm{LL}}(q_x)\delta_{\gamma(j)1}}{\omega^2-\omega^2_{\mathrm{LL}}(q_x)} \right\}.$$

The functions $\gamma(s)$, $\vartheta(s)$, and $\varphi(s)$ (s integer) relate the 6 indices α, β, n, m, l, and k of eqs. (261) and (262) to the new indices i and j. All matrices are filled as follows: Start in the upper left corner of the matrix with $\alpha=\beta=x$ and $n=m=l=k=1$. Staying in the first line and moving to the right change k form 1 to M. Then, put $l=2$ and again change k from 1 to M and so on until after NM elements it is $\alpha=\beta=x$, $n=m=1$, $l=N$, and $k=M$. Then, put $\beta=y$, start with $l=k=1$ and move to $l=N$ and $k=M$. Putting $\beta=z$ and following again the same procedure fills in the $3NM$ elements of the first line. In the second line the only difference is that $m=2$ for all $3NM$ elements. In the third line, $m=3$ and so on until $m=M$. In the $(M+1)$-th line, put $n=2$ and start again with $m=1$. Continuing like this, the first NM lines of the matrix are filled. In the $(NM+1)$-th line, put $\alpha=y$ and proceed as from the first line of the matrix. Then, in the $(2NM+1)$-th line, put $\alpha=z$ and start again as in the first line of the matrix. This procedure corresponds to $\alpha=\gamma(i)$, $\beta=\gamma(j)$, $n=\vartheta(i)$, $m=\varphi(i)$, $l=\vartheta(j)$, and $k=\varphi(j)$ where ($x\hat{=}1$, $y\hat{=}2$, $z\hat{=}3$)

$$\gamma(s) = \mathrm{int}\left[\frac{s-1}{NM}\right]+1, \tag{273}$$

$$\vartheta(s) = \mathrm{int}\left[\frac{\mathrm{mod}\left(\frac{s}{NM}\right)-1}{M}\right]+1, \tag{274}$$

$$\varphi(s) = \mathrm{mod}\left[\frac{\mathrm{mod}\left(\frac{s}{NM}\right)}{M}\right], \tag{275}$$

where int$[u/v]$ gives the integer part of u/v, cutting all decimals and here

$$\mathrm{mod}\left(\frac{u}{v}\right) := v\left[\left(\frac{u}{v}\right) - \mathrm{int}\left[\frac{u}{v}\right] + \delta_{u/v,\mathrm{int}[u/v]}\right]. \tag{276}$$

A.2.2 Discretized Local Electric Field

When the external field is either longitudinal or transverse, the discretized local field equations are

$$\boldsymbol{M_{AB}}^{-1}(q_x,\omega)\cdot\vec{\mathcal{E}}_{\mathrm{A}}(q_x,\omega) = \vec{\mathcal{E}}_{\mathrm{B,ext}}(q_x,\omega), \tag{277}$$

where A and B stand for L and T. Following the usual technique for the solution of coupled linear equations [285], the i-th component of the discretized local field vector is

$$\left(\vec{\mathcal{E}}_{\mathrm{A}}(q_x,\omega)\right)_i = \frac{\det[\boldsymbol{M}_{\mathbf{AB}}^{\mathbf{ext},i}(q_x,\omega)]}{\det[\boldsymbol{M_{AB}}^{-1}(q_x,\omega)]}, \tag{278}$$

where the matrix $\boldsymbol{M}_{\mathbf{AB}}^{\mathbf{ext},i}$ follows from $\boldsymbol{M_{AB}}^{-1}$ by replacing the i-th column in $\boldsymbol{M_{AB}}^{-1}$ by the vector $\vec{\mathcal{E}}_{\mathrm{B,ext}}$,

$$\boldsymbol{M}_{\mathbf{AB}}^{\mathbf{ext},i} = \begin{pmatrix} \left(\boldsymbol{M_{AB}}^{-1}\right)^{1\,1} & \cdots & (\vec{\mathcal{E}}_{\mathrm{B,ext}})_1 & \cdots & \left(\boldsymbol{M_{AB}}^{-1}\right)^{1\;3NM} \\ \left(\boldsymbol{M_{AB}}^{-1}\right)^{2\,1} & \cdots & (\vec{\mathcal{E}}_{\mathrm{B,ext}})_2 & \cdots & \left(\boldsymbol{M_{AB}}^{-1}\right)^{2\;3NM} \\ \cdots & \cdots & \cdots & \cdots & \cdots \\ \left(\boldsymbol{M_{AB}}^{-1}\right)^{3NM\;1} & \cdots & (\vec{\mathcal{E}}_{\mathrm{B,ext}})_{3NM} & \cdots & \left(\boldsymbol{M_{AB}}^{-1}\right)^{3NM\;3NM} \end{pmatrix}. \tag{279}$$

Eq. (278) gives the local field at discrete values of $\vec{Q}$, namely at those values chosen for the abscissas. In order to obtain the local field at any $\vec{Q}$, one has to intrapolate between the discrete values. Below, in appendix A.2.5 it is shown how these expressions can be used in order to estimate the magnitude of the induced transverse field.

When the matrix $\boldsymbol{M_{AB}}^{-1}$ is singular, i.e. its determinant is zero, the local field diverges even for an arbitrarily small external field. Strictly speaking, the expression for the components of the discrete local field vector is only valid when $\boldsymbol{M_{AB}}^{-1}$ is not singular. However, one must not forget the small imaginary parts iη present in $g_0(\vec{q},\omega)$ in eq. (253) and in $\chi_{0000}(q_x,\omega)$ in eq. (256). They make sure that the discretized local field vector is well defined for real q_x and ω. The limit $\eta\to 0$ is to be performed at the end of the calculations, after the Fourier transform from $\vec{q}$ to $\vec{r}$.

The local field as a function of $\vec{r}$ and t is

$$E_{\mathrm{A}}^{\alpha}(\vec{r},t) = \frac{1}{(2\pi)^4}\int \mathrm{d}\vec{q}\int \mathrm{d}\omega\, \mathrm{e}^{-\mathrm{i}\vec{q}\vec{r}-\mathrm{i}\omega t}E_{\mathrm{A}}^{\alpha}(\vec{q},\omega). \tag{280}$$

For a monochromatic external field, $\vec{E}_{\mathrm{A,ext}}(\vec{r},t)\propto \mathrm{e}^{-\mathrm{i}\omega_{\mathrm{ext}}t}$, also the local field is monochromatic and $\vec{E}_{\mathrm{A}}(\vec{q},\omega)\propto 2\pi\delta(\omega-\omega_{\mathrm{ext}})$. Substituting q_β by $4q'_\beta/d$ for $\beta=y,z$ and discretizing the Fourier integrals with respect to q'_β using the same abscissas as in the discretization of the local field integral equations, the local field $E_{\mathrm{A}}^{\alpha}(\vec{r},t)$ is

approximated by

$$E_{\mathrm{A}}^{\alpha}(\vec{r},t) = \frac{1}{(2\pi)^3}\left(\frac{4}{d}\right)^2 \mathrm{e}^{-\mathrm{i}\omega_{\mathrm{ext}}t}\int \mathrm{d}q_x\, \mathrm{e}^{-\mathrm{i}q_x x}\sum_{s,p=1}^{N,M} w_{N,s}w_{M,p}\,\mathrm{e}^{\nu_{N,s}^2+\nu_{M,p}^2} \quad (281)$$
$$\times\ \mathrm{e}^{-\mathrm{i}4(\nu_{N,s}\,y+\nu_{M,p}\,z)/d}\,\frac{\det[\boldsymbol{M}_{\mathbf{AB}}^{\mathbf{ext},\boldsymbol{\zeta}(\boldsymbol{s},\boldsymbol{p},\boldsymbol{\alpha})}(q_x,\omega_{\mathrm{ext}})]}{\det[\boldsymbol{M}_{\mathbf{AB}}{}^{-1}(q_x,\omega_{\mathrm{ext}})]},$$

where $\zeta(s,p,\alpha) = NM(\alpha-1)+M(s-1)+p$ and x,y,z correspond to $1,2,3$.

A.2.3 Discretized Dielectric Function

Following eqs. (108) and (109), the dielectric tensors of the parabolic quantum wire are defined via

$$\vec{E}_{\mathrm{L,ext}}(\vec{q},\omega) = \int \mathrm{d}\vec{Q}\,'\,\boldsymbol{\epsilon}_{\mathbf{L}}(\vec{q},\vec{Q}\,',\omega)\,\vec{E}_{\mathrm{L}}(q_x,\vec{Q}\,',\omega), \quad (282)$$

$$\vec{E}_{\mathrm{T,ext}}(\vec{q},\omega) = \frac{\omega^2}{c^2q^2-\omega^2}\int \mathrm{d}\vec{Q}\,'\left\{\frac{c^2q^2}{\omega^2}\,\delta(\vec{Q}-\vec{Q}\,')\,\mathbf{1}-\boldsymbol{\epsilon}_{\mathbf{T}}(\vec{q},\vec{Q}\,',\omega)\right\} \quad (283)$$
$$\times\ \vec{E}_{\mathrm{T}}(q_x,\vec{Q}\,',\omega).$$

These two integral equations can be discretized in exactly the same manner as the local-field integral equations in section A.2.1, leading to

$$\vec{\mathcal{E}}_{\mathrm{L,ext}}(q_x,\omega) = \boldsymbol{M}_{\boldsymbol{\epsilon}_{\mathbf{L}}}(q_x,\omega)\cdot\vec{\mathcal{E}}_{\mathrm{L}}(q_x,\omega) \quad (284)$$

$$\vec{\mathcal{E}}_{\mathrm{T,ext}}(q_x,\omega) = \boldsymbol{M}_{\boldsymbol{\epsilon}_{\mathbf{T}}}(q_x,\omega)\cdot\vec{\mathcal{E}}_{\mathrm{T}}(q_x,\omega), \quad (285)$$

where

$$(\boldsymbol{M}_{\boldsymbol{\epsilon}_{\mathbf{L}}}(q_x,\omega))^{ij} = \left(\frac{4}{d}\right)^2 w_{N,\vartheta(j)}w_{M,\varphi(j)}\,\mathrm{e}^{\nu_{N,\vartheta(j)}^2+\nu_{M,\varphi(j)}^2} \quad (286)$$
$$\times\ \epsilon_{\mathrm{L},\vartheta(i)\varphi(i)\vartheta(j)\varphi(j)}^{\gamma(i)\gamma(j)}(q_x,\omega),$$

$$(\boldsymbol{M}_{\boldsymbol{\epsilon}_{\mathbf{T}}}(q_x,\omega))^{ij} = \frac{q_x^2d^2+(4\nu_{N,\vartheta(i)})^2+(4\nu_{M,\varphi(i)})^2}{q_x^2d^2+(4\nu_{N,\vartheta(i)})^2+(4\nu_{M,\varphi(i)})^2-(\omega d/c)^2}\,\delta_{i,j} \quad (287)$$
$$-\ \left(\frac{4}{d}\right)^2\frac{(d\omega/c)^2\cdot w_{N,\vartheta(j)}w_{M,\varphi(j)}\,\mathrm{e}^{\nu_{N,\vartheta(j)}^2+\nu_{M,\varphi(j)}^2}}{q_x^2d^2+(4\nu_{N,\vartheta(i)})^2+(4\nu_{M,\varphi(i)})^2-(\omega d/c)^2}$$
$$\times\ \epsilon_{\mathrm{T},\vartheta(i)\varphi(i)\vartheta(j)\varphi(j)}^{\gamma(i)\gamma(j)}(q_x,\omega).$$

Comparison of eqs. (284) and (285) with eqs. (263) and (264) shows that $\boldsymbol{M}_{\boldsymbol{\epsilon}_{\mathbf{L}}} = \boldsymbol{M}_{\mathbf{LL}}{}^{-1}$ and $\boldsymbol{M}_{\boldsymbol{\epsilon}_{\mathbf{T}}} = \boldsymbol{M}_{\mathbf{TT}}{}^{-1}$. The discretized components of the longitudinal and transverse dielectric functions thus are

$$\epsilon_{\mathrm{L},nmlk}^{\alpha\beta}(q_x,\omega) = \frac{d^2\,\mathrm{e}^{-\nu_{N,n}^2-\nu_{M,m}^2}}{16\,w_{N,n}w_{M,m}}\left(\boldsymbol{M}_{\mathbf{LL}}{}^{-1}(q_x,\omega)\right)^{\zeta(n,m,\alpha)\ \zeta(l,k,\beta)}, \quad (288)$$

$$\begin{aligned}\epsilon^{\alpha\beta}_{\mathrm{T},nmlk}(q_x,\omega) &= \frac{d^2\,\mathrm{e}^{-\nu_{N,n}^2-\nu_{M,m}^2}}{16\,w_{N,n}w_{M,m}}\,\frac{q_x^2d^2+(4\nu_{N,n})^2+(4\nu_{M,m})^2-(\omega d/c)^2}{(\omega d/c)^2} \\ &\times \left[\frac{q_x^2d^2+(4\nu_{N,n})^2+(4\nu_{M,m})^2}{q_x^2d^2+(4\nu_{N,n})^2+(4\nu_{M,m})^2-(\omega d/c)^2}\,\delta_{\zeta(n,m,\alpha)\,\zeta(l,k,\beta)}\right. \\ &- \left.\left(\boldsymbol{M_{\mathbf{TT}}}^{-1}(q_x,\omega)\right)^{\zeta(n,m,\alpha)\;\zeta(l,k,\beta)}\right],\end{aligned} \tag{289}$$

where $\zeta(s,p,\alpha) = NM(\alpha-1)+M(s-1)+p$ and x,y,z correspond to $1,2,3$.

A.2.4 Local-Field Eigenmodes

The condition for the existence of a local-field eigenmode is that a local field can exist also in the absence of an external field, i.e. that the equation

$$\boldsymbol{M_{\mathbf{AB}}}^{-1}(q_x,\omega)\cdot\vec{\mathcal{E}}_{\mathrm{A}}(q_x,\omega)=\vec{0}, \tag{290}$$

has a solution for the local field other than the trivial solution. One thus has to search for the values of q_x and ω for which $\det[\boldsymbol{M_{\mathbf{AB}}}^{-1}]=0$. As all matrices $\boldsymbol{M_{\mathbf{AB}}}$ are related to $\boldsymbol{M_{\mathbf{TT}}}$, the zeroes of $\det[\boldsymbol{M_{\mathbf{TT}}}^{-1}]$ are considered first.

General Argument on when a Matrix Cannot be Singular
One knows that an arbitrary square matrix $A=a^{ij}$ of dimension $N\times N$ is not singular when

$$|a^{ii}|>\sum_{j\neq i}|a^{ij}|, \tag{291}$$

for any i with $1\leq i\leq N$ [293, 294]. The size of the diagonal elements of the matrix $\boldsymbol{M_{\mathbf{TT}}}^{-1}$ can be estimated using $|a-b|\geq||a|-|b||$, $|a+b|\leq|a|+|b|$ and $|T^{\gamma(i)\gamma(j)}_{\vartheta(i)\varphi(i)}(q_x)|\leq 1$ for all q_x, i, and j,

$$\begin{aligned}\left|\left(\boldsymbol{M_{\mathbf{TT}}}^{-1}(q_x,\omega)\right)^{ii}\right| &\geq \left|1-\frac{Z\,w_{N,\vartheta(i)}\,w_{M,\varphi(i)}}{\pi\,d^2\left|q_x^2+\left(\frac{4\nu_{N,\vartheta(i)}}{d}\right)^2+\left(\frac{4\nu_{M,\varphi(i)}}{d}\right)^2-\left(\frac{\omega}{c}\right)^2\right|}\right. \\ &\times \left.\left\{1+\delta_{\gamma(i)1}\,\mathrm{e}^{-2\nu_{N,\vartheta(i)}^2-2\nu_{M,\varphi(i)}^2}\,\frac{\omega_{\mathrm{LL}}^2(q_x)}{|\omega^2-\omega_{\mathrm{LL}}^2(q_x)|}\right\}\right|,\end{aligned} \tag{292}$$

where

$$Z=\frac{4e^2}{\pi^2\hbar\epsilon_0 c}\,\frac{v_{\mathrm{F}}}{c} \tag{293}$$

is a number of the order $\approx 3\times10^{-2}\cdot(v_{\mathrm{F}}/c)$. The weights $w_{N,\vartheta(i)}$ and $w_{M,\varphi(i)}$ are smaller than $\sqrt{\pi}$ for any N, M, and i. The fraction in the first part on the right hand side of eq. (292) diverges for $\omega^2=c^2q^2$ while the fraction in the second part diverges for $\omega^2=\omega_{\mathrm{LL}}^2(q_x)$. Away from these poles and for a realistic value of the Fermi velocity around 10^5 m/s, the diagonal elements are of the order of 1 for any N, M and i due to the small value of Z.

The sum over the off-diagonal elements can be interpreted in terms of an integral. Performing the Gaussian quadrature backwards and moving from the sum to a double integral, where for the specific situation at hand the integral is bigger than or equal to the sum [299], and using $|a+b| \leq |a| + |b|$ and $|T^{\gamma(i)\gamma(j)}_{\vartheta(i)\varphi(i)}(q_x)| \leq 1$, the sum over the off-diagonal elements is

$$\begin{aligned} \sum_{i \neq j} \left| \left(\boldsymbol{M_{\mathrm{TT}}}^{-1}(q_x, \omega) \right)^{ij} \right| \quad &\leq \quad \frac{Z}{d^2 \left| q_x^2 + \left(\frac{4\nu_{N,\vartheta(i)}}{d} \right)^2 + \left(\frac{4\nu_{M,\varphi(i)}}{d} \right)^2 - \left(\frac{\omega}{c} \right)^2 \right|} \\ &\times \quad \left\{ 3 + \mathrm{e}^{-\nu^2_{N,\vartheta(i)} - \nu^2_{M,\varphi(i)}} \, \frac{\omega^2_{\mathrm{LL}}(q_x)}{|\omega^2 - \omega^2_{\mathrm{LL}}(q_x)|} \right\}. \end{aligned} \tag{294}$$

Away from the poles the expression in eq. (294) is of the order of Z or smaller.

Following eq. (291), one can conclude that away from the poles the matrix $\boldsymbol{M_{\mathrm{TT}}}^{-1}$ is non-singular, and thus no eigenmode exists. When ω and $\vec{q}$ are close to the light or the Luttinger dispersion, however, the sum over the off-diagonal elements may become larger than the diagonal element. In that regime an eigenmode might be found. For ω and $\vec{q}$ approaching both poles simultaneously at the crossing of light and Luttinger dispersion, one does not need to go as close to the poles as in the case where only one fraction diverges in order to make the sum over the off-diagonal elements larger than the corresponding diagonal element. This already indicates a repulsion of the eigenmode dispersions at the crossing of light and Luttinger dispersion.

Note that it is not yet cleat if eigenmodes exist at all. It was only shown that, if they exist, their dispersion relation follows closely either the dispersion of the light or the dispersion of the collective excitations of the Luttinger liquid.

Plasmon and Photon Dispersions

The branches of the dispersion relation of the eigenmode of the transverse local field are expected to lie close to the dispersion relations of the light and of the collective excitations of the Luttinger liquid. The greatest deviation of the eigenmode dispersion from the light and the Luttinger dispersions is expected to appear near the crossing of these two dispersions. Following eqs. (50) and (53), one can estimate the positions of the crossings between the photon dispersion for $\vec{q}$ parallel to the wire, $\omega_{\mathrm{Ph}\|} = cq_x$, and the Luttinger dispersion to be at $q_{1\|} = 0$ and $q_{2\|} \approx \sqrt{8}\,\mathrm{e}^{-8/Z}$. The light dispersion for a wave vector $\vec{q}$ that has a component perpendicular to the wire, $\omega_{\mathrm{Ph}\perp} = c(q_x^2 + Q^2)^{1/2}$, intersects the Luttinger dispersion at $q_{1\perp}$ and $q_{2\perp}$. These two positions cannot be estimated analytically, but one knows $q_{1\|} < q_{1\perp} < q_{2\perp} < q_{2\|}$, see figure 3 on page 59. However, the dispersions $\omega_{\mathrm{Ph}\perp}$ and ω_{LL} only cross when the component of $\vec{q}$ that is perpendicular to the wire is sufficiently small. The photon and Luttinger dispersions are displayed in figure 3 on page 59 as functions of q_x and in figure 4 as functions of q_x and Q on page 59.

Analytic Approach for $N = 3$ and $M = 1$

The region of the crossing between light and Luttinger dispersion cannot be reached

numerically for realistic values of the Fermi velocity, but it can be approached analytically in the limit of very few abscissas. Choose $N = 3$ and $M = 1$, then $\nu_{3,3} = -\nu_{3,1} = \sqrt{6}/2$ and $\nu_{3,2} = \nu_{1,1} = 0$. The weights are $w_{3,1} = w_{3,3} = \sqrt{\pi}/6$, $w_{3,2} = 2\sqrt{\pi}/3$, and $w_{1,1} = \sqrt{\pi}$. The matrix $\boldsymbol{M_{TT}}^{-1}$ is of dimension 9×9, 41 of its elements are zero. It can be transformed into a structure consisting of four block matrices along the diagonal and its determinant thus is

$$\left|\boldsymbol{M_{TT}}^{-1}(q_x,\omega)\right| = \left|\boldsymbol{M_1}(q_x,\omega)\right| \cdot \left|\boldsymbol{M_2}(q_x,\omega)\right| \cdot \left|\boldsymbol{M_3}(q_x,\omega)\right| \cdot \left|\boldsymbol{M_4}(q_x,\omega)\right|, \tag{295}$$

where $|\ldots|$ denotes the determinant and

$$\boldsymbol{M_1} = -\left(\boldsymbol{M}_{\mathrm{TT}}{}^{-1}\right)^{22}, \tag{296}$$

$$\boldsymbol{M_2} = \begin{pmatrix} 2\left[\left(\boldsymbol{M}_{\mathrm{TT}}{}^{-1}\right)^{11} + \left(\boldsymbol{M}_{\mathrm{TT}}{}^{-1}\right)^{13}\right] & \left(\boldsymbol{M}_{\mathrm{TT}}{}^{-1}\right)^{14} - \left(\boldsymbol{M}_{\mathrm{TT}}{}^{-1}\right)^{16} \\ \left(\boldsymbol{M}_{\mathrm{TT}}{}^{-1}\right)^{41} + \left(\boldsymbol{M}_{\mathrm{TT}}{}^{-1}\right)^{43} & \frac{1}{2}\left[\left(\boldsymbol{M}_{\mathrm{TT}}{}^{-1}\right)^{44} - \left(\boldsymbol{M}_{\mathrm{TT}}{}^{-1}\right)^{46}\right] \end{pmatrix}, \tag{297}$$

$$\boldsymbol{M_3} = \begin{pmatrix} \frac{1}{2}\left[\left(\boldsymbol{M}_{\mathrm{TT}}{}^{-1}\right)^{11} - \left(\boldsymbol{M}_{\mathrm{TT}}{}^{-1}\right)^{13}\right] & \left(\boldsymbol{M}_{\mathrm{TT}}{}^{-1}\right)^{15} & \left(\boldsymbol{M}_{\mathrm{TT}}{}^{-1}\right)^{14} + \left(\boldsymbol{M}_{\mathrm{TT}}{}^{-1}\right)^{16} \\ \left(\boldsymbol{M}_{\mathrm{TT}}{}^{-1}\right)^{41} - \left(\boldsymbol{M}_{\mathrm{TT}}{}^{-1}\right)^{43} & 2\left(\boldsymbol{M}_{\mathrm{TT}}{}^{-1}\right)^{45} & 2\left[\left(\boldsymbol{M}_{\mathrm{TT}}{}^{-1}\right)^{44} + \left(\boldsymbol{M}_{\mathrm{TT}}{}^{-1}\right)^{46}\right] \\ 0 & \left(\boldsymbol{M}_{\mathrm{TT}}{}^{-1}\right)^{55} & 2\left(\boldsymbol{M}_{\mathrm{TT}}{}^{-1}\right)^{54} \end{pmatrix}, \tag{298}$$

$$\boldsymbol{M_4} = \begin{pmatrix} \left(\boldsymbol{M}_{\mathrm{TT}}{}^{-1}\right)^{77} & \left(\boldsymbol{M}_{\mathrm{TT}}{}^{-1}\right)^{78} & \left(\boldsymbol{M}_{\mathrm{TT}}{}^{-1}\right)^{79} \\ \left(\boldsymbol{M}_{\mathrm{TT}}{}^{-1}\right)^{87} & \left(\boldsymbol{M}_{\mathrm{TT}}{}^{-1}\right)^{88} & \left(\boldsymbol{M}_{\mathrm{TT}}{}^{-1}\right)^{89} \\ \left(\boldsymbol{M}_{\mathrm{TT}}{}^{-1}\right)^{97} & \left(\boldsymbol{M}_{\mathrm{TT}}{}^{-1}\right)^{98} & \left(\boldsymbol{M}_{\mathrm{TT}}{}^{-1}\right)^{99} \end{pmatrix}. \tag{299}$$

The determinant of $\boldsymbol{M_1}$ has no root. The determinant of $\boldsymbol{M_2}$ is zero under two conditions for $(\omega d/c)^2$ which are in lowest order in Z

$$\begin{aligned} \left(\frac{\omega d}{c}\right)^2 &\approx (q_x d)^2 + (4\nu_{3,1})^2 + \frac{2\, w_{3,1} w_{1,1}\, \mathrm{e}^{-\nu_{3,1}^2}(Z/\pi)}{(q_x d)^2 + (4\nu_{3,1})^2} \\ &\times \left\{ (4\nu_{3,1})^2 \mathrm{ch}(2\nu_{3,1}^2) + (q_x d)^2 \mathrm{sh}(2\nu_{3,1}^2) \right. \\ &+ \left. \frac{(4\nu_{3,1})^2 (\omega_{\mathrm{LL}}(q_x) d/c)^2}{\left[(q_x d)^2 + (4\nu_{3,1})^2 - (\omega_{\mathrm{LL}}(q_x) d/c)^2\right]} \right\}, \end{aligned} \tag{300}$$

$$\begin{aligned} \left(\frac{\omega d}{c}\right)^2 &\approx \left(\frac{\omega_{\mathrm{LL}}(q_x) d}{c}\right)^2 - \frac{2\, w_{3,1} w_{1,1}\, \mathrm{e}^{-\nu_{3,1}^2}(Z/\pi)}{(q_x d)^2 + (4\nu_{3,1})^2} \\ &\times \frac{(4\nu_{3,1})^2 (\omega_{\mathrm{LL}}(q_x) d/c)^2}{\left[(q_x d)^2 + (4\nu_{3,1})^2 - (\omega_{\mathrm{LL}}(q_x) d/c)^2\right]}. \end{aligned} \tag{301}$$

The first condition yields a frequency slightly above $\omega_{\mathrm{Ph}\perp}$ with $|\vec{q}|d = [q_x^2 d^2 + (4\nu_{3,1})^2]^{1/2}$. The second condition yields a frequency slightly below ω_{LL}. The two expansions in Z are valid for

$$Z \ll (q_x d)^2 + (4\nu_{3,1})^2 - (\omega_{\mathrm{LL}}(q_x) d/c)^2, \tag{302}$$

$$Z\,(\omega_{\mathrm{LL}}(q_x) d/c)^2 \ll \left[(q_x d)^2 + (4\nu_{3,1})^2 - (\omega_{\mathrm{LL}}(q_x) d/c)^2\right]^2, \tag{303}$$

i.e. for ω and q_x away from the crossing of the light and the Luttinger dispersions. For values of Qd as large as $4|\nu_{3,1}| = 2\sqrt{6}$, these two dispersions do not cross at all.

The determinant of $\boldsymbol{M_3}$ is zero under the conditions, given in lowest order in Z,

$$\left(\frac{\omega d}{c}\right)^2 \approx (q_x d)^2 + (4\nu_{3,1})^2 + \frac{2\, w_{3,1} w_{1,1}\, \mathrm{e}^{-\nu_{3,1}^2}(Z/\pi)}{(q_x d)^2 + (4\nu_{3,1})^2} \times \left[(4\nu_{3,1})^2 \mathrm{sh}(2\nu_{3,1}^2) + (q_x d)^2 \mathrm{ch}(2\nu_{3,1}^2)\right], \tag{304}$$

$$\left(\frac{\omega d}{c}\right)^2 \approx (q_x d)^2 + w_{3,2} w_{1,1}(Z/\pi). \tag{305}$$

Here, the dispersions of the eigenmodes lie slightly above $\omega_{\mathrm{Ph}\perp}$ and $\omega_{\mathrm{Ph}\parallel}$. The two expansions are valid for

$$Z \ll (4\nu_{3,1})^2, \tag{306}$$

and for the expression in eq. (305) also

$$Z \ll (q_x d)^2. \tag{307}$$

However, evaluating the zeroes of the determinant at $q_x d = 0$ in any order in Z one obtains the same result as in eqs. (304) and (305) when setting $q_x d = 0$. The determinant of $\boldsymbol{M_4}$ is zero for,

$$\left(\frac{\omega d}{c}\right)^2 \approx (q_x d)^2 + (4\nu_{3,1})^2 + 2\, w_{3,1} w_{1,1}\, \mathrm{e}^{-\nu_{3,1}^2}\, \mathrm{ch}(2\nu_{3,1}^2)\, (Z/\pi), \tag{308}$$

$$\left(\frac{\omega d}{c}\right)^2 \approx (q_x d)^2 + w_{3,2} w_{1,1}(Z/\pi), \tag{309}$$

in lowest order in Z. These expansions are valid for

$$Z \ll (4\nu_{3,1})^2, \tag{310}$$

and in addition

$$Z \ll (q_x d)^2, \tag{311}$$

for the expression in eq. (309). Again, evaluating the zeroes of the determinant at $q_x d = 0$ in any order in Z one obtains here the same result as in eqs. (308) and (309) when setting $q_x d = 0$.

The dispersions of the eigenmodes close to $\omega_{\mathrm{Ph}\perp}$ in eqs. (300), (304), and (308) are not identical. This is probably due to the rather crude approximation using so few abscissas. In the limit $(q_x d)^2 \ll (4\nu_{3,1})^2$, it is also $(\omega_{\mathrm{LL}}(q_x)d/c)^2 \ll (4\nu_{3,1})^2$ for any realistic value of the Fermi velocity and the above six conditions for $(\omega d/c)^2$ can be merged into three eigenmode dispersions for the local transverse field,

$$\left(\frac{\omega_{\mathrm{T,LL}}(q_x)d}{c}\right)^2 \approx \left(\frac{\omega_{\mathrm{LL}}(q_x)d}{c}\right)^2 \left[1 - \frac{\mathrm{e}^{-3/2}\, Z}{72}\right], \tag{312}$$

$$\left(\frac{\omega_{\mathrm{T,Ph}\parallel}(q_x)d}{c}\right)^2 \approx (q_x d)^2 + \frac{2\, Z}{3}, \tag{313}$$

$$\left(\frac{\omega_{\mathrm{T,Ph}\perp}(q_x)d}{c}\right)^2 \approx (q_x d)^2 + (4\nu_{3,1})^2 + \frac{\mathrm{e}^{3/2}\, Z}{6}. \tag{314}$$

These results are displayed qualitatively in figure 5 on page 60.

Analytic Approach for $N = 1$ and $M = 1$

The dispersions ω_{LL} and $\omega_{\mathrm{Ph}\perp}$ do not intersect for $N = 3$ and $M = 1$ as $Qd = 4\nu_{3,1}$ is too large. In the limit of infinitely many abscissas, there are values of $\nu_{N,n}$ and $\nu_{M,m}$ leading to a Q small enough in order to allow for an intersection of ω_{LL} and $\omega_{\mathrm{Ph}\perp}$. But that limit cannot be approached analytically. In order to find qualitative results for the crossing of ω_{LL} and $\omega_{\mathrm{Ph}\perp}$, choose $N = M = 1$ and then shift $\nu_{N=1,1}$ slightly to the left and to the right, splitting it into two abscissas: $\nu_{N=1,1} \to \pm\varepsilon$, where $0 < \varepsilon \ll 1$. The weight $w_{N=1,1}$ has to be changed accordingly; for a well-behaved function under the integral, $w_\varepsilon = w_{1,1}/2 - \delta$ with $|\delta| \ll 1$. The matrix $\boldsymbol{M_{TT}}^{-1}$ is of dimension 6×6, 16 of its elements are zero. Its determinant can be written in terms the determinants of three block matrices along the diagonal,

$$\left|\boldsymbol{M_{TT}}^{-1}(q_x,\omega)\right| = |\boldsymbol{M_5}(q_x,\omega)| \cdot |\boldsymbol{M_6}(q_x,\omega)| \cdot |\boldsymbol{M_7}(q_x,\omega)|\,, \tag{315}$$

with

$$\boldsymbol{M_5} = \begin{pmatrix} 2\left[(\boldsymbol{M_{TT}}^{-1})^{11} + (\boldsymbol{M_{TT}}^{-1})^{12}\right] & (\boldsymbol{M_{TT}}^{-1})^{13} - (\boldsymbol{M_{TT}}^{-1})^{14} \\ (\boldsymbol{M_{TT}}^{-1})^{31} + (\boldsymbol{M_{TT}}^{-1})^{32} & \frac{1}{2}\left[(\boldsymbol{M_{TT}}^{-1})^{33} - (\boldsymbol{M_{TT}}^{-1})^{34}\right] \end{pmatrix}, \tag{316}$$

$$\boldsymbol{M_6} = \begin{pmatrix} \frac{1}{2}\left[(\boldsymbol{M_{TT}}^{-1})^{11} - (\boldsymbol{M_{TT}}^{-1})^{12}\right] & (\boldsymbol{M_{TT}}^{-1})^{13} + (\boldsymbol{M_{TT}}^{-1})^{14} \\ (\boldsymbol{M_{TT}}^{-1})^{31} - (\boldsymbol{M_{TT}}^{-1})^{32} & 2\left[(\boldsymbol{M_{TT}}^{-1})^{33} + (\boldsymbol{M_{TT}}^{-1})^{34}\right] \end{pmatrix}, \tag{317}$$

$$\boldsymbol{M_7} = \begin{pmatrix} (\boldsymbol{M_{TT}}^{-1})^{55} & (\boldsymbol{M_{TT}}^{-1})^{56} \\ (\boldsymbol{M_{TT}}^{-1})^{65} & (\boldsymbol{M_{TT}}^{-1})^{66} \end{pmatrix}. \tag{318}$$

Only $\boldsymbol{M_5}$ contains a coupling between $\omega_{\mathrm{Ph}\perp}$ and ω_{LL}. The corresponding eigenmode dispersions are

$$\begin{aligned} \left(\frac{\omega_{\mathrm{T}\pm}(q_x)d}{c}\right)^2 &= \frac{1}{2}\Bigg\{\left[(q_xd)^2 + (4\varepsilon)^2 + \left(\frac{\omega_{\mathrm{LL}}(q_x)d}{c}\right)^2\right] \\ &+ 2w_\varepsilon w_{1,1}\,\mathrm{e}^{-\varepsilon^2}\,(Z/\pi)\left[\frac{(4\varepsilon)^2\cosh(2\varepsilon^2)}{(q_xd)^2+(4\varepsilon)^2} + \frac{(q_xd)^2\sinh(2\varepsilon^2)}{(q_xd)^2+(4\varepsilon)^2}\right]\Bigg\} \\ &\pm \frac{1}{2}\Bigg\{\Bigg(\left[(q_xd)^2 + (4\varepsilon)^2 - \left(\frac{\omega_{\mathrm{LL}}(q_x)d}{c}\right)^2\right] \\ &+ 2w_\varepsilon w_{1,1}\,\mathrm{e}^{-\varepsilon^2}\,(Z/\pi)\left[\frac{(4\varepsilon)^2\cosh(2\varepsilon^2)}{(q_xd)^2+(4\varepsilon)^2} + \frac{(q_xd)^2\sinh(2\varepsilon^2)}{(q_xd)^2+(4\varepsilon)^2}\right]\Bigg)^2 \\ &+ 8w_\varepsilon w_{1,1}\,\mathrm{e}^{-\varepsilon^2}\,(Z/\pi)\frac{(4\varepsilon)^2}{(q_xd)^2+(4\varepsilon)^2}\left(\frac{\omega_{\mathrm{LL}}(q_x)d}{c}\right)^2\Bigg\}^{1/2}. \end{aligned} \tag{319}$$

At $q_xd = 0$, neglecting higher orders in ε^2 and Z and taking $w_\varepsilon \approx w_{1,1}/2$,

$$\left(\frac{\omega_{\mathrm{T}\pm}(q_x=0)d}{c}\right)^2 \approx \begin{cases} (4\varepsilon)^2 + Z \\ 0 \end{cases}. \tag{320}$$

As $\varepsilon^2 \ll Z$, the relative deviation of the eigenmode dispersion from the light dispersion $\omega_{\mathrm{Ph}\perp}$ is huge at $q_x d = 0$. At the intersections of the dispersions,

$$d\kappa_i := (q_{i\perp} d)^2 + (4\varepsilon)^2 = \left(\frac{\omega_{\mathrm{LL}}(q_{i\perp}) d}{c} \right)^2 , \tag{321}$$

one obtains in lowest order in ε^2

$$\left(\frac{\omega_{\mathrm{T}\pm}(q_x = q_{i\perp}) d}{c} \right)^2 \approx \begin{cases} (d\kappa_i)^2 + Z \frac{(4\varepsilon)^2}{(d\kappa_i)^2} \\ (d\kappa_i)^2 \end{cases} . \tag{322}$$

It is $\varepsilon/(d\kappa_i) < 1$ and the deviation of the photon mode $\omega_{\mathrm{T}+}$ from the photon dispersion $\omega_{\mathrm{Ph}\perp}$ is thus smaller at $q_x d = q_{i\perp} d$ than at $q_x d = 0$ and it is further smaller at $q_{2\perp} d$ than at $q_{1\perp} d$. The deviation of the plasmon mode $\omega_{\mathrm{T}-}$ from the Luttinger dispersion is of higher order in ε^2 than the expression given in eq. (322) and thus much smaller than the deviation of the photon mode from $\omega_{\mathrm{Ph}\perp}$. The repulsion of the two eigenmodes at $q_{i\perp} d$ is in lowest order in ε^2

$$\left(\frac{\omega_{\mathrm{T}+}(q_x = q_{i\perp}) d}{c} \right)^2 - \left(\frac{\omega_{\mathrm{T}-}(q_x = q_{i\perp}) d}{c} \right)^2 = Z \frac{(4\varepsilon)^2}{(d\kappa_i)^2}. \tag{323}$$

It increases with increasing v_{F}. The results are displayed qualitatively in figure 6 on page 62.

Discussion of the Matrices $\boldsymbol{M_{\mathrm{TL}}}$, $\boldsymbol{M_{\mathrm{LL}}}$, and $\boldsymbol{M_{\mathrm{LT}}}$

So far, only the eigenmodes of the local transverse field in response to an external transverse field are obtained. In order to determine the eigenmodes of the local transverse field in response to an external longitudinal field, one has to check under which conditions the determinant of the matrix $\boldsymbol{M_{\mathrm{TL}}}^{-1}$ is zero. Following eq. (267) it is $\boldsymbol{M_{\mathrm{TL}}}^{-1} = (\mathbf{1} - \boldsymbol{M_{\mathrm{TT}}}^{-1})^{-1} \cdot \boldsymbol{M_{\mathrm{TT}}}^{-1}$. The zeroes of $|\boldsymbol{M_{\mathrm{TT}}}^{-1}|$ were discussed above and in section 4.4.2. As the determinant of the inverse of a matrix, $|\boldsymbol{A}^{-1}|$, is equal to the inverse of the determinant of $\boldsymbol{A}$, $|(\mathbf{1} - \boldsymbol{M_{\mathrm{TT}}}^{-1})^{-1}|$ is zero when $|\mathbf{1} - \boldsymbol{M_{\mathrm{TT}}}^{-1}|$ diverges. For finite N and M, it can only diverge when at least one of its elements diverges. From eq. (266) it can be seen that this is the case when q_x and ω lie exactly on the Luttinger or the light dispersion. This situation, however, does not lead to a zero of $|(\mathbf{1} - \boldsymbol{M_{\mathrm{TT}}}^{-1})^{-1} \cdot \boldsymbol{M_{\mathrm{TT}}}^{-1}|$, as the determinant of $\boldsymbol{M_{\mathrm{TT}}}^{-1}$ also diverges when q_x and ω hit exactly the Luttinger or the light dispersion and the diverging terms cancel. Thus, the transverse field eigenmodes are equivalent for a transverse and a longitudinal external driving and are given by the zeroes of $|\boldsymbol{M_{\mathrm{TT}}}^{-1}|$.

Following eq. (290), the eigenmodes of the local longitudinal field are determined by the condition that either $|\boldsymbol{M_{\mathrm{LL}}}^{-1}| = 0$ or $|\boldsymbol{M_{\mathrm{LT}}}^{-1}| = 0$. The first condition is equivalent to $|\mathbf{1} + \boldsymbol{M} \cdot \boldsymbol{M_{\mathrm{TT}}}| \to \infty$, see eq. (268). The elements of the matrix $\boldsymbol{M}$ diverge for ω and q_x exactly at the Luttinger dispersion, see eq. (270), but the elements of $\boldsymbol{M_{\mathrm{TT}}}$ are zero under this condition as $|\boldsymbol{M_{\mathrm{TT}}}^{-1}|$ diverges. Thus, $|\mathbf{1} + \boldsymbol{M} \cdot \boldsymbol{M_{\mathrm{TT}}}|$ only diverges when the elements of $\boldsymbol{M_{\mathrm{TT}}}$ diverge which happens of the zeroes of $|\boldsymbol{M_{\mathrm{TT}}}^{-1}|$. The second condition, $|\boldsymbol{M_{\mathrm{LT}}}^{-1}| = 0$, is equivalent to

$|\boldsymbol{M_{TT}}^{-1}| = 0$ or $|\boldsymbol{M}| \to \infty$, see eq. (269). The elements of $\boldsymbol{M}$, see eq. (270), diverge for $\omega = \omega_{\rm LL}(q_x)$. Again, in that situation, also the elements of $\boldsymbol{M_{TT}}^{-1}$ diverge and the determinant of the product of $\boldsymbol{M_{TT}}$ and $\boldsymbol{M}$ remains finite. Thus, the eigenmodes of the local longitudinal field are equivalent to the eigenmodes of the local transverse field.

A.2.5 Induced Transverse Field

Based on the analytic discussion of the local field eigenmodes for small N and M in appendix A.2.4, we estimate the magnitude of the induced transverse field. We choose the external field to be transverse and following appendix A.2.2, we evaluate the determinants of the matrices $\boldsymbol{M_{TT}^{ext,i}}$ and $\boldsymbol{M_{TT}}^{-1}$ in order to determine the x-component of the discretized local transverse field.

On the one hand, choosing $N = M = 1$ with the abscissas $\nu_{N,n} = \nu_{M,m} = 0$ leads to a zero induced transverse field, the approximation is too crude. On the other hand, as the dimension of the matrices $\boldsymbol{M_{TT}^{ext,i}}$ and $\boldsymbol{M_{TT}}^{-1}$ is $(3NM \times 3NM)$, already for $N = 3$ and $M = 1$ the evaluation of the determinants of $\boldsymbol{M_{TT}^{ext,i}}$ and $\boldsymbol{M_{TT}}^{-1}$ becomes extremely tedious. Therefore, following the approach used in appendix A.2.4, we use $N = M = 1$ and then split the abscissa $\nu_{N,n} = 0$ into $\nu_{N,n} = \pm\varepsilon$. The dimension of $\boldsymbol{M_{TT}^{ext,i}}$ and $\boldsymbol{M_{TT}}^{-1}$ then is (6×6).

The determinant of $\boldsymbol{M_{TT}}^{-1}$ was evaluated in appendix A.2.4. The matrix $\boldsymbol{M_{TT}}^{-1}$ was written in terms of 3 block matrices along the diagonal denoted by $\boldsymbol{M_5}$, $\boldsymbol{M_6}$, and $\boldsymbol{M_7}$. The determinant of $\boldsymbol{M_{TT}}^{-1}$ is then given by the product of the determinants of $\boldsymbol{M_5}$, $\boldsymbol{M_6}$, and $\boldsymbol{M_7}$. It turns out below that of these determinants only the one of $\boldsymbol{M_5}$ is needed explicitly. It is

$$\det[\boldsymbol{M_5}(q_x,\omega)] = \frac{[(\omega d/c)^2 - (\omega_{\rm T+}(q_x)d/c)^2]\,[(\omega d/c)^2 - (\omega_{\rm T-}(q_x)d/c)^2]}{[(\omega d/c)^2 - (q_x d)^2 - (4\varepsilon)^2]\,[(\omega d/c)^2 - (\omega_{\rm LL}(q_x)d/c)^2]}, \qquad (324)$$

where the dispersion relation of the branches of the eigenmode, $\omega_{\rm T\pm}(q_x)$, are given in eq. (319).

In order to evaluate the determinant of $\boldsymbol{M_{TT}^{ext,i}}$ one has to specify the external field. We assume an external transverse field parallel to the wire, $E^x_{\rm T,ext}(\vec{r},t)$. The Fourier transform is $E^x_{\rm T,ext}(\vec{q},\omega)$. The components of the discretized external field vector are, see appendix A.2.1,

$$\left(\vec{\mathcal{E}}_{\rm T,ext}(q_x,\omega)\right)_i = \begin{cases} E_{\rm T,ext}(q_x, q_y = -4\varepsilon/d, q_z = 0, \omega) & ; i = 1 \\ E_{\rm T,ext}(q_x, q_y = +4\varepsilon/d, q_z = 0, \omega) & ; i = 2 \\ 0 & ; \text{else} \end{cases}, \qquad (325)$$

for $1 \le i \le 6$. We assume for simplicity that the components of $\vec{\mathcal{E}}_{\rm T,ext}$ for $i = 1$ and $i = 2$ can be approximated by $E_{\rm T,ext}(q_x, q_y = 0, q_z = 0, \omega)$. As the field $E_{\rm T,ext}(q_x,\vec{Q},\omega)$ at $|\vec{Q}| = 0$ corresponds to $E_{\rm T,ext}(q_x,\vec{R},\omega)$ averaged with respect to $\vec{R}$, we call it $E_{\rm T,ext,av}(q_x,\omega)$ and obtain

$$\left(\vec{\mathcal{E}}_{\rm T,ext}(q_x,\omega)\right)_i \approx \begin{cases} E_{\rm T,ext,av}(q_x,\omega) & ; i = 1,2 \\ 0 & ; \text{else} \end{cases}. \qquad (326)$$

The x-component of the local transverse field is then given by $(\vec{\mathcal{E}}_{\rm T}(q_x,\omega))_i$ for $i=1,2$, see eq. (278). It corresponds to the the local transverse field at $q_y=\pm 4\varepsilon/d$ and $q_z=0$,

$$\left(\vec{\mathcal{E}}_{\rm T}(q_x,\omega)\right)_i = \begin{cases} E^x_{\rm T}(q_x, q_y=-4\varepsilon/d, q_z=0;\omega) & ;i=1 \\ E^x_{\rm T}(q_x, q_y=+4\varepsilon/d, q_z=0;\omega) & ;i=2 \end{cases}. \tag{327}$$

Now, insert the discretized external field into the matrix $\boldsymbol{M}^{\mathbf{ext},i}_{\mathbf{TT}}$ and evaluate its determinant for $i=1,2$. One obtains

$$\det[\boldsymbol{M}^{\mathbf{ext,1}}_{\mathbf{TT}}] = \det[\boldsymbol{M}^{\mathbf{ext,2}}_{\mathbf{TT}}] \tag{328}$$

with

$$\begin{aligned} \det[\boldsymbol{M}^{\mathbf{ext,1}}_{\mathbf{TT}}] &\approx E_{\rm T,ext,av}(q_x,\omega)\det[\boldsymbol{M_6}]\det[\boldsymbol{M_7}], \\ &\times \left\{1+\frac{Z\,(q_xd)^2}{[(q_xd)^2+(4\varepsilon)^2-(\omega d/c)^2]\,[(q_xd)^2+(4\varepsilon)^2]}\right\}, \end{aligned} \tag{329}$$

where Z is given in eq. (293). It was used $w_{1,1}=\sqrt{\pi}$, $w_\varepsilon \approx w_{1,1}/2$ and $\mathrm{e}^{\pm\varepsilon^2}\approx 1$. Dividing $\det[\boldsymbol{M}^{\mathbf{ext,1}}_{\mathbf{TT}}]$ by $\det[\boldsymbol{M}_{\mathbf{TT}}{}^{-1}]$ following appendix A.2.2, the determinants of $\boldsymbol{M_6}$ and $\boldsymbol{M_7}$ cancel.

From the discussion in appendix A.2.4 and section 4.4.2 we know that the deviation of the dispersion relation of the local-field eigenmode from the dispersion relations of the uncoupled systems is of the order of Z or smaller. We thus write

$$\left(\frac{\omega_{\rm T+}(q_x)d}{c}\right)^2 = (q_xd)^2+(4\varepsilon)^2+\zeta_+(q_x,\varepsilon), \tag{330}$$

$$\left(\frac{\omega_{\rm T-}(q_x)d}{c}\right)^2 = \left(\frac{\omega_{\rm LL}(q_x)d}{c}\right)^2-\zeta_-(q_x,\varepsilon), \tag{331}$$

where the functions $\zeta_\pm(q_x,\varepsilon)$ can be obtained by comparison with eq. (319). They are of the order Z or smaller. One then obtains for the induced transverse field, i.e. the local transverse field minus the external transverse field,

$$\begin{aligned} E^x_{\rm T,ind}(q_x, q_y=\pm 4\varepsilon/d, q_z=0,\omega) &\approx E_{\rm T,ext,av}(q_x,\omega) \\ &\times \left\{\frac{\zeta'_+(q_x,\varepsilon)}{[(\omega d/c)^2-(\omega_{\rm T+}(q_x)d/c)^2]}-\frac{\zeta_-(q_x,\varepsilon)}{[(\omega d/c)^2-(\omega_{\rm T-}(q_x)d/c)^2]}\right. \\ &- \left.\frac{\zeta'_+(q_x,\varepsilon)\,\zeta_-(q_x,\varepsilon)}{[(\omega d/c)^2-(\omega_{\rm T+}(q_x)d/c)^2]\,[(\omega d/c)^2-(\omega_{\rm T-}(q_x)d/c)^2]}\right\}, \end{aligned} \tag{332}$$

where

$$\zeta'_+(q_x,\varepsilon) = \zeta_+(q_x,\varepsilon)-\frac{Z\,(q_xd)^2}{[(q_xd)^2+(4\varepsilon)^2]}, \tag{333}$$

hence also $\zeta'_+(q_x,\varepsilon)$ is of the order Z.

Consider the Fourier transform of $E^x_{\mathrm{T,ind}}$ from q_x to x. The integral with respect to q_x over the expression given in eq. (332) times $\mathrm{e}^{-\mathrm{i}q_x x}$ can be solved via residue. This implies that the branches of the dispersion relation of the local-field eigenmode determine the behaviour of the induced transverse field along x. The magnitude of the induced transverse field is then given by the terms in the numerators in eq. (332) which are $\zeta'_+(q_x,\varepsilon)$, $\zeta_-(q_x,\varepsilon)$, and the product of these two functions. But these functions are of the order of Z or smaller and Z is dominated by v_F/c! Hence, the induced transverse field as a function of x is suppressed with respect to the external transverse field by a factor of v_F/c. Its influence on transport can therefore be neglected.

That the induced transverse field is strongly suppressed with respect to the external field remains true also for an external longitudinal field. One then has to replace the determinant of the matrix $\boldsymbol{M_{\mathbf{TT}}}^{-1}$ by the determinant of $\boldsymbol{M_{\mathbf{TL}}}^{-1}$. According to eq. (267) it is

$$\det[\boldsymbol{M_{\mathbf{TL}}}^{-1}(q_x,\omega)] = \frac{\det[\boldsymbol{M_{\mathbf{TT}}}^{-1}(q_x,\omega)]}{\det[\mathbf{1}-\boldsymbol{M_{\mathbf{TT}}}^{-1}(q_x,\omega)]}. \tag{334}$$

Hence, when the external field is longitudinal, the induced transverse field derived above has to be multiplied by a factor $\det[\mathbf{1}-\boldsymbol{M_{\mathbf{TT}}}^{-1}(q_x,\omega)]$. As all elements of the matrix $\mathbf{1}-\boldsymbol{M_{\mathbf{TT}}}^{-1}(q_x,\omega)$ are of the order of Z, the factor $\det[\mathbf{1}-\boldsymbol{M_{\mathbf{TT}}}^{-1}(q_x,\omega)]$ is also of the order of Z or smaller.

Even though this result was obtained for a very small number of abscissas we believe it to be generally valid. With increasing N and M, the number of factors consisting of $(\omega d/c)^2$ minus the branches of the eigenmode dispersion in the numerator of $\det[\boldsymbol{M_{\mathbf{TT}}}^{-1}]$ increases. Further, the number of factors consisting of $(\omega d/c)^2$ minus the branches of the dispersion relations of the uncoupled systems in the denominator of $\det[\boldsymbol{M_{\mathbf{TT}}}^{-1}]$ increases. But the overall structure of $\det[\boldsymbol{M_{\mathbf{TT}}}^{-1}]$ remains unchanged. And this structure is responsible for the result obtained for the induced transverse field.

B Dirty Quantum Wire

A general expression for the x-component of the current density in the dirty quantum wire is derived in appendix B.1. Explicit expressions for the dc and the ac current for specific choices of the external driving field are given in appendix B.2 and appendix B.3. The local transverse field in the wire is estimated in section B.4.

B.1 Transport Equation

The current density is related to the bosonic field operator $\vartheta(x,t)$, see eq. (60), via

$$J^x(\vec{r},t) = -\frac{e}{\sqrt{\pi}}\, B^x_{00}(\vec{R})\, \langle \partial_t \vartheta(x,t) \rangle. \tag{335}$$

The task is to determine the expectation value of the time evolution of $\vartheta(x)$.

Consider the current at the position of the barrier,

$$J^x(x=0,\vec{R},t) = -\frac{e}{\sqrt{\pi}}\, B^x_{00}(\vec{R})\, \langle \partial_t \vartheta(x=0,t) \rangle, \tag{336}$$

and assume the barrier potential to be very high. Then, following the Hamiltonian describing the barrier, see eq. (177), the bosonic field $\vartheta(x=0)$ assumes only discrete values, namely those leading to a minimum of the potential energy. The assumption of discrete values for $\vartheta(x=0)$ is equivalent to the statement that the electrons tunnel through the barrier in integer units [63]. The initial value of $\vartheta(x=0)$ is fixed, $\vartheta(x=0,t=0) \equiv 0$, corresponding to a homogeneous particle density distribution in the undisturbed system at $t=0$. The expectation value of $\vartheta(x=0,t)$ is then given by a sum over all possible discrete final values of $\vartheta(x=0,t)$, $n\sqrt{\pi}$, multiplied by the probability that the system evolves during time t from the fixed initial value to a certain final value, $P_n(t)$,

$$\langle \vartheta(x=0,t) \rangle = \sqrt{\pi} \sum_n n P_n(t). \tag{337}$$

A change of $\langle \vartheta(x=0,t) \rangle$ from $n\sqrt{\pi}$ to $(n \pm 1)\sqrt{\pi}$ indicates that one electron has tunneled through the barrier. The current density becomes

$$J^x(x=0,\vec{R},t) = -e\, B^x_{00}(\vec{R}) \sum_n n\, \partial_t P_n(t). \tag{338}$$

The probability $P_n(t)$ has still to be evaluated.

Path Integral Approach

The problem to be solved here, namely the evaluation of $\langle \vartheta(x=0,t) \rangle$, can be related to the problem of determining the dynamics of a single particle coupled to a set of harmonic oscillators. The latter system is often employed in order to model open quantum systems, i.e. in order to account for dissipation in quantum systems: One couples a system with few degrees of freedom, e.g. a single particle,

to a reservoir with many degrees of freedom, e.g. a set of harmonic oscillators. As one is only interested in the dynamics of the particle and not in the dynamics of the reservoir, the degrees of freedom of the reservoir are integrated out. The reduced density matrix that governs the dynamics of the single particle can be expressed via path integrals. The influence of the reservoir on the dynamics of the single particle is contained in a so-called influence functional. For details on this approach see [300, 301, 302]. Here, the bosonic field $\vartheta(x,t)$ at $x=0$ is interpreted as the "single particle" and $\vartheta(x,t)$ at $x\neq 0$ is interpreted at the reservoir. The probability $P_n(t)$ then corresponds to the diagonal elements of the reduced density matrix.

Based on the Luttinger model, one obtains for $P_n(t)$ [63, 179, 303],

$$P_n(t) = \int \mathcal{D}\vartheta_0(t') \int \mathcal{D}\vartheta_0'(t')\, \mathcal{A}[\vartheta_0(t')]\, \mathcal{A}^*[\vartheta_0'(t')]\, \mathcal{I}[\vartheta_0(t'), \vartheta_0'(t')], \tag{339}$$

where $\mathcal{D}\vartheta_0(t')$ denotes a path integration. The initial value of $\vartheta_0(t') := \vartheta(x=0,t')$ at $t'=0$ is zero and the final value at $t'=t$ is $n\sqrt{\pi}$. Further, $\mathcal{A}[\vartheta_0(t)]$ is the amplitude of $\vartheta_0(t)$ in the absence of the coupling to the "reservoir" modes $\vartheta(x\neq 0)$ [63, 179, 303],

$$\mathcal{A}[\vartheta_0(t)] = \mathrm{e}^{-\mathrm{i}\{S_{\mathrm{bar}}[\vartheta_0(t)]+S_{\mathrm{em,eff}}[\vartheta_0(t)]\}/\hbar}, \tag{340}$$

where S_{bar} is the action derived from the barrier Hamiltonian, see eq. (177),

$$S_{\mathrm{bar}}[\vartheta_0(t)] = -U_{\mathrm{bar}} \int_0^t \mathrm{d}t' \cos[2\sqrt{\pi}\vartheta_0(t')]. \tag{341}$$

Further, $S_{\mathrm{em,eff}}[\vartheta_0(t)]$ is the action containing an effective driving voltage $V_{\mathrm{eff}}(t)$ that drops at the barrier,

$$S_{\mathrm{em,eff}}[\vartheta_0(t)] = -\frac{e}{\sqrt{\pi}} \int_0^t \mathrm{d}t' V_{\mathrm{eff}}(t')\vartheta_0(t'). \tag{342}$$

The effective driving voltage is related to the projected driving field $E^x_{\mathrm{ext,1b}}$, see eq. (140), via [9]

$$V_{\mathrm{eff}}(t) = \int_{-\infty}^{\infty} \mathrm{d}x \int_{-\infty}^{t} \mathrm{d}t'\, E^x_{\mathrm{ext,1b}}(x,t')\, r(x,t-t'), \tag{343}$$

where $r(x,\omega)$ is determined by the conductivity of the clean quantum wire of zero diameter, see eq. (145),

$$r(x,\omega) = \frac{\sigma^{xx}_{\mathrm{1b},d=0}(x,\omega)}{\sigma^{xx}_{\mathrm{1b},d=0}(0,\omega)}. \tag{344}$$

The influence functional $\mathcal{I}[\vartheta_0(t'), \vartheta_0'(t')]$ takes into account the effect of the reservoir modes $\vartheta(x\neq 0)$ onto the time evolution of $\vartheta_0(t)$ [63, 179, 303],

$$\mathcal{I}[\vartheta_0(t'), \vartheta_0'(t')] = \mathrm{e}^{-\Phi_{\mathcal{I}}[\vartheta_0(t'),\vartheta_0'(t')]/\hbar}, \tag{345}$$

with

$$\Phi_{\mathcal{I}}[\vartheta_0(t'),\vartheta_0'(t')] = -\frac{\hbar}{\pi}\int_0^t \mathrm{d}t_2 \int_0^{t_2} \mathrm{d}t_1 \left[\dot{\vartheta}_0(t_2)-\dot{\vartheta}_0'(t_2)\right] \times \left[W(t_2-t_1)\dot{\vartheta}_0(t_1) - W^*(t_2-t_1)\dot{\vartheta}_0'(t_1)\right]. \quad (346)$$

The kernel $W(t)$ consists of a real part $S(t)$ and an imaginary part $R(t)$,

$$W(t) = S(t) + \mathrm{i}R(t). \quad (347)$$

with [10, 282],

$$W(t) = \frac{e^2}{\pi\hbar}\int_0^\infty \frac{\mathrm{d}\omega}{\omega}\,\mathrm{Re}\left(\frac{1}{\sigma^{xx}_{1\mathrm{b},d=0}(x=0,\omega)}\right) \times \left\{[1-\cos(\omega t)]\coth(\hbar\omega\beta/2) + \mathrm{i}\sin(\omega t)\right\}. \quad (348)$$

Here, $\beta = 1/k_\mathrm{B}T$ denotes the inverse temperature. For a general spatial shape of the interaction potential, $W(t)$ has to be evaluated numerically. For a zero-range interaction potential, it is [9]

$$S(t) = \frac{1}{g}\log(1+\omega_\mathrm{c}^2 t^2) + \frac{2}{g}\log\left[\frac{\hbar\beta}{\pi t}\sinh\left(\frac{\pi t}{\hbar\beta}\right)\right], \quad (349)$$

$$R(t) = \frac{2}{g}\arctan(\omega_\mathrm{c} t). \quad (350)$$

The interaction parameter g is given in eq. (51). The quantity $\hbar\omega_\mathrm{c}$ is a cut-off necessary whenever a zero-range interaction is considered. In order to exclude inter-band transitions the cut-off should be of the order of the band gap between the first (occupied) and the second (empty) subband.

Current at the Barrier

Next, a tunneling probability Δ^2 independent of $\vartheta_0(t)$ is introduced. Tunneling of one particle through the barrier is proportional to Δ^2. Tunneling of n particles is correspondingly of order $(\Delta^2)^n$. For a large barrier and hence a small Δ^2, tunneling of more than one particle is neglected and $n = \pm 1$ is considered. The paths $\vartheta_0(t)$ then range from the initial value 0 to the final values $\pm\sqrt{\pi}$. The path integral over $\vartheta_0(t)$ can be represented by sums and $P_{\pm 1}$ can be evaluated. One obtains for the current density at the position of the barrier [63, 179, 303]

$$J^x(x=0,\vec{R},t) = e\Delta^2\, B^x_{00}(\vec{R}) \int_0^\infty \mathrm{d}\tau\, \mathrm{e}^{-S(\tau)} \sin[R(\tau)] \sin\left[\frac{e}{\hbar}\int_{t-\tau}^{t} \mathrm{d}t'\, V_\mathrm{eff}(t')\right]. \quad (351)$$

Originally, this result was derived for a longitudinal driving field, i.e. an electric driving field based on a scalar electric potential [63, 179, 303]. However, it was shown in [295] that for a transverse driving, i.e. an electric driving field based on a magnetic vector potential, the result is equivalent to the one in eq. (351).

Current at any Position x

Now, the current at the position of the barrier is known, but the current at an arbitrary position x is still unknown. The current at position $x \neq 0$ can be related to the current at the barrier by repeating the above approach fixing two values of the bosonic field $\vartheta(x,t)$, namely at $x = 0$ and another certain position x. Then [176],

$$\Delta J^x(x,\vec{R},\omega) = r(x,\omega)\Delta J^x(x=0,\vec{R},\omega), \tag{352}$$

with

$$\Delta J^x(x,\vec{R},\omega) = J^x(x,\vec{R},\omega) - J^x_{\text{clean}}(x,\vec{R},\omega), \tag{353}$$

where J^x and J^x_{clean} are the current densities in the quantum wire with and without barrier, respectively, and $r(x,\omega)$ is given in eq. (344). Note that the expression in eq. (352) was originally derived for a true 1D wire of zero diameter [176]. The current at any position x hence is

$$\begin{aligned} J^x(x,\vec{R},\omega) &= J^x_{\text{clean}}(x,\vec{R},\omega) - \frac{\sigma^{xx}_{1\text{b},d=0}(x,\omega)}{\sigma^{xx}_{1\text{b},d=0}(0,\omega)}\, J^x_{\text{clean}}(0,\vec{R},\omega) \\ &+ \frac{\sigma^{xx}_{1\text{b},d=0}(x,\omega)}{\sigma^{xx}_{1\text{b},d=0}(0,\omega)}\, J^x(0,\vec{R},\omega). \end{aligned} \tag{354}$$

For a delta-form electric field localized at the barrier, an infinitely thin wire, and a zero-range interaction potential, it is [9]

$$J^x(x,\vec{R},\omega) = \mathrm{e}^{\mathrm{i}|x|\omega g/v_{\text{F}}} J^x(x=0,\vec{R},\omega). \tag{355}$$

The current is distributed symmetrically around the barrier as it depends on the modulus of x. It further oscillates as a function of x with a period of $2\pi v_{\text{F}}/\omega g$.

B.2 DC Transport

For a time-independent effective voltage, V_{dc}, the current density in eq. (351) is

$$J^x_{\text{dc}}(\vec{R},V_{\text{dc}}) = e\Delta^2\, B^x_{00}(\vec{R}) \int_0^\infty \mathrm{d}\tau\, \mathrm{e}^{-S(\tau)} \sin[R(\tau)]\, \sin\left(\frac{eV_{\text{dc}}\tau}{\hbar}\right). \tag{356}$$

Inserting $S(\tau)$ and $R(\tau)$ for a zero-range interaction potential, see eqs. (349) and (350), and performing the integration with respect to τ [304] yields

$$\begin{aligned} J^x_{\text{dc}}(\vec{R},V_{\text{dc}}) &= B^x_{00}(\vec{R})\, \frac{\hbar\omega_{\text{c}}}{eR_{\text{T}}\pi} \left(\frac{\hbar\beta\omega_{\text{c}}}{2\pi}\right)^{1-2/g} \cdot \frac{\left|\Gamma\left(\frac{1}{g} + \frac{\mathrm{i}eV_{\text{dc}}\beta}{2\pi}\right)\right|^2}{\Gamma(2/g)} \\ &\times \sinh\left(eV_{\text{dc}}\beta/2\right). \end{aligned} \tag{357}$$

The symbol Γ denotes the gamma function. The parameter g is given in eq. (51). The tunneling resistance R_{T} is defined as

$$R_{\text{T}} = \frac{2\omega_{\text{c}}^2\hbar}{\pi e^2\Delta^2}. \tag{358}$$

It has to be large in comparison to h/e^2.

Performing the zero-temperature limit, $\beta \to \infty$, one obtains for the dc current with the help of [281]

$$J^x_{\rm dc}(\vec{R}, V_{\rm dc}) = \frac{B^x_{00}(\vec{R})}{R_{\rm T}\Gamma(2/g)} \left(\frac{e|V_{\rm dc}|}{\hbar\omega_{\rm c}}\right)^{2/g-2} V_{\rm dc}. \tag{359}$$

For a repulsive interaction, $g < 1$, the non-linear current is suppressed with respect to the linear current ($g = 1$) at small voltages. The stronger the interaction, the more pronounced is the suppression. With increasing driving voltage, the non-linear current becomes larger than the linear one for $eV_{\rm dc}/\hbar\omega_{\rm c} > 1$; but only voltages smaller than the cut-off, $eV_{\rm dc} < \hbar\omega_{\rm c}$, are physically reasonable, otherwise one leaves the range of validity of the model.

B.3 AC Transport

B.3.1 DC Component of the AC Current

Choose a 3D screened Coulomb potential with an inverse screening length α, see section 3.2, projected onto the quantum wire of diameter d, see section 3.1, and consider the regime $\alpha^{-1} \ll d$. For the projected driving electric field choose

$$E^x_{\rm ext,1b}(x,t) = E^x_{\rm dc}(x) + E^x_{\rm ac}(x)\cos(\omega_{\rm ext}t). \tag{360}$$

The voltages $V_{\rm dc}$ and $V_{\rm ac}$ are defined as

$$V_{\rm dc/ac} \equiv -\int\limits_{-\infty}^{\infty} {\rm d}x\, E_{\rm dc/ac}(x). \tag{361}$$

The spatial shape of $E^x_{\rm ac}(x)$ is

$$E^x_{\rm ac}(x) = E^x_{\rm ac}{\rm e}^{-|x|/\Lambda}, \tag{362}$$

where Λ denotes the range of the electric field. The effective driving potential, see eq. (343), then is [10]

$$V_{\rm eff}(t) = V_{\rm dc} + \frac{\hbar\omega_{\rm ext}}{e}\,|z|\,\cos(\omega_{\rm ext}t - \varphi_z). \tag{363}$$

Here, $|z|$ and φ_z are, respectively, modulus and argument of the complex quantity

$$z = \frac{e}{\hbar\omega_{\rm ext}} \int\limits_{-\infty}^{\infty} {\rm d}x\, E^x_{\rm ac}(x)\, r(x,\omega_{\rm ext}), \tag{364}$$

where the function $r(x,\omega)$ is given in eq. (344). The argument φ_z leads to a phase shift of the higher harmonics of the current and is not needed here as only the dc component of the current is studied. The modulus of z is

$$|z| = \frac{eV_{\rm ac}}{\hbar\omega_{\rm ext}} \frac{1}{\sqrt{1+\Lambda^2 k^2_{\rm LL}(\omega_{\rm ext})}}\, \mathcal{F}\left(\frac{\omega_{\rm ext}}{v_{\rm F}\alpha}, \frac{k_{\rm LL}(\omega_{\rm ext})}{\alpha}, \alpha\Lambda\right), \tag{365}$$

where $k_{\rm LL}(\omega)$ is the inverse of the dispersion relation of the elementary excitations of the Luttinger liquid, see section 3.2, and the function $\mathcal{F}(u,v,w)$ is

$$\mathcal{F}(u,v,w) = \sqrt{\frac{1}{1+u^2}\left[1+v^2\frac{(u+wv)^2}{(uw+v^2)^2}\right]}. \tag{366}$$

The effective driving voltage is monochromatic and hence the phase factor in the expression for the current in eq. (351) can be represented by a sum over Bessel functions [281]. The dc component of the ac current then is

$$\begin{aligned} J^x_{\rm ac,dc}(x=0,\vec{R}) &= e\Delta^2\, B^x_{00}(\vec{R}) \int\limits_0^\infty {\rm d}\tau\, {\rm e}^{-S(\tau)} \sin[R(\tau)]\, \sin\left(\frac{eV_{\rm dc}\tau}{\hbar}\right) \\ &\times \; J_0\left(2|z|\sin(\omega_{\rm ext}\tau/2)\right), \end{aligned} \tag{367}$$

where J_0 denotes a Bessel function of the first kind [281] and the index "ac,dc" at the current denotes that the expression gives the dc component of the ac current. By expanding the Bessel function of the sine in eq. (367) into a sum over Bessel functions [281], one obtains

$$J^x_{\rm ac,dc}(x=0,\vec{R}) = \sum_{n=-\infty}^{\infty} J_n^2(|z|)\, J^x_{\rm dc}(\vec{R}, V_{\rm dc}+n\hbar\omega_{\rm ext}/e) \tag{368}$$

where the current $J^x_{\rm dc}(\vec{R},V_{\rm dc})$ is the true dc current given in eq. (357).

In the limit of a delta-like electric field localized at the tunneling barrier, $\Lambda \to 0$, the integral in eq. (364) can be evaluated approximately and one obtains $|z| = eV_{\rm ac}/\hbar\omega_{\rm ext}$, i.e. $|z|$ scales with frequency as $|z| \propto \omega_{\rm ext}^{-1}$, see also [214]. In the limit of a homogeneous electric field that does not depend on position, $\Lambda \to \infty$, the integral in eq. (364) represents the spatial average of the function $r(x,\omega_{\rm ext})$. One then obtains $|z| \propto \omega_{\rm ext}^{-2}$.

B.3.2 Harmonic Components of the AC Current

Assume an external ac voltage that drops at the barrier and varies with time as

$$V_{\rm ext}(t) = V_{\rm dc} + V_{\rm ac}\cos(\omega_{\rm ext}t). \tag{369}$$

For zero-range interactions, the effective driving voltage, see eq. (343), is equivalent to the external voltage. The voltage phase factor in eq. (351) can for a monochromatic driving be expressed in terms of Bessel functions, $J_k(z)$, see [281]. The resulting expression for the current at the barrier is [9],

$$J^x(x=0,\vec{R},t) = B^x_{00}(\vec{R}) \sum_{n=-\infty}^{\infty} A_n(\omega_{\rm ext}){\rm e}^{-{\rm i}n\omega_{\rm ext}t}. \tag{370}$$

The complex current amplitudes are

$$\begin{aligned} A_n(\omega_{\rm ext}) &= {\rm i}^{n-1}\,\frac{e\Delta^2}{2}\int\limits_0^\infty {\rm d}\tau\,{\rm e}^{-S(\tau)}\sin[R(\tau)]\,{\rm e}^{{\rm i}n\omega_{\rm ext}\tau/2} \\ &\times\; J_n\left(\frac{2eV_{\rm ac}}{\hbar\omega_{\rm ext}}\sin\left[\frac{\omega_{\rm ext}\tau}{2}\right]\right)\,\left[{\rm e}^{{\rm i}eV_{\rm dc}\tau/\hbar}-{\rm e}^{-{\rm i}(eV_{\rm dc}\tau/\hbar+n\pi)}\right]. \end{aligned} \tag{371}$$

Using summation rules for the Bessel functions in eq. (371) [281] and splitting the complex current amplitude into real and imaginary parts, one obtains

$$A_n(\omega_{\rm ext}) = A_n^{(+)}(\omega_{\rm ext}) + {\rm i}A_n^{(-)}(\omega_{\rm ext}) \tag{372}$$

with

$$\begin{aligned} A_n^{(\pm)}(\omega_{\rm ext}) &= \frac{1}{2}\sum_{k=-\infty}^{\infty} C^{(\pm)}(V_{\rm dc}+k\hbar\omega_{\rm ext}/e)J_k\left(\frac{eV_{\rm ac}}{\hbar\omega_{\rm ext}}\right) \\ &\times\; \left[J_{k+n}\left(\frac{eV_{\rm ac}}{\hbar\omega_{\rm ext}}\right)\pm J_{k-n}\left(\frac{eV_{\rm ac}}{\hbar\omega_{\rm ext}}\right)\right]. \end{aligned} \tag{373}$$

The signs $(\pm)$ at the function C denote the real, $(+)$, and imaginary, $(-)$, parts of

$$C(\zeta) = {\rm i}e\Delta^2\int\limits_0^\infty {\rm d}\tau\,{\rm e}^{-S(\tau)}\sin[R(\tau)]\,{\rm e}^{-{\rm i}e\zeta\tau/\hbar}. \tag{374}$$

The real part of this expression is equivalent to the dc current, see eq. (356).

Based on eq. (371), one can show that the in-phase part of the current scales in leading order as $\omega_{\rm c}^{-2/g}$ for all g. The out-phase part scales in leading order as $\omega_{\rm c}^{-2/g}$ for $g > g_{\rm c}(n)$, where $g_{\rm c}(n) = 2/(n+2+s)$ with $s = [1+(-1)^n]/2$. For $g < g_{\rm c}(n)$, the out-phase current scales in leading order as $\omega_{\rm c}^{-(n+2+s)}$ [10]. For $g > g_{\rm c}(n)$, the function C, see eq. (374), is in leading order in $\omega_{\rm c}$

$$C(z) = \frac{{\rm i}\hbar\omega_{\rm c}}{eR_{\rm T}\pi}\left(\frac{\hbar\beta\omega_{\rm c}}{2\pi}\right)^{1-2/g}\frac{|\Gamma\left(\frac{1}{g}+\frac{{\rm i}ez\beta}{2\pi}\right)|^2}{\Gamma(2/g)}\,\frac{\sin\left(\pi\left[\frac{1}{g}-\frac{{\rm i}ez\beta}{2\pi}\right]\right)}{\cos(\pi/g)}. \tag{375}$$

At zero temperature, $\beta\to\infty$, the complex current amplitude is in leading order in $\omega_{\rm c}$ [281]

$$\begin{aligned} A_n^{(+)}(\omega_{\rm ext}) &= \frac{\hbar\omega_{\rm c}}{eR_{\rm T}}\left(\frac{\omega}{\omega_{\rm c}}\right)^{2/g-1}\frac{1}{2\Gamma(2/g)}\sum_{k=-\infty}^{\infty}J_k\left(\frac{eV_{\rm ac}}{\hbar\omega_{\rm ext}}\right) \\ &\times\; \left[J_{k+n}\left(\frac{eV_{\rm ac}}{\hbar\omega_{\rm ext}}\right)+J_{k-n}\left(\frac{eV_{\rm ac}}{\hbar\omega_{\rm ext}}\right)\right]\left|k+\frac{eV_{\rm dc}}{\hbar\omega_{\rm ext}}\right|^{2/g-1} \\ &\times\; {\rm sgn}\left(k+\frac{eV_{\rm dc}}{\hbar\omega_{\rm ext}}\right), \end{aligned} \tag{376}$$

$$A_n^{(-)}(\omega_{\rm ext}) = \frac{\hbar\omega_{\rm c}}{eR_{\rm T}}\left(\frac{\omega}{\omega_{\rm c}}\right)^{2/g-1}\frac{1}{2\Gamma(2/g)}\tan(\pi/g)\sum_{k=-\infty}^{\infty}J_k\left(\frac{eV_{\rm ac}}{\hbar\omega_{\rm ext}}\right) \quad (377)$$
$$\times \left[J_{k+n}\left(\frac{eV_{\rm ac}}{\hbar\omega_{\rm ext}}\right) - J_{k-n}\left(\frac{eV_{\rm ac}}{\hbar\omega_{\rm ext}}\right)\right]\left|k+\frac{eV_{\rm dc}}{\hbar\omega_{\rm ext}}\right|^{2/g-1}.$$

The interaction strengths for which these results are valid are $g > 2/3$ for $n = 1$, $g > 2/5$ for $n = 2$ and $n = 3$, $g > 2/7$ for $n = 4$ and $n = 5$ and so on.

For low frequencies, $\hbar\omega_{\rm ext} < \max(eV_{\rm dc}, k_{\rm B}T/g)$, one can expand the expression for the complex current amplitude in eq. (371) for $\omega_{\rm ext}\tau \ll 1$. Then, the real part becomes independent of frequency and the imaginary part is smaller than the real part by a factor $n\hbar\omega_{\rm ext}/eV_{\rm ac}$ for $V_{\rm dc} \ll V_{\rm ac}$ or by $n\hbar\omega_{\rm ext}/eV_{\rm dc}$ for $V_{\rm dc} \gg V_{\rm ac}$ [9]. One obtains for $V_{\rm dc} \ll V_{\rm ac}$,

$$A_n^{(+)}(V_{\rm dc}, V_{\rm ac}, g) \propto \left(\frac{V_{\rm dc}}{V_{\rm ac}}\right)^s \left(\frac{eV_{\rm ac}}{\hbar\omega_{\rm c}}\right)^{2/g-1}, \quad (378)$$

and for $V_{\rm dc} \gg V_{\rm ac}$,

$$A_n^{(+)}(V_{\rm dc}, V_{\rm ac}, g) \propto \left(\frac{eV_{\rm ac}}{\hbar\omega_{\rm c}}\right)^n \left(\frac{eV_{\rm dc}}{\hbar\omega_{\rm c}}\right)^{2/g-n-1}. \quad (379)$$

The proportionality constants omitted here contain neither the frequencies nor the voltages.

At finite temperature the above results remain valid as long as $k_{\rm B}T/g < eV_{\rm dc}$ or $eV_{\rm ac} > k_{\rm B}T/g > eV_{\rm dc}$. When $eV_{\rm ac} < k_{\rm B}T/g$ the cut-off of the τ-integration in eq. (371) is given by T instead of $V_{\rm dc}$,

$$A_n^{(+)}(V_{\rm dc}, V_{\rm dc}, T, g) \propto \left(\frac{eV_{\rm ac}}{\hbar\omega_{\rm c}}\right)^n \left(\frac{eV_{\rm dc}}{k_{\rm B}T}\right)^s \left(\frac{k_{\rm B}T}{\hbar\omega_{\rm c}}\right)^{2/g-n-1}. \quad (380)$$

B.4 Local Field Effects

The induced transverse field is related to the transverse part of the current via, see eq. (209),

$$\vec{E}_{\rm T,ind}(\vec{q},\omega) = {\rm i}\mu_0\omega\, g_0(\vec{q},\omega)\vec{J}_{\rm T}(\vec{q},\omega), \quad (381)$$

with $g_0(\vec{q},\omega)$, see eq. (86),

$$g_0(\vec{q},\omega) = \lim_{\eta\to 0}\frac{1}{q^2 - \left(\frac{\omega}{c}+{\rm i}\eta\right)^2}. \quad (382)$$

The time-dependent non-linear current in the wire has only an x-component and the x-component of the transverse part of this current then is, following eqs. (78) and (80),

$$J_{\rm T}^x(\vec{q},\omega) = J^x(\vec{q},\omega) - \frac{q_x^2}{|\vec{q}\,|^2}J^x(\vec{q},\omega). \quad (383)$$

Inserting this expression for the transverse part of the current into eq. (381) yields for the induced transverse field

$$E^x_{\mathrm{T,ind}}(\vec{q},\omega) \;=\; \mathrm{i}\mu_0\omega\, g_0(\vec{q},\omega)\,[1 - q_x^2\epsilon_0 V^{\mathrm{C}}_{\mathrm{ee}}(\vec{q})/e^2]\, J^x(\vec{q},\omega), \tag{384}$$

where it was used that the Fourier transform of the 3D Coulomb interaction potential is $V^{\mathrm{C}}_{\mathrm{ee}}(\vec{q}) = e^2/\epsilon_0|\vec{q}|^2$.

Next, take the expression for the non-linear ac current at the barrier given in eq. (196), Fourier transform it to ω, multiply it with the phase factor given in eq. (187) in order to obtain the current at any position x and then Fourier transform the whole expression to $\vec{q}$-space,

$$J^x(\vec{q},\omega) \;=\; \mathrm{i}4\pi\,\frac{(\omega g/v_{\mathrm{F}})}{(\omega g/v_{\mathrm{F}})^2 - q_x^2}\, B^x_{00}(\vec{Q}) \sum_{n=-\infty}^{\infty} A_n(\omega_{\mathrm{ext}})\,\delta(\omega - n\omega_{\mathrm{ext}}). \tag{385}$$

Insert this into eq. (384),

$$\begin{aligned} E^x_{\mathrm{T,ind}}(\vec{q},\omega) \;&=\; 4\pi\mu_0\,\frac{w^2 g}{v_{\mathrm{F}}}\,\frac{B^x_{00}(\vec{Q})\,[1 - q_x^2\epsilon_0 V^{\mathrm{C}}_{\mathrm{ee}}(\vec{q})/e^2]}{[q_x^2 - (\omega g/v_{\mathrm{F}})^2]\,[q_x^2 + Q^2 - (\omega/c)^2]} \\ &\times\; \sum_{n=-\infty}^{\infty} A_n(\omega_{\mathrm{ext}})\,\delta(\omega - n\omega_{\mathrm{ext}}). \end{aligned} \tag{386}$$

As the non-linear ac current as a function of the position x was derived for a wire of zero diameter, one should replace $B^x_{00}(\vec{R})$ by a delta-function and hence $B^x_{00}(\vec{Q})$ by 1. Further, as the expression for the current in eq. (385) is valid for zero-range interactions, $V^{\mathrm{ZR}}_{\mathrm{ee}}(\vec{r}-\vec{r}\,') = V_0\delta(\vec{r}-\vec{r}\,')$, one should for consistency replace the Fourier transform of the interaction potential in eq. (386) by V_0, where V_0 is independent of $\vec{q}$. From the expression for the projected zero-range interaction potential in eq. (58) in section 3.2 one can see that $V^{\mathrm{ZR}}_{1\mathrm{b}}$ diverges for a wire of zero diameter, $d \to 0$, if V_0 is not proportional to d^2. This implies that the term V_0 in eq. (386) should vanish for a wire of zero diameter. This strange situation is an artefact of the rather unphysical assumption of a zero-range interaction. However, it turns out that the choice of the interaction potential in eq. (386) has no influence on the qualitative statement that can be made at the end about the magnitude of the induced transverse field, see below.

Now, proceed by Fourier transforming the field in eq. (386) to $\vec{r}$-space

$$\begin{aligned} E^x_{\mathrm{T,ind}}(\vec{r},\omega) \;&=\; \frac{4\pi\mu_0}{(2\pi)^3}\,\frac{w^2 g}{v_{\mathrm{F}}}\,\left\{\sum_{n=-\infty}^{\infty} A_n(\omega_{\mathrm{ext}})\,\delta(\omega - n\omega_{\mathrm{ext}})\right\} \\ &\times\; \int \mathrm{d}q_x\,\mathrm{e}^{-\mathrm{i}q_x x}\int \mathrm{d}\vec{Q}\,\mathrm{e}^{-\mathrm{i}\vec{Q}\vec{R}}\,\frac{1}{[q_x^2 - (\omega g/v_{\mathrm{F}})^2]\,[q_x^2 + Q^2 - (\omega/c)^2]}. \end{aligned} \tag{387}$$

The integration with respect to q_x can be performed explicitly for $x \neq 0$; one obtains two terms and for one of them also the integration with respect to $\vec{Q}$ can be

performed,

$$
\begin{aligned}
E^x_{\mathrm{T,ind}}(\vec{r},\omega) &= \frac{-\mathrm{i}\mu_0}{2\pi}\,\frac{w^2 g}{v_\mathrm{F}}\,\left\{\sum_{n=-\infty}^{\infty} A_n(\omega_\mathrm{ext})\,\delta(\omega-n\omega_\mathrm{ext})\right\} \\
&\times\ 2\pi\,\mathrm{e}^{\mathrm{i}\omega g|x|/v_\mathrm{F}}\cdot\frac{v_\mathrm{F}}{\omega g}\cdot K_0\left(\sqrt{\left(\frac{\omega g}{v_\mathrm{F}}\right)^2-\left(\frac{\omega}{c}\right)^2}\,|\vec{R}|\right) \\
&+\ \frac{\mathrm{i}\mu_0}{2\pi}\,\frac{w^2 g}{v_\mathrm{F}}\,\left\{\sum_{n=-\infty}^{\infty} A_n(\omega_\mathrm{ext})\,\delta(\omega-n\omega_\mathrm{ext})\right\} \\
&\times\ \int \mathrm{d}\vec{Q}\,\frac{\mathrm{e}^{-\mathrm{i}\vec{Q}\vec{R}+\mathrm{i}|x|\sqrt{(\omega/c)^2-Q^2}}}{(\omega g/v_\mathrm{F})^2-(\omega/c)^2+Q^2}\cdot\frac{1}{\sqrt{(\omega/c)^2-Q^2}},
\end{aligned}
\tag{388}
$$

where $x\neq 0$ and $K_0(z)$ is a modified Bessel function [281]. One can see that the first term on the right hand side of eq. (388) diverges for $|\vec{R}|=0$ while the second does not. As for a wire of zero diameter, the current is proportional to $\delta(\vec{R})$ one actually expects the induced field to reflect this delta-function. As we are only interested in the effect of the induced field onto the current in the wire, i.e. at $|\vec{R}|=0$, the second term on the right hand side of eq. (388) is neglected with respect to the first.

Averaging then the first term on the right hand side of eq. (388) with respect to $\vec{R}$, i.e. integrating it with respect to $\vec{R}$, yields

$$
E^x_{\mathrm{T,ind,av}}(x\neq 0,\omega) \approx -\frac{\mathrm{i}2\pi\mu_0\omega\,\mathrm{e}^{\mathrm{i}\omega g|x|/v_\mathrm{F}}}{(\omega g/v_\mathrm{F})^2-(\omega/c)^2}\,\sum_{n=-\infty}^{\infty} A_n(\omega_\mathrm{ext})\,\delta(\omega-n\omega_\mathrm{ext}). \tag{389}
$$

Neglecting ω/c with respect to $\omega g/v_\mathrm{F}$, for $v_\mathrm{F}/c\ll 1$ and g not too small, and replacing μ_0 by $1/\epsilon_0 c^2$ yields

$$
E^x_{\mathrm{T,ind,av}}(x\neq 0,\omega) \approx -\frac{\mathrm{i}}{\epsilon_0\omega}\left(\frac{v_\mathrm{F}/g}{c}\right)^2 J^x_\mathrm{av}(x,\omega), \tag{390}
$$

where $J^x_\mathrm{av}(x,\omega)$ is the averaged time-dependent non-linear current

$$
J^x_\mathrm{av}(x,\omega) = 2\pi\,\mathrm{e}^{\mathrm{i}\omega g|x|/v_\mathrm{F}}\,\sum_{n=-\infty}^{\infty} A_n(\omega_\mathrm{ext})\,\delta(\omega-n\omega_\mathrm{ext}). \tag{391}
$$

Following eq. (390), it is clear the induced transverse field that causes a correction to the non-linear current is suppressed by a factor $(v_\mathrm{F}/gc)^2$ with respect to this current. Hence, the linear current induced by $E^x_{\mathrm{T,ind,av}}$ is negligible with respect to the current $J^x_\mathrm{av}(x,\omega)$.

The above calculations can be repeated keeping the Coulomb interaction potential instead of assuming a zero-range potential. Also then, the transverse induced field consists of one part diverging at $|\vec{R}|=0$ and another part remaining finite at $|\vec{R}|=0$. Keeping only the part that diverges inside the wire and averaging it with respect to $\vec{R}$ yields in the limit $\omega/c\ll\omega g/v_\mathrm{F}$ exactly the result given in eq. (390).

Finally, note that when evaluating the longitudinal part of the induced field for a wire of zero diameter, this induced field is finite outside the wire as the longitudinal part of the current is finite outside the wire. Such a result is in contradiction to the discussion in section 3.3 according to which the longitudinal and transverse parts of the current are zero outside the wire and consequently the longitudinal field is zero outside the wire. The contradiction is due to the strange nature of a wire of zero diameter with a total current density that is proportional to $\delta(\vec{R})$ in $\vec{r}$-space. Strictly speaking, a delta-function only makes sense in connection with an integration.

References

[1] L. V. Keldysh, in *The Dielectric Function of Condensed Systems*, edited by L. V. Keldysh, D. A. Kirzhnitz, and A. A. Maradudin (North-Holland, Amsterdam, 1989), Chap. 1, p. 1.

[2] O. Keller, Phys. Rep. **268**, 85 (1996).

[3] D. Pines and P. Nozières, *The Theory of Quantum Liquids* (W. A. Benjamin, New York, 1966).

[4] *Quantum Theory of the Optical and Electronic Properties of Semiconductors*, edited by H. Haug and S. W. Koch (World Scientific, Hong Kong, 1993).

[5] R. Loudon, in *Collective Excitations in Solids*, Vol. B88 of *NATO ASI*, edited by B. di Bartolo (Plenum Press, New York, 1983), Chap. 11, p. 479.

[6] J. Voit, Rep. Prog. Phys. **58**, 977 (1995).

[7] A. Fechner, M. Sassetti, and B. Kramer, in *24th International Conference on the Physics of Semiconductors*, edited by D. Gershoni (World Scientific, Singapore, 1998), section VII, A28 (on CD).

[8] A. Fechner, M. Sassetti, and B. Kramer, Microelec. Eng. **47**, 341 (1999).

[9] A. Fechner, M. Sassetti, and B. Kramer, Europhys. Lett. **45**, 693 (1999).

[10] G. Cuniberti, A. Fechner, M. Sassetti, and B. Kramer, Europhys. Lett. **48**, 66 (1999).

[11] G. Cuniberti, A. Fechner, M. Sassetti, and B. Kramer, in *Proceedings of the 7th International Specialist Workshop on Nonlinear Dynamics of Electronic Systems*, edited by W. Schwarz (Dezernat Öffentlichkeitsarbeit TU Dresden, Dresden, 1999).

[12] A. Fechner, G. Cuniberti, M. Sassetti, and B. Kramer, Adv. Phys. **8**, SI65 (1999).

[13] J. Bardeen and W. H. Brattain, Phys. Rep. **74**, 230 (1948).

[14] J. Bardeen and W. H. Brattain, Phys. Rep. **75**, 1208 (1949).

[15] G. E. Moore, Electr. Mag. **38**, 114 (1965).

[16] Y. Imry, *Introduction to Mesoscopic Physics* (Oxford University Press, Oxford, 1997).

[17] T. J. Thornton, Rep. Prog. Phys. **58**, 311 (1995).

[18] C. G. Smith, Rep. Prog. Phys. **59**, 235 (1996).

[19] G. Bergmann, Phys. Rep. **107**, 1 (1984).

[20] S. Washburn and R. A. Webb, Adv. Phys. **35**, 375 (1986).

[21] D. Wharam, in *Electronic Transport Properties*, edited by B. Kramer (Springer Press, Berlin, 2000), Vol. III/34A.

[22] A. Fechner, in *Electronic Transport Properties*, edited by B. Kramer (Springer Press, Berlin, 2000), Vol. III/34A.

[23] L. Jacak, P. Hawrylak, and A. Wójs, *Quantum Dots* (Springer Press, Berlin, 1998).

[24] T. Dittrich *et al.*, *Quantum Transport and Dissipation* (Wiley-VCH, Weinheim, 1998).

[25] G. B. Stringfellow, Rep. Prog. Phys. **45**, 469 (1982).

[26] *Molecular Beam Epitaxy and Heterostructures*, Vol. E87 of *NATO ASI*, edited by L. L. Chang and K. Ploog (Nijhoff Publishing, Dordrecht, 1984).

[27] B. A. Joyce, Rep. Prog. Phys. **48**, 1637 (1985).

[28] K. A. Valiev, *The Physics of Submicron Lithography* (Plenum Press, New York, 1992).

[29] *Nanolithography: A Borderland between STM, EB, IB, and X-Ray Lithographies*, Vol. E264 of *NATO ASI*, edited by M. Gentili, C. Giovannella, and S. Selci (Kluwer Academic Publishers, Dordrecht, 1994).

[30] *Low-Dimensional Structures in Semiconductors: From Basic Physics to Applications*, Vol. B281 of *NATO ASI*, edited by A. R. Peaker and H. G. Grimmeiss (Plenum Publishing Corporation, New York, 1992).

[31] *Physics and Technology of Submicron Structures*, Vol. 83 of *Solid-State Sciences*, edited by H. Heinrich, G. Bauer, and F. Kuchar (Springer Press, Berlin, 1988).

[32] *Science and Engineering of One- and Zero-Dimensional Semiconductors*, Vol. B214 of *NATO ASI*, edited by S. P. Beaumont and C. M. S. Torres (Plenum Publishing Corporation, New York, 1990).

[33] T. J. Thornton, Superlatt. Microstruct. **23**, 601 (1998).

[34] D. Kaufman *et al.*, Phys. Rev. B **59**, R10433 (1999).

[35] B. Dwir *et al.*, Physica B **259-261**, 1025 (1999).

[36] *Nanostructures and Mesoscopic Systems*, edited by W. P. Kirk and M. A. Reed (Academic Publishing Corporation, Boston, 1992).

[37] A. Yacoby *et al.*, Phys. Rev. Lett. **77**, 4612 (1996).

[38] B. L. Al'tshuler, A. G. Aronov, D. E. Khmel'nitskii, and A. I. Larkin, in *Quantum Theory of Solids*, edited by I. M. Lifshits (MIR Publishers, Moscow, 1984), Chap. 1.

[39] B. L. Al'tshuler and A. G. Aronov, in *Electron-electron interaction in disordered systems*, edited by A. L. Efros and M. Pollak (North-Holland, Amsterdam, 1985), Chap. 1, p. 1.

[40] M. Kaveh and N. Wiser, Adv. Phys. **33**, 257 (1984).

[41] C. C. Dean and M. Pepper, J. Phys. C **17**, 5663 (1984).

[42] K. K. Choi, D. C. Tsui, and S. C. Palmateer, Phys. Rev. B **32**, 5540 (1985).

[43] T. J. Thornton *et al.*, Phys. Rev. Lett. **56**, 1198 (1986).

[44] R. P. Taylor *et al.*, J. Phys.: Condens. Matter **1**, 10413 (1989).

[45] H. Taniguchi *et al.*, Jpn. J. Appl. Phys. **29**, 2321 (1990).

[46] J. P. Bird *et al.*, J. Phys.: Condens. Matter **3**, 2897 (1991).

[47] S. Chakravarty and A. Schmid, Phys. Rep. **140**, 193 (1986).

[48] D. K. Ferry and S. M. Goodnick, *Transport in Nanostructures* (Cambridge University Press, Cambridge, 1997).

[49] R. G. Wheeler *et al.*, Phys. Rev. Lett. **49**, 1674 (1982).

[50] K. K. Choi, D. C. Tsui, and K. Alavi, Phys. Rev. B **36**, 7751 (1987).

[51] T. Hiramoto, K. Hirakawa, Y. Iye, and T. Ikoma, Appl. Phys. Lett. **54**, 2103 (1989).

[52] Y. K. Fukai, S. Yamada, and H. Nakano, Appl. Phys. Lett. **56**, 2123 (1990).

[53] J. P. Bird *et al.*, J. Phys.: Condens. Matter **2**, 7847 (1990).

[54] A. Ramon, M. Heiblum, and H. Shtrikman, Semicond. Sci. Technol. **8**, 2176 (1993).

[55] M. Noguchi *et al.*, J. Appl. Phys. **80**, 5138 (1996).

[56] P. Mohanty, E. M. Q. Jariwala, and R. A. Webb, Phys. Rev. Lett. **78**, 3366 (1997).

[57] J. H. F. Scott-Thomas *et al.*, Phys. Rev. Lett. **62**, 583 (1989).

[58] U. Meirav, M. A. Kastner, M. Heiblum, and S. J. Wind, Phys. Rev. B **40**, 5871 (1989).

[59] S. B. Field *et al.*, Phys. Rev. B **42**, 3523 (1990).

[60] U. Meirav, M. A. Kastner, and S. J. Wind, Phys. Rev. Lett. **65**, 771 (1990).

[61] H. J. Schulz, in *Les Houches École d'Été de Physique Théorique* (Elsevier Science Publishers, New York, 1995), Vol. LXI, p. 553.

[62] H. J. Schulz, G. Cuniberti, and P. Pieri, in *Field Theories for Low Dimensional Systems*, Vol. 131 of *Solid-State Sciences*, edited by G. Morandi, A. Tagliacozzo, and P. Sodano (Springer Press, Berlin, 2000), (cond-mat preprint, 9807366).

[63] M. Sassetti, in *Quantum Transport in Semiconductor Submicron Structures*, Vol. E326 of *NATO ASI*, edited by B. Kramer (Kluwer Academic Publishers, Dordrecht, 1996), p. 95.

[64] F. P. Milliken, C. P. Umbach, and R. A. Webb, Solid State Comm. **97**, 309 (1996).

[65] C. Kane and M. P. A. Fisher, Phys. Rev. B **46**, 15233 (1992).

[66] C. Kane and M. P. A. Fisher, Phys. Rev. Lett. **68**, 1220 (1992).

[67] X. G. Wen, Phys. Rev. Lett. **64**, 2206 (1990).

[68] X. G. Wen, Phys. Rev. B **41**, 12838 (1990).

[69] X. G. Wen, Phys. Rev. B **43**, 11025 (1991).

[70] X. G. Wen, Phys. Rev. B **44**, 5708 (1991).

[71] K. Moon *et al.*, Phys. Rev. Lett. **71**, 4381 (1993).

[72] P. Fendley, A. W. W. Ludwig, and H. Saleur, Phys. Rev. Lett. **74**, 3005 (1995).

[73] A. M. Chang, L. N. Pfeiffer, and K. W. West, Phys. Rev. Lett. **77**, 2538 (1996).

[74] A. M. Chang, L. N. Pfeiffer, and K. W. West, Physica A **249-251**, 383 (1998).

[75] M. Grayson *et al.*, Phys. Rev. Lett. **80**, 1062 (1998).

[76] R. Egger and A. Gogolin, Phys. Rev. Lett. **79**, 5082 (1997).

[77] C. Kane, . Balents, and M. P. A. Fisher, Phys. Rev. Lett. **79**, 5086 (1997).

[78] M. Bockrath *et al.*, Nature **397**, 598 (1999).

[79] D. H. Cobden, J. Nygard, M. Bockrath, and P. L. McEuen, in *Proceedings of the XIII. International Winterschool on Electronic Properties of Novel Materials (IWEPNM)*, edited by H. Kuzmany (American Institute of Physics, Woodbury, 1999), (cond-mat preprint, 9904179).

[80] S. V. Zaitsev-Zotov, Y. A. Kumzerov, Y. A. Firsov, and P. Monceau, J. Phys.: Condens. Matter **12**, L303 (2000).

[81] O. M. Auslaender *et al.*, Phys. Rev. Lett. **84**, 1764 (2000).

[82] K. S. Ralls *et al.*, Phys. Rev. Lett. **52**, 228 (1984).

[83] S. Feng, in *Mesoscopic Phenomena in Solids*, edited by B. L. Al'tshuler, P. A. Lee, and R. A. Webb (Elsevier Science Publishers, Amsterdam, 1991), Chap. 4, p. 107.

[84] P. M. Mankiewich *et al.*, J. Vac. Sci. Technol. B **4**, 380 (1986).

[85] Y. Ochiai *et al.*, Superlatt. Microstruct. **6**, 337 (1989).

[86] D. Mailly, M. Sanquer, J.-L. Pichard, and P. Pari, Europhys. Lett. **8**, 471 (1989).

[87] A. A. Bykov *et al.*, JETP Lett. **49**, 135 (1989).

[88] A. Ohata, A. Toriumi, M. Iwase, and K. Natori, J. Appl. Phys. **68**, 200 (1990).

[89] D. Mailly and M. Sanquer, Surf. Sci. **229**, 260 (1990).

[90] R. J. Haug, H. Munekata, and L. L. Chang, Jpn. J. Appl. Phys. **31**, L127 (1992).

[91] G. M. Gusev, Z. D. Kvon, and E. B. Olshanetskii, Sov. Phys. JETP **74**, 735 (1992).

[92] R. A. Smith and H. Ahmed, J. Appl. Phys. **81**, 2699 (1997).

[93] R. A. Webb, A. Hartstein, J. J. Wainer, and A. B. Fowler, Phys. Rev. Lett. **54**, 1577 (1985).

[94] P. G. N. de Vegvar *et al.*, Phys. Rev. B **38**, 4326 (1988).

[95] A. A. Bykov, G. M. Gusev, and Z. D. Kvon, Sov. Phys. JETP **70**, 742 (1990).

[96] A. A. Bykov *et al.*, Superlatt. Microstruct. **10**, 287 (1991).

[97] A. R. Long *et al.*, Superlatt. Microstruct. **9**, 35 (1991).

[98] A. R. Long *et al.*, Semicond. Sci. Technol. **8**, 39 (1993).

[99] J. Wróbel *et al.*, Surf. Sci. **263**, 261 (1992).

[100] V. I. Belinicher and B. I. Sturman, Sov. Phys. Usp. **23**, 1999 (1980).

[101] V. I. Fal'ko and D. E. Khmel'nitskii, Sov. Phys. JETP **68**, 186 (1989).

[102] A. A. Bykov *et al.*, JETP Lett. **49**, 13 (1989).

[103] J. M. Shilton *et al.*, J. Phys.: Condens. Matter **8**, L531 (1996).

[104] T. H. Oosterkamp *et al.*, in *Proceeding of the International Summer School on Nanophysics (Helsinki, Finnland, 1998)*, (cond-mat preprint, 9904359).

[105] H. D. Jensen and J. M. Martinis, Phys. Rev. B **46**, 13407 (1992).

[106] L. R. C. Fonseca, A. N. Korotkov, and K. K. Likharev, J. Appl. Phys. **79**, 9155 (1996).

[107] I. L. Aleiner and A. V. Andreev, Phys. Rev. Lett. **81**, 1286 (1998).

[108] L. J. Geerligs *et al.*, Phys. Rev. Lett. **64**, 2691 (1990).

[109] H. Pothier *et al.*, Physica B **169**, 573 (1991).

[110] A. A. Odintsov, Appl. Phys. Lett. **58**, 2695 (1991).

[111] L. P. Kouwenhoven *et al.*, Phys. Rev. Lett. **67**, 1626 (1991).

[112] L. P. Kouwenhoven *et al.*, Phys. Rev. Lett. **73**, 3443 (1994).

[113] R. H. Blick *et al.*, Appl. Phys. Lett. **67**, 3924 (1995).

[114] T. Fujisawa and S. Tarucha, Superlatt. Microstruct. **21**, 247 (1997).

[115] T. H. Oosterkamp *et al.*, Phys. Rev. Lett. **78**, 1536 (1997).

[116] B. di Bartolo, in *Collective Excitations in Solids*, Vol. B88 of *NATO ASI*, edited by B. di Bartolo (Plenum Press, New York, 1983), Chap. 1, p. 19.

[117] D. L. Mills and E. Burstein, Rep. Prog. Phys. **37**, 817 (1974).

[118] E. Burstein, in *Elementary Excitations in Solids*, edited by A. A. Maradudin and G. F. Nardelli (Plenum Press, New York, 1969), p. 367.

[119] Y. A. Il'inskii, L. V. Keldysh, and V. Kisin, *Electromagnetic Response of Material Media* (Plenum Press, New York, 1994).

[120] R. Claus, L. Merten, and J. Brandmüller, *Light Scattering by Phonon-Polaritons* (Springer Press, Berlin, 1975).

[121] C. H. Henry and J. J. Hopfield, Phys. Rev. Lett. **15**, 964 (1965).

[122] A. Otto, Z. Phys. **216**, 398 (1968).

[123] S. John, Phys. Rev. Lett. **53**, 2169 (1984).

[124] P. E. Wolf and G. Maret, Phys. Rev. Lett. **55**, 2696 (1985).

[125] M. P. van Albada and A. Lagendijk, Phys. Rev. Lett. **55**, 2692 (1985).

[126] I. Freund, M. Rosenbluh, R. Berkovits, and M. Kaveh, Phys. Rev. Lett. **61**, 1214 (1988).

[127] E. Akkermans, P. E. Wolf, and R. Maynard, Phys. Rev. Lett. **56**, 1417 (1986).

[128] M. J. Stephen and G. Cwilich, Phys. Rev. B **34**, 7564 (1986).

[129] F. C. MacKintosh and S. John, Phys. Rev. B **37**, 1884 (1988).

[130] R. Dalichaouch *et al.*, Nature **354**, 53 (1991).

[131] J. Kroha, C. M. Soukoulis, and P. Wölfle, Phys. Rev. B **47**, 11093 (1993).

[132] B. A. van Tiggelen and E. Kogan, Phys. Rev. A **49**, 708 (1994).

[133] M. P. van Albada, B. A. van Tiggelen, A. Lagendijk, and A. Tip, Phys. Rev. Lett. **66**, 3132 (1991).

[134] M. Rusek and A. Orlowski, Phys. Rev. E **51**, R2763 (1995).

[135] H. Drexler *et al.*, Appl. Phys. Lett. **67**, 2816 (1995).

[136] M. H. Pedersen and M. Büttiker, Phys. Rev. B **58**, 12993 (1998).

[137] A. L. Fetter and J. D. Walecka, *Quantum Theory of Many-Particle Physics* (McGraw-Hill Book Company, New York, 1971).

[138] C. Kittel, *Quantum Theory of Solids* (John Wiley & Sons, New York, 1966).

[139] D. Pines, in *Solid State Physics*, edited by F. Seitz and D. Turnbull (Academic Press, New York, 1955), Vol. I, p. 367.

[140] G. D. Mahan, *Many-Particle Physics* (Plenum Press, New York, 1981).

[141] W. Kohn and P. Vashishta, in *Theory of the Imhomogeneous Electron Gas*, edited by S. Lundqvist and N. H. March (Plenum Press, New York, 1983), Chap. 2, p. 79.

[142] P. Fulde, *Electron Correlations in Molecules and Solids* (Springer Press, Berlin, 1995).

[143] A. Georges, G. Kotliar, W. Krauth, and M. J. Rozenberg, Rev. Mod. Phys. **68**, 13 (1996).

[144] C. Bourbonnais and L. G. Caron, Int. J. Mod. Phys. **5**, 1033 (1991).

[145] S. R. White, Phys. Rep. **301**, 187 (1998).

[146] A. Luther and I. Peschel, Phys. Rev. B **9**, 2911 (1974).

[147] S. Eggert, A. E. Mattsson, and J. M. Kinaret, Phys. Rev. B **56**, R15537 (1997).

[148] M. Fabrizio and A. O. Gogolin, Phys. Rev. B **51**, 17827 (1995).

[149] S. Eggert, H. Johannesson, and A. Mattsson, Phys. Rev. Lett. **76**, 1505 (1996).

[150] A. H. C. Neto, C. de C. Chamon, and C. Nayak, Phys. Rev. Lett. **79**, 4629 (1997).

[151] M. Sassetti and B. Kramer, Phys. Rev. Lett. **80**, 1485 (1998).

[152] M. Sassetti and B. Kramer, Eur. Phys. J. B **4**, 357 (1998).

[153] M. Sassetti, F. Napoli, and B. Kramer, Phys. Rev. B **59**, 7297 (1999).

[154] V. V. Ponomarenko, Phys. Rev. B **52**, R8666 (1995).

[155] D. L. Maslov and M. Stone, Phys. Rev. B **52**, R5539 (1995).

[156] I. Safi and H. J. Schulz, Phys. Rev. B **52**, R17040 (1995).

[157] A. Y. Alekseev, V. V. Cheianov, and J. Fröhlich, Phys. Rev. B **54**, R17320 (1996).

[158] I. Safi and H. J. Schulz, in *Quantum Transport in Semiconductor Submicron Structures*, Vol. E326 of *NATO ASI*, edited by B. Kramer (Kluwer Academic Publishers, Dordrecht, 1996), p. 159.

[159] Y. V. Nazarov, A. A. Odintsov, and D. V. Averin, Europhys. Lett. **37**, 213 (1997).

[160] V. V. Ponomarenko and N. Nagaosa, Phys. Rev. B **60**, 16865 (1999).

[161] V. A. Sablikov and B. S. Shchamkhalova, JETP Lett. **67**, 196 (1998).

[162] V. A. Sablikov and B. S. Shchamkhalova, Phys. Rev. B **58**, 13847 (1998).

[163] R. Egger and H. Grabert, Phys. Rev. Lett. **79**, 3463 (1997).

[164] P. Fendley, A. W. W. Ludwig, and H. Saleur, Phys. Rev. Lett. **75**, 2196 (1995).

[165] Y. Oreg and A. M. Finkel'stein, Phys. Rev. Lett. **74**, 3668 (1995).

[166] A. Kawabata, J. Phys. Soc. Jap. **65**, 30 (1996).

[167] A. Shimizu, J. Phys. Soc. Jap. **65**, 1162 (1996).

[168] Y. Oreg and A. M. Finkel'stein, Phys. Rev. B **54**, R14265 (1996).

[169] G. Cuniberti, M. Sassetti, and B. Kramer, J. Phys.: Condens. Matter **8**, L21 (1996).

[170] G. Cuniberti, M. Sassetti, and B. Kramer, Phys. Rev. B **57**, 1515 (1998).

[171] P. Fendley, A. W. W. Ludwig, and H. Saleur, Phys. Rev. B **52**, 8934 (1995).

[172] F. Lesage, H. Saleur, and P. Simonetti, Phys. Rev. B **56**, 7598 (1997).

[173] K. Leung, R. Egger, and C. H. Mak, Phys. Rev. Lett. **75**, 3344 (1995).

[174] D. L. Maslov, Phys. Rev. B **52**, R14368 (1995).

[175] R. Egger and H. Grabert, Phys. Rev. Lett. **77**, 538 (1996).

[176] M. Sassetti and B. Kramer, Phys. Rev. B **54**, R5203 (1996).

[177] F. Guinea, G. G. Santos, M. Sassetti, and M. Ueda, Europhys. Lett. **30**, 561 (1995).

[178] H. H. Lin and M. P. A. Fisher, Phys. Rev. B **54**, 10593 (1996).

[179] M. Sassetti, U. Weiss, and B. Kramer, Solid State Comm. **97**, 605 (1996).

[180] M. Ogata and H. Fukuyama, Phys. Rev. Lett. **73**, 468 (1994).

[181] M. Ogata and H. Fukuyama, Jpn. J. Appl. Phys. **34**, 4284 (1995).

[182] Y. Oreg and A. M. Finkel'stein, Phys. Rev. Lett. **76**, 4230 (1996).

[183] Y.-L. Liu, Phys. Rev. B **59**, 7937 (1999).

[184] R. Egger and H. Grabert, Phys. Rev. Lett. **75**, 3505 (1995).

[185] K. A. Matveev and L. I. Glazman, Phys. Rev. Lett. **70**, 990 (1993).

[186] M. Sassetti, F. Napoli, and U. Weiss, Phys. Rev. B **52**, 11213 (1995).

[187] H. Maurey and T. Giamarchi, Europhys. Lett. **38**, 681 (1997).

[188] R. Egger and H. Grabert, Phys. Rev. B **55**, 9929 (1997).

[189] M. Sassetti, G. Cuniberti, and B. Kramer, Solid State Comm. **101**, 915 (1997).

[190] M. Sassetti and B. Kramer, Phys. Rev. B **55**, 9306 (1997).

[191] G. Cuniberti, M. Sassetti, and B. Kramer, Europhys. Lett. **37**, 421 (1997).

[192] H. J. Schulz, Phys. Rev. Lett. **71**, 1864 (1993).

[193] H. Maurey and T. Giamarchi, Phys. Rev. B **51**, 10833 (1995).

[194] T. Giamarchi and H. J. Schulz, Phys. Rev. B **37**, 325 (1988).

[195] A. Furusaki and N. Nagaosa, Phys. Rev. B **47**, 4631 (1993).

[196] R. Landauer, Z. Phys. **68**, 217 (1987).

[197] M. Büttiker, Phys. Rev. Lett. **57**, 1761 (1986).

[198] Y. Imry, in *Directions in Condensed Matter Physics*, edited by G. Grinstein and G. Mazenko (World Scientific, Singapore, 1986), p. 101.

[199] M. Büttiker, A. Prêtre, and H. Thomas, Phys. Rev. Lett. **70**, 4114 (1993).

[200] M. Büttiker, H. Thomas, and A. Prêtre, Phys. Lett. A **180**, 364 (1993).

[201] M. Büttiker, J. Phys.: Condens. Matter **5**, 9361 (1993).

[202] M. Büttiker, H. Thomas, and A. Prêtre, Z. Phys. B **94**, 133 (1994).

[203] A. Prêtre, H. Thomas, and M. Büttiker, Phys. Rev. B **54**, 8130 (1996).

[204] M. Büttiker and T. Christen, in *Quantum Transport in Semiconductor Submicron Structures*, Vol. E326 of *NATO ASI*, edited by B. Kramer (Kluwer Academic Publishers, Dordrecht, 1996), p. 263.

[205] M. Büttiker, Journal of Low Temperature Physics **118**, 519 (2000).

[206] Z. Ma, J. Wang, and H. Guo, Phys. Rev. B **57**, 9108 (1998).

[207] P. G. N. de Vegvar, Phys. Rev. Lett. **70**, 837 (1993).

[208] H. Tang and Y. Fu, Phys. Rev. Lett. **67**, 485 (1991).

[209] Y. M. Blanter and M. Büttiker, Europhys. Lett. **42**, 535 (1998).

[210] Y. M. Blanter, F. W. J. Hekking, and M. Büttiker, Phys. Rev. Lett. **81**, 1925 (1998).

[211] V. A. Sablikov and B. S. Shchamkhalova, JETP Lett. **66**, 41 (1997).

[212] V. V. Ponomarenko, Phys. Rev. B **54**, 10328 (1996).

[213] J. R. Tucker and M. J. Feldman, Rev. Mod. Phys. **57**, 1055 (1985).

[214] P. K. Tien and J. R. Gordon, Phys. Rev. **129**, 647 (1963).

[215] J. Iñarrea and G. Platero, Europhys. Lett. **34**, 43 (1996).

[216] G. Platero and R. Aguado, Appl. Phys. Lett. **70**, 3546 (1997).

[217] X.-G. Zhao, G. A. Georgakis, and Q. Niu, Phys. Rev. B **56**, 3976 (1997).

[218] A. Wacker, A.-P. Jauho, S. Zeuner, and S. J. Allen, Phys. Rev. B **56**, 13268 (1997).

[219] R. Aguado and G. Platero, Phys. Rev. Lett. **81**, 4971 (1998).

[220] D. Sokolovski, Phys. Rev. B **37**, 4201 (1988).

[221] W. R. Frensley, Superlatt. Microstruct. **4**, 497 (1988).

[222] L. Y. Chen and C. S. Ting, Phys. Rev. Lett. **64**, 3159 (1990).

[223] L. Y. Chen and C. S. Ting, Phys. Rev. B **43**, 2097 (1991).

[224] E. Runge and H. Ehrenreich, Phys. Rev. B **45**, 9145 (1992).

[225] Y. Fu and M. Willander, J. Appl. Phys. **72**, 3593 (1992).

[226] C. L. Fernando and W. R. Frensley, Phys. Rev. B **52**, 5092 (1995).

[227] H. C. Liu, J. Appl. Phys. **69**, 2705 (1991).

[228] H. C. Liu, Phys. Rev. B **43**, 12538 (1991).

[229] H. M. Pastawski, Phys. Rev. B **46**, 4053 (1992).

[230] Y. Fu and S. C. Dudley, Phys. Rev. Lett. **70**, 65 (1993).

[231] C. Jacoboni and P. J. Price, Phys. Rev. Lett. **71**, 464 (1993).

[232] Y. Fu and S. C. Dudley, Phys. Rev. Lett. **71**, 466 (1993).

[233] N. S. Wingreen, A.-P. Jauho, and Y. Meir, Phys. Rev. B **48**, 8487 (1993).

[234] A.-P. Jauho, N. S. Wingreen, and Y. Meir, Phys. Rev. B **50**, 5528 (1994).

[235] A. D. Stone, M. Y. Azbel, and P. A. Lee, Phys. Rev. B **31**, 1707 (1985).

[236] H. C. Liu, Appl. Phys. Lett. **52**, 453 (1988).

[237] C. Jacoboni and P. J. Price, Solid State Comm. **75**, 193 (1990).

[238] A.-P. Jauho, Phys. Rev. B **41**, 12327 (1990).

[239] P. Johansson, Phys. Rev. B **41**, 9892 (1990).

[240] W. Cai *et al.*, Phys. Rev. Lett. **65**, 104 (1990).

[241] S. A. Gurvitz, Phys. Rev. B **44**, 11924 (1991).

[242] I. Bar-Joseph and S. A. Gurvitz, Phys. Rev. B **44**, 3332 (1991).

[243] P. Johansson and G. Wendin, Phys. Rev. B **46**, 1451 (1992).

[244] J. Iñarrea, G. Platero, and C. Tejedor, Semicond. Sci. Technol. **9**, 515 (1994).

[245] Y. Dakhnovskii and H. Metiu, Phys. Rev. B **51**, 4193 (1995).

[246] M. P. Anantram and S. Datta, Phys. Rev. B **51**, 7632 (1995).

[247] R. Aguado, J. Iñarrea, and G. Platero, Phys. Rev. B **53**, 10030 (1996).

[248] Q. Sun and T. Lin, Phys. Rev. B **56**, 3591 (1997).

[249] J. Iñarrea, R. Aguado, and G. Platero, Europhys. Lett. **40**, 417 (1997).

[250] J. Iñarrea, G. Platero, and C. Tejedor, Phys. Rev. B **50**, 4581 (1994).

[251] K. Flensberg, Phys. Rev. B **55**, 13118 (1997).

[252] M. Wagner, Phys. Rev. B **49**, 16544 (1994).

[253] M. Wagner, Phys. Rev. A **51**, 798 (1995).

[254] Y. Goldin and Y. Avishai, Phys. Rev. B **55**, 16359 (1997).

[255] L. Y. Gorelik, F. A. Maao, R. I. Shekhter, and M. Jonson, Phys. Rev. Lett. **78**, 3169 (1997).

[256] M. Wagner, Phys. Rev. Lett. **76**, 4010 (1996).

[257] M. Wagner, Phys. Rev. B **55**, R10217 (1997).

[258] C. Bruder and H. Schoeller, Phys. Rev. Lett. **72**, 1076 (1994).

[259] M. H. Hettler and H. Schoeller, Phys. Rev. Lett. **74**, 4907 (1995).

[260] N. C. Kluksdahl, A. M. Kriman, D. K. Ferry, and C. Ringhofer, Phys. Rev. B **39**, 7720 (1989).

[261] F. A. Buot and A. K. Rajagopal, Phys. Rev. B **48**, 17217 (1993).

[262] J. Iñarrea and G. Platero, Europhys. Lett. **33**, 477 (1996).

[263] P. W. Brouwer and M. Büttiker, Europhys. Lett. **37**, 441 (1997).

[264] M. P. Anantram, J. Phys.: Condens. Matter **10**, 9015 (1998).

[265] G. Gómes-Santos, Phys. Rev. Lett. **76**, 4223 (1996).

[266] P. F. Williams and A. N. Bloch, Phys. Rev. B **10**, 1097 (1974).

[267] J. Alsmeier, C. Sikorski, and U. Merkt, Phys. Rev. B **37**, 4314 (1988).

[268] T. Demel, D. Heitmann, P. Grambow, and K. Ploog, Appl. Phys. Lett. **53**, 2176 (1988).

[269] G. Berthold *et al.*, Semicond. Sci. Technol. **8**, 735 (1993).

[270] Y. S. Tang *et al.*, Phys. Rev. B **45**, 13799 (1992).

[271] Y. S. Tang, G. Jin, and C. D. W. Wilkinson, Solid State Comm. **85**, 189 (1993).

[272] C. Lettau *et al.*, Phys. Rev. B **50**, 2432 (1994).

[273] F. D. M. Haldane, Phys. Rev. Lett. **47**, 1840 (1981).

[274] F. D. M. Haldane, J. Phys. C **14**, 2585 (1981).

[275] J. M. Luttinger, J. Math. Phys. **4**, 1154 (1963).

[276] D. C. Mattis and E. H. Lieb, J. Math. Phys. **6**, 304 (1965).

[277] S. Tomonaga, Prog. Theor. Phys. **5**, 544 (1950).

[278] V. J. Emery, in *Highly conducting One-Dimensional Solids*, edited by J. T. Devreese, R. P. Evrard, and V. E. van Doren (Plenum Press, New York, 1979).

[279] J. Sólyom, Adv. Phys. **28**, 201 (1979).

[280] E. Mariani, M. Sassetti, and B. Kramer, Europhys. Lett. **49**, 224 (2000).

[281] *Handbook of Mathematical Functions*, 9 ed., edited by M. Abramowitz and I. A. Stegun (Dover Publications, New York, 1972).

[282] G. Cuniberti, Ph.D. thesis, University of Genova, 1997.

[283] D. A. Kirzhnitz, in *The Dielectric Function of Condensed Systems*, edited by L. V. Keldysh, D. A. Kirzhnitz, and A. A. Maradudin (North-Holland, Amsterdam, 1989), Chap. 2, p. 41.

[284] O. Keller, Phys. Rev. B **33**, 990 (1986).

[285] R. Courant and D. Hilbert, *Methods of Mathematical Physics* (Interscience Publishers, New York, 1953).

[286] P. M. Morse and H. Feshbach, *Methods of Theoretical Physics* (McGraw-Hill Book Company, New York, 1953).

[287] O. Svelto and D. C. Hanna, *Principles of Lasers* (Plenum Press, New York, 1989).

[288] A. Furusaki and N. Nagaosa, Phys. Rev. B **54**, R5239 (1996).

[289] W. Apel and T. M. Rice, Phys. Rev. B **26**, 7063 (1982).

[290] S. Tarucha, T. Honda, and T. Saku, Solid State Comm. **94**, 413 (1995).

[291] A. D. Stone and A. Szafer, IBM J. Res. Develop. **32**, 384 (1988).

[292] Z. Kopal, *Numerical analysis* (Chapman & Hall, London, 1961).

[293] H. S. Wilf, *Mathematics for the Physical Sciences* (John Wiley & Sons, New York, 1962).

[294] E. Bodewig, *Matrix calculus* (North-Holland, Amsterdam, 1959).

[295] T. Kleimann, Master's thesis, University of Hamburg, 1999.

[296] J. D. Jackson, *Classical Electrodynamics* (John Wiley & Sons, New York, 1962).

[297] R. P. Feynman and A. R. Hibbs, *Quantum Mechanics and Path Integrals* (McGraw-Hill Book Company, New York, 1965).

[298] L. S. Schulman, *Techniques and Applications of Path Integration* (John Wiley & Sons, New York, 1981).

[299] P. J. Davis and P. Rabinowitz, *Methods of Numerical Integration* (Academic Press, New York, 1975).

[300] A. O. Caldeira and A. J. Legget, Phys. Rev. Lett. **46**, 211 (1981).

[301] A. O. Caldeira and A. J. Legget, Ann. Phys. **149**, 374 (1983).

[302] U. Weiss, *Quantum Dissipative Systems* (World Scientific, Singapore, 1993).

[303] A. Fechner, Master's thesis, University of Hamburg, 1996.

[304] I. S. Gradshteyn and I. M. Ryzhik, *Table of Integrals, Series and Products* (Academic Press, New York, 1980).

Acknowledgement

I thank Bernhard Kramer and Maura Sassetti for the uncountable physical discussions we had and for their strong personal support.

I thank Ole Halfpap who always found the time to listen.

I gratefully acknowledge the financial support of the SFB 508 at the university of Hamburg, of the European TMR program, of the WE-Heraeus-Stiftung, and of the Graduiertenkolleg at the university of Hamburg.